eman ta zabal zazu

Universidad del País Vasco
Euskal Herriko Unibertsitatea

Faculty of chemistry
University of the Basque county
and
Faculty of Science
Pavol Jozef Šafárik University in Košice

Thesis

Presented to obtain

THE DEGREE OF DOCTOR OF PHILOSOPHY
at the

UNIVERSITY OF THE BASQUE COUNTRY
and at the

PAVOL JOZEF ŠAFÁRIK UNIVERSITY IN KOŠICE

by
Jakub MIŇO

Subject:

Functional magnetic materials prepared by rapid quenching

Table of content

Table of figures

Acknowledgement

The thesis is a result of cooperation between Pavol Jozef Šafárik university in Košice (UPJŠ) and University of the Basque country (UPV/EHU) within the frame of cotutelle agreement. In total, I have spent one year at UPV/EHU and three years at UPJŠ I studied one year at UPJŠ without cotutelle program because of different length of PhD. study in Slovakia.

First of all, I would like to thank my Slovak and Spanish supervisor Rastislav Varga and Arcady Zhukov for all provided help with research and as well with all the difficult administration work.

My gratitude also belongs to my colleagues from the Laboratory of magnetic optic and transport properties at UPJŠ, Laboratory of applied physics at UPV/EHU, Slovak Academy of Science and Technical University.

Also, I would like to thank my family for support, especially my wife, Jana, for continuous support through my PhD. study and for the grammar corrections.

Finally, I thank to following agencies and grants for financial support:

NanoCEXmat Project Grant ITMS 26220120019, Slovak Grant Agency VEGA Project Grant 1/0060/13, Grant APVV-0027-11, Spanish MINECO MAT2013-47231-C2-1-P, VVGS-PF-2015-495 and VVGS-PF-2016-72614.

Technical and human support provided by SGIker is gratefully acknowledged.

Introduction

Materials become everyday part of life. Development of new materials leads to improvement of living standards. Beginning of human progress is associated with materials like stone, wood a metal, but through the centuries we developed advanced materials for various purposes. With the beginning of digital age, attention of majority of material research turns towards so-called smart materials. These materials have one or more physical properties that significantly alter in controlled fashion after external stimulus. In simple words, they can be used as sensors and actuators. Smartphones, computers, cars, and even home appliances start to rely on smart materials. In modern smartphones, sensors are used to rotate display, to show cardinal direction, to measure ambient temperatures, etc. Displays are often equipped by light sensor that change brightness of displays based on ambient light. Car parking is much easier with sensors. Moreover, typical house appliance items can cooperate together through co-called Internet of Things. Windows equipped with smart materials can react to the amount of sunlight and make themselves more or less transparent. Sensor system in the household can turn on or off the light in the room if someone is inside. Smart materials reached also to wearables items like photochromic sunglasses that automatically, and without any electricity, change their transparency depending on the sunlight. Smartwatches are becoming more and more popular, because they provide information about blood pressure and pulse during the sport or inform about the number of steps that we have taken during the day. In the medicine, smart materials are used as stents, braces, implants. Nowadays, there are new potential applications coming out every week.

This is the main motivation for the present work, to make the life simpler. We chose materials that are able to recover their former shape after deformation caused by strain also called shape memory alloys and magnetoresistive materials that significantly change their resistance after applying of high external magnetic field. Shape memory materials are widely used in many fields as biomedicine, automotive industry, and robotics. There is still high demand for these materials in mentioned field and more possible application in new field (e.g. construction).

Interesting group of materials was discovered in 1903, when Fridrich Heusler found an alloy, that is composed from the non-magnetic materials, but as alloy, it acts as ferromagnet. Later, it was found that specific composition of Heusler alloys belongs also to the smart materials. Selected compositions have one more interesting property:

ferromagnetism. This is especially useful for shape memory material, where smart material effect is caused by phase transformation with different magnetic properties of both phases. Magnetic properties change is then proportional to the progress of shape memory effect. Material actuate and also sense it’s change in the same time.

Nobel prize winning discovery in 1988 brings us to the second studied type of materials with giant magnetoresistance. The developing of new read-heads in storage devices based on giant magnetoresistance boosted the development of information technologies. Nowadays, there is high demand in spintronics for new material that can greatly enhance the computational power of modern computers.

The aim of the present work is to prepare these materials by rapid quenching methods and enhance their properties or lower the cost and time necessary for production. The first and the second chapters deals with theoretical background of shape memory alloy and materials with giant magnetoresistance, respectively. There is explanation of the phenomena and the most typical problems that occur during the work with them. The aim of the chapter three is to put the most typical so-far prepared compositions and materials together in a small review. The forth chapter explains all the methods and devices used during the experimentation to achieve the goals. Finally, the most important chapter five sums up all the results and discuss the possible explanations.

Fig. 1 The examples of smart materials

1 Shape memory alloys

Shape memory alloys are materials with a specific property which restore their original shape after a thermal load is applied, or in the case of superelastic alloys, after deformation caused by strain [1]. Shape memory effect and superelasticity are associated with the crystallographically reversible nature of the martensitic transformation which appears in shape memory alloys [2]. This phenomenon is triggered by temperature change or, in the case of superelastic alloys, by unloading material (superelasticity) [3]. Elastic strain is limited up to 0.2% in the typical metallic materials [4]. However, polycrystalline shape memory alloys are capable of straining up to 13% [5], in the case of monocrystals even up to 20% [4]. Shape memory alloys were discovered in 1932 by Dr. Arne Ölander [6] and shape memory effect was described for the first time in 1941 by Dr. Vernon [7]. Shape memory alloys are widely used in robotics, biomedicine, aeronautic or automotive industries [1].

1.1 Shape memory alloys and superelasticity

Extensive research has been conducted upon shape memory alloys since their discovery. Therefore, mechanism of shape memory effect is well described [1,3,5,9,11]. There are four ways how shape memory effect can be performed (Fig. 2):

- One-way shape memory effect:

  The alloy retains in deformed shape after unloading external force. Heating will activate shape recovery.

- Two-way shape memory effect:

  The alloy remembers deformed and original shape at low and at high temperature. Shape transformation occurs without mechanical straining. Unfortunately, two-way shape memory alloys are less efficient. So far, only half of strain can be achieved (comparing to one-way shape memory effect) and also the two-way shape memory alloys require training.

- Pseudoelasticity (also called superelasticity, however it is the same phenomenon):

  The alloy returns to its original shape immediately after removing mechanical stress without any need of thermal activation.

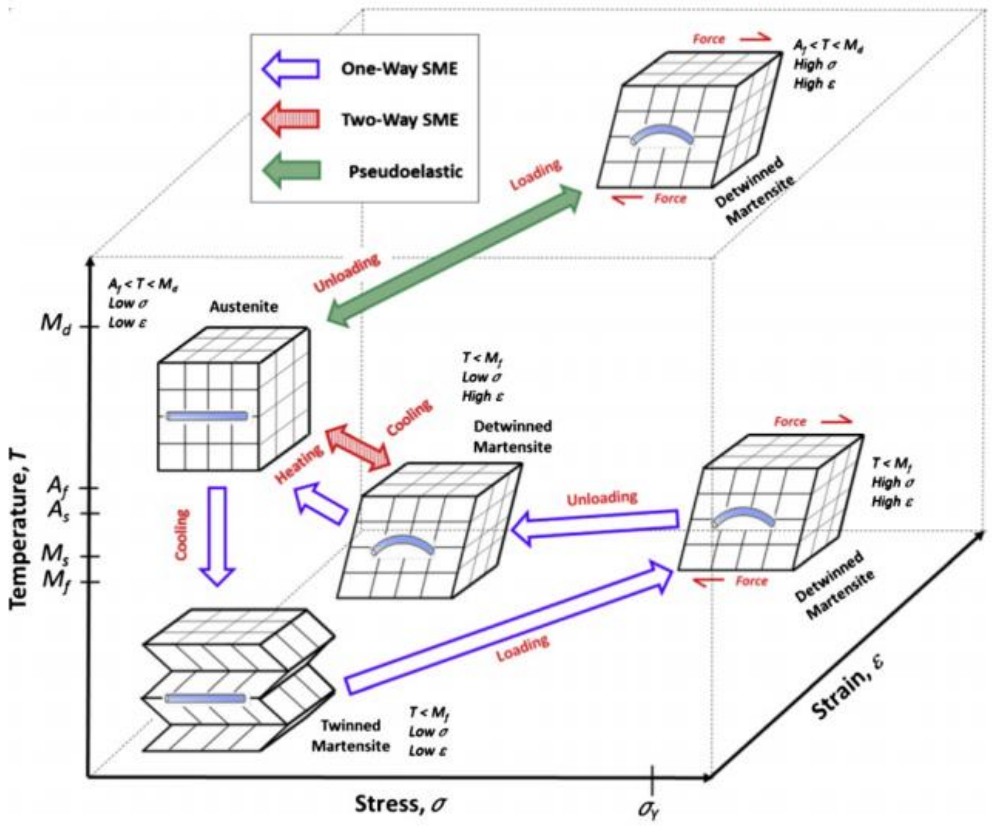

Fig. 2 Representation of all phases, lattices and transformations in shape memory alloys and their dependence on stress and temperature [3]

1.2 Martensitic transformation

Shape memory effect is carried by diffusion-less solid-to-solid phase transformation, generally known as martensitic transformation. It was described for the first time in the iron-based alloys (steels). Martensitic transformation occurs between low temperature martensite phase (stabilized by stress) and high temperature austenite phase (stable without stress) [8]. Its general property is cooperative relocation of atoms limited by atomic bonds range, which also maintain strict nearest crystallographic neighbourhood of atoms during the transformation [9]. Simplified version of martensitic transformation is shown in the Fig. 3. Force induced martensitic transformation is not observed only in shape memory alloys but it is well-described phenomenon in rustles or carbon steels [8].

Martensitic transformation on the contrary to plastic deformation progresses without relocating nearest crystallographic neighbourhood. The difference between plastic and superelastic deformation is shown in the Fig. 3a, where neighbour atoms A,

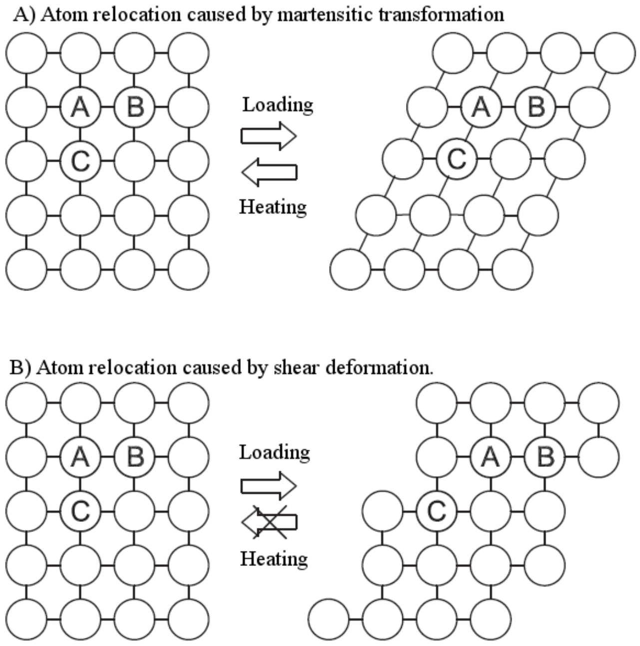

Fig. 3 The difference between shear deformation and martensitic transformation is defined by the local arrangement between the nearest neighbours [8]

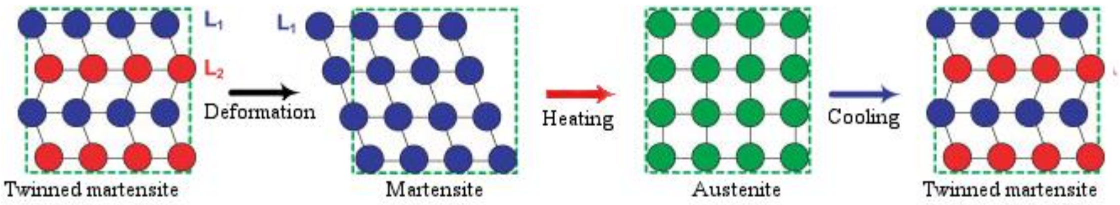

Fig. 4 Martensitic transformation for one-way shape memory effect [5]

B, and C are unchanged by deformation. In the case of shear deformation (shown in the Fig. 3b) this mechanism is not present [8].

Martensitic transformation (depicted in Fig. 4) for one way shape memory effect progress as follows: at the beginning, the alloy is in the state of twinned martensite, which is stable at low temperatures. Deformation removes twinning and causes shape change which remains after tension is unloaded. The heating induces transformation into high temperature phase, austenite which is followed by change recovering. Cooling causes transformation back into martensite but without shape changing due to the twinning. Practically, shape memory alloy exists in two different phases with three diverse crystal structures (two variants of martensite and austenite) and they operate through six possible transformations [1]. All of these are depicted in (Fig. 2)

1.2.1 Martensitic transformation temperatures

Shape memory alloys can operate only in the exact temperature range, in which martensitic transformation takes place. The transformation temperatures are important characteristics of shape memory alloy and they are referred as:

- Austenite start temperature (A_s) is a specific temperature when austenite starts to transform to martensite. From macroscopic point of view, it is when first sign of shape recovery is observed.
- Austenite finish temperature (A_f) defines the moment when martensitic transformation ends and no transformation is about to continue. The shape of alloy is totally recovered.
- Martensite start temperature (M_s) is observed during cooling process. Martensite starts to develop together with twinning process that ensures no observable shape change (only for one-way shape memory effect).
- Martensite finish temperature (M_f) represents the moment when alloy is composed only from martensitic phase.

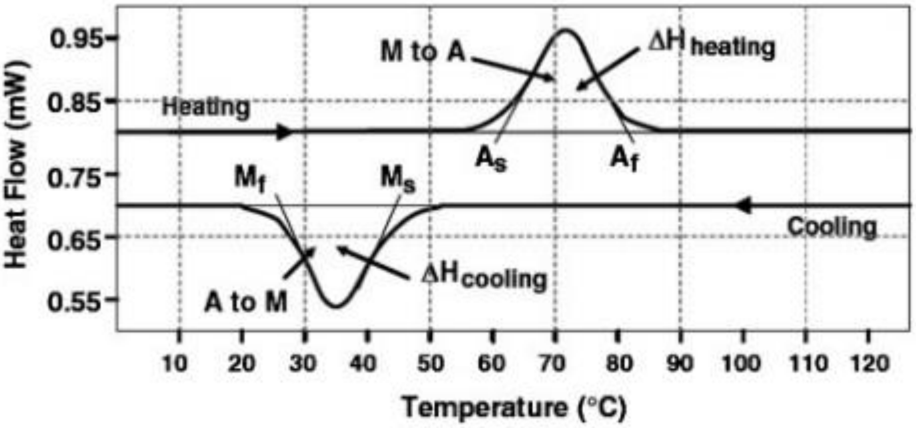

Fig. 5 DSC measurements used to determine transformation temperatures [5]

These temperatures belong to main characteristics for shape memory alloy. They, together with M_d temperature (the upper limit of temperature for occurrence of martensitic transformation), determine application fields for shape memory alloys [10]. Transformation temperatures can be detected by differential scanning calorimetry (depicted in Fig. 5), from temperature dependence on electrical resistivity, or from dilatometry measurements [5]. Other important characteristics of shape memory alloys are listed in Chapter 1.3.

Shape memory effect progresses with re-orientation of twinning structure of martensite. Superelastic effect is activated by martensitic transformation itself (induced by stress). Twinning processes are not responsible for superelasticity [5]. Martensitic transformation can be activated by stress or by temperature. This dependency is schematically expressed by Clausius-Clapeyron equation:

$$\frac{\mathrm{d}\sigma_c}{\mathrm{dT}} = -\frac{\Delta S}{\varepsilon . V_m} \tag{1.1}$$

where σ_c represents critical stress for inducing martensitic transformation, T is a temperature, ΔS expresses a change of entropy between martensite and austenite, ε is a strain, and V_m represents mole volume [12]. Transformation temperatures follow this dependence meaning that stress and temperature manipulation adjust each transformation temperature [5]. In the case of ferromagnetic alloys (i. e. Heusler alloys), shape memory effect can be induced by magnetic field.

1.3 Maximum strain and working stress in shape memory alloys

Properties of shape memory alloy are well described by following characteristics: maximum stress σ_{max}, recoverable strain ε_{rec}, and irrecoverable strain ε_{irr}. Stress-strain curves are usually executed to determine these parameters. As it is seen in Fig. 6, recoverable strain is divided into two subgroups: shape memory strain ε_{sme} or superelastic ε_{se}, and elastic strain ε_{el}. All groups and subgroups are fully described as follows:

- Irrecoverable strain ε_{irr} represents a fraction of the strain, which is caused by plastic deformation thus making it irreversible. It is mainly generated by creating and moving dislocations, but also by martensite stabilization, which have not been transformed to austenite after heating. However, ε_{irr}

can be minimalized through training process (many-times repeated stress-strain cycle).

- Recoverable strain ε_{rec} is divided into 2 subgroups:
    - Recoverable strain ε_{sme} (shape memory) or ε_{se} (superelasticity) is caused by martensitic transformation and its value is determined by crystal lattices differences and its parameters.
    - Elastic strain ε_{se} progresses inseparably with ε_{sme} or ε_{se} and it is described by Young's modulus *E* and written as follows:

$$E = \frac{\sigma}{\varepsilon} = \frac{FL_0}{A_0 \Delta L} \tag{1.2}$$

where *F* represents tensile force, A_0 is cross–section area, L_0 is length of unstressed material before and ΔL represents change in length. Young modulus is characteristic for all materials not only for shape memory alloys.

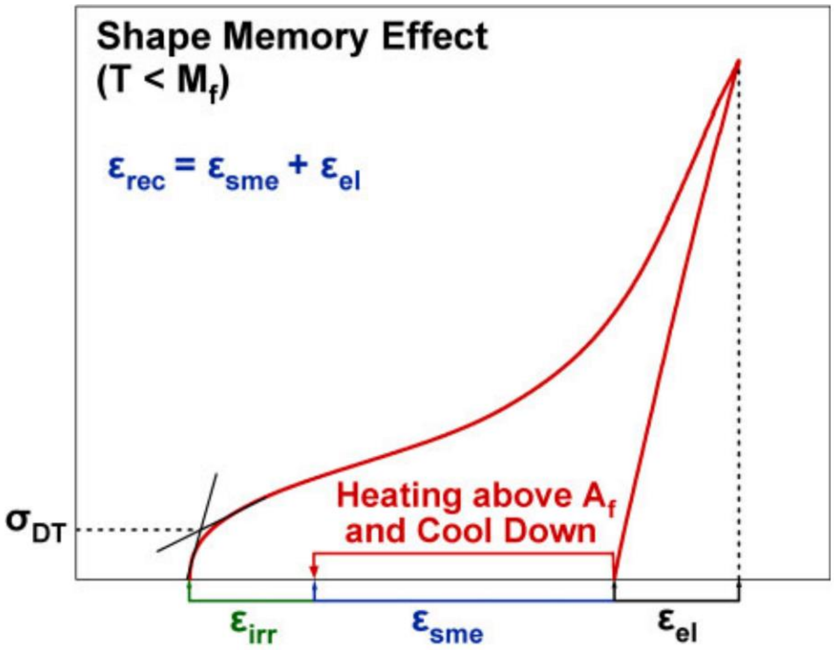

Fig. 6 Stress-strain curve for one-way shape memory effect [5].

Superelastic strain is caused by differences in crystal lattices of both phases. If tension is used in particular direction, maximum strain ε_{max} can be evaluated using formula:

$$\varepsilon_{max} = \frac{\sqrt{2}a - a_0}{a_0} \times 100 \tag{1.3}$$

where a represents lattice parameter of martensitic phase, a_0 is a lattice parameter of austenitic phase. However, Eq. 1.3 can be used only for samples prepared as monocrystals. Orientation of each grain influence maximum strain in polycrystalline samples [13,14].

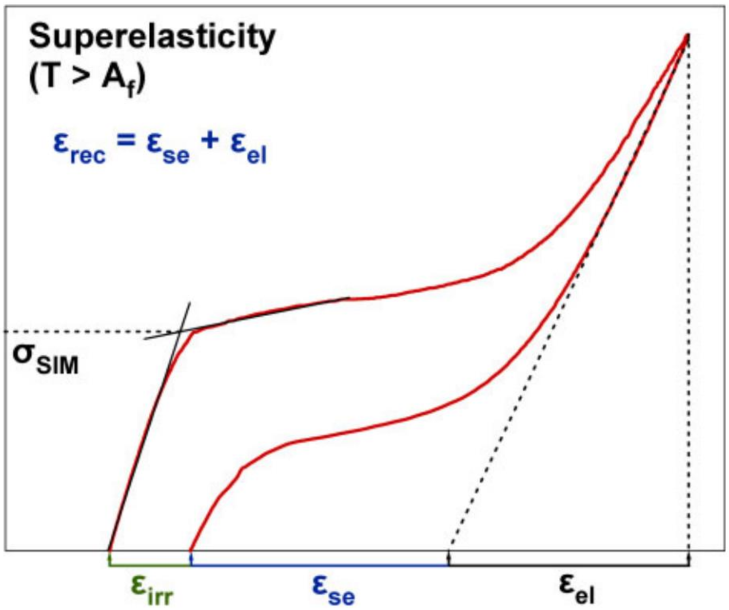

Fig. 7 Stress-strain curve for superelasticity [5]

1.3.1 Plastic deformation and training of shape memory alloys

Plastic deformation is a part of each shape memory cycle. Local internal stress can become higher than external stress while martensitic transformation takes place. This causes irreversible plastic deformation even if yield strength σ_y was not exceeded. Therefore, materials with high yield strength σ_y perform better with low irrecoverable deformation ε_{irr}. Stress, at which detwinning or reorientation of martensite occurs, is called detwinning or reorientation stress σ_{DT} (σ_{SIM} for superelasticity). Yield strength is an important property of shape memory alloys and it can be improved by hardening methods. Cold working directly increases σ_y and also stabilises the phase, in which cold working takes place. For example, cold working at martensitic temperature stabilises martensite phase and increases reverse transformation temperatures. However, many of shape memory or superelastic alloy are intermetallic and they have a limited ductility, so processing them becomes more complicated. Additionally, superelastic and shape memory effect can be improved through training. Training represents mechanical (Fig. 8) or thermal (Fig. 9) multiple cycling between austenite and martensite for several times.

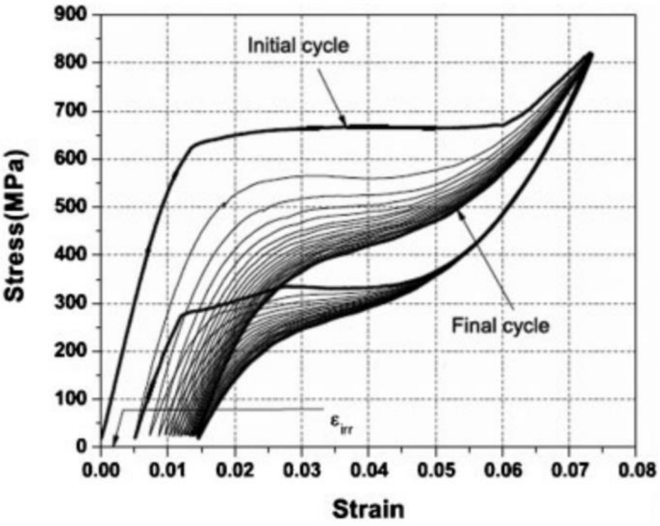

Fig. 8 Stress strain curves before and after training [5]

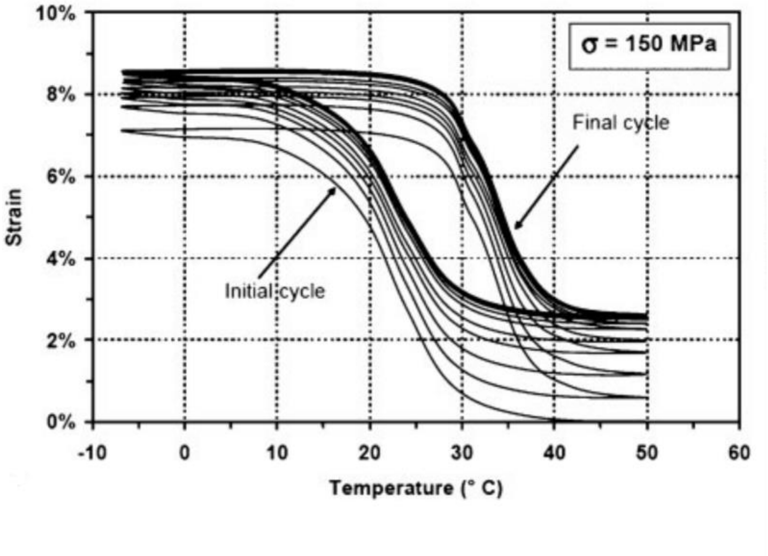

Fig. 9 Temperature cycling with constant load [5]

Irrecoverable strain takes place during cycling, but it gradually become saturated as cycling continues. The main reason why training helps is that dislocations or residuals of martensite are generated by martensitic transformation itself, therefore are placed in particular locations.

2 Giant magnetoresistance

Magnetoresistance (MR) is the change of electrical resistivity due to an external magnetic field. MR exists in all real metals, and the magnitude and behaviour of MR are different for various types of metals. The effect of giant magnetoresistance (GMR) is a significant change of electrical resistivity R depending on magnetization of magnetic material in non-magnetic matrix either as multi-layered films or granular materials. GMR has been observed for the first time in 1988 by two independent research groups led by A. Fert and P. Grünberg on multi-layer film consisting of Fe-Cr-Fe [15,16]. It should be noted that discovery of GMR was awarded by the Nobel prize in Physics in 1997 [17]. Discovery of GMR have started an extensive research era of these materials with new chemical composition. Initially GMR effect has been observed only in the magnetic multilayer geometry. Multi-layered films are usually prepared by single crystal growth [16] or by spattering layers [26]. Later, GMR has been discovered in granular systems [26,27].

2.1 Electrical resistance and magnetoresistance

The electrical resistance depends on scattering of free electrons in a crystal lattice. Scattering is caused by collision with impurities, lattice imperfections, and phonons [18]. The key role in the electrical resistance plays electron-phonon interactions, which makes temperature dependence of resistance linear at higher temperature. However, phonon vibrations are partially diminished at helium temperature (~ 4K). Thus, collisions with mechanical imperfections and impurities dominate the major influence of phonons [19]. Various resistance behaviours can be observed at low temperature as shown in Fig. 10. Black curve represents a typical metal without magnetic impurities or superconductivity, red curve is an example of Kondo effect and green line is usual for superconductors [20]. Temperature dependence of resistance for metals is well described by the Bloch-Grüneisen formula [19]:

$$\rho(T) = \rho(0) + \rho_{el-ph}(T) \tag{2.1}$$

$$\rho_{el-ph}(T) = \alpha_{el-ph}\left(\frac{T}{\Theta_R}\right)^n \int_0^{\frac{\Theta_R}{T}} \frac{x^n}{(e^x - 1)(1 - e^{-x})}dx \qquad (2.2)$$

where $\rho(0)$ is the residual resistivity as a result of impurities and defects, electron-phonon interaction is described by the temperature dependence part ρ_{el-ph}, n is the constant and represents nature of interaction (values are 2,3 or 5). The part α_{el-ph} is constant which arises from Debye and plasma frequency, and electron phonon constant. Θ_R represents Debye temperature obtained from resistivity measurements.

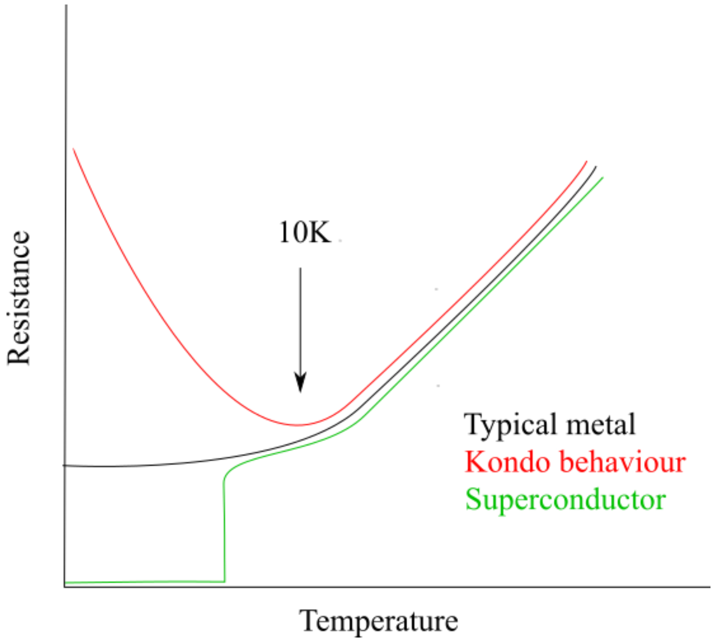

Fig. 10 Temperature-resistance curves for various types of material

Moreover, magnetic field can also affect resistivity in the material in so-called magnetoresistance effect. As mentioned above, magnetoresistance is the change of electrical resistivity due to an external magnetic field. In the most ferromagnets, the effect is observed as an increase in resistance as the angle θ between the current I and the saturated magnetization M_s decreases. The value of resistance change $\Delta R/R$ is usually very small. For example, magnetoresistance of nickel and iron is about 2 and 0.3 percent respectively [21]. Magnetoresistance ratio is usually defined by following term:

$$MR(H) = \Delta R/R_0 = (R_H - R_0)/R_0, \qquad (2.3)$$

where R_H and R_0 represents resistance measured with and without the external magnetic field, respectively. From this equation it is clear, that magnetoresistance can only reach values between 0% and 100%. However, it is possible to find another equation in the literature [25]:

$$MR(H) = \Delta R/R_H = (R_H - R_0)/R_H. \tag{2.4}$$

Use of this equation may lead to magnetoresistance values above 100%.

2.2 Giant magnetoresistance

The giant magnetoresistance was described for the first time by two independent research groups of A. Fert [15] and R. Grünberg [16]. The phenomenon has been observed on thin films of Fe-Cr-Fe composition. Structure of thin films used in the first stage of GMR research consisted of very thin chromium layer (1nm) between two ferrous thin films (25 nm) [16]. Considerable change of resistance was observed. Few year later, GMR was found also in granular materials [26,27] formed by immiscible elements. The mechanism of the giant magnetoresistance of multilayers or granular materials is fundamentally different from mechanism of magnetoresistance in ferromagnetic, homogeneous bulk and other alloys (known as anisotropic magnetoresistance). The maximum resistance changes of GMR can be higher by one order of magnitude [28]. The name “giant” was taken from one of the first reports [15].

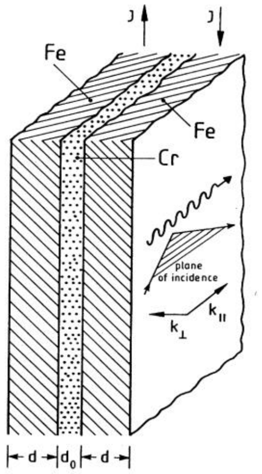

Fig. 11 Sketch of multi-layered film used by Grunberg’s research team in 1988 [16]

It has been found, that resistance change in multilayered films under magnetic field is caused by spin-dependent scattering of conducting electrons when travelling through nanoscale non-magnetic metal spacer between two magnetic layers. If external magnetic field is not present, the resistance is higher, because magnetic layers would have opposite magnetization. Application of magnetic field changes the magnetization of one layer to be equal. This allows half of the electrons with same spin orientation as magnetization to pass through the layers without scattering [28] (Fig. 12).

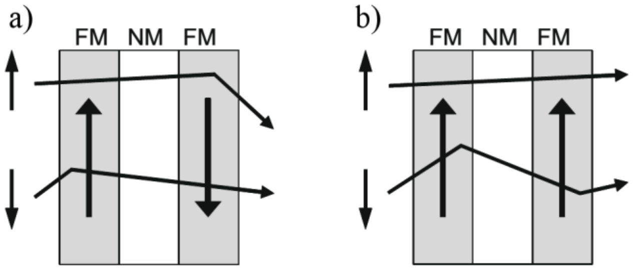

Fig. 12 Interactions of electrons depend on electron spin and on the direction of magnetization in each layer. If the direction of magnetization in the layers is opposite ↑↓ (a), electron with spin ↑ and ↓ are scattered during transport. The same direction of magnetization ↑↑ (b) allows electron with spin ↑ to pass through the layers without scattering, thus lowering the total resistance of material [28].

The increase of magnetic field gradually increases the magnetoresistance until material reaches saturated magnetization. However, the magnetoresistance in the small fields is quite high. When a single domain state (uniform magnetization) is reached (slightly beyond technical saturation ($H > H_s$), magnetoresistance is saturated as well. Only relative orientation of magnetization and electrical current is required to reach sufficient magnetoresistance change [29,30] (Fig. 13).

A granular magnetic alloy is composed from non-magnetic matrix and from small ferromagnetic particles embedded into it. Usually, such a material is prepared by producing a solid solution of ferromagnetic metal in non-magnetic metal matrix. For example: most frequently used preparation procedures are:

- Preparation of GMR material in the form of thin film or layer using non-equilibrium deposition techniques such as an evaporation, electrodeposition, or sputtering.
- Using rapid quenching techniques like melt spinning to produce ribbons or Taylor-Ulitovsky method to produce microwires.

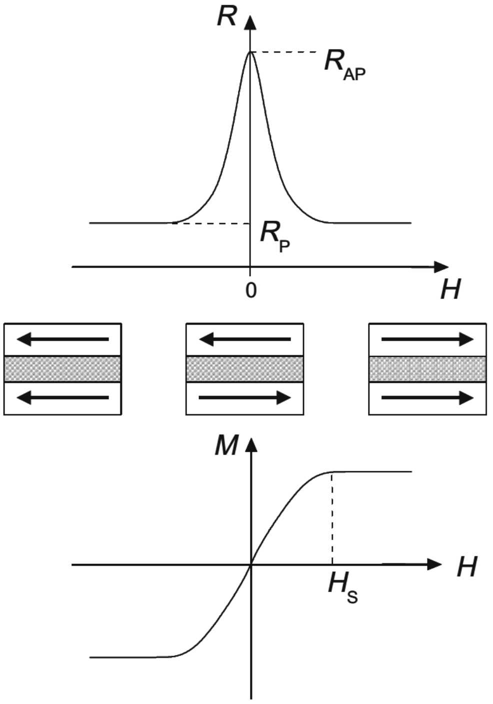

Fig. 13 Top picture depicts the change of the resistance with external magnetic field. Medium sketch represents paramagnetic spacer between two ferromagnetic layers with arrow showing the direction of magnetization in ferromagnetic layer. Bottom graph shows correlation between saturated magnetization and saturated resistance change [28].

If the metals are immiscible, their solid solution is metastable. It is possible to enhance the formation of the granules in the prepared sample by applying heat treatment. Size of the particles can be controlled by varying the annealing time and separation (density) of the granules and by changing ratio between non-magnetic and ferromagnetic elements. Ferromagnetic particles often exhibit so-called superparamagnetic behaviour in granular GMR materials. This phenomenon can be achieved by reducing the size of the particles below the critical size that depends not only on the particle size, but also on following material parameters: ferromagnetic exchange coupling, magnetocrystalline anisotropy constants, and strength between atomic moments [31]. Particle starts to act superparamagnetic when its thermal energy *kT* becomes larger than its total anisotropy energy KV, where V represents particle volume and K is constant of the resultant anisotropy from any sources. The magnetisation curve of assembled non-interactive SPM particles will be shown without hysteresis (Fig. 14). The saturation of such particles requires large magnetic field.

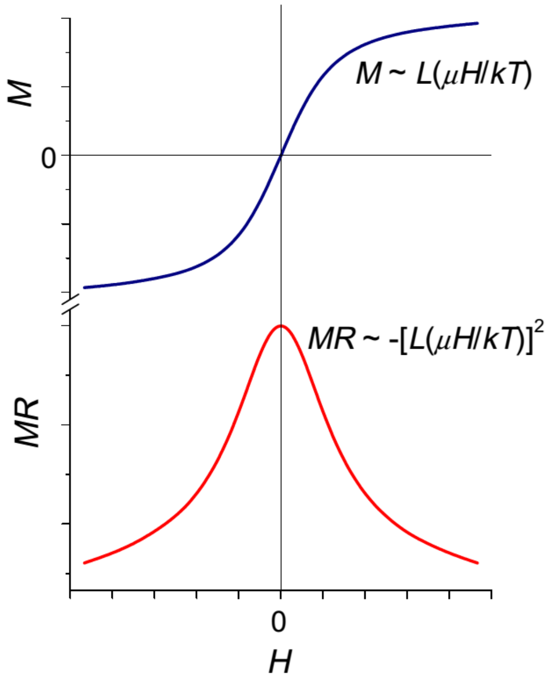

Fig. 14 Magnetic field dependence of the magnetization (top) and magnetoresistance change (bottom) for an ideal granular material consisting of ferromagnetic particles in paramagnetic or diamagnetic matrix [28].

If superparamagnetic particles are sufficiently separated in non-magnetic matrix, there is no magnetic interaction between their magnetic moments. In that case, conduction electron will be polarized by the magnetic moment of mentioned particle. If the same electron will encounter another superparamagnetic particle in time shorter than its spin-memory time (original spin orientation), then it will undergo a spin dependent scattering due to the uncorrelated spin orientation of both particles (Fig. 15). This spin-dependent scattering increases the resistance of granular materials just like in the case of multi-layered thin films. Relation between the field dependence of magnetization and the magnetoresistance is proportional to the Langevin function:

$$M(H) \propto L(\mu H/kT) \tag{2.5}$$

Electron movement from one particle to another was considered as a quantitative contribution to the magnetoresistance by Gittleman et al. [32]. Correlation between the magnetic moment orientations of neighbouring superparamagnetic particles and it has been shown as a probability of the electron scattering.

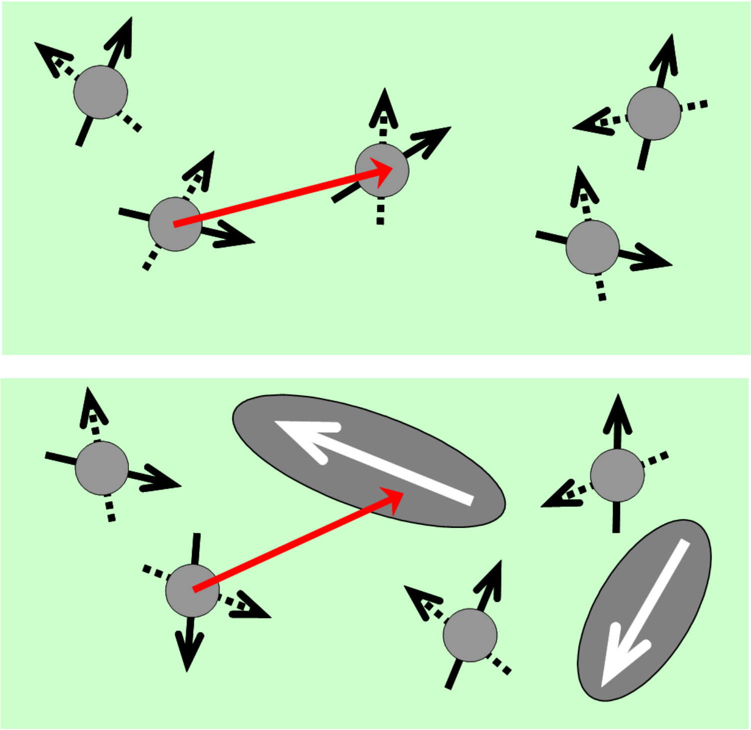

Fig. 15 Superparamagnetic particles in non-magnetic matrix [28]. The arrows attached to the circles represent random thermal fluctuation of magnetic moment. The red arrow connecting two magnetic particles (grey) represents path of a travelling conduction electron between particles. Top: Superparamagnetic particles (pictured as grey circles) with random orientation of magnetic moments. Bottom: Mixture of superparamagnetic (circles) and ferromagnetic (ellipsoid). The magnetic moment orientation of ferromagnetic particles is fixed mostly by the shape anisotropy.

Therefore, magnetoresistance is proportional to htw magnetic moment vectors of initial μ_1 and final μ_2 superparamagnetic particles that determine the path of the scattered electron [28]. It follows this equation:

$$MR(H) \propto -\langle \mu_1 \cdot \mu_2 \rangle = \langle \mu_1 \cdot n_H \rangle \langle \mu_2 \cdot n_H \rangle = -[M(H)]^2 = -\left(L \frac{\mu H}{kT} \right)^2 \quad (2.6)$$

where n_H is a unit vector in the direction of magnetic field. However, not every granular system has efficiently small particles that act superparamagnetically [33]. Systems with mixed superparamagnetic and ferromagnetic clusters are quite common. Giant magnetoresistance may contain three different contributions with the simultaneous presence of both type of clusters (Fig. 16):

- $\mathrm{GMR}_{\mathrm{SPM\text{-}SPM}}$ – ideal granular structure, scattering occurs on path: superparamagnetic region A → non-magnetic region → superparamagnetic region B

- GMR_{FM-FM} – ideal multi-layered film, scattering occurs on path: ferromagnetic region A → non-magnetic region → ferromagnetic region B
- s GMR_{SPM-FM}, GMR_{FM-SPM} – mixed magnetic structure, scattering occurs on path: ferromagnetic region A → non-magnetic region → superparamagnetic region B, or on the path superparamagnetic region A → non-magnetic region → ferromagnetic region B

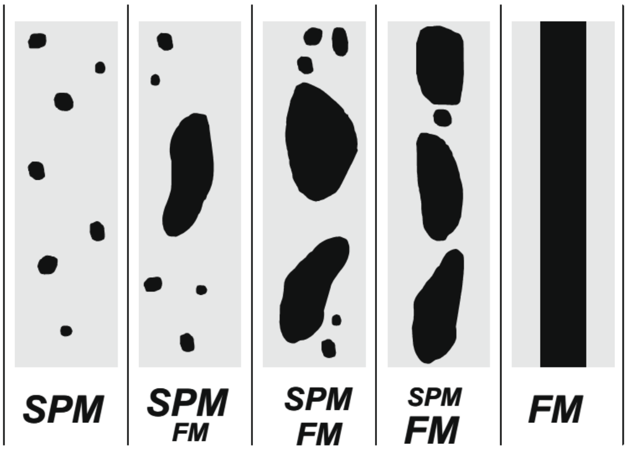

Fig. 16 Gradual transition from ideal granular alloys (left) to ideal magnetic/non-magnetic multilayers [22]

In conclusion, giant magnetoresistance in both multi-layered film or granular magnetic alloys arises from spin-dependent scattering that occurs on the electron path from magnetic region through non-magnetic region to second magnetic region. Magnetization of both magnetic regions must be oriented differently in the moment, when electron enters these regions.

2.3 Kondo effect

Kondo effect describes specific resistivity-temperature behaviour. Firstly, resistivity decreases with decreasing temperature as it is expected in metals, but then tends to increase as temperature decreases down to liquid helium temperature [20,23]. This phenomenon was discovered in 1934 [24] but satisfactory theoretical explanation was not provided until 1964 by Jun Kondo [23]. Kondo effect is found in diluted alloys containing a sufficiently small concentration of magnetic impurities [20,23,34]. Therefore, conducting electrons are affected by magnetic moments of impurity atoms. It resembles that magnetic impurities interact magnetically with conduction electrons [23]. Before Kondo's paper, resistivity phenomenon was considered as one-electron problem. Kondo proposed a solution by treating the back-scattering of electrons from magnetic impurities as many-body problem [34].

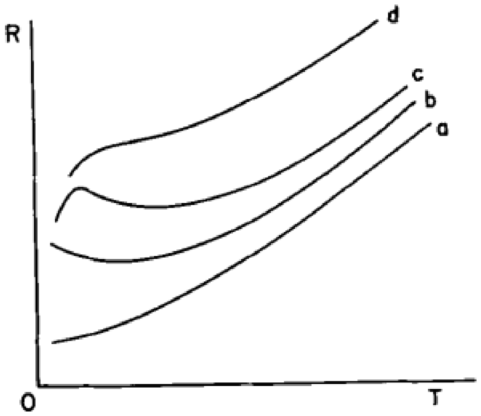

Fig. 17 Temperature dependence of resistance for various types of alloys [20]

a) non-magnetic typical alloy b) magnetic impurities (resistance minimum)
c) large fraction of magnetic impurities d) still larger fraction

The Kondo effect is greatly influenced by the concentration of magnetic impurities. This influence is observed in Fig. 17, where curve *b* shows behaviour with small portion of magnetic impurities. Curve *c* represents higher concentration of impurities and curve *d* depicts higher increase in concentration, which shifts expected

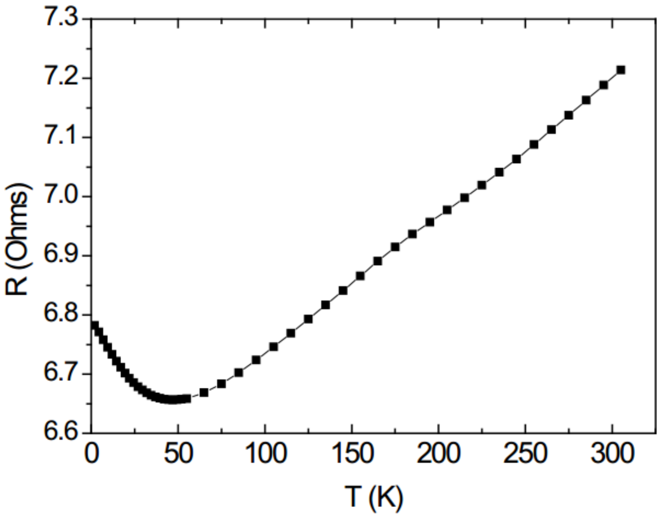

Fig. 18 Temperature dependence of resistivity (sample $Cu_{95}Co_5$)

minimum to higher temperatures and thus diminish minimum. Temperature dependence of resistance for purely non-magnetic alloys without impurities is displayed by curve a [34]. The typical dilution of magnetic alloys varies from 0.0005% [36] to 0.2% [20]. However, systems with 5 at. % of magnetic impurities with Kondo-like behaviour have been found as it is seen in Fig. 18 [37]. It is necessary to point out that also other physical phenomena may have contributed to resistance minimum (such an electron-electron interaction or scattering conduction electrons by structural two level system) [37].

2.3.1 Kondo effect principle

Temperature dependence of electrical resistivity including the Kondo effect is described by:

$$\rho(T) = \rho_0 + aT^2 + c_m ln\frac{\mu}{T} + bT^5 \qquad (2.3)$$

where ρ_0 is the residual resistance; aT^2 shows the contribution from the Fermi liquid properties; the term bT^5 arises from the lattice vibrations; a, b, and c_m are constants. Jun Kondo derived the third logarithmic term. Later calculations refined this result to produce a finite resistivity but retained the feature of a resistance minimum at a non-zero temperature. Kondo's calculation correctly describes resistance increase only above so-called Kondo temperature (K_T). Anderson introduced model which describes impurity interaction in 1961 [38]. Anderson's model predicts one electron level with energy ε_0 and in this case, electron tunnels quantum-mechanically from impurity and escape with its energy above Fermi level. However, this exchange process may end with flipped spin of conducting electron or even impurity. The spin exchange changes the energy spectrum of the system. If many of these processes are taken at the same time, new state is developed – the Kondo resonance, which scatters conductive electrons very effectively.

3 Material properties

Properties of studied materials determine their magnetic and structural order, thus explanation of materials properties is essential.

3.1 Heusler alloys

Currently, the group of alloys named Heusler alloys consist of more than 1500 alloys with different chemical composition [39-40]. Heusler alloys are divided into two main groups: full Heusler alloys with stoichiometric composition X_2YZ and half-Heusler alloys with stoichiometric composition XYZ. Heusler alloys are perspective materials with many possible applications, some of them have shape memory effect and superelasticity.

3.1.1 Historical background

Discovery of Heusler alloys is dated back to 1903 [41] when German chemist and mine engineer Fridrich Heusler found out that addition of element *Z* (with valence electrons from *s* and *p* layers) to the mixture of X and Y atoms, leads to ferromagnetic behaviour without any ferromagnetic element present in the sample [42]. The research on Heusler alloys was at quite slow pace during the first half of 20th century. Crystal structure of one of the first Heusler alloys was examined by X-ray diffraction in 1929, which led to discovery of so-called Heusler *fcc* superlattice (explained in Chapter 3.1.4)[43]. Bradley and Rogers [44] found out by X-ray measurements that ferromagnetism is not granted only by chemical composition, but mostly by short range ordering. New Heusler alloys compositions were found during 1950's and 1960's years, element *X* (*Cu*) was successfully replaced by some other noble metals (*Ag*, *Au*, *Pd*), nickel, or cobalt. Final samples also exhibit ferromagnetic behaviour despite paramagnetic or diamagnetic nature of its components.

Discovery of new, unknow Heusler alloys led to the extensive research on Heusler alloys, on theirs magnetic, structural and transport properties. Step by step, more interesting properties of Heusler alloys have been discovered. One of the first functional Heusler materials was alloy with composition *CuZnAl* having shape memory effect in 1976 [46]. The first highly spin-polarized Heusler alloy was discovered in 1983 having composition *NiMnSb* [47].

3.1.2 Structure of Heusler alloys

Felser and Perkins model was used to explain structural properties of Heusler alloys [39,40]. The model describes very well the structure of Heusler alloys and it stands mostly on electronegativity of each element in alloy. Atomic arrangement in the Heusler structure can be easily described through electronegativity. It should be mentioned, that term anions and cations do not refer to ionic nature of bonds in Heusler alloys, it only refers to differences in electronegativity of mentioned atoms and serves only to simplify the explanation.

Heusler alloys are not only characterized by stoichiometric composition, but mostly by well-defined crystal structure. Properties of Heusler alloy are strictly defined by correct atom arrangement. Small change in structure may lead to huge change of desired properties [47]. Two main types of Heusler alloys are recognized:

- Half-Heusler alloys have stoichiometric formula XYZ and crystalize mostly in cubic structure without central symmetry (space group No. 216, $F\bar{4}3m$, $C1_b$)
- Full-Heusler alloys have stoichiometric formula X_2YZ and crystalize mostly in cubic structure (space group No. 225 $Fm\bar{3}m$, $L2_1$) [39,40]

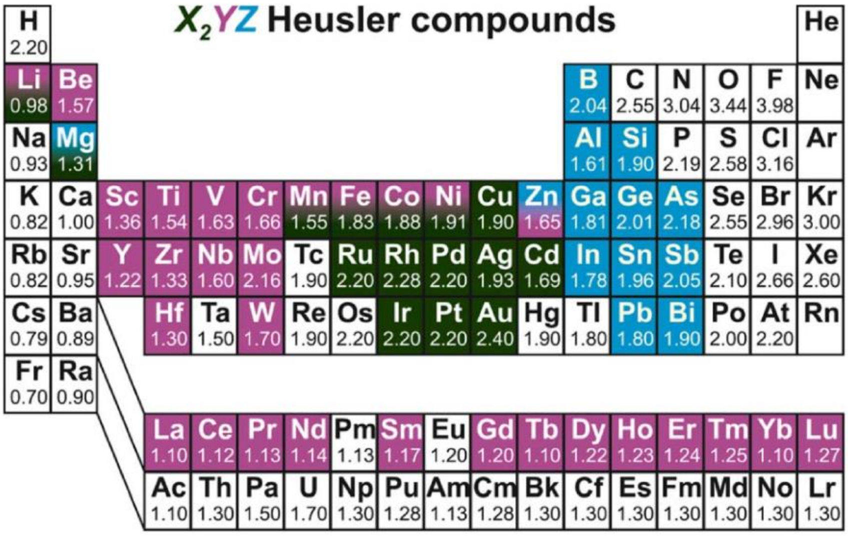

Fig. 19 Composition variations of all possible Heusler alloys [39].

Atomic arrangement is strongly correlated to the properties of Heusler alloys. Even small amount of impurities may alter atomic ordering and thus physical properties of material. Therefore, it is important to understand the rules of hte structural ordering in Heusler alloys. Elements that form Heusler alloys are viewed in Fig. 19, where dark green, purple, and blue colours represent possible *X*, *Y*, and *Z* variations of elements, respectively. Some of elements can occupy more positions (not simultaneously) in the atomic arrangement.

3.1.3 Half-Heusler alloys

Characteristic feature of half-Heusler alloys is occurrence of three interpenetrating fcc lattices, each of them are occupied by *X*, *Y* or *Z* atoms. Wyckoff position for these atoms are *4a* (0,0,0), *4b* (1/2,1/2,1/2), and *4c* (1/4,1/4,1/4), respectively. However, inequivalent atomic arrangements are possible, but if electronic calculation is made, then is important to know exact site arrangement, since it is crucial for the obtained electron structure.

Half-Heusler alloy may be viewed as a *ZnS*-sublattice with Wyckoff position *4a* and *4c* (see Fig. 20a). This sublattice is characterized by covalent bonding. On the other hand, *NaCl*-sublattice has strongly ionic character and occupies position 4a and 4b (see

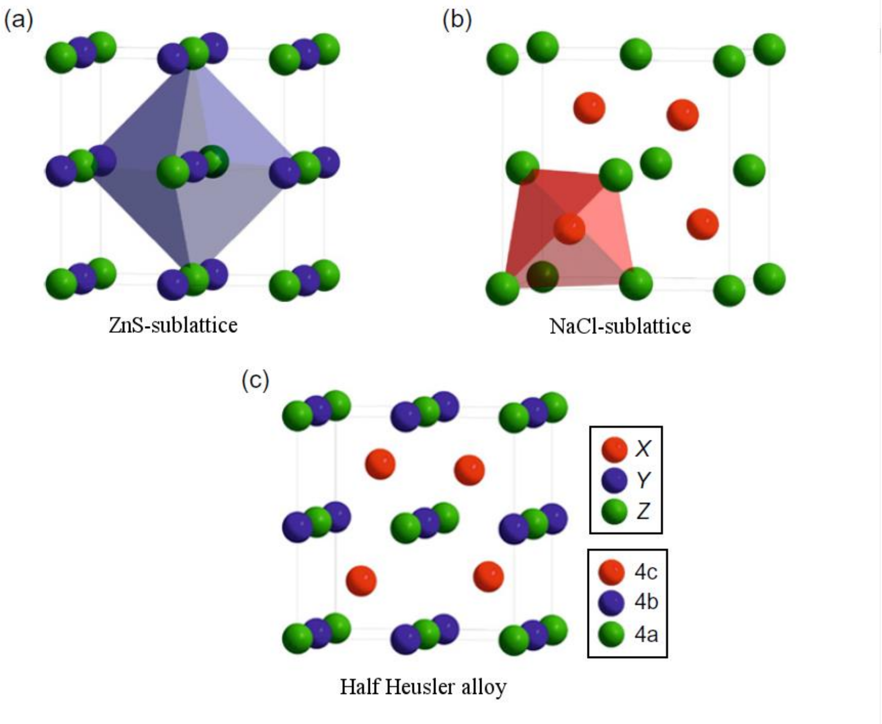

Fig. 20 Sublattices that build up Half-Heusler alloy [40].

Fig. 20b), that form between the most and the least electronegative elements. Therefore, mutual arrangement of atoms is dependent on chemical composition of alloy [39].

Half-Heusler lattice can be explained by its prototype alloy *MgAgAs* [39]. In this case, silver atom and anionic arsenic form the covalent *ZnS*-sublattice. Magnesium with silver form *NaCl*-sublattice. Consequently, arsenic is eightfold coordinated by divalent and monovalent atoms. However, majority of the other Half-Heusler alloys crystallize differently. Proper example for most of the Half-Heusler alloys can be *MgCuSb*, where copper and anionic antimony form ZnS-sublattice, while manganese cation forms *NaCl*-sublattice together with anionic antimony.

What type of atomic arrangement is preferred? It depends on atomic radius of each element and also on chemical properties of each element (e.g. electronegativity). If the difference in atomic radii of atoms is small (like in the case of magnesium and silver), then the anion is surrounded by eight cations and each cation by four anions. Some elements as manganese, silver and lithium have tendency to form covalent bonds. Therefore, occurrence of these elements in the alloy promote *ZnS*-sublattices (e.g. *LiAlSi*, *LiMgSb*, and aforementioned *MgAgAs*) Elements that promote metal bonds and there is significant difference in atomic radii of atoms are presented in the alloy *MgCuSb*. In this case, antimony anions have four copper cations in coordination sphere and copper cation are surrounded by four magnesium cations and four antimony anions. Magnesium is then surrounded by four magnesium cations. This type is characterized mostly by Heusler alloy, which contain two transition metals.

3.1.4 Full-Heusler alloys

Full-Heusler alloys with stoichiometric formula X_2YZ crystallize in cubic structure in space group No. 225, $Fm\bar{3}m$, with model Cu_2MnAl ($L2_1$). Atom *X* occupies Wyckoff position 8c (1/4,1/4,1/4) and *Y*, *Z* have Wyckoff position *4a* (0,0,0) and *4b* (1/2,1/2,1/2), respectively. Full Heusler alloys are formed by four interpenetrating sub-lattices, while two of them are equally occupied by *X*. Full Heusler alloys are formed by *NaCl* sub-lattices between the most and the least electronegative element. This sub-lattice has strong ionic character and it is formed in octahedral arrangement. On the other hand, all tetrahedral positions are occupied by atom *X*. Structure of full-Heusler alloy may be constructed by *ZnS*-sublattices similarly to half-Heusler alloys. However, there are twice as more *X* atoms, so all tetrahedral holes are filled.

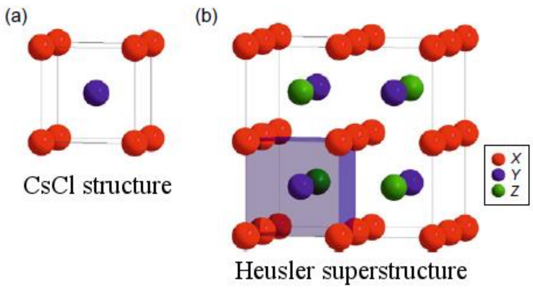

Fig. 21 Heusler superstructure [40]

Heusler CsCl superstructure is commonly used term in the scientific literature. It may be viewed by shifting crystal lattice by (1/4,1/4,1/4) considering previous space group $Fm\bar{3}m$. Superstructure is formed by combination of two $CsCl$ sub-lattices, where Y and Z atoms fill octahedral holes.

3.1.5 Disorders of Heusler alloys

Crystallization of Heusler alloys may result in many types of crystal disorders (Table 1). All disorders have similar atomic arrangement and carry typical properties of Heusler alloys. Disorders shown in the Table 2 marked with numbers 3 to 8 are derived from full-Heusler alloys. Disorders 3 to 8 have fulfilled octahedral holes similarly to full-Heusler alloys (Fig. 23).

Table 1 Types of Heusler alloys disorder with the help of Inorganic Crystal Structure Database (ICSD), Strukturberichte (SB) and Pearson databases.

No.	Lattice site occupation	Stoichiometric formula	Structure type			Space group
			ICSD	SB	Pearson	
1	$X=X,Y,Z$	X_2YZ	Cu_2MnAl	$L2_1$	$cF16$	$Fm\bar{3}m$
2	X,Y,Z	XYZ	$MgAgAs$	$C1_b$	$cF12$	$F\bar{4}3m$
3	X,X',Y,Z	$XX'YZ$	$LiMgPdSn$	Y	$cF16$	$F\bar{4}3m$
4	$X,X'=Y,Z$	XX'_2Z	$CuHg_2Ti$	X	$cF16$	$F\bar{4}3m$
5	$X=X'=Y,Z$	X_3Z	BiF_3	DO_3	$cF16$	$Fm\bar{3}m$
6	$X=X',Y=Z$	X_2Y_2	$CsCl$	$B2$	$cP2$	$Pm\bar{3}m$
7	$X=Y,X'=Z$	$X_2X'_2$	$NaTl$	$B32a$	$cF16$	$Fd\bar{3}m$
8	$X=X'=Y=Z$	X_4	W	$A2$	$cI2$	$Im\bar{3}m$

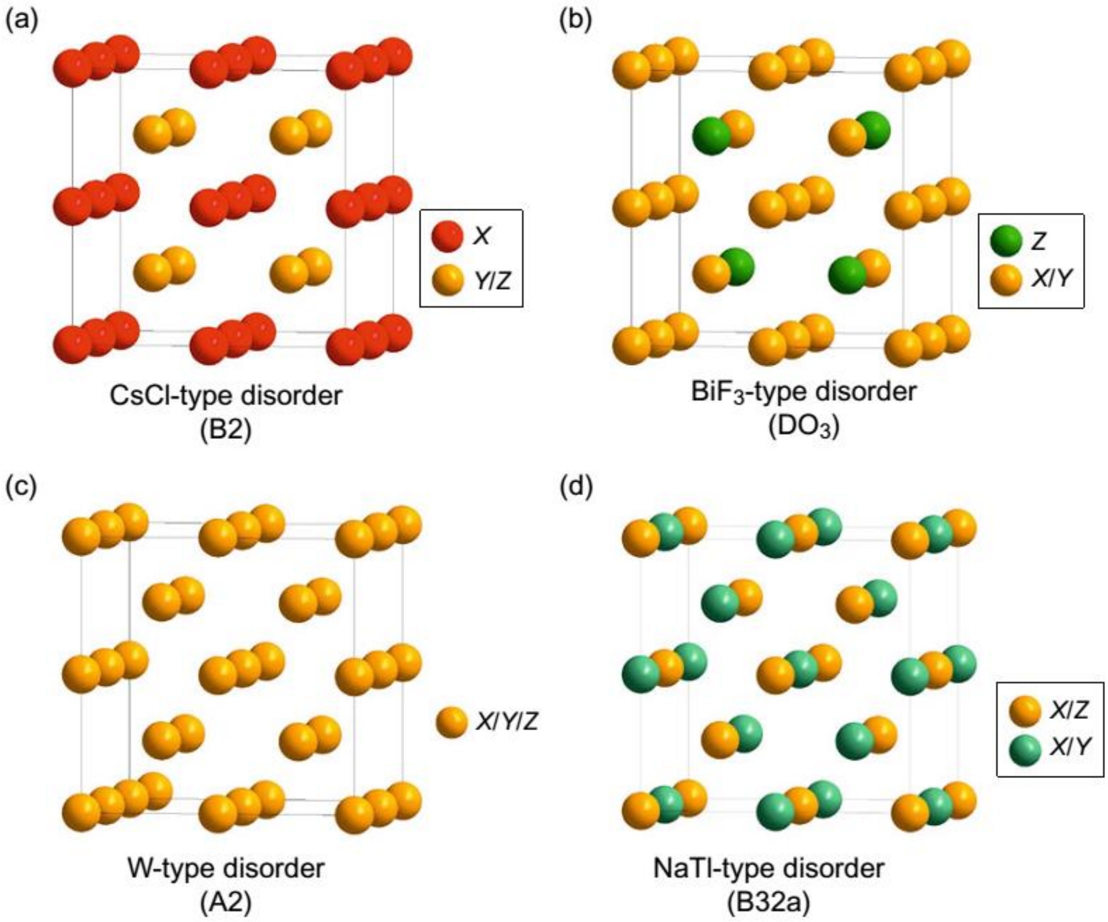

Fig. 22 Summary of the most common disorders in the Heusler alloys [40]

The most important disorder for this dissertation is *A2*, *B2*, and DO_3 cubic structure (Fig. 22). Disorder *A2* is formed when all positions are equally occupied by *X*, *Y*, or *Z* elements. *B2* disorder occurs when *Z* and *Y* elements are equally distributed, so

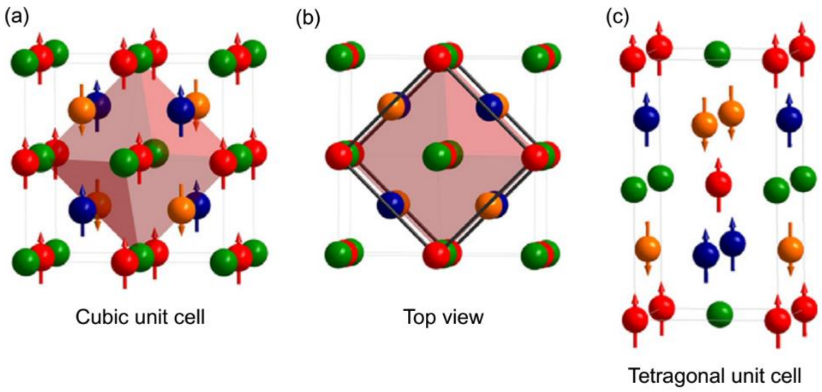

Fig. 23 Inverse and quaternary Heusler alloy [40]

Wyckoff positions *4a* and *4b* positions are even. With this disorder, CsCl-sublattices form the Heulser alloy. Disorded DO_3 is characterized by BiF_3 structure. It represents equal distribution of X and Y atoms. This leads to reduction of symmetry and results in $Pm\bar{3}m$ space group. In the case of Heusler alloys with shape memory effect, tetragonal structures may form the martensite phase. Cubic cell of austenite phase is then contracted along one axis (001) and extended along two others [40]. Martensite phase has to store large amount of stress during martensitic transformation. Strain energy loads are accommodated in martensitic microstructure in the form of crystallographic domains called variants. Typical martensite consists of mixture of variants. Two adjacent variants have common well-defined interface, called twin plane.

3.2 Materials for shape memory and superelasticity

Nowadays, there are many materials having shape memory effect. However, not many of them were implemented in commercial applications.

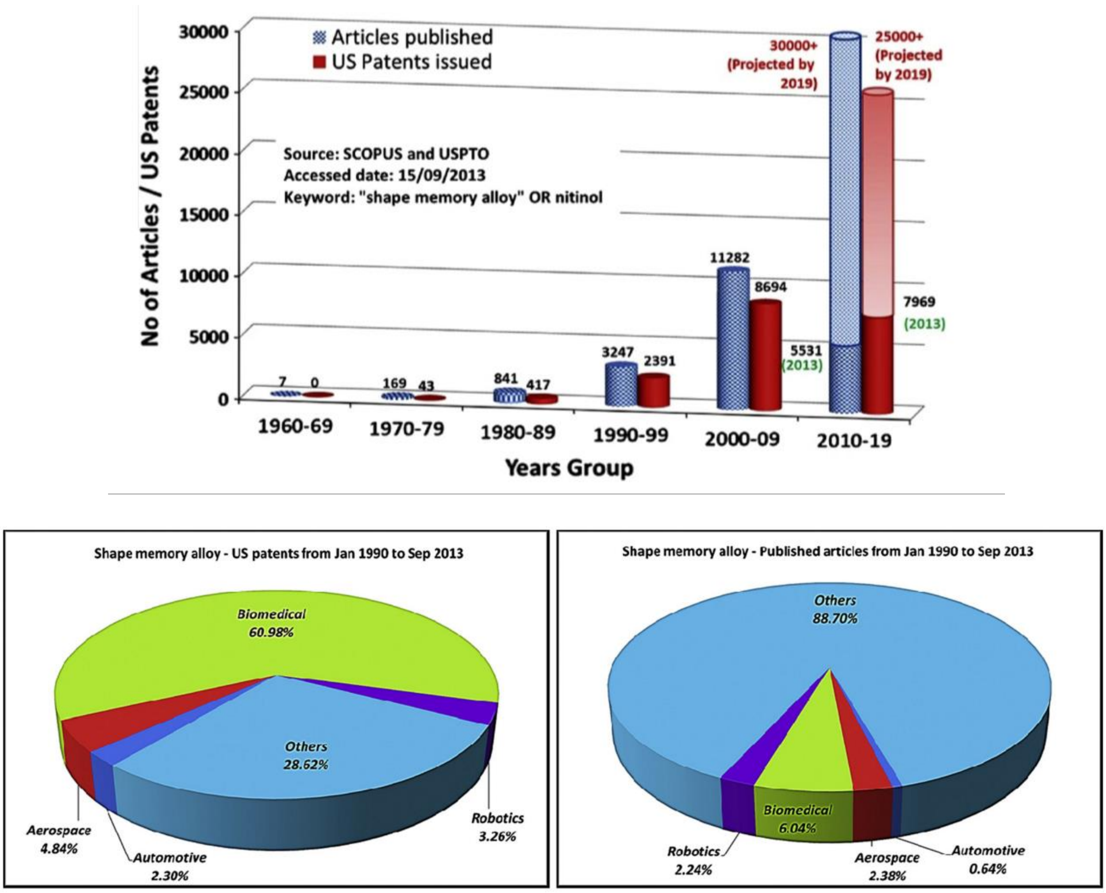

Fig. 24 Interest in shape memory alloys. Top panel: Evolution of shape memory alloy research, Bottom panels: scope of research as s number of patents (right) and articles (left) (2013) [3].

Without doubt, the most commercially used shape memory alloy is NiTi alloy called Nitinol (more than 90% all SMA applications are based on NiTi) [1]. Research on shape memory alloy has growing tendency, so it may be considered as a promising field of study (Fig. 24) [3].

Various alloys with shape memory effect have been discovered. Table 2 presents the widely-used shape memory alloys:

Table 2 The most used shape memory alloys

Category	Examples	
Room temperature	NiTi-based alloys	NiTi, NiTiCu, NiTiPd, NiTiFe, NiTiCo
	Cu-based alloys	CuZn, CuZnAl, CuAlNi, CuAlNiMn, CuSn
	Fe-based alloys	FePt, FeMnSi, FeNiC,
	Ag-based alloys	AgCd
	Au-based alloys	AuCd
	Co-based alloys	CoNiAl
High temperature	NiTi-based alloys	TiNiPd, TiNiPt, NiTiHf, NiTiZr
	Zr-based alloys	ZrRh, ZrCu, ZrCuNiCo
	Ti-based alloys	TiMo, TiNb, TiTa, TiAu
	Other alloys	UNb, TaRu, NbRu, FeMnSi
Magnetic	NiMn-based alloys	NiMnGa, NiMnAl, NiMnIn
	Fe-based	FePd, FePt,
	Others	CoNiGa, Dy, Tb, LaSrCuO

The main reason why designers choose shape memory alloys lies in their superior properties in high energy density and high actuation stress and strain [3]. However, low response time and low energy efficiency limit practical use of shape memory alloys. Current research trends in shape memory alloys are divided into three main groups:

Automotive and aerospace:

- self-healing and sensing structures/components (smart tyre and airbags),
- morphing capability for aerodymanic and aesthetic features,
- high temperature actuators,
- noise, vibration and harchness (NVH) dampers/isolators,

- rotary actuators,

Robotics:

- Micro and fast actuators
- Efficient, stable and accurate actuators
- Rotary actuator

Biomedical:

- Artificial muscles
- Shape memory implants
- Biocompatible (toxic free) shape memory alloys

3.2.1 Examples of shape memory alloys

NiTi alloys were developed in the military sector. Namely, in the Naval Ordnance Laboratory [50], when William Buehler was a supervisor in charge to select metal alloys for the nose of the water-air-water missiles (Subroc, UUM-44A) [1]. The aim of the research was to find suitable material for penetrating enemy defences, thus necessary properties were high impact resistance and high melting temperature. Some of the properties of NiTi were discovered by very peculiar way in 1959. The NiTi bar was carried to the workshop and during transport it fell on ground. It made a very loud dull sound. Buehler was intrigued by this sound and returned to the furnace and repeated the fall with the hot NiTi bar. Instead, they heard a very shrill sound. This led to the discovery of two different, coexistent, reversible phases in the NiTi bars at different temperatures. Different atomic arrangement of high and low temperature phase led to different levels of sound damping. However, shape memory effect and superelasticity have been discovered 3 years later when they tried to demonstrate a high resistance to fatigue in front of the commission. One of the committee member was not satisfied by their answers about origin of high resistance to fatigue, so he examined the sample himself. He took a piece of wire and folded it. Then he took his lighter and heated the wire. The wire returned to its original shape with a great astonishment of all present.

First commercially used application of NiTi shape memory alloy was “shrink to fit” pipe for F-14 Tomcat in 1969 and it was followed by practical use of NiTi superelastic alloy as orthodontic wire. The difference between using NiTi both as the superelastic and

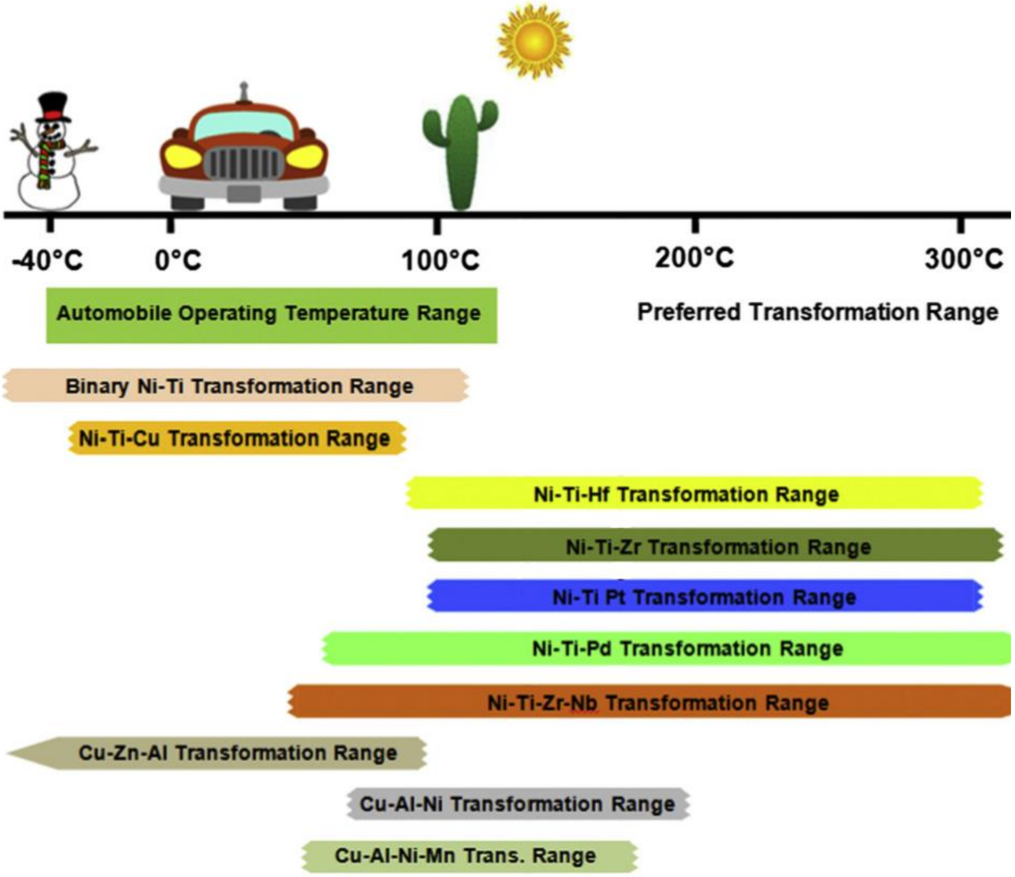

Fig. 25 Transformation temperature for various shape memory alloys [1]

as the shape memory alloy lies in the annealing. As-cast wire has superelastic properties and annealed material is used for its shape memory properties. The search for new shape memory materials does not stop despite superior mechanical properties of NiTi alloys. There is still great demand for materials with high or wide temperature range, and also discovery of the ferromagnetic shape memory alloys opens new applications, where actuator can serve also as a sensor.

NiTi alloys may be improved by adding elements like Pd, Pt, Zr, Hf, and Nb to shift martensitic transformation to higher temperatures. These elements also affect strain, its reversibility and thermal hysteresis so it is advantageous to choose proper composition for each application (Fig. 25).

3.2.2 Examples of ferromagnetic shape memory alloys

The ferromagnetic shape memory alloys exhibit large strains in a presence of external magnetic field (Fig. 26) [51]. Because of that, they are considered to be smart materials. Basic requirements for the magnetic shape memory alloy are: the presence of ferromagnetic phases in the temperature range of martensitic transformation and also the magnetic anisotropy energy must be higher than the energy required to move a twin boundary [1]. Other similar phenomenon that deals with change of dimensions under magnetic field is magnetostriction, but it does not meet the aforementioned requirements. However, even the materials with exceptionally large magnetostriction, like alloy Tb-Dy-Fe (terfenol D), show strains only up to 0.1% [52,53]. On the other side, ferromagnetic shape memory alloy may produce magnetically induced strain up to 10% contrary to the magnetostriction materials. The most studied ferromagnetic shape memory alloy is Ni-Mn-Ga, others also well-known are: Co-Ni-Ga, Fe-Pd, La-Sr-Cu-O4, Fe-Pt, and Cu-Al-Ni.

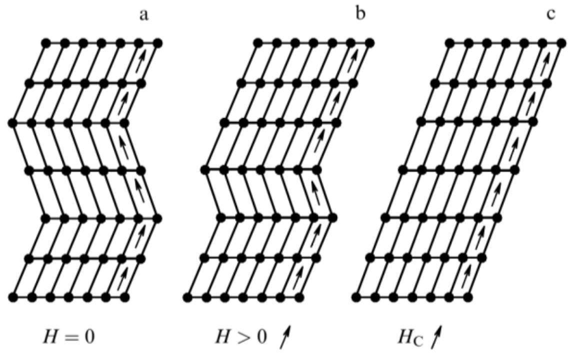

Fig. 26 Martensite variant reorientation after application of magnetic field [51]

The phenomenon of magnetically induced strain has been observed for the first time by Ullako et al. [54] in Ni-Mn-Ga. The achieved strain was 0.2% in a magnetic field 8 kOe and martensitic start temperature 276K. Following experiment by Tickle et al. [55] achieved 1.3 % irreversible strain and 0.5 % reversible cyclic strain in magnetic field of 10 kOe for composition $Ni_{51.3}Mn_{24}Ga_{24.7}$. Much later, considerable strain 6 % was realized by Heczko [56] and Murray [57] in Ni-Mn-Ga single crystals with non-stoichiometric compositions. The ferromagnetic shape memory effect is well studied in Ni-Mn-Ga alloys on various stoichiometric compositions and it revealed strong correlation between chemical composition and reversible strain (Table 3). It was found that slight excess of manganese (from 28% to 31%) provides largest strains. For example, difference between 25.4% and 28.5% at. percent of manganese leads to massive difference 0.4% and 6% strain, respectively.

Recently, progress has been made on optimization of stoichiometry [63,64,65] of Ni-Mn-Ga and improvements of production capabilities [65,66,67] made it possible to prepare large Ni-Mn-Ga single crystals with perfect magneto-mechanical properties suitable for applications. Consequently, some prototypes of ferromagnetic shape memory actuators have been proposed [68,69].

Table 3 Comparison of Ni-Mn-Ga compositions

Chemical composition (at. %)	Martensitic start transformation temperature M_s (K)	Magnetically induced strain (%)	Reference
$Ni_{52}Mn_{22}Ga_{25.8}$	289	0.3	[58]
$Ni_{48}Mn_{31}Ga_{21}$	301	5.1	[56,59]
$Ni_{49.8}Mn_{28.5}Ga_{21.7}$	318	6.0	[57]
$Ni_{48.2}Mn_{30.8}Ga_{21}$	307	7.3	[60]
$Ni_{48.1}Mn_{29.4}Ga_{22.5}$	270	0.3	[60]
$Ni_{49.5}Mn_{25.4}Ga_{25.1}$	289	0.4	[61]
$Ni_{52}Mn_{23}Ga_{32}$	310	0.27	[62]

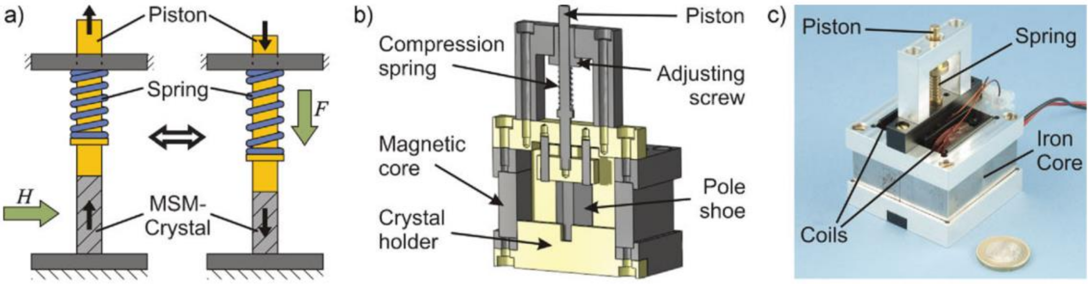

Fig. 27 One of Ni-Mn-Ga prototype of spring actuator [68]

It is possible to exchange the Ga in Ni-Mn-Ga for Al to get ordered high temperature phase with magnetic shape memory. Ni-Mn-Al crystalizes in B2 structure after annealing above 1000°C (it crystalizes in $L2_1$ after ageing at 350-400°C). Shape memory effect in Fe-Pd alloys was discovered in 1980 [70]. They are know to have small hysteresis but the highest temperature where martensitic transformation begins approx. at

273 K and it tends to decrease with incresing content of Pd [71], Addition of Ni or Co also lowers start of martensitic transformation.

The highest magnetically induced cycling strain was 0.6% measured in the single crystals [72]. 3% strain was achieved in single crystal only once, during the first turn of magnetic field change and then the reversible strain the was only 0.1% during other cycles [73].

3.3 GMR materials

Since the discovery of the giant magnetoresistance effect in magnetic multilayered films [15,16] and later in granular materials [26,27] numerous studies on a variety of systems have been reported [15-27,28,79,86]. Discovery of GMR effect was preceded by development of thin film technologies in the 1970 - 1980s as an evaporation, sputtering and molecular beam epitaxy [70]. The biggest challenge for materials technology was to prepare very thin defect-free layers suitable for application of giant magnetoresistance. For example, if layer thickness is nanometer thick, it has only 5 atomic layers [28]. One-nanometer layers are widely used in the materials utilizing giant magnetoresistance [15,16].

3.3.1 Thin films

There are many mulitlayered thins films with different compositions that have been reported to exhibit giant magnetoresistance (e. g. Co–Cu/Cu, Ni–Cu/Cu, Co–Ag/Ag, Co–Au/Au, Co–Ru/Ru, Co–Ni–Cu/Cu, Fe–Ni–Cu/Cu, Fe–Co–Cu/Cu, Co(–Cu)–Zn/Cu, Fe–Co–Ni–Cu/Cu) [28]. Early research on thin films was focused on optimal microstructural (e.g. interface roughness) and magnetic properties. These properties are important for achieving the maximum magnetoresistance change [sensors] to the level that could be used for sensor application. Most of the papers on the GMR on thin film were dealing with Co-Cu/Cu multilayers. The reason for extended study of cobalt and copper materials lies in the highest measured giant magnetoresistance up to 50% in sputtered thin films [75,76,77] (electrodeposited thin films only up to 20%).

New type of hard-disk read-heads based on giant magnetoresistance is the first industrial application of magnetoresistive thin films (Fig. 28). It was developed in the 1997 [78]. Giant magnetoresistance based sensor on read-head is used to detect the magnetization of the bits on the recording medium. New read-heads have better sensitivity so bit size could be reduced (so storage density increased).

GMR thin films are also used in automotive industry where they work as sensors of rotational speed, angle, and position [80-83]. Also, biomedicine sensors have been developed [84] for measurements of specific molecules detection. This type of sensors was presented in prototypes of “lab on a chip” device with 32 GMR sensors.

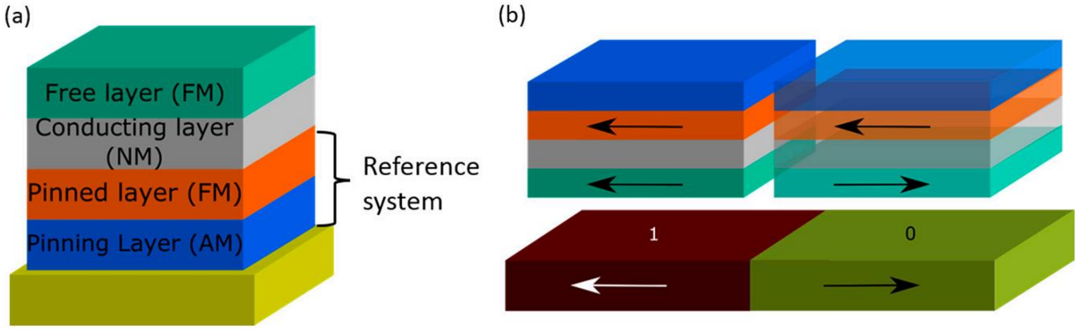

Fig. 28 A) schematic setup of giant magnetoresistance sensor used in hard-disk read-head. B) when sensor moves above bits, magnetization of free layer in sensor is changed, thus increasing or decreasing the resistance [85]

3.3.2 Granular GMR materials

Granular or inhomogeneous materials, which are typically formed by immiscible elements (Co, Fe, Ni)-(Cu, Pt, Au, Ag), have attracted considerable attention since the beginning of 1990s [26,27, 79,86]. The main interest in granular materials is related to a substantial economic difference between the preparation cost of a multilayered thin films and granular materials: multilayered materials must be fabricated with multi-source molecular beam epitaxy and sputtering. On the other hand, granular materials can be fabricated with much simpler technology, like rapid quenching or ball milling [86,87]. The main interest in granular materials is related to the GMR effect [87]. The origin of the GMR effect in granular materials has been attributed to spin-dependent scattering of conduction electrons within magnetic granules, as well as at interfaces between magnetic granules and nonmagnetic matrix [26,27,79,86]. Granular structure can be usually obtained after the recrystallization of the metastable alloys prepared from immiscible elements (typically Co-Cu or Co-Ag) through the annealing. Formation of such structure is related to the phase diagram of the immiscible elements. Typically, the phase diagram of immiscible alloys at room temperature presents quite low solubility of the ferromagnetic elements in the metallic matrix. Consequently, after rapid quenching from the melt the obtained alloys usually form a supersaturated solid solution at room temperature [26,27,86,88]. Annealing at adequate conditions allows formation of aforementioned granular structure consisting of fine magnetic precipitations within the non-magnetic conductive metallic matrix [26,27,86]. It is possible to prepare a variety of materials with amorphous, nanocrystalline or granular structures by using rapid quenching from the melt [86,89-91]. Highest interest in rapidly quenched materials is related to the soft magnetic properties of amorphous and nanocrystalline ferromagnetic alloys [91,92]. Additionally, rapid quenching technique can be successfully employed for fast preparation of metastable and granular materials [86,88].

It is worth mentioning that the granular structure is not the unique origin of the GMR effect in materials prepared from immiscible elements: the alternative interpretation of GMR effect involves Co particles embedded in Cu matrix [90], Co clusters within a Cu matrix [93] or homogeneous spinodal decomposition characterized by long parallel Co-excess stripes [94].

One of the routes allowing miniaturization of rapidly quenching materials is the utilization of novel techniques for preparation of composite materials. Thus, Taylor-Ulitovsky technique involving simultaneous rapid quenching from the melt of thin metallic microwire coated by glass gained considerable attention [88,95].

4 Experimental part

Measurements of magnetic, structural and physical properties have been carried out at Univerzity of Pavol Jozef Šarárik in Košice (UPJŠ), at Institute of experimental physics of Slovak academy of Sciences (SAV), at University of Basque Country (UPV/EHU) in San Sebastian. Experimental work consists of sample preparation by rapid quenching in form of ribbons and glass-coated microwires. Each of the sample forms have their own specific properties, advantages and disadvantages and they will be discussed here.

4.1 Preparation of material

Rapid quenching methods offer many advantages:

- solubility of each element is increased, often by orders
- allows to form supersaturated solution
- possibility of formation of non-equilibrium or metastable phases
- decrease the number or volume of segregated phases
- possibility of creation amorphous structure in classically crystalline materials

however, many of these advantages require specific conditions and many times it is impossible to achieve required properties. Right now, there exist many methods offering rapid quenching. For this work, we have used following techniques:

- Melt-spinning method
- Taylor-ulitovsky technique

4.1.1 Arc Melting method

The arc melting method has been used to produce master alloys (ingots) for further processing with rapid quenching method. This step of preparation is necessary mostly because of homogenization step in the fabrication protocol. Direct use of pure elements in rapid quenching method does not provide sufficient homogeneity. Therefore, arc melting method is used to produce homogenous sample, which can be directly used in advanced rapid quenching techniques in the Laboratory of magnetic, transport, and optic properties at Pavol Jozef Šafárik University Arc Furnace, *Compact Arc Melter MAM-1* (

Fig. 29). Arc melter is capable of achieving temperature up to 3500°C and is ready to prepare ingots from 5 to 20 grams. Device has two electrodes: tungsten and copper. Copper electrode serves as a stand with moulds and also serves for cooling (with built-in water capillary). Arc melting method requires argon atmosphere to ionize atmosphere as it is necessary in order to prevent the formation of oxides [96]. Following procedure was used:

Precisely weighed (on analytical balance) amount of each element is placed on copper crucible base plate. In the next step, chamber is hermetically closed and vacuum is achieved. Usually, previous step is few times repeated to ensure pure argon atmosphere. Argon pressure is set to 0.7 bar. Applying voltage on the tungsten electrode form the arc between material and electrode. Current flow heats and melts the elements together. Consequently, sample has been re-melted three times to achieve sufficient homogeneity.

Fig. 29 Arc Melter MAM 1 with closed eye cover protection

4.1.2 Melt-spinning method

Melt-spinning is one of the most used rapid quenching method. *Edmund Bühler Melt Spinner SC* is located in the Laboratory of magnetic, transport, and optic properties at Pavol Jozef Šafárik University. Cooling rates on copper wheel can achieve values up to 10^{-6} K.s^{-1} [98,99].

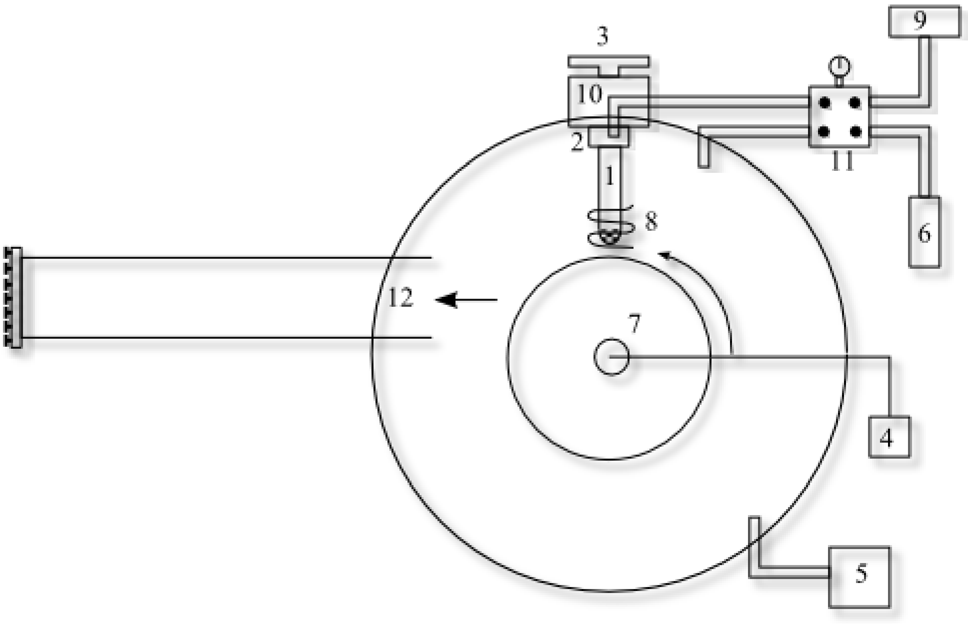

Fig. 30 Scheme of Melt-spinning method

1) crucible with master alloy 2) crucible thread 3) crucible gap regulation 4) wheel rotation velocity regulation 5) vacuum pumps 6) helium canister 7) rotating copper wheel 8) induction coil 9) pressure chamber 10) pyrometer in holder 11) valve plate 12) catching tube for casted ribbons

Melt-spinning procedure starts with mounting a crucible (1) into thread (2). It is necessary to adjust gap between the wheel and crucible (3). Afterwards, the chamber is closed and the sufficient vacuum rate is reached. Second diffusion vacuum pump is used to achieve a vacuum up to $5x10^{-5}$ mbar. However, high vacuum is not an efficient way to prepare rapid quenched ribbons. Helium atmosphere is required for heat transfer and for preventing of oxides formation. The alloy is melted using high frequency induction coil (8). Flow of molten metal through a hole in crucible is restricted by high viscosity of molten metal. When pressure chamber (9) is opened, alloy is forced through the tube's hole onto copper wheel. Tangential velocity of the cold copper wheel shoots the casted ribbon into catching tube (12) cooling it during the flight.

Following parameters of melt-spinning method are adjustable:

- gap between crucible,
- tangential velocity of copper wheel,
- overpressure value,
- temperature of the molten metal.

These parameters determine possibility of ribbon's production and its properties.

4.1.3 Taylor-Ulitovsky technique

Glass coated microwires have been prepared at UPV/EHU and at RV magnetics in Košice. Main advantages of this method are:

- reproducibility and scalability of microwires with same properties in mass production,
- large variation of parameters (geometric or physical),
- opportunity to produce long pieces of microwire (up to 10km),
- possibility to control and adjust geometrical parameters (diameter of metallic core or diameter of glass coating).

Following procedure has been used to produce microwires: a small amount of sample is placed into closed glass tube (1). Subsequently, it is necessary to connect glass

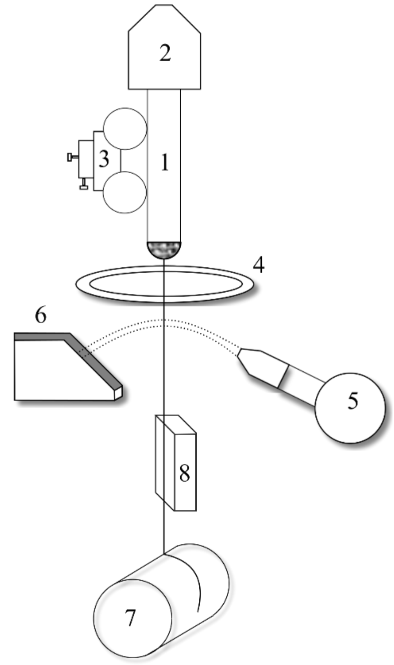

Fig. 31 Microwire production

1) glass tube with master alloy 2) vacuum unit 3) feeding mechanism 4) AC inductor 5) crystallizer 6) water catcher 7) bobbin 8) antenna

tube into exhaust system (2) to keep the sample up. Glass feeding mechanism (3) is used to ensure constant supply of glass. High frequency AC inductor (4) is used to melt alloy. Alloy is relocated to the area of inductor by means of accelerated glass tube feeding (speed 130mm/min). Then it is necessary to wait until molten alloy softens glass. When softened glass and melt are stable a microwire can be withdrawn. Touching the glass + melt tube with a glass stick will force melt to get into a glass due to the capillary effect. First, microwire drawing is realized by hands, then it is possible to catch it on winding mechanism and wrap it around a bobbin cap (7). Antenna (8) provides information on microwire homogeneity during the preparation. Electrical resistance is important for determining a thickness of the metallic core. Second parameter is capacitance, which is used to estimate thickness of the glass-coating. After stabilization of the process, microwire can be wrapped around bobbin body. Cooling is provided by water jet flowing from crystallizer (5) to bath (6) with 60-litter canister.

The biggest challenge is to prepare the microwire with chemical composition that can react with atmosphere or with the glass. In general, it is problematic to prepare microwire composed of metals like titanium, chromium, molybdenum, tungsten, niobium, aluminium, sodium, and the most of the rare earth metals. For example, aluminium reacts with a glass forming aluminium oxide.

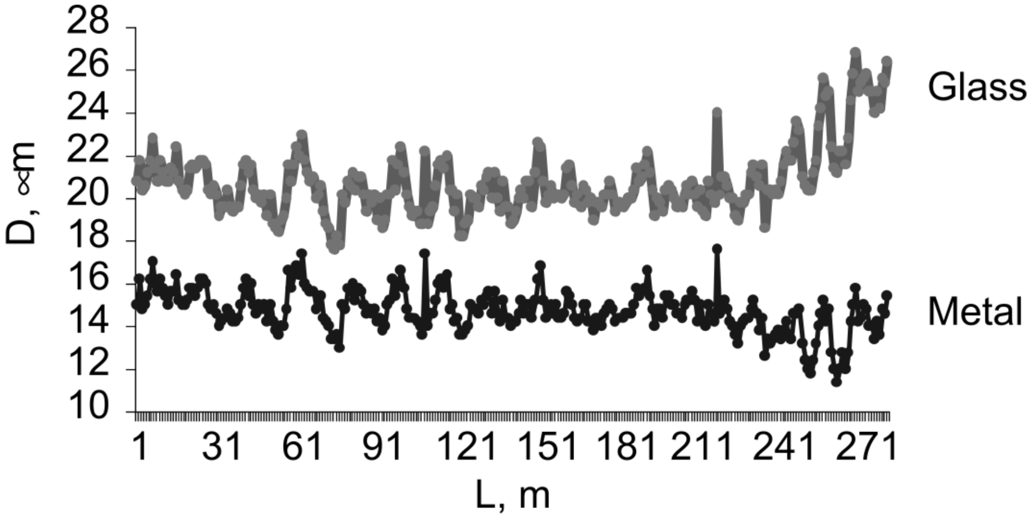

Fig. 32 Variation of total diameter (glass) and metal core (metal) diameter

Typical geometrical parameters of metallic core thickness vary between 0.8 – 30 μm and glass thickness varies between 2 – 15 μm. Thickness of the metallic core and glass coating slightly varies along the microwire (Fig. 32). Moreover, glass coating applies internal stresses on the metallic core. This happens mostly due to the differences between thermal expansion coefficient.

4.2 Structural study

Structural order determines all physical properties. Therefore, structural measurements have been performed first.

4.2.1 Electron microscopy

Structure of both types of materials have been studied using electron microscopy. Superelastic alloy have been studied by scanning electron microscope (SEM) at UPJŠ in Košice and GMR materials have been studied using two high angle annular dark field transmission electron microscopes (HAADF-STEM) at UPV/EHU, one in Leiola and the other one in San Sebastián.

Electron microscopy is in many ways similar to light microscopy but instead of visible light wave properties of electrons are used. Electrons follow analogous rules like light in geometrical optics [100]. In general, all electron microscopes have similar structure, which consists of electron beam, magnetic lenses, sample holder and detector (Fig. 33). Electron beam is produced by electron gun. Magnetic lenses direct electron beam on the sample and they reflect towards the detector together with other types of radiation.

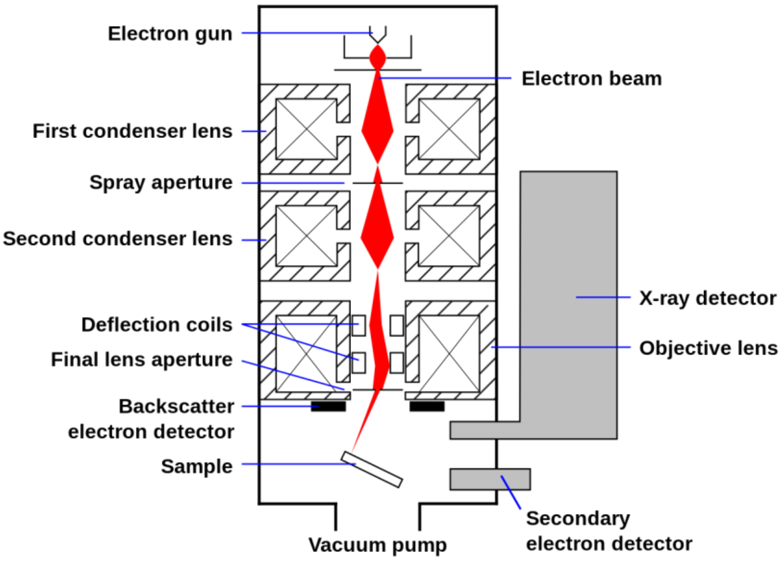

Fig. 33 Structure of scanning electron microscope

Interaction of electron beam with a sample produces various signals as visible light, electrons and X-ray photons (see Fig. 34). Electrons emitted by cathode interact with sample by inelastic and elastic scattering. Elastic scattering progresses with almost no energy loss and electrons are scattered back after they hit electron core, so-called backscattered electrons. Inelastic scattering proceeds with energy transfer between electrons from primary beam, and free or shell electrons. These electrons, so-called secondary electrons, are then emitted from atoms and detected. These two types of

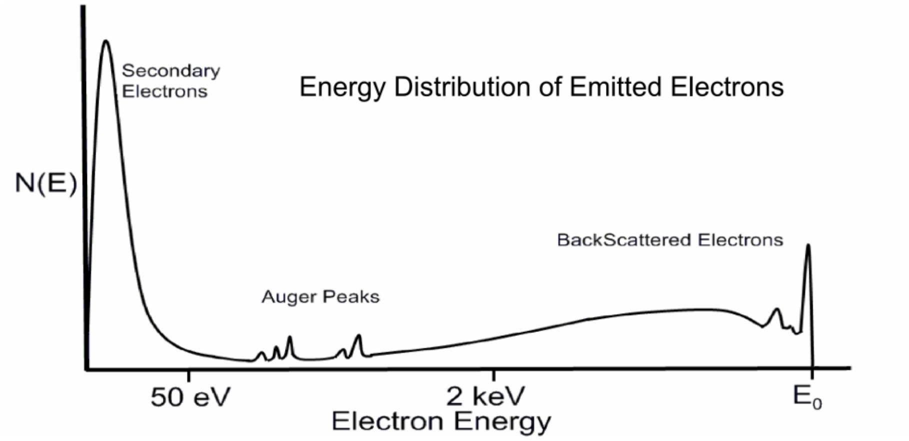

Fig. 35 Energy distribution of emitted electrons

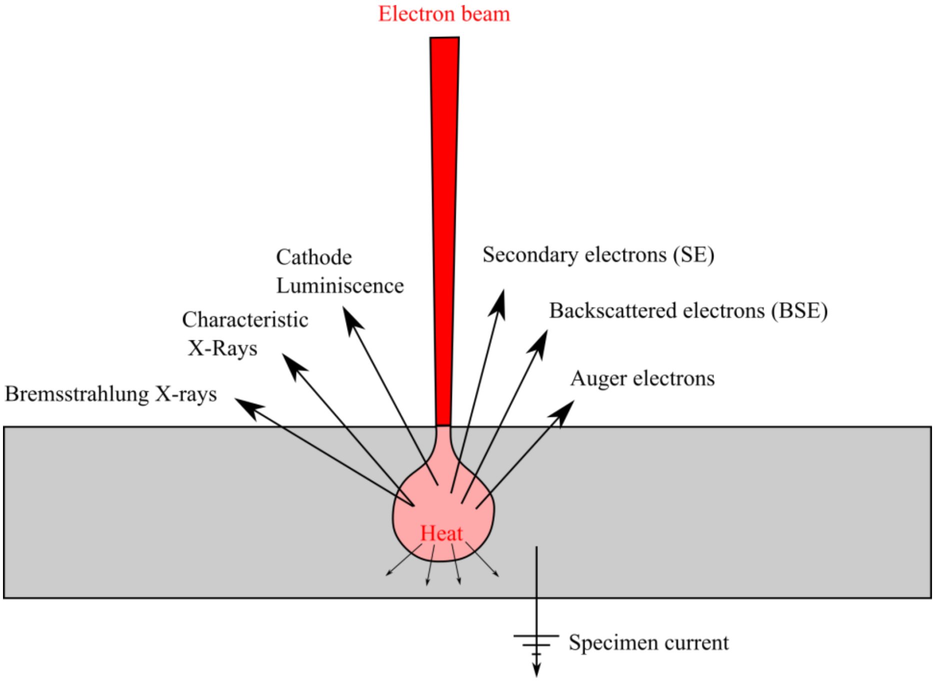

Fig. 34 Interaction of incident beam with sample

electron (secondary and backscattered) can be easily distinguished by comparing their energies to energy of electron beam. Energy of backscattered electrons is slightly smaller, but energy of secondary electrons is lower by orders (Fig. 35).

Secondary electrons belonged to the electron shell, thus they should be replaced by electron from higher energy levels. This emits X-Rays with specific energies for each element. Energy dispersive X-ray spectroscopy (EDX/EDS) uses this property to characterize chemical composition of sample. It is possible to obtain quantitative chemical composition by comparing intensities of each EDX signals. EDX analysis has been widely used in this work to confirm nominal composition of sample. However, this method has its limitation and it is difficult to have high precision when the surface of observed sample is rough. One needs to count with ±2% derivation from real composition.

4.3 X-Ray diffraction spectroscopy

X-Ray diffraction is used to determine crystal structure of material, thus symmetry and properties of its lattice. In crystal, atomic ordering structure (crystal lattice) repeatedly occurs in space. Therefore, homogenous material may be created by repeating its crystal lattices infinitely so it generates perfect symmetry. Each arbitrarily selected point in crystal structure has given position to other random point given by lattice vector R_n:

$$R_n = n_1 a + n_2 b + n_3 c \tag{4.1}$$

where n_1, n_2 a n_3 are integers and a, b, c are lattice parameters [102].

X-Ray is electromagnetic radiation with wavelength λ 0,01–10 nm. It is produced by impact of high energy particles with matter. X-rays then collides with atoms in the sample. Atoms cores are without any change after impact, but electrons oscillate with the same frequency and becomes the source of secondary radiation with the same energy (wavelength). This type of interaction is called elastic (coherent) scattering. Atoms in crystals diffract the radiation after impact. However, most of the waves cancel out each other through destructive interference. Only few waves that meet the conditions of Braag’s law add constructively:

$$n\lambda = 2d_{hkl}\sin(\theta) \tag{4.2}$$

where, *n* is any integer, λ represents the wavelength of the radiation, *d* is the spacing between the atoms planes, and θ is the incident angle. These reflections on diffraction patter are used to determine the crystal structure.

4.4 Magnetic measurements

Magnetic measurements have been used to provide following information:

1. Hysteresis loops and virgin curves have been taken at various temperatures to determine easy axis of magnetization and saturated magnetization of different phases in the sample.
2. Temperature dependences of magnetization have been taken to determine structural transformation.
3. Magnetic permeability dependence on strain has been evaluated to identify sensing properties of the superelastic sample.
4. Resistivity dependences on magnetic field have been measured at various temperatures to characterize the magnetoresistance phenomena of microwire.
5. Resistivity dependences on temperature have been measured at various magnetic fields to observe Kondo-like behaviour.

Vibration sample magnetometer has been used to obtain information from hysteresis loops and temperature dependence of magnetic field. These apertures are located on both laboratories at UPJŠ and UPV/EHU in PPMS and MPMS by Quantum Design.

4.4.1 Vibrating sample magnetometry

Vibrating sample magnetometer (VSM) belongs to the best instruments to measure magnetic properties and it is widely used since 1959 [103]. The method is based on vibrations of magnetic sample in uniform magnetic field, which induces voltage in pickup coils. Picked up voltage is then proportional to magnetic moment of sample. In our case, small piece of ribbon of the rectangular shape has been used. Sample should be mounted on non-magnetic holder which vibrates in the presence of pickup coils. Oscillating sample is magnetized by the uniform magnetic field; thus, it induces magnetic field in the pickup coils, which's magnitude is proportional to magnetic moment of the sample. The direction of magnetic field has been perpendicular to the sample's axis in all measurements.

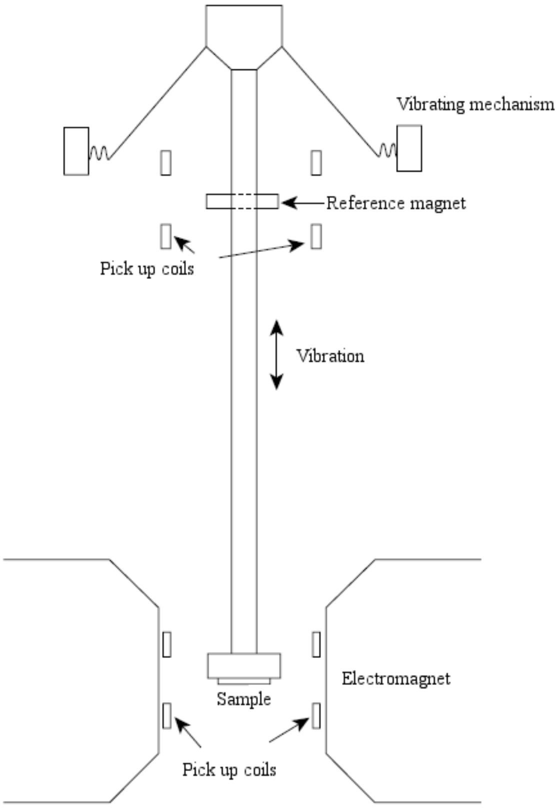

Fig. 36 Scheme of vibrating sample magnetometer

4.5 Measurements of electrical properties

The most used technique for measuring electrical resistance is four-point probe set on studied materials [28]. Four-point probe measurements have an advantage over two-points probes. Two contacts are used to measure voltage and other two to apply the current. Thus, four probe method is more precise because it is not measuring the resistance of connecting wires. This method is widely used in the measuring of electrical resistance wires. However, measuring magnetoresistance in microwires is trickier due to glass coating. Microwire must have glass removed from the both sides.

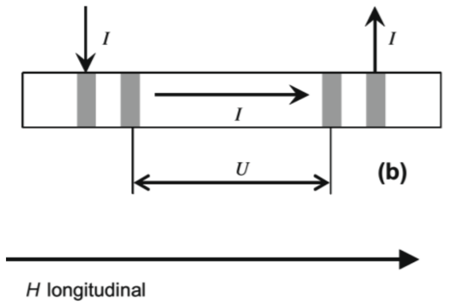

Fig. 37 Strip geometry used to measure GMR measurement with arrangements of contacts [28]

4.6 Superelasticity measurements

Measurements of strain have been carried out on the “lab-made” setup and also on the TA instruments Q800 DMA at Technical University in Košice.

DMA is capable of measuring in temperature range from -180°C to 600°C. Device is very precious with stress resolution 0.01 mN and strain resolution 1 nm [104]. Thus,

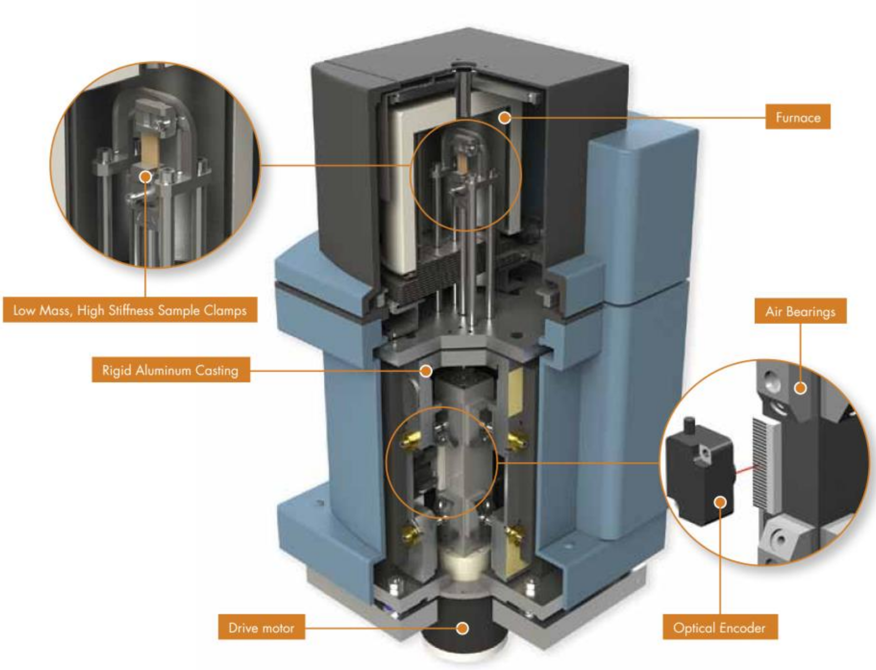

Fig. 38 Scheme of DMA analysis [104]

DMA is especially good device for precious measurements of stress-strain curves at different temperatures. However, width and thickness have to be known before measurement in order to count stress in MPa. During the measurement, the sample is placed in tension between a fixed a moveable clamp. These clamps are suitable for both ribbons and microwires.

However, it is not possible to measure magnetic properties change during phase transition. For this reason, “lab made” setup has been developed. Force gauge FG20KG-RS23 has been used to measure the stress. Strain was measured using Digimatic Indicator ID-XC 543-390B. For sample straining Lustron Test Stand FS-1001 was used. The magnetic permeability was measured by Hameg HM8118 LCR-Bridge with test frequency of 100 kHz. All the devices have been working together as pictures in Fig. 39. Handle of test stand (1) is used to apply stress on the sample. Sample holder (3) is located on the force gauge (2). Sample is held by a sand paper and glued. There are markings in the sample holder so it is possible to check possible displacement after measurement.

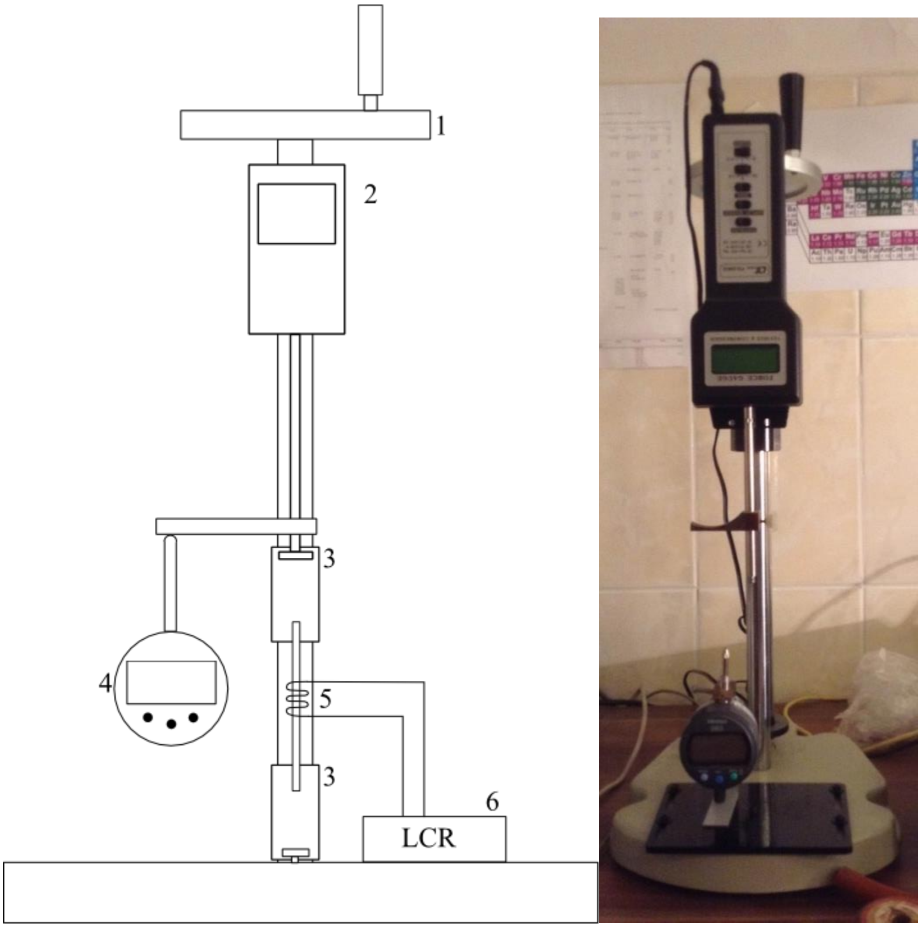

Fig. 39 Lab made setup for measuring stress-strain curves

Applied stress causes strain that is measured by digital indicator (4). Coil around the middle of ribbon is used to measure induction by the LCR meter (5).

5 Results and Discussion

This part of work deals with the experimental results of selected superelastic and magnetoresistive materials. Samples in the form of ribbons, and microwires have been prepared by suction-casting, melt-spinning, and by Taylor-Ulitovsky method, respectively. Following compositions have been prepared:

Table 4 Geometrical parameters of prepared samples

Ribbon	Application	Width	Thickness	Length*
$Co_{37}Ni_{34}Al_{29}$	Superelastic	1 mm	25-45 μm	1-10 cm
$Co_{49}Ni_{21}Ga_{30}$	Superelastic	1-1,5 mm	10-30 μm	1 cm
$Fe_{43.5}Mn_{34}Al_{15}Ni_{7.5}$	Superelastic	1-3mm	40 μm	approx. 3 m
Microwire	Application	Diameter core	Diameter total	
$Co_{51}Cr_{27}Ga_{11}Si_{11}$	Superelastic	7 μm	20 μm	
$Cu_{80}Co_{20}$	GMR	13 μm	20 μm	
$Cu_{90}Co_{10}$	GMR	15 μm	20 μm	
$Cu_{95}Co_{5}$	GMR	13 μm	17 μm	

* Typical length of unbroken piece

High purity elements have been used to prepare the samples (Al = 99,9%, Co = 99,9+%, Cr = 99,99%, Fe = 99,98%, Ga = 99,99%, Mn = 99,9%, Ni = 99,95+%), Geometrical parameters of all samples are listed in the Table 2. Ribbon's geometrical parameters vary from 1-3 mm in width. Thickness of ribbons is usually from 25 to 45 μm. Ribbons of composition $Co_{37}N_{34}iAl_{29}$ and $Co_{49}Ni_{21}Ga_{30}$ are quite brittle and longest unbroken pieces have up to 4 cm. On the other hand, $Fe_{43.5}Mn_{34}Al_{15}Ni_{7.5}$ sample have good mechanical properties and ribbon was prepared in one long piece up to 3 m.

5.1 Superelastic sample $Co_{49}Ni_{21}Ga_{30}$

First sample is known for its superelasticity since 2001 [106]. In the original paper, sample was prepared by arc melting with consequent heat treatment at high temperatures (1073 K-1573 K). Single phase alloys prepared by Oikawa et. al. [106] were too brittle to perform stress-strain measurements. However, they measured 2% strain on the sample

Fig. 41 $Co_{49}Ni_{21}Ga_{30}$ ribbon next to the ruler

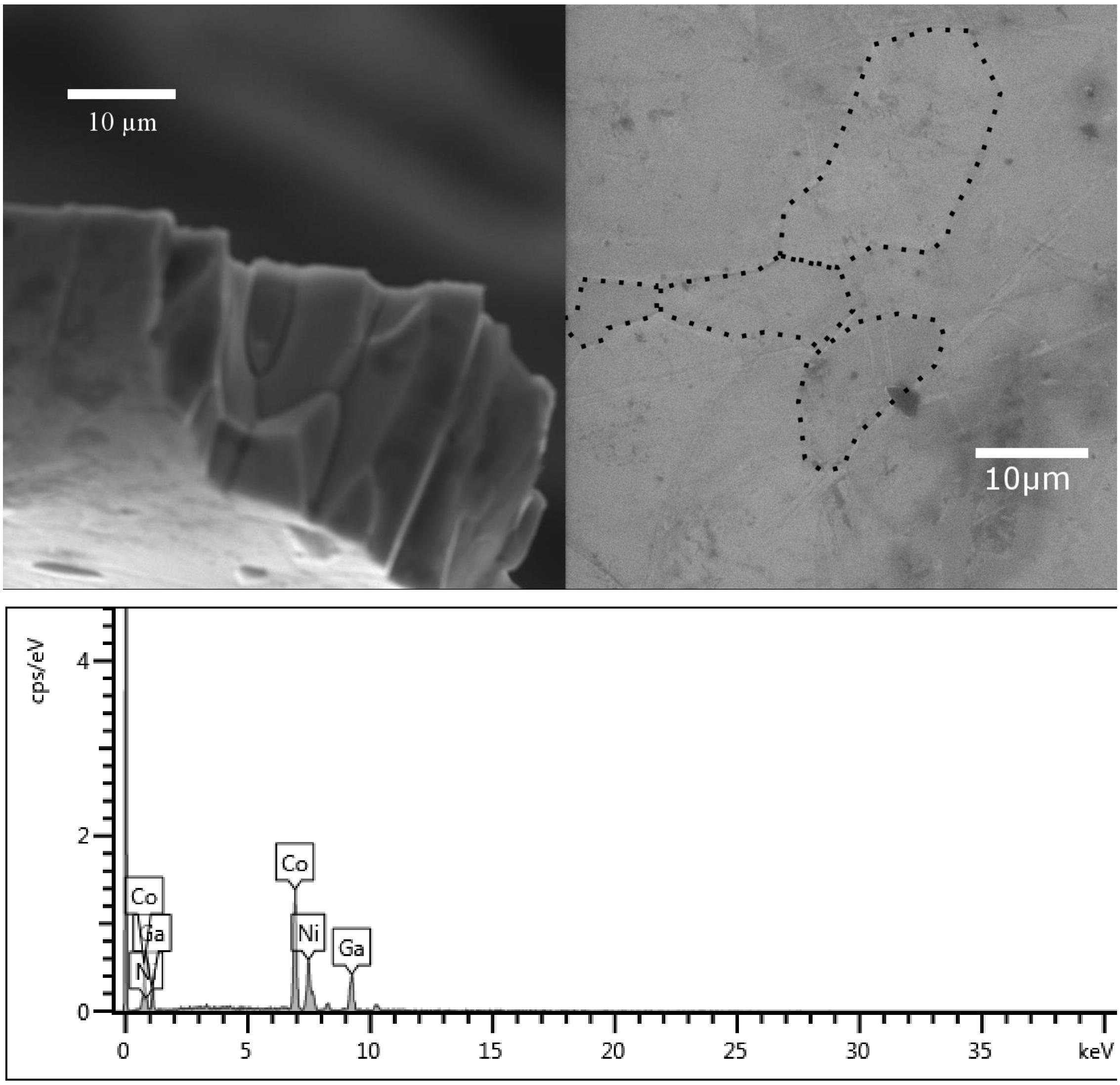

Fig. 40 SEM picture and EDX analysis of $Co_{49}Ni_{21}Ga_{30}$ ribbon's cross section (left) and the surface of ribbon's plane (right) with marked grains

containing two phases. Our sample was prepared by melt spinning technique and it was too brittle so it shattered on the walls of the machine during the preparation. Pieces of sample are pictured in Fig. 41 with a ruler to compare. It can be seen that only small pieces of the sample have been prepared. The longest pieces of sample have up to 1 cm.

SEM picture (Fig. 40) of ribbon's cross section revealed polycrystalline microstructure with grain's size varying between 10 to 30 µm. Ribbon is 40 µm thick. Moreover, columnar crystalline growth perpendicular to the ribbons plane is observed. This is most probably caused by strong thermal gradient created during rapid quenching. Analyses performed by EDX were taken from three different pieces of ribbon (in total on five different sites). The averaged chemical composition was $Co_{49.4}Ni_{20.6}Ga_{30.0}$. Deviation from nominal composition was ±1.49 %. Sufficient homogeneity of the sample has been achieved without long-term annealing of master alloys comparing to ref. [107].

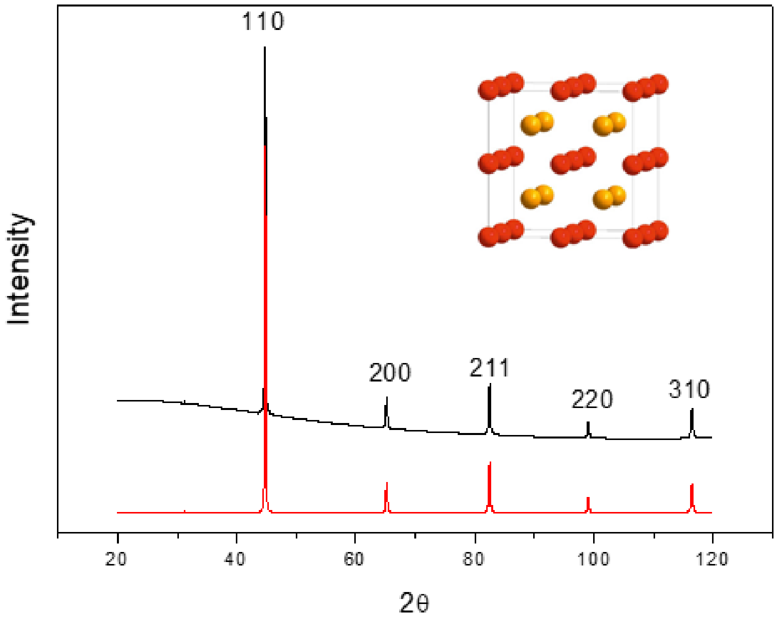

Fig. 42 X-ray diffractogram of $Co_{49}Ni_{21}Ga_{30}$ ribbon taken at room temperature.

X-Ray diffractogram (Fig. 42) of $Co_{49}Ni_{21}Ga_{30}$ shows single phase at room temperature. It is considered to have B2 crystal structure ($Pm\bar{3}m$), which is Y-Z disorder variant of $L2_1$ Heusler alloy (see Chapter 3.1.5) [40]. Lattice parameter for the phase was determined to be 2.857 Å. This phase is considered to be the high temperature austenite phase, which participates in martensitic transformation. Results correspond well to the ref. [108]. According to it, martensitic phase should crystalize in face centred tetragonal structure (fct).

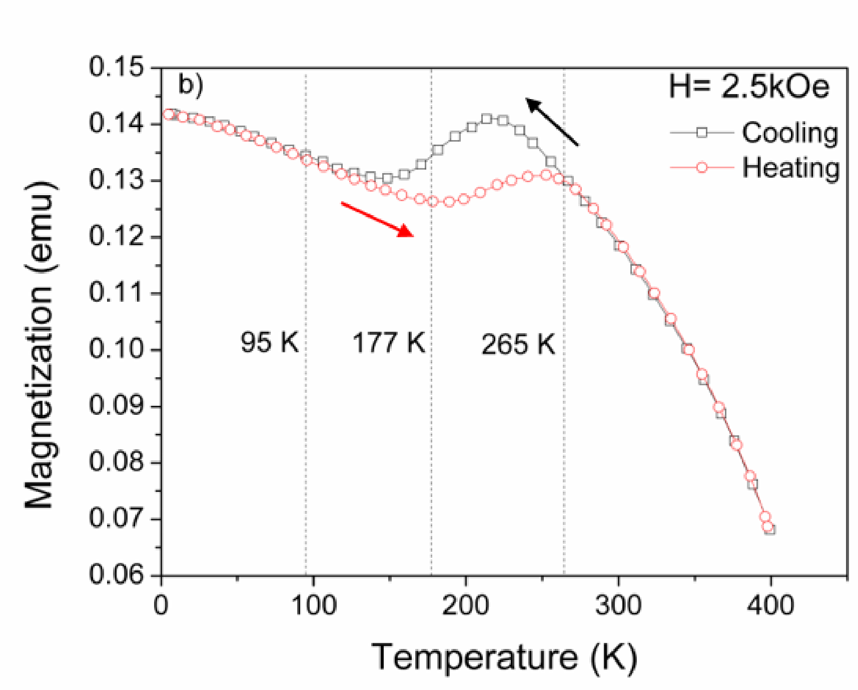

Fig. 44 Temperature dependence of magnetization of $Co_{49}Ni_{21}Ga_{30}$ ribbon shows structural transition.

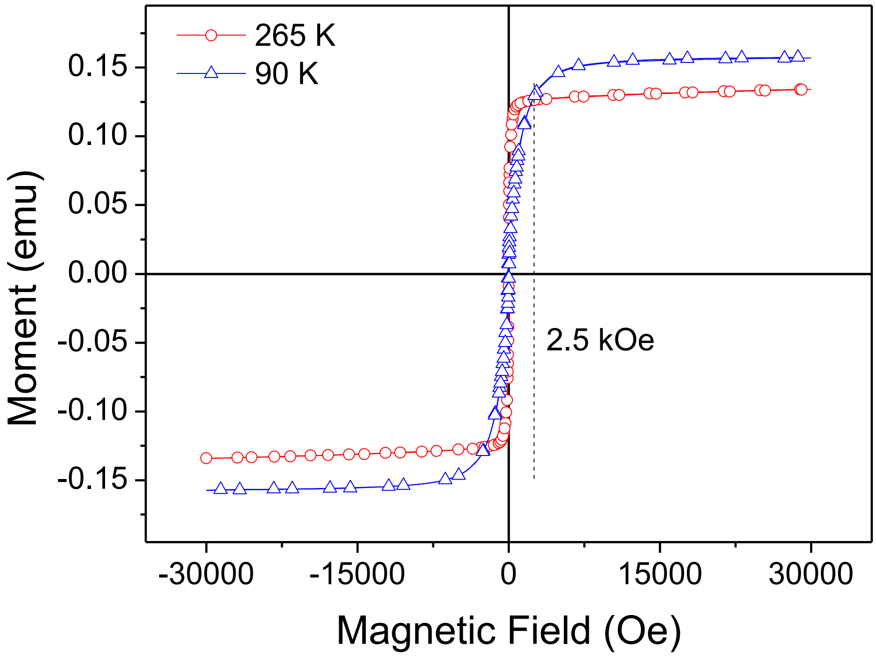

Fig. 43 Magnetic field dependence of magnetization of $Co_{49}Ni_{21}Ga_{30}$ ribbon. It is clear, that high temperature phase has lower saturated magnetization and it is easier to magnetize.

Structural transition has been revealed by magnetic measurements at the temperatures below room temperature. The phase transformation exhibits a hysteresis, from which martensitic transformation temperatures have been obtained. Austenite start temperature was determined to be 179 K austenite finish temperature is 252 K. Martensite phase transformation starts at 216 K and finishes at 149 K. Martensitic transformation temperatures have been evaluated from the first points out from expected temperature dependence of magnetization. Measurements of hysteresis loops show that each phase has different magnetocrystalline anisotropy and saturated magnetization. Hysteresis loops (shown in Fig. 43) taken at different temperatures (at full-martensite state - 90 K, at full austenite state - 265 K) indicate that low-temperature phase is more anisotropic. Magnetocrystalline anisotropy was determined by comparing the saturation field of both phases, which was 1 250 Oe and 7 000 Oe for high and low temperature, respectively.

Temperature dependence of resistance shows that martensitic transformation is shifted (contrary to magnetic measurements) to the range 214 K and 155 K martensite start and martensite finish temperatures, respectively. Additionally, higher magnetic field

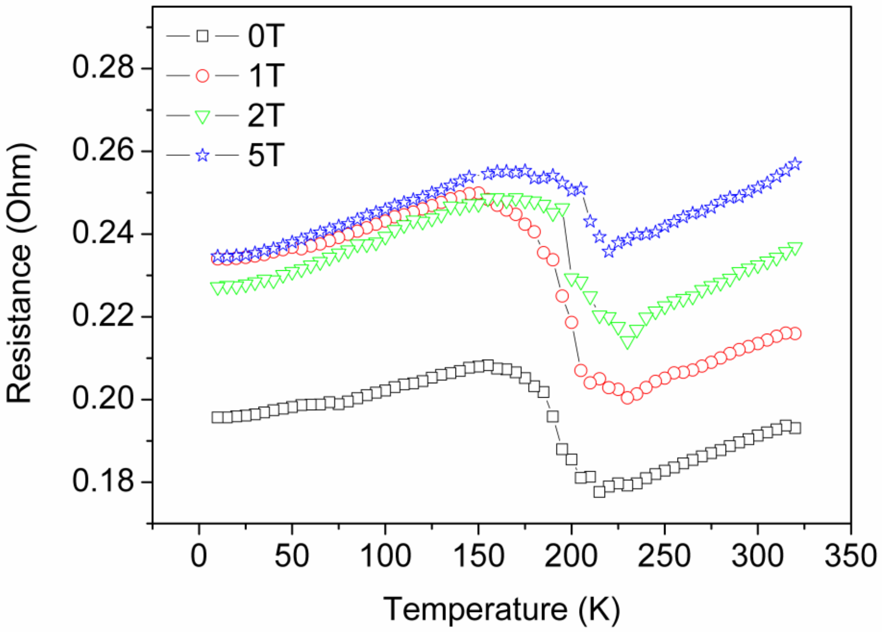

Fig. 45 Temperature dependence of resistance for $Co_{49}Ni_{21}Ga_{30}$ ribbon shows influence of magnetic field on martensitic transformation temperatures. Higher field shifts martensite start and finish temperatures to the higher temperature.

influences martensitic transformation by shifting it to higher temperatures comparing to zero field measurements. Martensitic start temperature rose from 215 K up to 230 K, and martensitic finish temperature shifted from 155 K to 164 K. Usually, first points out of linear dependence are considered to represent transformation temperatures. However, nature of resistivity measurement causes differences in transformation temperatures with respect to magnetic measurements. Resistivity is more sensitive to local atomic changes. Due to the fact, inflex points have been evaluated to locate temperature where the most of transition takes place (Table 5). Measurement at all magnetic fields has been executed on the same piece of sample, therefore temperature training may influence the results.

Table 5 Shift of martensitic transformation temperatures

	0T	1T	2T	5T
Martensite start	215	230	230	220
Inflex point	191	200	199	210
Martensite finish	155	151	163	164

5.2 Superelastic sample $Co_{37}N_{34}iAl_{29}$

Superelasticity in $Co_{37}N_{34}iAl_{29}$ has been also discovered in 2001 [106]. Also, high temperature annealing was applied to enhance its properties. Moreover, particles with this

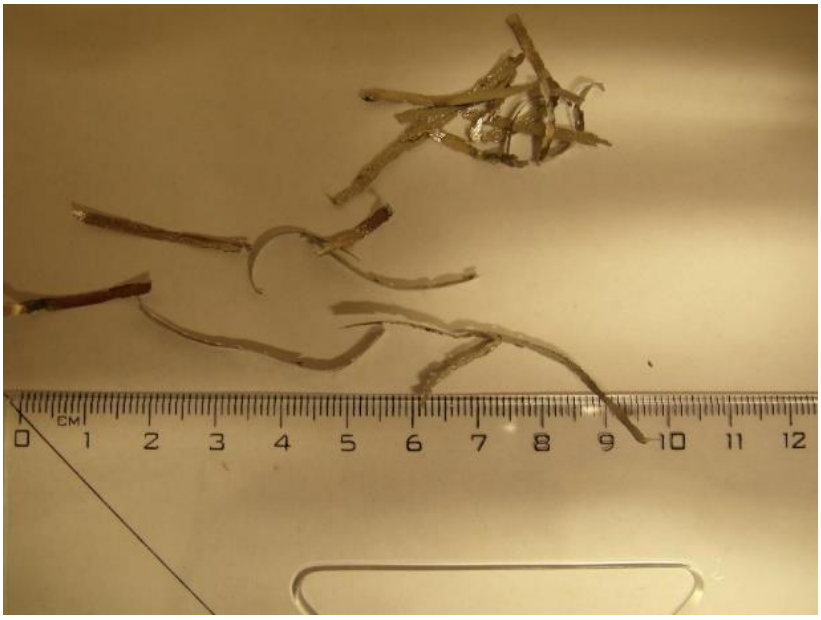

Fig. 46 $Co_{37}N_{34}iAl_{29}$ ribbon next to the ruler

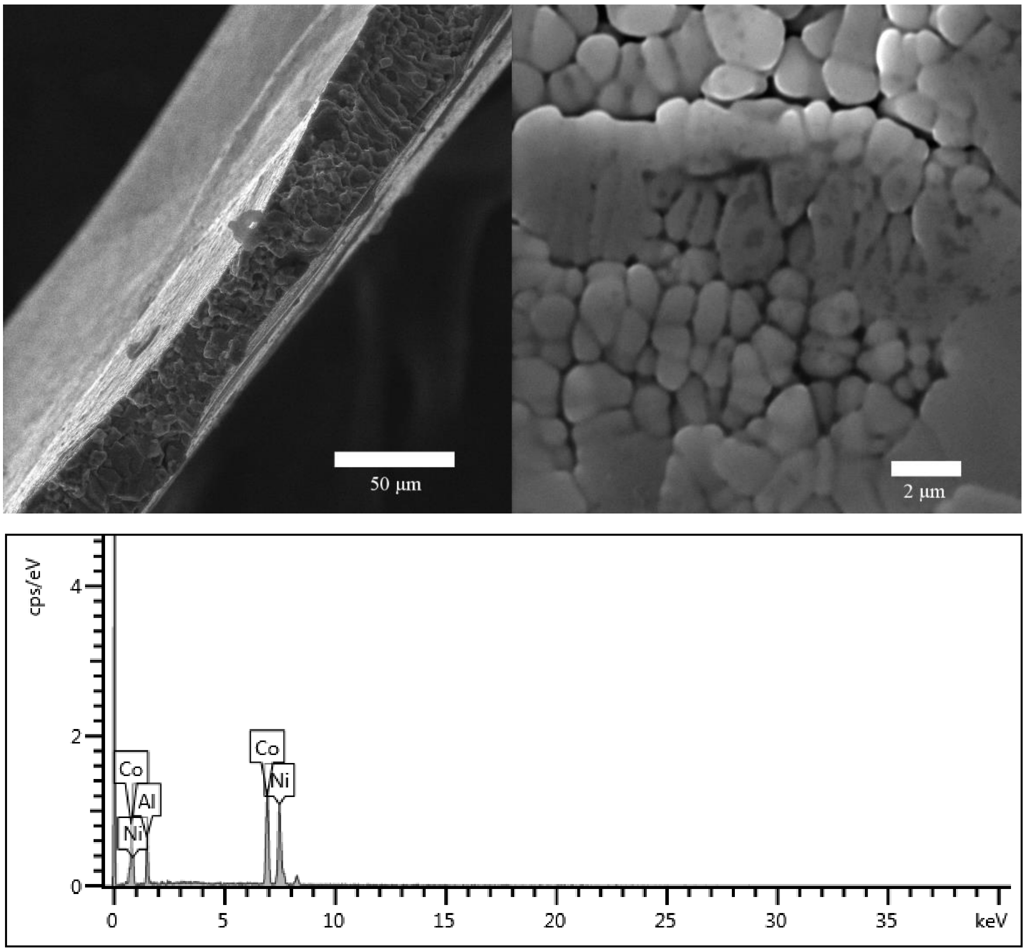

Fig. 47 SEM micrograph of $Co_{37}N_{34}iAl_{29}$ ribbon wit EXD analysis graph.

composition have been successfully embedded in the metal matrix to sense deformation of matrix [109].

$Co_{37}N_{34}iAl_{29}$ analysis of the microstructure was made on the ribbon section and surface and it revealed polycrystalline structure (Fig. 47). Size of the crystallites varies between 1-2 µm. The thickness of ribbon varies from 25 to 45µm. Regions with spherical and with columnar crystalline are present on the ribbon fracture. Small crystallites have advantage because martensitic transformation propagate faster through the material, which is important for developing an efficient actuator. Chemical analysis was made on 3 different pieces of sample and the average composition was $Co_{38.3}Ni_{33.4}Al_{28.2}$ with differences between nominal and real composition of ±2.7%.

XRD measurement revealed a single phase at room temperature (Fig. 49). It is considered to be B2 variant of $L2_1$ variant of Heusler alloy (Y-Z disorder) also known as

$Pm\bar{3}m$. Lattice parameter for the phase was determined to be 2.8499 Å, which can be compared to the ref. [110,111].

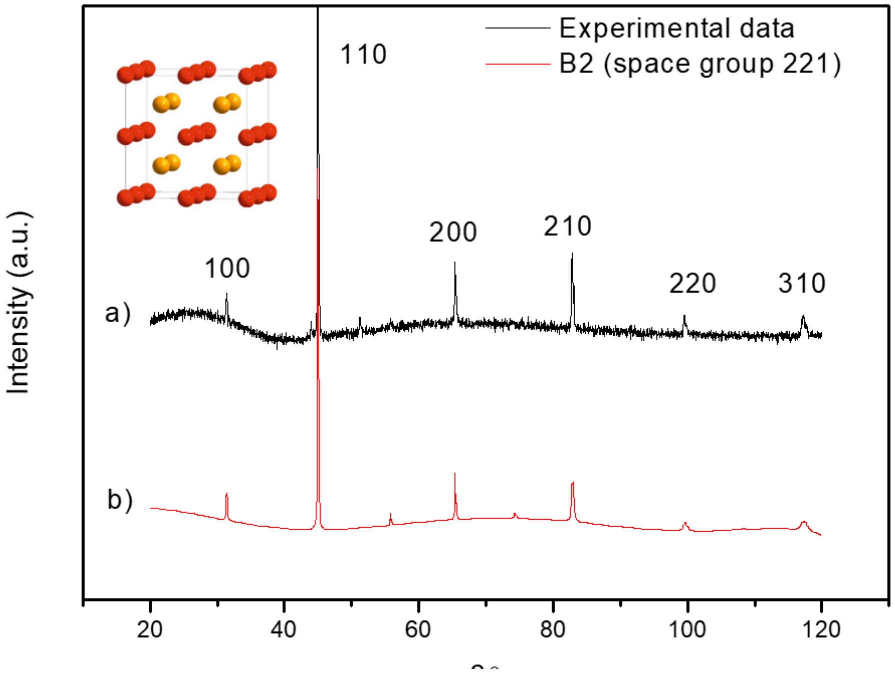

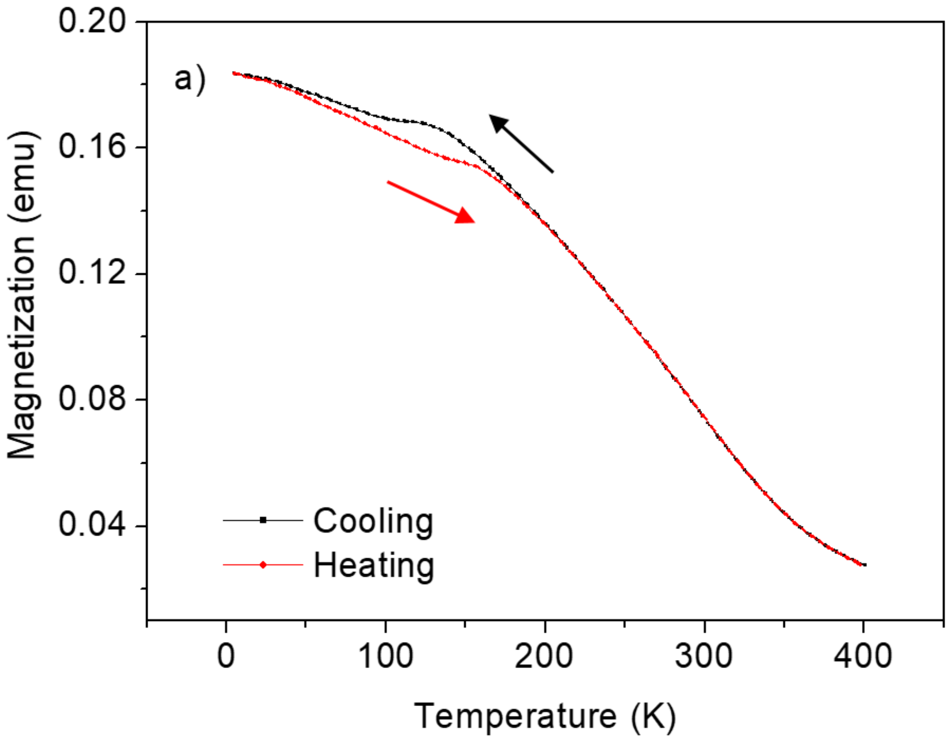

Fig. 48 Temperature dependence of magnetization for Co$_{37}$N$_{34}$iAl$_{29}$ ribbon shows martensitic transformation.

Martensitic transformation is visible on the temperature dependence of magnetization as the hysteresis between cooling and heating cycle. Transformation temperature have been obtained from first derivation of the dependence. Martensitic start and finish temperatures have been evaluated to be 150 K and 75 K, respectively. Austenite start and finish are considered to be 80 K and 170 K.

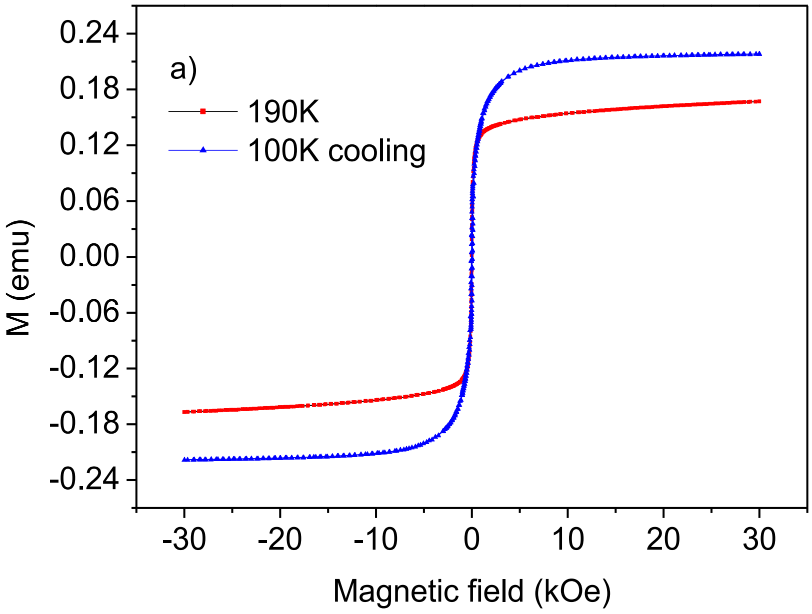

Fig. 50 Hysteresis loops of $Co_{37}N_{34}iAl_{29}$ ribbon. Only small differences between two magnetic phases could be evaluated.

However, the hysteresis does not have clear boundaries as it is in the case of $Co_{49}Ni_{21}Ga_{30}$. Hysteresis loops were taken at 2 different temperatures; before the beginning of martensitic transformation (10 K) and after it's end (190 K). However, the shape of hysteresis loops does not provide us insight into magnetic properties, such as magnetocrystalline anisotropy and saturated magnetization, due to the similarities of both phases. There are only small differences between 2 phases visible on the hysteresis loops, mostly in coercivity and saturated magnetization. Moreover, saturated magnetization is mostly influenced by temperature difference between two measurements as seen in Fig. 50. On the other hand, we can clearly see differences from the virgin curves in saturation field of high temperature phase (Fig. 51). Virgin curves taken at the same temperature follow hysteresis between high and low temperature phases considering cooling or heating cycle. This could be seen at virgin curve taken during cooling cycle at 100 K (red, circle dots), which follows curve taken at 190 K due to the hysteresis of martensitic transformation. The same applies to 100 K virgin curve taken during heating and 10 K curve. High temperature phase is considered to have higher magnetocrystalline anisotropy due to the saturation field differences between low temperature phase (9 kOe) and high temperature phase (4 kOe)

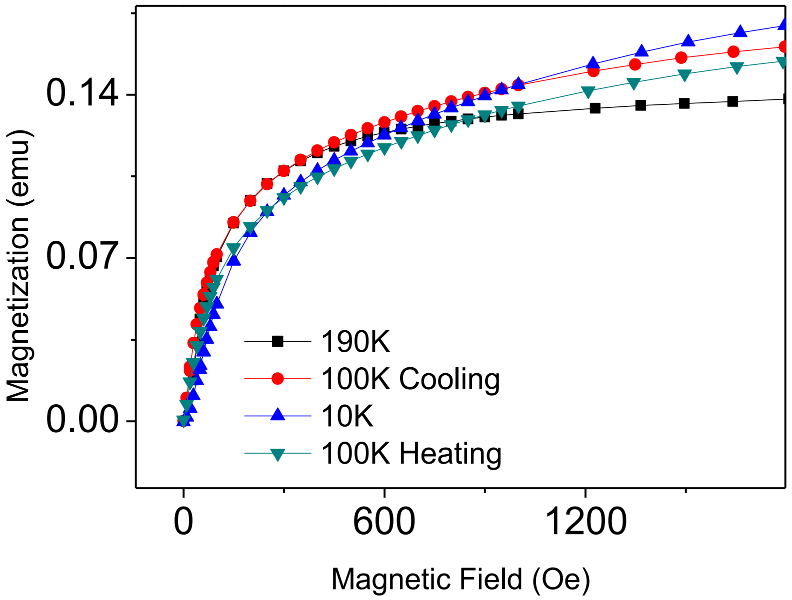

Fig. 51 Virgin curves of $Co_{37}N_{34}iAl_{29}$ ribbon. It is possible to see hysteresis in martensitic transformation through different magnetic properties of both phases. Measurements on the same temperature tend to follow the curve of their corresponding phases.

Resistivity measurements (Fig. 52) have been made in order to confirm martensitic transformation and its influence on magnetic field. Obtained martensitic transformation temperatures are shown in Table 6. Magnetic field has negligible influence on martensite start and austenite finish temperatures, but martensite finish and austenite start temperatures rose which made martensitic transformation narrow.

Table 6 Martensitic transformation shift under magnetic field

Condition	M_s	M_f	A_s	A_f
M(T)	150 K	75 K	80 K	170 K
R(T) 1T	175 K	95 K	65 K	175 K
R(T) 2T	160 K	100 K	105 K	165 K
R(T) 5T	165 K	105 K	110 K	170 K

M (T) stands for temperature dependence of magnetization

R (T) stands for temperature dependence of resistance

Negligible influence of magnetic field on martensitic transformation may be explained by low difference in saturation magnetization between austenite and martensite phases, which leads to small change of Zeeman energy. If the difference in Zeeman energy of both phases is high, then it is possible to shift martensitic transformation, because total change of energy will decrease.

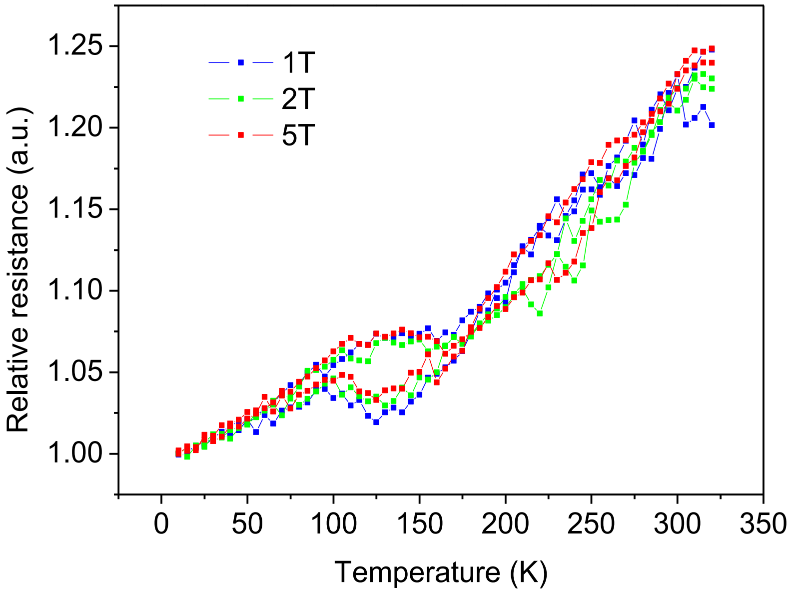

Fig. 52 Temperature dependence of resistance for $Co_{37}N_{34}iAl_{29}$ ribbon

It was possible to measure stress strain curves with improved mechanical properties of $Co_{37}N_{34}iAl_{29}$. Force was applied with a rate 2N/min and the maximum force was 18 N. Applied stress was calculated from cross section of the ribbon. The maximum achieved reversible strain was 0.7%. Irreversible strain was quite low 0.2%. However, the sample is still quite fragile so it was mounted with caution and the strain 0.3% in the region with lowest stress is most probably caused by straightening the sample and it is not associated with shape memory mechanism. Yield test revealed maximum strain of 1.7% at 400 MPa stress. Also, 0.8% strain was caused by straightening sample.

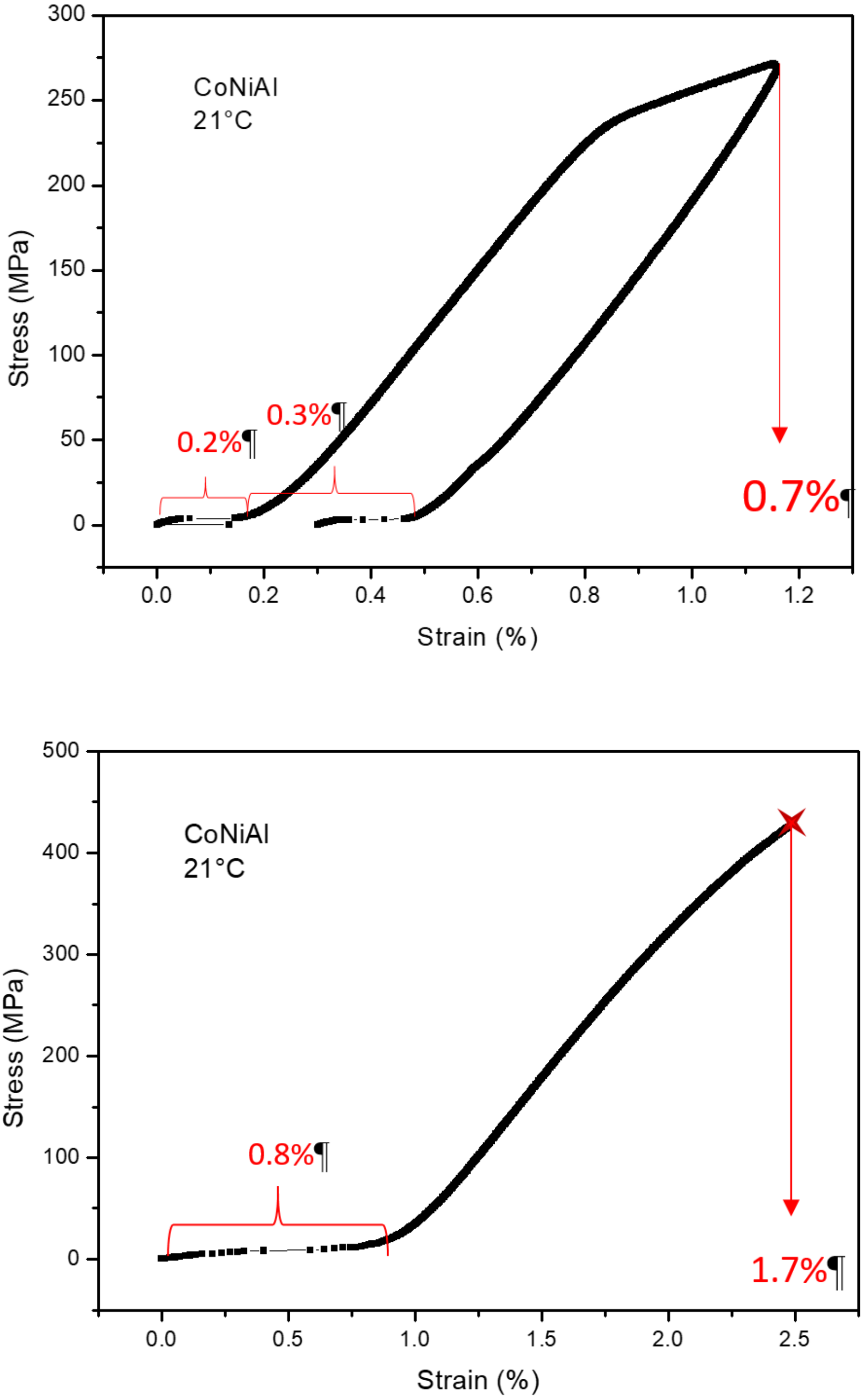

Fig. 53 Stress strain curves for Co$_{37}$N$_{34}$iAl$_{29}$ ribbon. Top panel: Reversible stress strain curves. Bottom panel: Yield test

5.3 Superelastic sample $Fe_{43.5}Mn_{34}Al_{15}Ni_{7.5}$

$Fe_{43.5}Mn_{34}Al_{15}Ni_{7.5}$ was discovered in 2011 with superelastic recoverable strain 5%. However, the alloy was prepared by arc melting with consequent thermal treatment for several hours. Sample is known to have perfect mechanical properties as ductility, which make it as a proper candidate to use it in construction applications [12].

Fig. 54 $Fe_{43.5}Mn_{34}Al_{15}Ni_{7.5}$ ribbon after preparation

SEM micrographs (Fig. 56) revealed columnar microstructure that is similar to the previous sample $Co_{49}Ni_{21}Ga_{30}$. Morever, layer of equiaxed crystallized grains is present at the wheel surface, which was in contact with copper wheel during preparation. The ribbon is around 40-55 μm thick. EXD analysis measured on three samples confirmed nominal composition.

X-Ray diffraction measurement (Fig. 55) measured at room temperature revealed two phases, α and γ'. α phase crystalizes in the face centred cubic phase and its lattice parameter is a_{fcc} = 0.36604. This phase represents austenite, high temperature phase. γ' phase crystalizes in body centred cubic structure. It is considered to be low temperature phase (martensite) with the lattice parameter a_{bcc} = 0.29086 nm. By comparing intensities of both phases, it possible to evaluate the volume of each phase in the alloy. Detailed

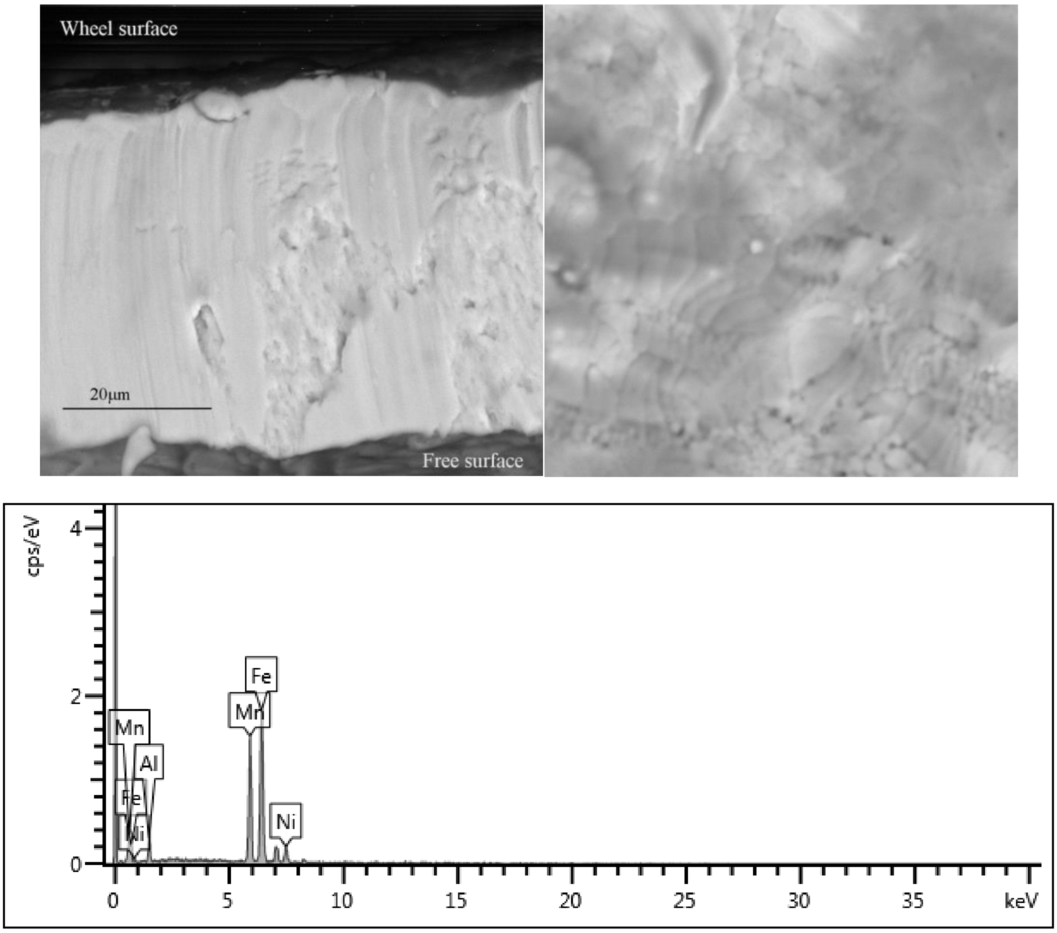

Fig. 56 SEM micrographs of $Fe_{43.5}Mn_{34}Al_{15}Ni_{7.5}$

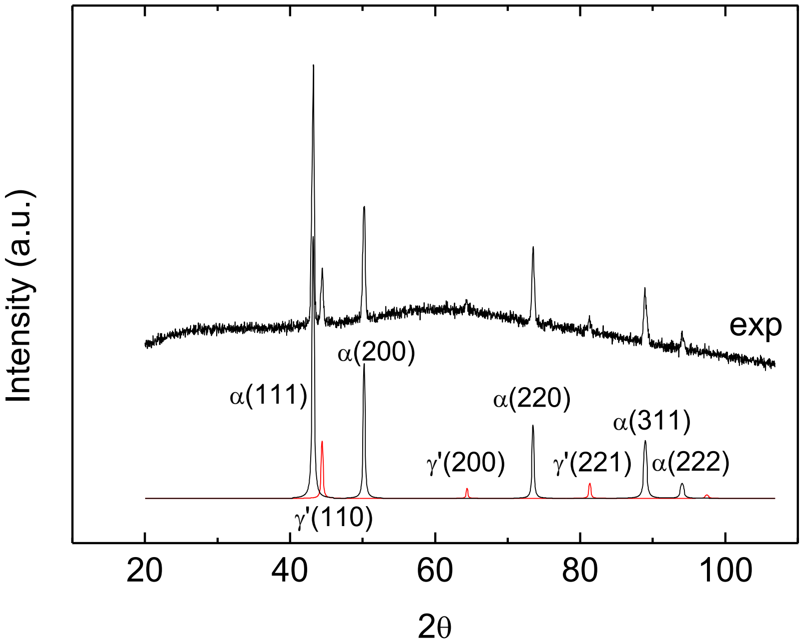

Fig. 55 X-ray diffraction of $Fe_{43.5}Mn_{34}Al_{15}Ni_{7.5}$ ribbon

XRD analysis showed the volume of the austenite phase is 88 % and remaining 12 % belongs to martensite at room temperature.

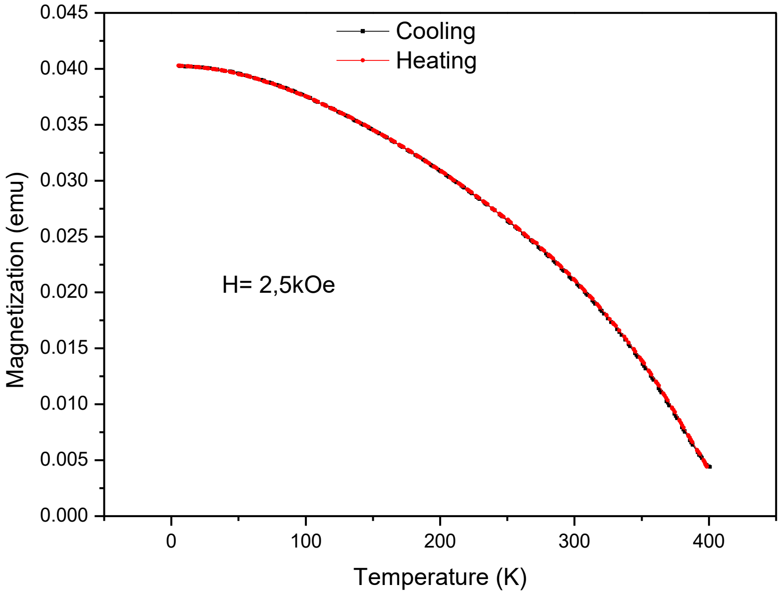

Fig. 58 Temperature dependence of magnetization for $Fe_{43.5}Mn_{34}Al_{15}Ni_{7.5}$ ribbon

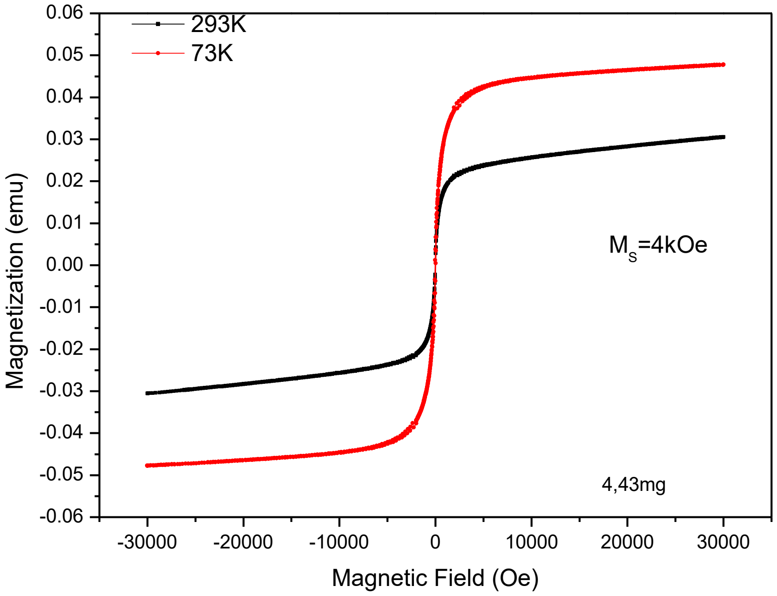

Fig. 57 Hysteresis loops of $Fe_{43.5}Mn_{34}Al_{15}Ni_{7.5}$ ribbon.

Magnetic measurements have been performed to confirm structural transition and to examine differences between both phases. However, there is almost no difference in magnetization dependence of temperature (Fig. 58) between cooling and heating cycle. That may be attributed to the long range of martensitic transformation making magnetization hysteresis low. Consequently, this measurement was not used for obtaining transformation temperatures. On the other hand, Curie temperature is around 125°C. It highlights the opportunity that $Fe_{43.5}Mn_{34}Al_{15}Ni_{7.5}$ ribbon may serve as sensor around

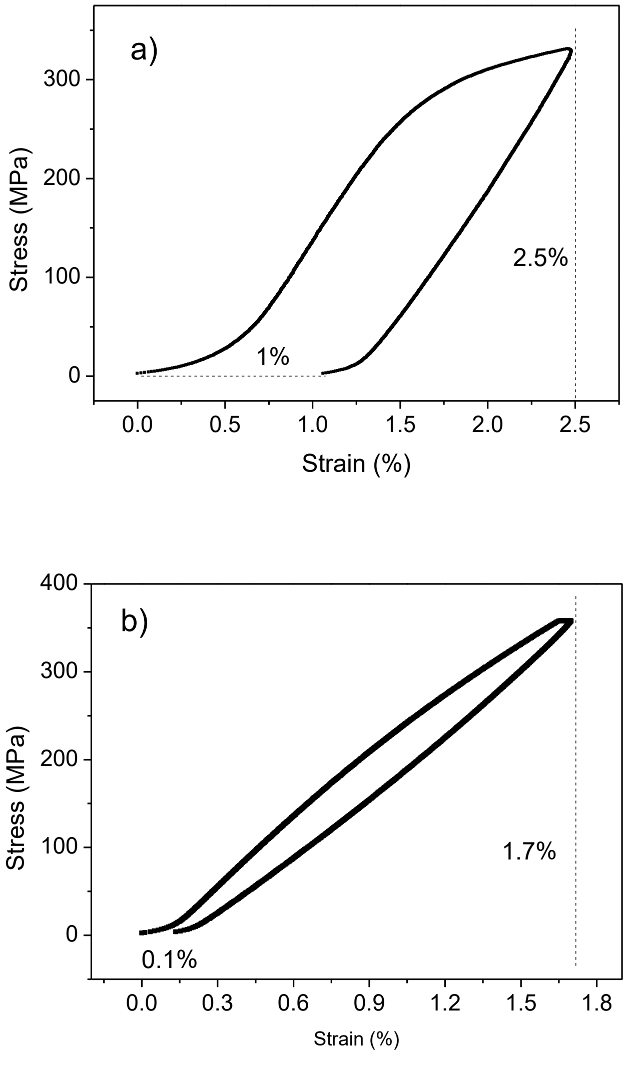

Fig. 59 Stress strain curves for $Fe_{43.5}Mn_{34}Al_{15}Ni_{7.5}$ measured on ribbon with remarkable change of irreversible strain, which drop down by 90%.

room temperatures. High temperature phase has saturation magnetization at field 6 kOe and low temperature phase saturates at 2.3 kOe. It suggests, that martensite has higher magnetocrystalline anisotropy. It is opposite situation to magnetic properties of $Co_{49}Ni_{21}Ga_{30}$. and $Co_{37}N_{34}iAl_{29}$ phases.

Stress strain curves have been measured on ribbons at various temperatures to confirm superelastic properties of the $Fe_{43.5}Mn_{34}Al_{15}Ni_{7.5}$. Graph in the Fig. 59 represents stress-strain curve on sample before and after the training process. Maximum achieved reversible superelastic strain was 1.7 %. During training process, irreversible strain was diminished down to 0.1 % from former 1 %.

Stress strain measurements have been improved by the measurements of permeability (Fig. 60). Maximum achieved strain was 1% and simultaneously permeability dropped by noticeable 12% change. It should be noticed, that there is only small hysteresis in permeability between loading and unloading cycles during the time when the most of stress takes place. Slim hysteresis is required for precise sensor or actuator [112]. In addition, the permeability at zero stress is different for two cases (before and after measurement), which points to the fact that permeability variations arise from structural transition between α and γ’ phases rather than from stress dependence of permeability.

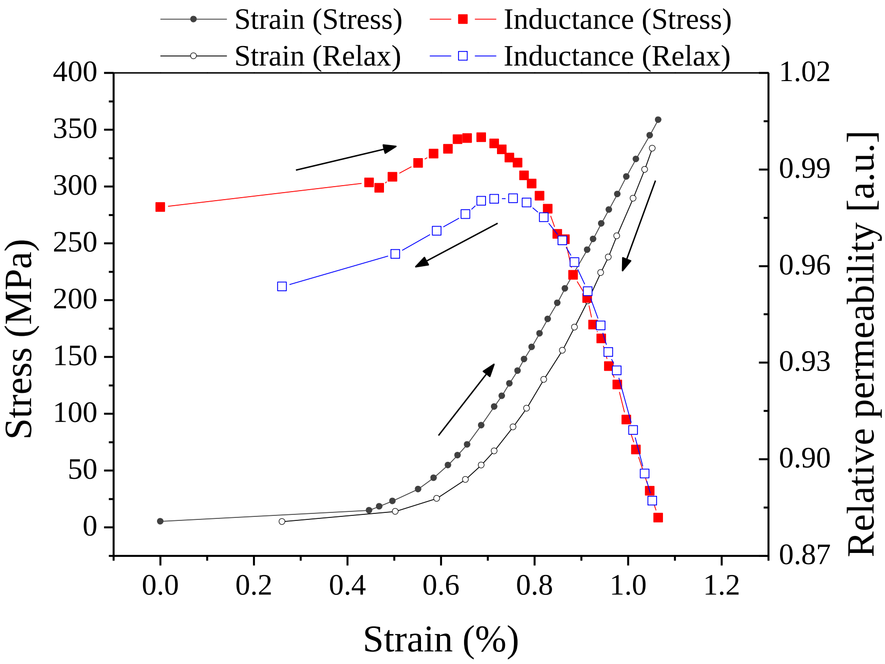

Fig. 60 Strain dependence of stress and relative permeability of $Fe_{43.5}Mn_{34}Al_{15}Ni_{7.5}$ ribbon

It should be mentioned that samples are usually annealed to release internal stresses. But studied samples were not annealead, neither in the case of $Fe_{43.5}Mn_{34}Al_{15}Ni_{7.5}$ and $Co_{49}Ni_{21}Ga_{30}$. This may explain the difference between typical stress-strain curve of superelastic samples (Fig. 7) and our measurements. Internal stresses are distributed randomly through the ribbon, thus the value superelastic stress of each grain may fluctuate depending on the value of internal stress affecting the grain. Equal distribution of superelastic stress during the loading is important feature of the sample. With it, sample may strain superelastically in the whole range, due to equally distributed superelastic stress and through the change of phase volume act as a sensor.

5.4 Superelastic sample $Co_{51}Cr_{17}Ga_{11}Si_{11}$

The sample is known for its inverse shape memory effect when shape memory change occurs after cooling, not heating. Superelasticity has been also reported on the sample in the temperature range close to room temperature [113]. Samples have been so far prepared by arc melting and subsequently annealed. Microwire with superelastic properties has been prepared by Taylor-Ulitovsky method. So, our goal was to prepare the sample in the form of microwire and to study the superelastic properties.

Fig. 61 Sample $Co_{51}Cr_{17}Ga_{11}Si_{11}$ prepared by Taylor Ulitovsky method

SEM micrographs (Fig. 62) revealed metallic core inside glass coating. Total diameter of sample was measured to be 25 μm and metallic core has 6.7 μm. However, polycrystalline character presented in previous samples was not observed in $Co_{51}Cr_{27}Ga_{11}Si_{11}$ microwire. EDX was measured on two pieces of microwire with uncovered metallic core. Result of EDX analysis was in accordance with a small difference (± 1 at. %) between prepared ($Co_{51.39}Cr_{25.99}Ga_{11.33}Si_{11.29}$) and desired composition.

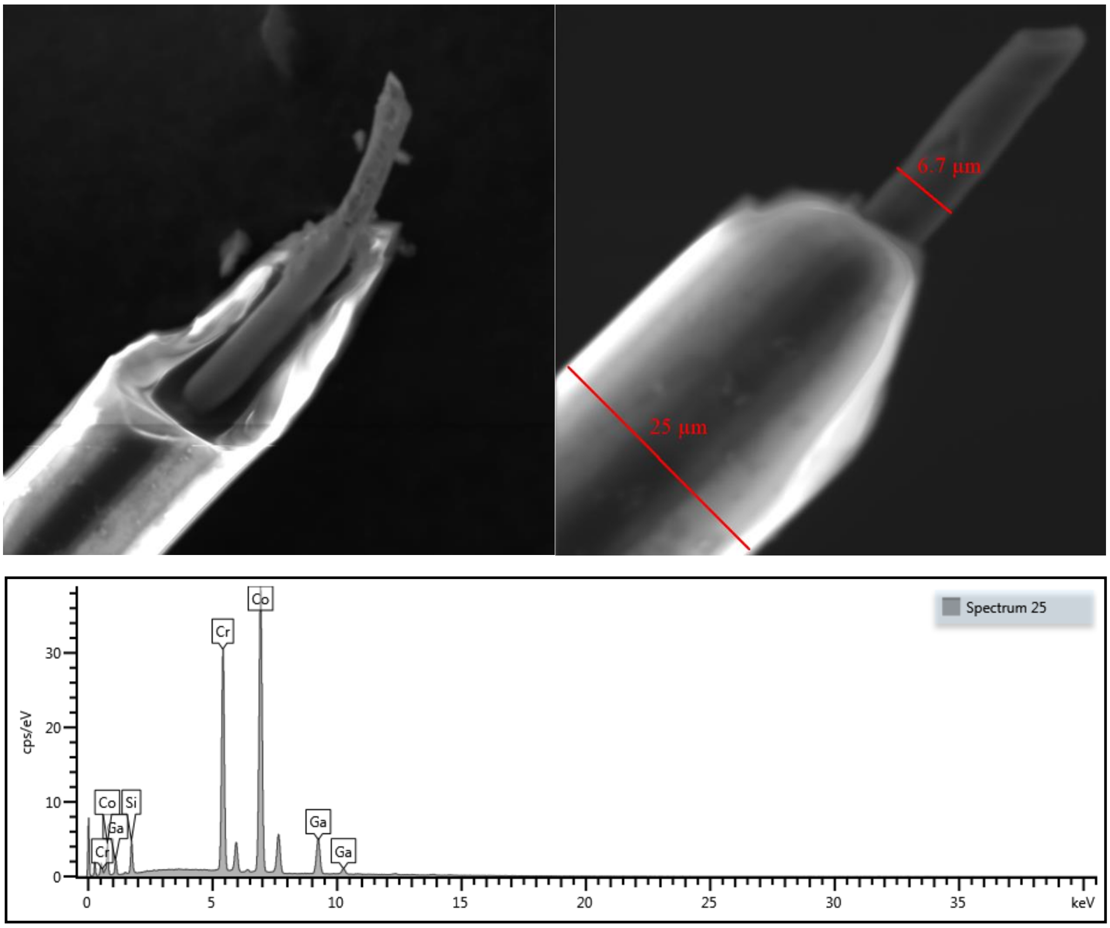

Fig. 62 SEM micrograph of superelastic, glass-coated microwire with marked diameter of glass coating and metallic core. Bottom graph represents spectrum of EDX analysis.

The presence of single phase was confirmed by X-Ray diffraction at room temperature. Sample crystallizes in B2 structure with space group symmetry $Pm\bar{3}m$. Lattice parameter was determined to be 2.8615. Relative intensities demonstrate the presence of preferred crystal orientation. The most interesting discovery has been provided by electron backscatter diffraction analysis, which was used to confirm or disprove presence of preferred orientation (Fig. 65). These measurements have been

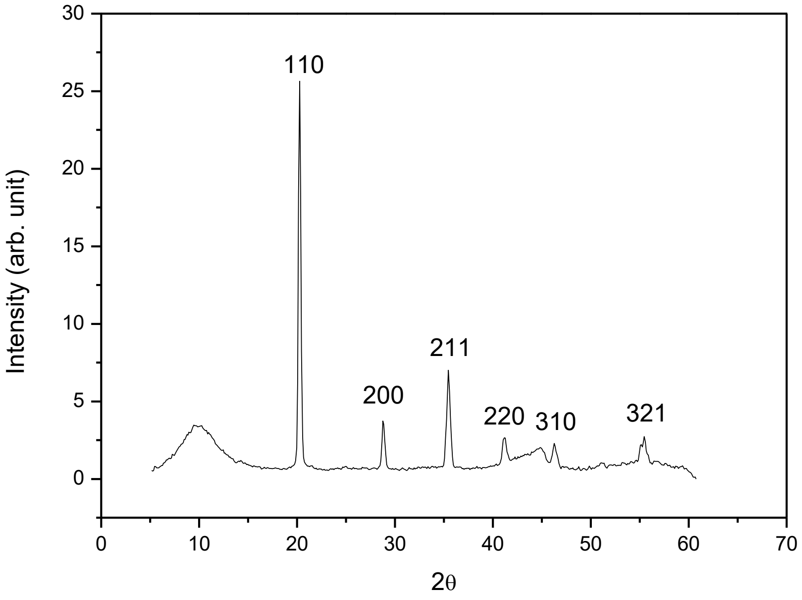

Fig. 63 X-ray diffraction for $Co_{51}Cr_{27}Ga_{11}Si_{11}$ microwire

conducted on many sites of microwires and always with the same results. All crystallographic orientations are in the direction <111> parallel to the microwire axis. No grain boundaries have been observed. There is pictured data map of examined site on the microwire on the top left corner of Fig. 65. This site has been selected due to the optimal location for EBSD measurement which requires a beam of electrons in approx. 70° angle. Coloured maps on the left top panel represent the portion of the microwire oriented in one way (the same colour means one orientation of crystal) for corresponding coordinates (X, Y, Z).

Bottom panel represents how much of the microware is oriented in the directions <001>, <101> and <111> for each coordinate. So far, microwire seems to be monocrystalline along the microwire with orientation <111>.

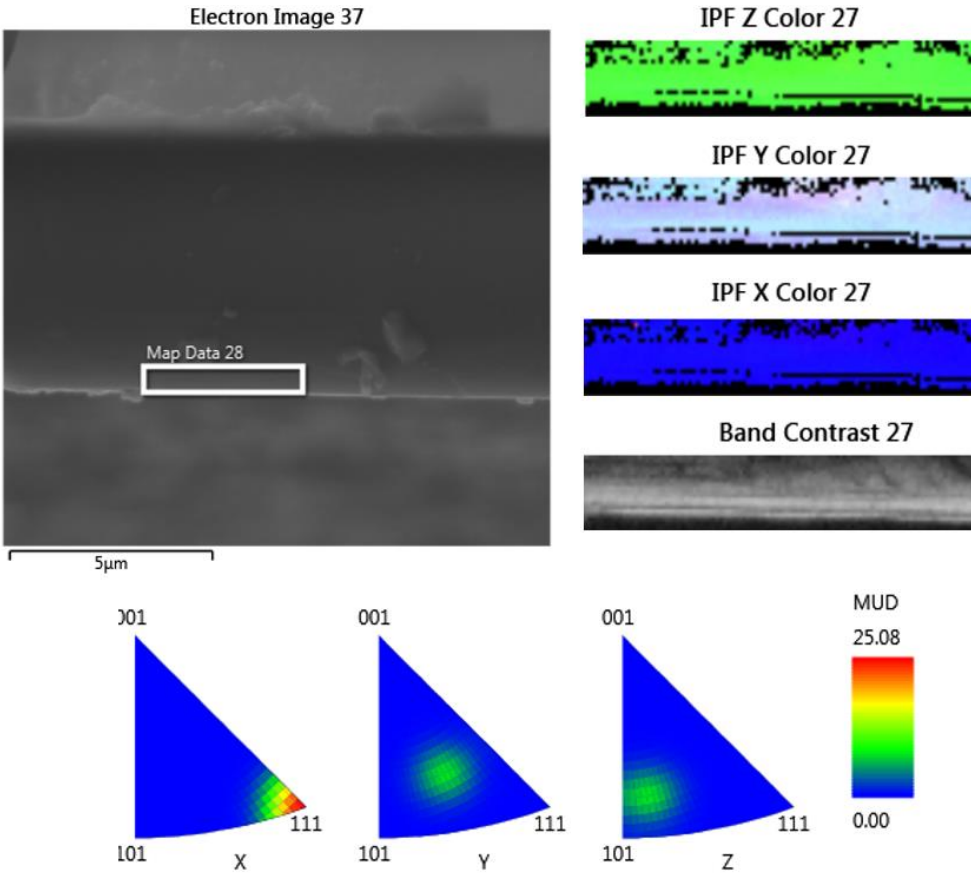

Fig. 65 Results of EBSD measurements revealed one crystal orientation

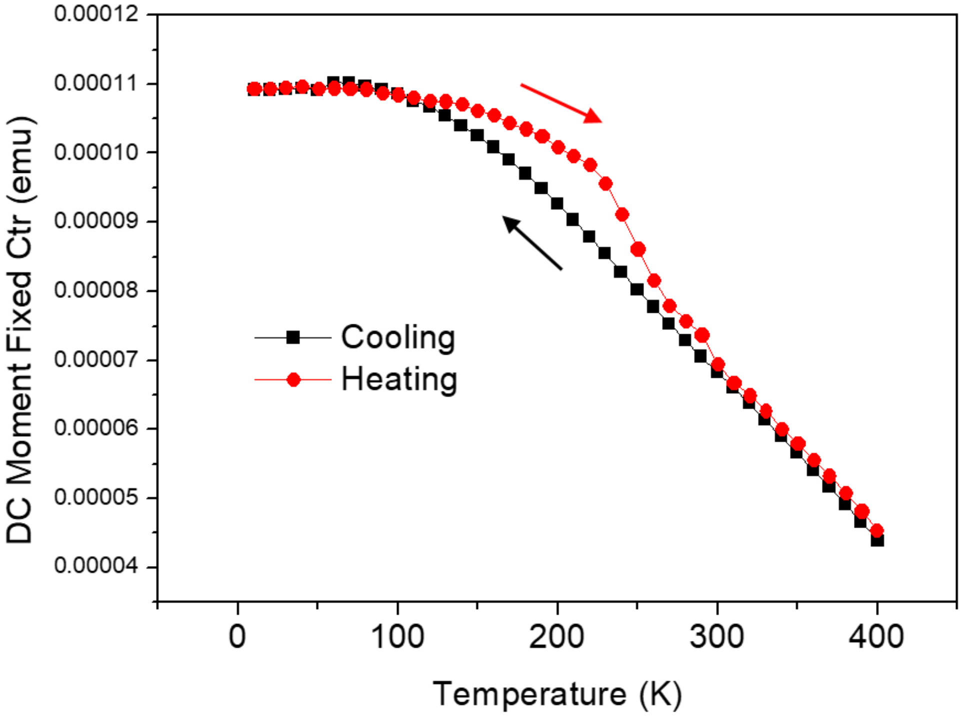

Fig. 64 Temperature dependence of magnetization for Co$_{51}$Cr$_{17}$Ga$_{11}$Si$_{11}$

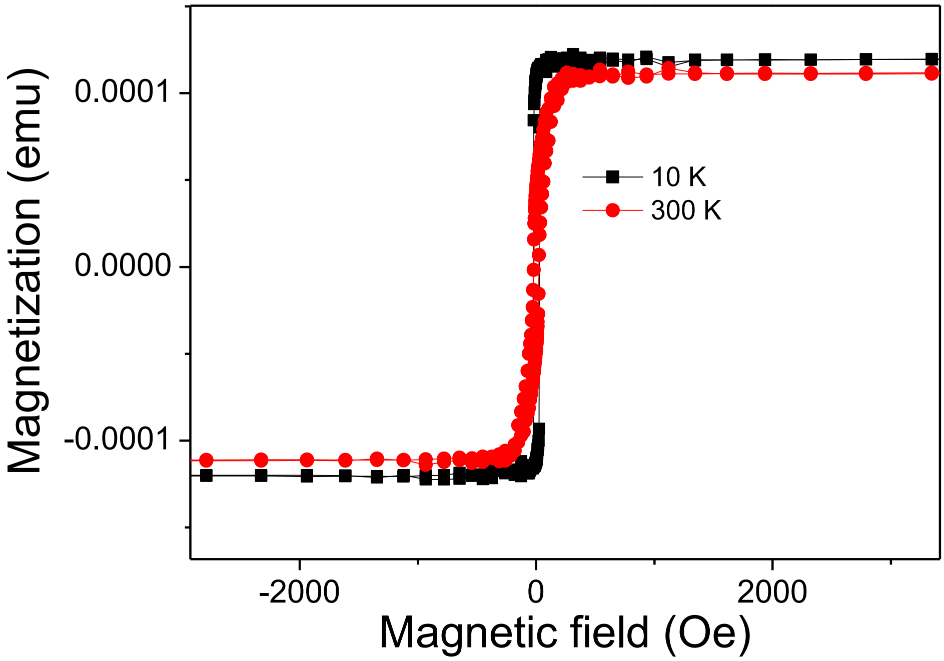

Fig. 66 Hysteresis loops for $Co_{51}Cr_{17}Ga_{11}Si_{11}$

Temperature dependence of magnetization revealed hysteresis in magnetization at the temperatures lower than room temperature (Fig. 64). Abnormal decrease in magnetization was observed during heating. However, it was not observed during cooling. Sign of phase transition during cooling phase may be attributed to the long temperature range of transition (it appears as an abnormally linear dependence) similar as in the Fig. 58 for $Fe_{43.5}Mn_{34}Al_{15}Ni_{7.5}$ ribbon. Temperature dependence of magnetization has confirmed martensitic transformation. Measurements of magnetic field dependence of magnetization have been measured at 10 K and 300 K (Fig. 66). These temperatures have been selected to see differences between low temperature phase and high temperature phase. Low temperature phase has lower magnetocrystalline anisotropy compared to the high temperature phase. It can be seen as a difference in saturation of magnetic field. Stress strain curves have been also measured on $Co_{51}Cr_{17}Ga_{11}Si_{11}$ microwires. Bunch of 19 microwires have been mounted into DMA device. Achieved reversible strain was 1.65% with very low irrecoverable strain of 0.13% (Fig. 67). Sample yielded at 2,5% strain (Fig. 68). It should be noted, that low irreversible strain was achieved without training, in other words, during the first measurement. That may be attributed to the monocrystalline microwire that is properly oriented. Considerable strain has been achieved without heat treatment as it was necessary for arc melted bulk materials [113].

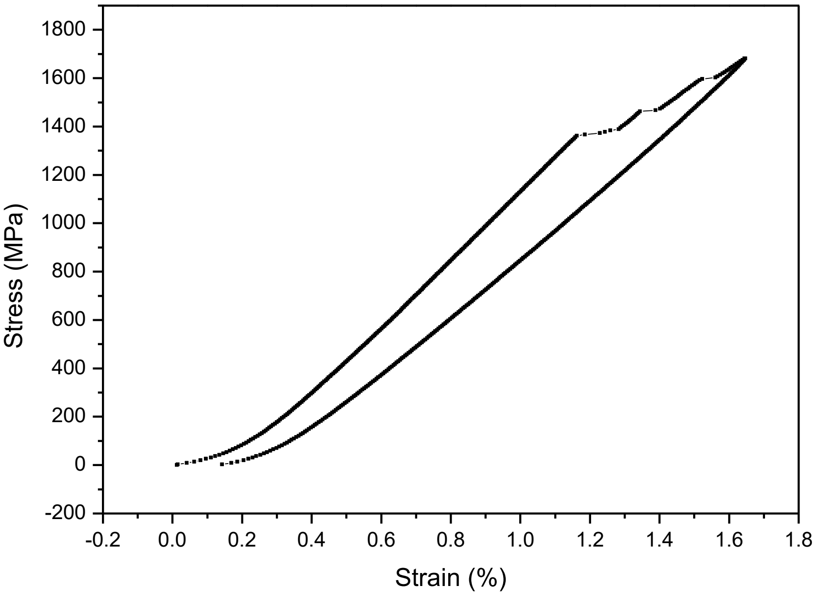

Fig. 67 Stress strain curve for $Co_{51}Cr_{17}Ga_{11}Si_{11}$

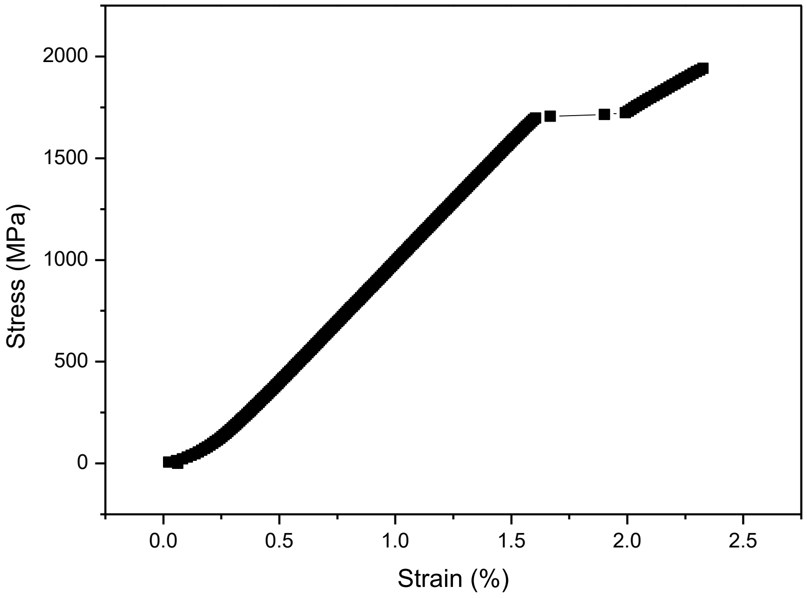

Fig. 68 Evaluation of critical strain for $Co_{51}Cr_{17}Ga_{11}Si_{11}$

5.5 Granular Cu-Co microwires with GMR effect

This subchapter deals with giant magnetoresistance found in granular structures prepared by Taylor-Ulitovsky technique. Our goal was to study the influence of annealing on giant magnetoresistance in the glass-coated microwires. Granular materials have advantage in fast and cheap preparation contrary to the thin films prepared by electrodeposition [114-116]. Taylor-Ulitovsky method offers easy way to prepare such a material.

Samples with composition $Cu_{80}Co_{20}$, $Cu_{90}Co_{10}$ a $Cu_{95}Co_5$ have been annealed for various times and at two different temperatures. The annealing time was 10, 30, 60 minutes and 2, 5, 10, 24 hours for heat treatment at 673 K. Additionally, samples were also annealed at isothermal temperature (T_{ann}= 373 K and 423 K) for 2, 10, and 24 hours.

5.5.1 X-Ray diffraction

Two phases have been identified in the CuCo samples, *hcp* α-Co and *ffc* Cu. Preferred grain orientation was observed from the XRD spectra (Fig. 69). *Fcc* phase is characterized by two main peaks at $2\Theta_1 \approx 43.23°$ and $2\Theta_2 \approx 50.35°$ corresponding with atomic spacing of 2.09 Å and 1.81 Å. Lattice parameters for hcp α-Co phase are 2.05 Å and 1.77 Å. Main peaks for this phase are at $2\Theta_1 \approx 44.12°$ and at $2\Theta_2 \approx 51.57°$. Therefore, these peaks are overlapped in many cases. The very first peak represents merged peaks of Cu phase and Co phase. Moreover, low content of Co in the samples makes it quite difficult to detect. The presence of preferred texture decreases the main α-Co peak at $2\Theta_1 \approx 44.12°$. Relative intensities of peaks have changed after annealing. Within annealing of the sample $Cu_{95}Co_5$, one can observe decreasing of the preferred orientation. The first peak is appreciably increased and the relative intensities change with the annealing. When we look at the detail, the peaks of Cu and Co are more separated with the annealing. Broadening of the peaks was also observed, especially for $Cu_{95}Co_5$. There is still the marked preferred orientation in the microwire after annealing of the sample $Cu_{90}Co_{10}$. For the sample $Cu_{80}Co_{20}$, annealing does not affect the structure changes in Co-Phase. The relative intensities of all the peaks are the same in the as-prepared and annealed samples. Samples had quite low magnetoresistance before annealing and broadening of peaks may suggest that average size of grains decreased, or the number of small size clusters increased.

To prove the stress relaxation effect, low temperature annealing was performed. XRD diffractograms on low temperature annealed samples were very similar to as-cast samples.

5.5.2 Electron microscopy

Transmission electron microscopy observations have been executed on all of Cu-Co samples. TEM has been used to find granular structures. The solubility of cobalt in copper is 6% at room temperatures, so it is expected to find granular structure in the sample with cobalt content above 6%. EDX analyses have been executed on all samples to confirm Co grains or clusters. Sites of EDX analyses for $Cu_{80}Co_{20}$ microwire are marked on the Fig. 70 and the generated data are displayed in the Table 7. EXD analyses have been also conducted on the other compositions, but the results have discovered just

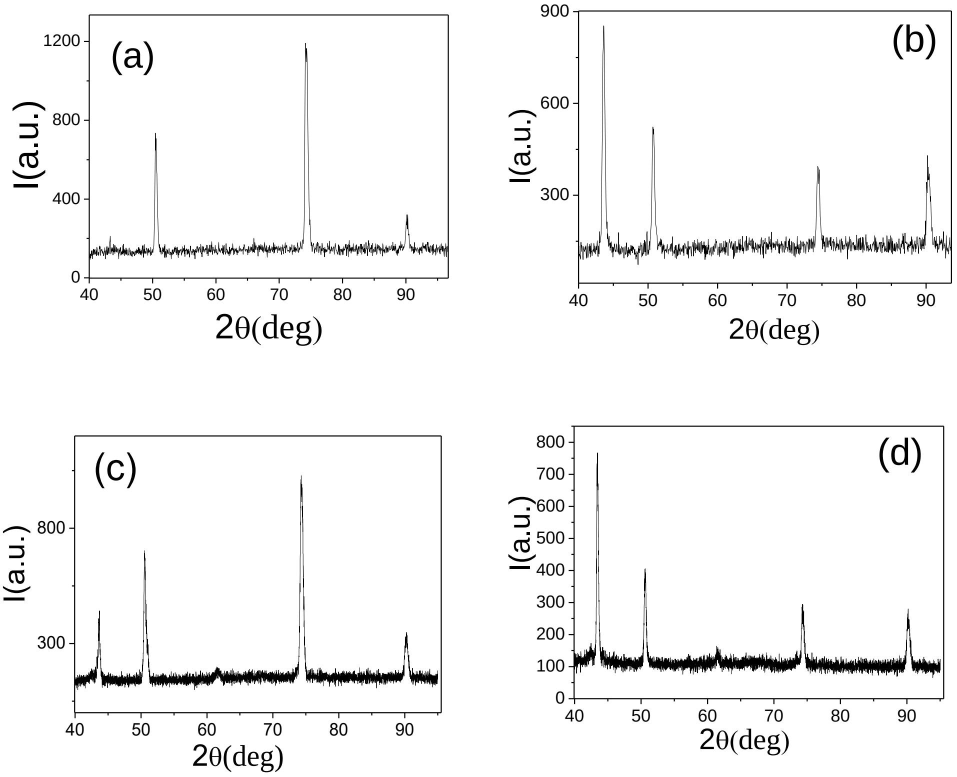

Fig. 69 XRD of as-prepared (a,b) and annealed at T_{ann}=673 K for 24 h (c,d) $Cu_{95}Co_5$ and $Cu_{80}Co_{20}$ microwires respectively.

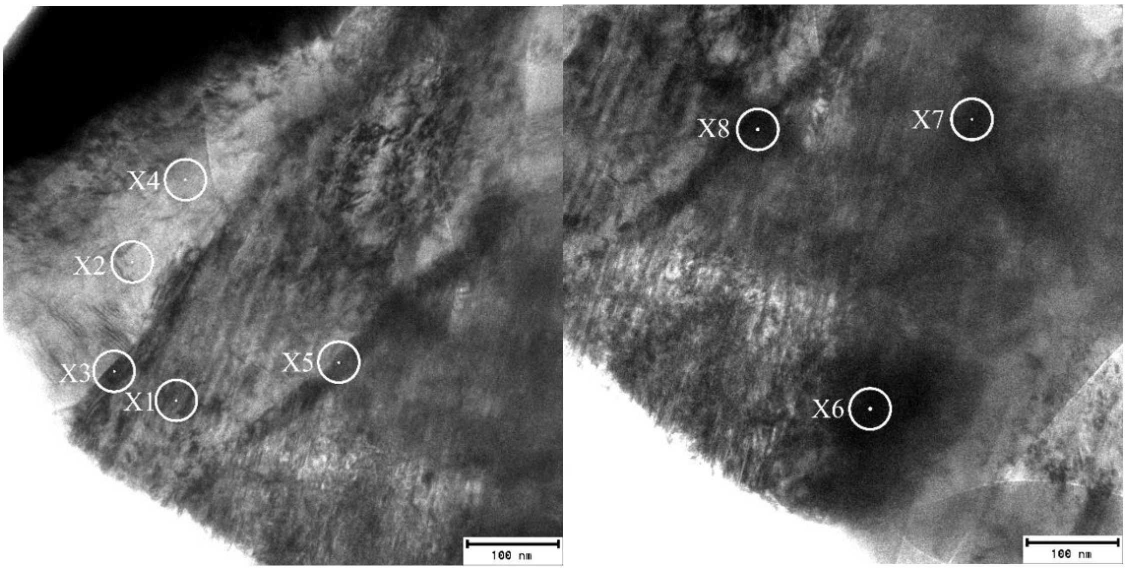

Fig. 70 TEM examination of $Cu_{80}Co_{20}$ microwire. Marked sites represent sites of EDX analyses

negligible composition differences on the examined place. The mark circles correctly represent the electron beam (which is 45 nm wide) showing from which place the information has been taken.

Data gathered by EDX point analyses suggest that there may be grains that cannot be easily distinguished by TEM examinations. Further examinations by HAADF-STEM (Fig. 71) have been conducted to finally confirm existence of Co grains. However, granular structure has been found only in the case of $Cu_{80}Co_{20}$ microwires.

Table 7 Results of EDX analyses on $Cu_{80}Co_{20}$ microwire

$Cu_{80}Co_{20}$	Cu (at. %)	Co (at. %)
X1	95.5	4.5
X2	92.7	7.3
X3	95.1	4.9
X4	96.0	4.0
X5	97.8	2.2
X6	59.7	40.3
X7	84.6	15.3
X8	95.1	4.9

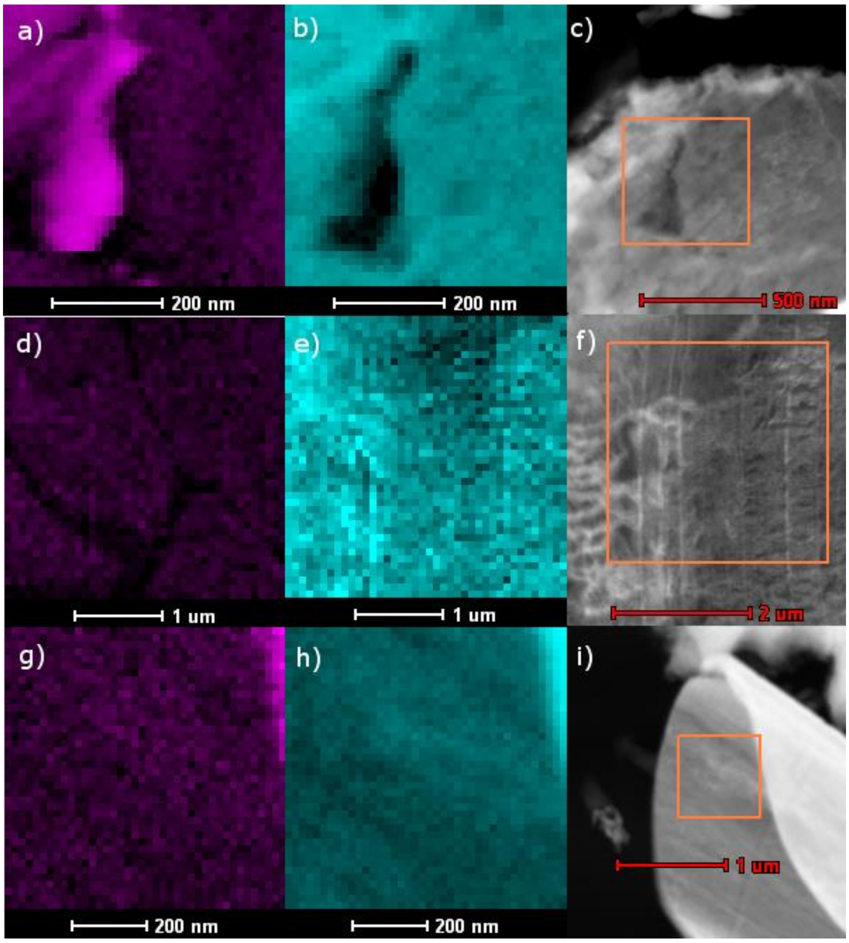

Fig. 71 STEM images of $Cu_{80}Co_{20}$ (a,b,c), $Cu_{90}Co_{10}$ (c,e,f), $Cu_{95}Co_5$ (g,h,i). Purple and teal colours represent Co and Cu atoms, respectively. (c,f,i) shows particular areas chosen for analysis.

5.5.1 Magnetic measurements

Magnetic measurements can provide more information on distribution of Co atoms in the Cu matrix. Hysteresis loops for the $Cu_{90}Co_{10}$ taken at different temperatures are linear in as-prepared state except of the hysteresis loop taken at 5 K (Fig. 72 left). However, hysteresis loops have changed after annealing and they exhibit, contrary to as-prepared samples, ferromagnetic behaviour also at higher temperatures than 5 K and this confirms the increase of ferromagnetic phase after annealing.

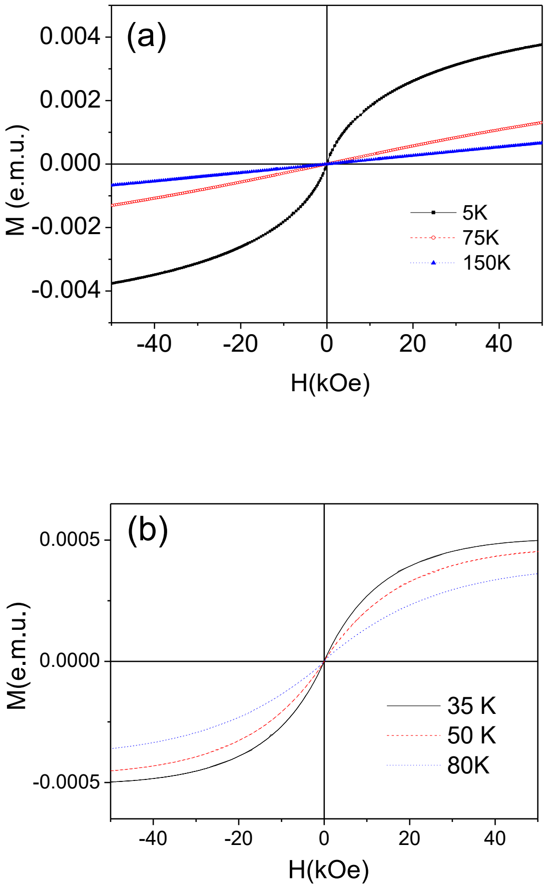

Fig. 72 Hysteresis loops for as-prepared (left) and for annealed (right) CuCo microwires at 400°C for 10 hours.

5.5.2 Magnetoresistance measurements

GMR effect was considerable enhanced after annealing at 673 K. As an example, increase of the GMR effect was observed from 1 to 7.5% in $Cu_{95}Co_5$ microwire (Fig. 73a) and *ΔR/R* increases from 8 to 19% in $Cu_{80}Co_{20}$ microwire for the same annealing conditions (2 hours at 673 K, Fig. 73b). Additionally, we can observe that there is a slight increasing of ΔR/R of $Cu_{80}Co_{20}$ sample after annealing. It can be attributed to the anisotropic resistance related to ferromagnetic grains presence. Observed *ΔR/R(H)* dependences are typical for GMR effect showing decrease of resistance R with increase of magnetic field (Fig. 73).

Brief summary of all GMR measurements is represented on the figures bellow as a dependence of t_{ann} on GMR effect in a magnetic field 5 T for studied CoCu microwires (Fig. 76). The results can be explained in three ways:

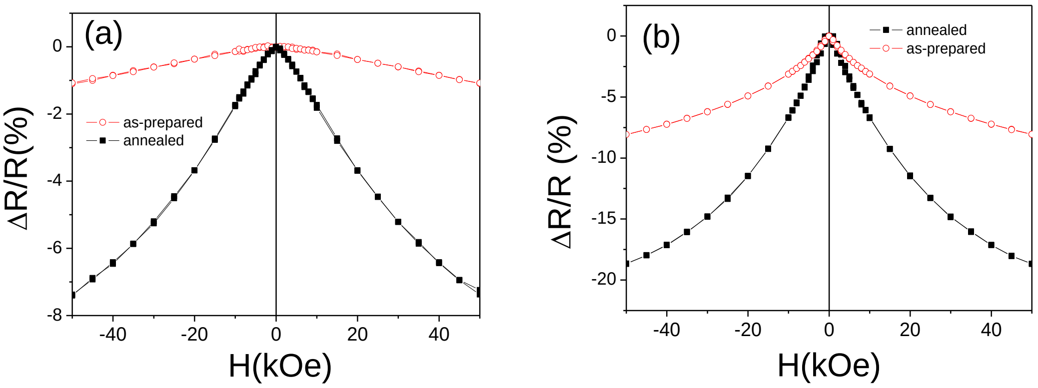

Fig. 73 ΔR/R(H) dependences for Co$_5$Cu$_{95}$ (a) and Co$_{20}$Cu$_{80}$ (b) microwires measured at 5 K in as-prepared and annealed at 673 K for 2 h.

1) Annealing can release the stresses, which in principle influences the metallic core structure. However, this option is the least likely; because the stress relaxation occurs near 373 K – 473 K [117] and measurements made on the samples which were annealed at low temperature show no considerable change to GMR effect.

2) Another potential explanation was offered by [118]. It can be described as fast aggregation and then re-dissolution of cobalt atoms in copper matrix after annealing. Increase of size and number of Co cluster may cause high MR in annealed samples.

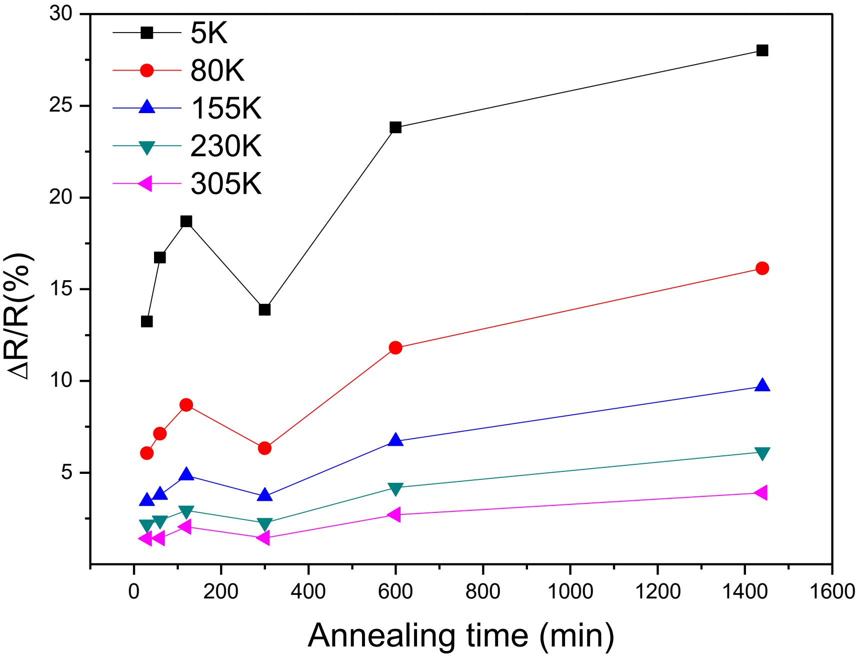

Fig. 74 Summary of all max ΔR/R(H) for Cu$_{80}$Co$_{20}$ microwires at 5 T.

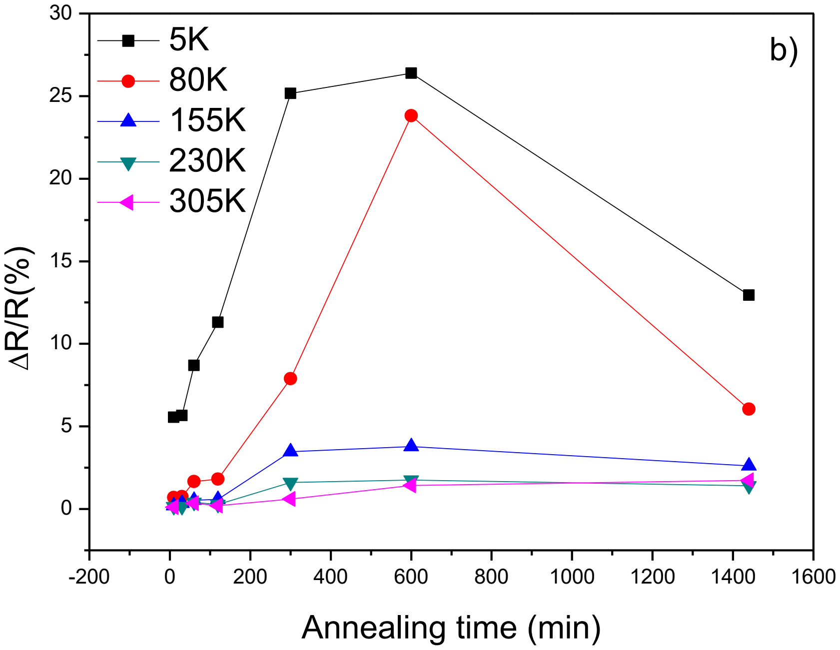

Fig. 75 Summary of all max ΔR/R(H) for $Cu_{90}Co_{10}$ microwires at 5 T.

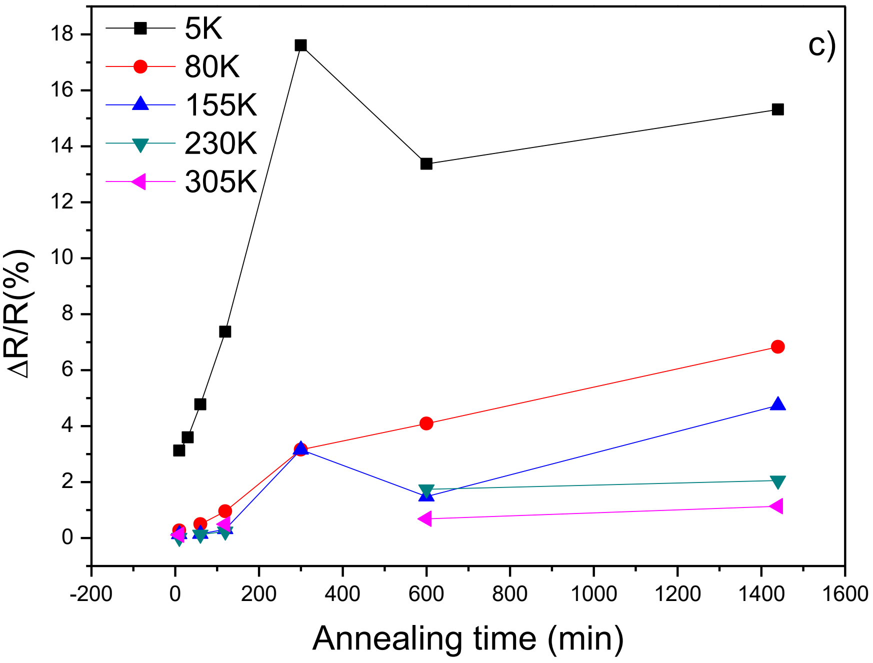

Fig. 76 Summary of all max ΔR/R(H) for $Cu_{95}Co_5$ microwires at 5 T.

3) Additionally, it is possible, that microwire have inhomogeneous parts with higher or lower Co content after production, so some samples have unpredictably high or low magnetoresistance.

Internal stresses result in considerable texture of all the samples. From the previous knowledge on stress relaxation in glass-coated microwires we can assume that the relaxation processes run with temperature starting from 373 K [119]. Stresses have been most probably released after low-temperature annealing (T_{ann}=150-200 °C), but XRD measurements on low temperature annealed samples show no considerable change comparing them to the as-prepared measurements. Moreover, GMR effect was also measured on the samples annealed at 423 K with annealing time 10 hours (Fig. 77) and it revealed only slight enhancement of GMR effect. Thus, it can be assumed that the stress relaxation is not the key factor that affects the MR increase of the studied samples. GMR increase does not seem to be related with the stress relaxation and must be attributed to the short-range ordering processes that cannot be distinguished by the XRD method.

In all GMR systems a high resistivity exists in a conducting medium which is magnetically inhomogeneous or disordered on the scale of the mean-free electron path.

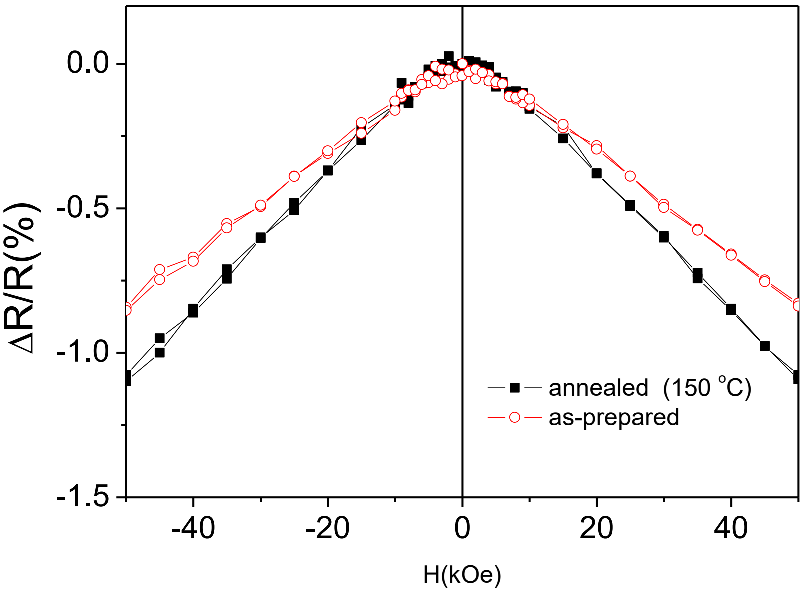

Fig. 77 ΔR/R(H) dependences measured in as-prepared and annealed at 423 K for 10 h $Cu_{95}Co_5$ microwires measured at 5 K.

On the other hand, the GMR appears only in samples with volume fraction X_v less than the percolation volume fraction X_p. At $X_v > X_p$, all the particles form a connecting network with large ferromagnetic domains and low coercivity as in homogeneous ferromagnetic alloys and GMR decreases. Therefore, although we cannot detect any change of phase composition by XRD, observed dependence of the $\Delta R/R$ on T_{ann} must be attributed to the grain size and content change after annealing. The other possible reason of observed changes can be appearance of the nanostructures typical for the spinodal decomposition after annealing [115,118].

On the other hand, there are still open questions as regarding the origin of the GMR effect in materials prepared from immiscible elements. Thus, Co particles embedded in Cu matrix, small Co clusters within a Cu matrix, homogeneous spinodal decomposition characterized by long parallel Co-excess stripes are considered by various authors [118,120]. Moreover Kondo-like behaviour reported even for $Cu_{95}Co_5$ microwires is quite unusual even for alloys containing more than 5%

5.5.3 Kondo-like behaviour

Regarding Kondo effect, even the sample with the lowest content of Co $Cu_{95}Co_5$ cannot be considered as the classical diluted Kondo system because of large amount of Co single-ion concentration but also because part of Co phase forms clusters with local magnetic fields and spin polarization of current carriers. The common explanation of the resistivity minimum is the Kondo effect related to the magnetic impurities in metals. In classical Kondo-systems where the content of magnetic impurities in a metal is small (0,002-0,02 %) it was recognized that the resistance minima is associated with magnetic impurities in the metallic host being one which has a local magnetic moment due to the spin of unpaired electrons in its atomic-like *d* or *f* shell [23]. The scattering processes from magnetic impurities (those in which the internal spin state of the impurity and scattered electron are exchanged) could give rise to a resistivity contribution behaving as ln(T), and hence provide a satisfactory explanation of the observed resistance minima. Additionally, magnetic field usually suppresses the resistivity minimum [121]. But usually the minimum temperature is much lower than observed in all CuCo samples in as-prepared state. In our case the Co content is much higher (5%) and consequently minimum temperature can be higher. To prove aforementioned mechanism, we measured the effect of magnetic field on resistance dependence of temperature for both as-prepared and annealed $Cu_{95}Co_5$ samples and plotted R-R_{min} versus ln T. In our case, some certain similarities with classical Kondo effect were observed (Fig. 78).

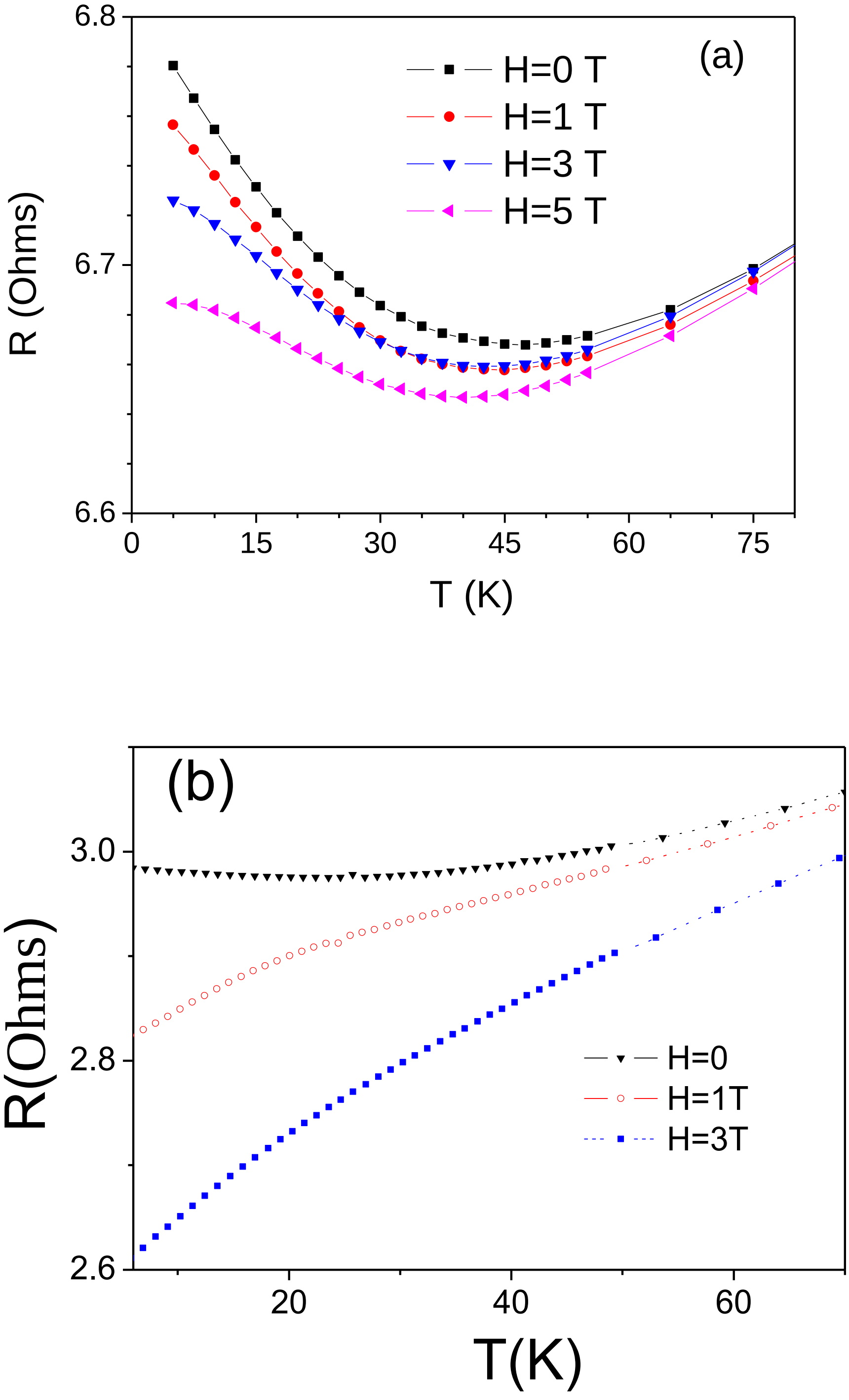

Fig. 78 Effect of magnetic field on temperature dependence of resistance, R, in as-prepared (a) and annealed at 673 K (b) $Cu_{95}Co_5$ microwires

Magnetic field considerably affects the resistivity minimum. It is worth mentioning that if the resistivity minimum of as-prepared samples $Cu_{95}Co_5$ is not completely suppressed even by high magnetic field (H = 5T), resistivity minimum of annealed sample is completely suppressed by H = 1T. Magnetization curves measured in Co-Cu microwires exhibit saturation at 5 K that can be associated with not uniform distribution of Co atoms in the Cu matrix, i.e. with the presence of Co inhomogeneities or clusters. Therefore, studied $Cu_{95}Co_5$ microwire is not a classical diluted Kondo system not only because of large Co single–ion concentration but also because a part of Co ions forms magnetic clusters and these clusters will create local magnetic fields and spin-polarization of current carriers [122].

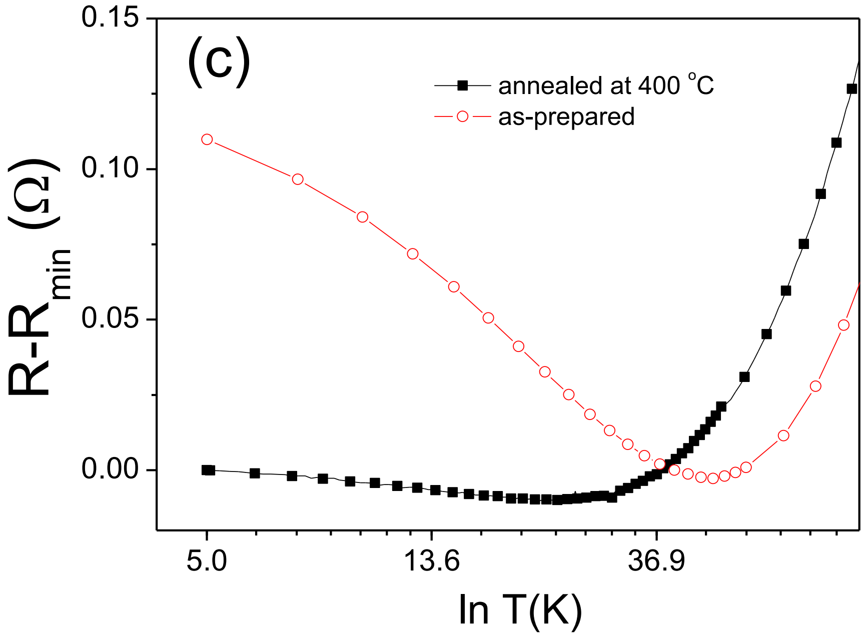

Fig. 79 Logarithmic dependence (ln T) for annealed and as prepared $Cu_{95}Co_5$ samples (c)

Consequently, both as-prepared and annealed $Cu_{95}Co_5$ microwires present certain features typical for the classical Kondo effect related to the magnetic impurities in metals. But the resistivity minimum in as-prepared sample is not completely suppressed even at 5 T, the temperature of resistivity minimum is quite high for diluted Kondo alloys and the concentration of the Co ions distributed randomly in the Cu- matrix is not low. Therefore, we cannot exclude interaction between magnetic Co-ions and, as a result, we can expect partial suppression of Kondo effect. Considering that studied samples present magnetic saturation at 5 K we must assume that the Co-ions are not uniformly distributed in the

Cu-matrix: the regions with higher Co-ions content are responsible for the presence of Co inhomogeneities or clusters, while the regions with lower Co-ions content behave as the magnetic impurities in the metallic host.

Surprisingly, in contrast to the other granular systems where R(T) minimum has been reported [124], we observed huge effect of annealing on minimum temperature, T_K: in our case T_K decreases after annealing from 47 to 22 K.

6 Conclusion

The work provides the basic review of shape memory alloys and materials with giant magnetoresistance. The first part (Chapters 1-3) of the thesis deals with theoretical background. The second part is devoted to experimental methods used (Chapter 4); and the results obtained (Chapter 5). In total, four shape memory materials have been prepared and studied. Moreover, the annealing effect on giant magnetoresistance was studied on three compositions of CuCo microwire. The first prepared sample is superelastic ribbon with $Co_{49}Ni_{21}Ga_{30}$ composition. Ribbon was brittle and only small pieces in length was prepared. The following properties of rapid quenched $Co_{49}Ni_{21}Ga_{30}$ alloy have been confirmed:

- SEM examination on $Co_{49}Ni_{21}Ga_{30}$ shows polycrystalline structure with ±1.49 % deviation from nominal compositions
- XRD revealed single phase at room temperature. Phase crystallize in B2 crystal structure ($Pm\overline{3}m$) with lattice parameter 2.857 Å.
- Magnetic measurement confirmed the presence of martensitic transformation which progresses at transformation temperatures between 179-252 K and 216-149 K for austenite and martensite phase, respectively. High temperature phase has lower magnetic anisotropy than low temperature phase.
- Temperature dependence of resistance confirmed martensitic transformation too. Application of magnetic field shifted start of martensitic transformation to the higher temperatures.
- Poor mechanical properties did not allow to measure the stress-strain curves.

The second prepared sample is superelastic ribbon with $Co_{37}N_{34}iAl_{29}$ composition. Following properties of rapid quenched $Co_{37}N_{34}iAl_{29}$ alloy have been confirmed:

- SEM examination of $Co_{37}N_{34}iAl_{29}$ shows polycrystalline structure with ±2.7% deviation from nominal compositions
- XRD revealed single phase at room temperature. Phase crystallizes in B2 crystal structure ($Pm\overline{3}m$) with lattice parameter 2.8499 Å.

- Magnetic measurements revealed martensitic transformation at low temperatures. High temperature phase shows lower magnetocrystalline anisotropy similarly to the previous sample.
- Resistance measurement showed that it is possible to slightly alter martensitic transformation temperatures and application of magnetic field made transformation range narrow.
- Better mechanical properties allowed to measure strain which reached up to 1.7%. Achieved reversible stress was 0.7%.

The third prepared sample is superelastic ribbon with $Fe_{43.5}Mn_{34}Al_{15}Ni_{7.5}$ composition. Contrary to the previous samples, this composition showed very good mechanical properties. Following properties of rapid quenched $Fe_{43.5}Mn_{34}Al_{15}Ni_{7.5}$ alloy have been confirmed:

- SEM examination revealed polycrystalline, columnar microstructure with a layer of equiaxed crystallized grains.
- XRD confirmed the presence of two phases. Austenite (crystalizes in *fcc*) and martensite (crystalizes in *bcc*), with lattice parameter a_{fcc} = 0.36604 nm and a_{bcc} = 0.29086 nm.
- Magnetic measurement does not show clear transition like in previous samples, but it may be explained in the terms of similar magnetic properties of both phases.
- Maximum achieved strain was 1.7% with very low irreversible strain 0.1% achieved after training.
- $Fe_{43.5}Mn_{34}Al_{15}Ni_{7.5}$ alloy was proved to be capable of sensing the deformation during 1% of strain due to lowering its magnetic permeability by 12%. It points to the fact, that it is possible to use it for contactless sensing of large strain.

The fourth superelastic sample is glass-coated microwire with composition $Co_{51}Cr_{17}Ga_{11}Si_{11}$. Following properties of rapid quenched $Co_{51}Cr_{17}Ga_{11}Si_{11}$ alloy have been confirmed:

- SEM micrographs revealed metallic core inside glass coating. Total diameter of sample was measured to be 25 μm and metallic core has 6.7 μm.
- Microwire crystallizes in B2 structure with space group symmetry $Pm\bar{3}m$ at room temperature. Lattice parameter was determined to be 2.8615 Å.
- We observed uniform orientation of grains in superelastic microwire $Co_{51}Cr_{27}Ga_{11}Si_{11}$ by EBSD analysis. No grain boundaries were found on the various sites of microwire. Preferred orientation in shape memory alloys can provide superior properties observed in studies of monocrystals with rapid quenching that benefit from cheap and fast production.
- Stress-strain curves have been also measured on $Co_{51}Cr_{17}Ga_{11}Si_{11}$ microwires. Achieved reversible strain was 1.65% with very low irrecoverable strain 0.13% (Fig. 67). Sample yielded at 2,5% strain.

Experimental results on CuCo microwires revealed these information:

1. X-ray diffraction revealed the existence of copper and cobalt phases in all compositions. Preferred orientation in as-cast samples decreases after annealing.
2. Areas with lower and higher content of Co have been found during TEM examinations on $Cu_{80}Co_{20}$ sample. Only negligible differences have been found on others composition.
3. GMR significantly increases after annealing. The highest observed GMR (32%) was found in the case of $Cu_{90}Co_{10}$. The best explanation is due to the spinodal decomposition that occurred during annealing.
4. Kondo-like behaviour appears in the temperature dependence of resistance and in the as-cast sample it is not possible to diminish it by application of strong magnetic field. On the other side, Kondo-like behaviour is diminished in the annealed samples by quite low magnetic fields. This also suggests the occurrence of spinodal decomposition.

7 Conclusion related to further development of scientific object and potential application.

The most interesting result of the shape memory research was found in $Fe_{43.5}Mn_{34}Al_{15}Ni_{7.5}$ ribbon and $Co_{51}Cr_{27}Ga_{11}Si_{11}$ microwire. $Fe_{43.5}Mn_{34}Al_{15}Ni_{7.5}$ ribbon may act as a sensor with good mechanical properties. Consequently, heat treatment may be applied to release internal stress in order to improve superelasticity. However, this need proper examination on the real material. Internal stress may play important role in critical stress value, which is necessary for beginning of the phase transformation.

No crystal boundaries have been found in superelastic $Co_{51}Cr_{27}Ga_{11}Si_{11}$ microwire so far. It points to the fact that $Co_{51}Cr_{27}Ga_{11}Si_{11}$ may be monocrystalline along entire length. SMA alloys strain more in their particular direction and monocrystals are known to have the biggest strain. Thus, more EBSD measurement should be carried out with the most important measurement of cross section to confirm or disprove this hypothesis. Easily prepared microwire with desired orientation of grains would have advantage because of lower price and lower time needed for preparation over other types of materials.

Although many applications have been developed so far, there is still a lot of ideas and potential uses of studied samples to work on. Brittle superelastic samples could be embedded into metal matrix to contactless sensing deformation in construction applications. Moreover, preparation of microwires would diminish ductility problem, because glass stabilises metal core, thus alloys may be used as sensors also on surface or inside of materials. Glass protection make the microwire biocompatible as well. This opens application in biomedicine field as contactless sensors of temperature or stress.

There are few ideas on CuCo microwires too. It would be very interesting to examine the progress of spinodal decomposition during annealing by evaluation of the STEM micrographs with chemical composition maps on the wires with different time of annealing. This would give us deeper understanding on how spinodal decomposition progresses.

8 Resumé in Slovak

Práca sa venuje príprave rýchlo chladených funkčných magnetických materiálov a charakterizácii ich vlastností. V prvých dvoch kapitolách sa nachádza teoretické vysvetlenie javu tvarovej pamäte, superelasticity a javu obrovskej magnetorezistencie. Jav tvarovej pamäte predstavuje proces, ktorý dovoľuje deformovanému materiálu vrátiť sa do pôvodného tvaru po tepelnej aktivácii. Superelasticita je špecifické správanie materiálu s javom tvarovej pamäte, ktorý nevyžaduje tepelnú aktiváciu a materiál nadobudne pôvodný tvar bez tepelnej aktivácie, ale okamžite po uvoľnení pnutia. Polykryštalické materiály sú schopné dosiahnuť superelastické predĺženia až o 13% a v prípade monokryštálov až do 20%. Tieto zliatiny sa už komerčne využívajú hlavne v robotike, v biomedicíne, v automobiloch a v letectve.

Jav tvarovej pamäte môže prebiehať troma hlavnými spôsobmi:

- Jednosmerný jav tvarovej pamäte: zliatina sa vracia do pôvodného tvaru po tepelnej aktivácii.
- Dvojsmerný jav tvarovej pamäte: zliatina si pamätá vysokoteplotný a nízkoteplotný tvar. Mechanická deformácia nie je nutná.
- Superelasticita: Zliatina nadobúda pôvodný tvar okamžite po odľahčení.

Pre zliatiny s javom tvarovej pamäti je nevyhnutná prítomnosť fázovej transformácie, ktorá prebieha výlučne v pevnom skupenstve medzi dvoma fázami. Tento proces sa bežne označuje ako martenzitická transformácia, pričom nízkoteplotná fáza (stabilizovaná pnutím) sa nazýva martenzit a vysokoteplotná fáza (stabilná bez pnutia) je označovaná ako austenit. Jav tvarovej pamäte je umožnený kooperatívnym presunom atómov na kratšie vzdialenosti ako medziatómová vzdialenosť. Martenzitická transformácia prebieha organizovane tak, aby susedné atómy ostali rovnaké, čím sa líši od plastickej deformácie. Pre opísanie javu tvarovej pamäte je potrebné definovať nasledujúce pojmy:

- Transformačné teploty: predstavujú teploty pri ktorých sa začína alebo končí prechod z jednej fázy do druhej, pre austenit a martenzit opisujeme ich štartovaciu a finálnu teplotu. Transformačné teploty tak určujú pracovný rozsah zliatin, v ktorom možno ich vlastnosti využiť.
- Predĺženie: pri opise jednotlivých súbežne prebiehajúcich zložiek predlženia sa používajú nasledovné termíny: nevratné predlženie ε_{irr} predstavuje

plastickú deformáciu. Vratné elastické predĺženie ε_{rec} je typické pre všetky materiály a riadi sa Youngovým modulom pružnosti. Vratné superelastické predĺženie je spôsobené javom tvarovej pamäte a jeho veľkosť určuje zmena kryštalickej štruktúry a zmena jej mriežkovej konštanty.

Za najpoužívanejšiu a najznámejšiu zliatinu s javom tvarovej pamäte je zliatina niklu a titanu, známa aj ako nitinol. Viac ako 90% aplikácii je založených práve na zliatinách na báze titanu a niklu. Avšak napriek tomu, výskum za účelom objavenia nových zliatin nekončí, ale výskum je zameraný na zliatiny, ktoré majú vhodnú pracovnú teplotu s vysokými hodnotami maximálneho predĺženia. Takisto objav feromagnetických zliatin s javom tvarovej pamäte otvoril celú škálu nových aplikácii, kde aktuátor môže zároveň slúžiť aj ako senzor.

Vybrané druhy Heuslerových zliatin sú súčasne feromagnetické a zároveň vykazujú jav tvarovej pamäte alebo superelasticitu. Heuslerove zliatiny sa delia medzi 2 základné kategórie:

- Polovičné Heuslerove zliatiny majú stechiometrický pomer prvkov XYZ a väčšinou kryštalizujú v kubickej štruktúre bez centrálnej symetrie (priestorová grupa č. 216, $F\bar{4}3m$, $C1_b$)
- Plné Heuslerove zliatiny majú štruktúrny vzorec X_2YZ a kryštalizujú v kubickej štruktúre (priestorová grupa č. 225, $Fm\bar{3}m$, $L2_1$)

Atóm na pozícii X spravidla patrí do druhej polovici d prvkov, prvok Y patrí medzi lantanoidy a prvú polovicu d prvkov a Z prvkom bývajú p kovy a polokovy. Ich vzájomné atómové usporiadanie je silno späté s vlastnosťami Heuslerových zliatin. Aj malé nečistoty môžu pozmeniť atómovú štruktúru, čiže aj vlastnosti Heuslerovych zliatin. Preto je veľmi dôležité poznať zákonitosti, ktorými sa ich štruktúra riadi.

Druhý typ vzoriek, ktorými sa táto práca zaoberá sú materiály s obrovskou magnetoresistenciou. Magnetorezistencia je zmena elektrického odporu vplyvom vonkajšieho magnetického poľa. Existuje vo všetkých reálnych kovoch a jej amplitúda sa jemne líši pre rôzne typy kovov, zvyčajne však ako malá zmena odporu do 0.1%. Jav obrovskej magnetorezistencie sa prejavuje ako výrazná zmena odporu v magnetickom poli (až do 50%), ktorá je spôsobená orientáciou magnetizácie v magnetických časticiach, ktoré sú obklopené vodivým, ale nemagnetickým materiálom, Zníženie odporu v magnetickom poli je spôsobené orientáciou magnetických momentov v magnetickej vrstve. V prípade, že je vonkajšie magnetické pole nulové (resp. dostatočne malé) sú magnetické momenty orientované náhodne. Ak vodivostné elektróny majú opačný spin ako magnetická vrstva dochádza k rozptylu elektrónov a vysokému odporu. Avšak pri zapnutí vonkajšieho magnetického poľa sa jednotlivé magnetické momenty natočia do jedného smeru. Takýto scenár dovoľuje prejsť časti voľných elektrónov bez rozptylu, čo znižuje odpor.

Prvýkrát bol tento jav zaznamenaný v roku 1988 dvoma nezávislými výskumnými skupina vedenými A. Fertom a P. Grünbergom, ktorí za tento objav získali Nobelovu cenu v roku 1997. Jav obrovskej magnetorezistencie objavili na tenkom filme zloženého z dvoch vrstiev železa, ktorá je predelená nemagnetickou vodivou vrstvou chrómu. Tenké vrstvy sa zvyčajne pripravujú naprašovaním alebo elektrodepozíciou. Tieto metódy patria medzi drahé a časovo náročné. Javom obrovskej magnetorezistencie bol však neskôr objavený aj v granulárnych materiálov, kde sú magnetické častice náhodne rozložené vo vodivom nemagnetickom materiáli. Príklad takéhoto materiálu je možné jednoducho pripraviť použitím Taylor-Ulitovského metódy s rýchlym chladením.

Metódy rýchleho chladenia ponúkajú radu výhod oproti bežným spôsobom prípravy vzoriek:

- zvyšujú rozpustnosť jednotlivých vzoriek, častokrát rádovo
- ponúkajú možnosť prípravy vzoriek s rozličným zložením
- dávajú možnosť pripraviť metastabilné a nerovnovážne fázy
- znižujú počet a veľkosť prípadných nevyžiadaných segregovaných fáz

Pre účely tejto práce boli využité dve metódy rýchleho chladenia; metóda liatia taveniny na rýchlo rotujúci valec za vzniku tenkých pások a Taylor-Ulitovského metóda prípravy sklom potiahnutých mikrodrôtov. Predzliatiny boli pripravené oblúkovým tavením a následne použité na prípravu rýchlo chladených materiálov.

Superelastické pásky so zložením $Co_{49}Ni_{21}Ga_{30}$., $Co_{37}N_{34}iAl_{29}$ a $Fe_{43.5}Mn_{34}Al_{15}Ni_{7.5}$ boli pripravené použitím metódy liatia taveniny na rotujúci valec. Pomocou tejto metódy je možné v našich podmienkach pripraviť polykryštalické pásky široké do 3 mm a tenké od 25-55 µm. Predzliatina je najprv uložená v skúmavke s dierou a roztavená indukčným ohrevom. Po nadobudnutí správnej teploty je vystrelená na rotujúci valec. Pásky sú vystrelené za prítomnosti ochrannej atmosféry hélia, ktorá zabraňuje oxidácii materiálu a zároveň umožňuje tepelnú výmenu. Rýchlosť rotácie pásky bola pri všetkých prípravách superelastických vzoriek nastavená na 20 ms^{-1}.

Taylor-Ulitovského metóda bola použitá na prípravu superelastického mikrodrôtu $Co_{51}Cr_{27}Ga_{11}Si_{11}$ a na prípravu magnetorezistívnych mikrodrôtov CuCo. Hlavná výhoda tejto metódy spočíva v možnosti:

- opakovať a škálovať produkciu pri masovej výrobe
- meniť a kontrolovať geometrické (priemer kovového jadra a hrúbku skla) vlastnosti počas prípravy drôtov a tým ovplyvňovať výsledné fyzikálne vlastnosti
- pripraviť dlhé kusy neprerušovaných mikrodrôtov až do dĺžky 10 km

Počas prípravy je predzliatina umiestnená v skúmavke a zahrieva sa indukčným tavením. Následne keď je zliatina roztavená a jej teplota je dosť vysoká na to, aby zmäkčila sklo je možné začať s prípravou mikrodrôtu. Dotykom sklenej tyčinky sa zachytí zmäknuté sklo a ťahaním nadol využitím kapilárneho efektu sa vytvára sklom potiahnutý mikrodrôt. Vzorky boli skúmané nasledovnými metódami:

- skenovacia elektrónová mikroskopia SEM (JEOL 6100),
  transmisná elektrónová mikroskopia TEM (Philips SuperTwin CM200 a TECNAI G2 20 TWIN),
- detekcia charakteristického röntgenového žiarenia EDX,
- difrakcia spätne odrazených elektrónov EBSD,
- difrakcia röntgenového žiarenia XRD (BRUKER D8 Advance),
- merania závislosti magnetizácie od magnetického poľa a teploty (Quantum design MPMS),
- merania závislosti odporu od magnetického poľa (Quantum design PPMS),
- merania napäťovo-deformačných kriviek (DMA TA Q800),
- merania napäťovo-deformačných kriviek na aparatúre s doplneným meraním na zmenu permeability.

Prvá pripravená vzorka vo forme pásky má zloženie $Co_{49}Ni_{21}Ga_{30}$. Boli pripravené iba krátke kúsky pásky vo veľkosti do 1 cm. Pozorovanie mikroštruktúry skenovacím elektrónovým mikroskopom odhalilo polykryštalický charakter vzorky. Takisto bol pozorovaný kolmý rast kryštálov na plochu pásky, ktorý je pravdepodobne spôsobený veľkým teplotným rozdielom vytvorený rýchlym chladením. Veľkosť kryštálov sa pohybovala od 10-30 μm. Analýza EDX bola prevedená na piatich rôznych miestach a na troch rôznych kúskoch pásky. Priemerné chemické zloženie pásky je $Co_{49.4}Ni_{20.6}Ga_{30.0}$. Odchýlka od želaného zloženia bola maximálne ±1,49 %. Dostatočná homogenita vzorky bola dosiahnutá aj bez potreby žíhania predzliatin a pripravených pások.

Röntgenová analýza pri izbovej teplote odhalila prítomnosť jednej fázy. Jedná sa o *B2* štruktúru s označením $Pm\bar{3}m$, kde dochádza k náhodnému obsadzovaniu Y a Z pozícií atómami niklu a gália. Mriežkový parameter pre túto fázu je 2,857 Å.

Z magnetických meraní vidno prítomnosť fázovej premeny, ktorá prebieha pod izbovou teplotou. Vykazuje hysterézu, z ktorej boli stanovené transformačné teploty. Austenitická štartovacia teplota bola stanovená na 179 K a jej finálna teplota na 252 K. Martenzit sa začína vytvárať pri teplote 216 K a končí pri 149 K. Hysterézne slučky boli namerané pri dvoch rôznych teplotách, pri 90 K, keď sa zliatina nachádza v plne martenzitickej fáze a pri 265 K, keď je zliatina v plne austenitickej fáze. Slučky ukazujú, že vysokoteplotná a nízkoteplotná fáza majú rôznu magnetokryštalickú anizotropiu. Hodnota poľa nasýtenej magnetizácie totiž dokazuje prítomnosť vyššej anizotropie v prípade nízkoteplotnej fázy. Tá ma nasýtenú magnetizáciu pri hodnote vonkajšieho magnetické poľa 1,25 kOe, zatiaľ čo nízkoteplotná fáza je nasýtená až pri poli 7 kOe.

Z teplotnej závislosti elektrického odporu možno vidieť posun martenzitickej transformácie k vyšším teplotám. Martenzitická štartovacia teplota sa posunula z 216 K až na 230 K.

Druhou pripravenou vzorkou bola páska so zložením $Co_{37}N_{34}iAl_{29}$. Po príprave pásky vznikli kúsky dlhé niekoľko centimetrov. Pod skenovacím elektrónovým mikroskopom bolo jasne vidieť polykryštalickú štruktúru a veľkosť jednotlivých zŕn sa pohybuje v rozmedzí 1-2 μm. Hrúbka pásky bola odmeraná v rozmedzí 25-40 μm. Takisto boli pozorované oblasti s kolmým rastom kryštálov na plochu pásky a náhodne orientovanú granulárnu štruktúru. Malé kryštály majú výhodu, pretože ich hranice fungujú ako nukleačné centrá pre fázovú premenu, ktorá takto prebieha rýchlejšie. Tým sa znižuje reakčný čas martenzitickej transformácie. Chemická analýza prebehla na troch rôznych kúskoch pásky a priemerné chemické zloženie je $Co_{38.3}Ni_{33.4}Al_{28.2}$ pričom maximálne rozdiely v zložení boli ± 2,7.

Röntgenová analýza pri izbovej teplota potvrdila prítomnosť jednej fázy, ktorá je považovaná za *B2* variant Heuslerovej fázy $L2_1$ podobne ako pri zliatine so zložením $Co_{49}Ni_{21}Ga_{30}$.. Mriežkový parameter pre túto fázu je 2.8499 Å.

Teplotná závislosť magnetizácie poukazuje na prítomnosť martenzitickej transformácie prebiehajúcou pod izbovou teplotou. Transformačné teploty nie sú jasne ohraničené. Začiatok fázovej premeny na martenzit bol stanovený z teplotnej závislosti magnetizácie na 150 K a jej koniec na 75 K. Austenit začína kryštalizovať pri teplote 80 K a končí pri teplote 170 K. Hysterézne slučky boli namerané pri teplote 10 K (zliatina je v martenzite) a pri 190 K (zliatina je v austenite). Z tvaru hysteréznych slučiek možno vyčítať, že vysokoteplotná fáza má vyššiu magnetokryštalickú anizotropiu. Tento fakt je ešte viac viditeľný na krivkách prvotnej magnetizácie. Nasýtená magnetizácia je totiž pre vysokoteplotnú fázu dosiahnutá už pri magnetickom poli 4 kOe a pre nízkoteplotnú fázu až pri poli 9 kOe. Merania odporu dokazujú prítomnosť fázovej premeny zatiaľ čo posúvajú martenzitickú a austenitickú štartovaciu teplotu k vyšším teplotám. Zmeny transformačných teplôt pre rôzne polia možno vidieť v tabuľke 1.

Tab. 1 Teploty martenzitickej transformácie a ich posun

Meranie	M_s	M_f	A_s	A_f
M(T)	150 K	75 K	80 K	170 K
R(T) 1T	175 K	95 K	65 K	175 K
R(T) 2T	160 K	100 K	105 K	165 K
R(T) 5T	165 K	105 K	110 K	170 K

M (T) predstavuje meranie teplotnej závislosti magnetizácie

R (T) predstavuje meranie teplotnej závislosti odporu

Maximálne dosiahnuté vratné predĺženie na vzorke $Co_{37}N_{34}iAl_{29}$ bolo 0,8 % s 0,3% nevratným predĺženia. Takisto bolo namerané predĺženie 0,2% pri takmer nulových pnutiach, ktoré je dosiahnuté iba narovnaním vzorky a nie je výsledkom superelasticity. Kritické predĺženie dosiahlo hodnotu 1,7%. spolu s 0,8% predĺžením spôsobeným narovnaním vzorky.

Tretia pripravená superelastická vzorka má zloženie $Fe_{43.5}Mn_{34}Al_{15}Ni_{7.5}$. Analýza elektrónovým mikroskopom odhalila polykryštalickú štruktúru s kolmým rastom kryštálov podobným ako u vzorky so zložením $Co_{49}Ni_{21}Ga_{30}$.. Navyše na strane ktorá bola v kontakte s chladeným valcom je možné pozorovať rast granulárnych kryštálov, ktoré naznačujú vysokú rýchlosť chladenia. Páska je hrubá okolo 40-55 μm.

Röntgenová analýza pri izbovej teplota poukázala na prítomnosť dvoch fáz označených ako α a γ', pričom α fáza kryštalizuje v kubickej plošne orientovanej mriežke a γ' kryštalizuje v priestorovo orientovanej kubickej mriežke. Za martenzitickú fázu je považovaná mriežka γ' s mriežkovým parametrom a_{bcc} = 2,9086 Å. Mriežkový parameter pre α fázu je a_{fcc} = 3,6604 Å. Porovnaním intenzít bolo možné určiť relatívny pomer objemu oboch fáz. Ukázalo sa, že pri izbovej teplote sa 88% zliatiny nachádza vo vysokoteplotnej austenitickej fáze a 12% fázy je v martenzitickej fáze.

Z teplotnej závislosti magnetizácie nebolo možné odhaliť prítomnosť martenzitickej transformácie. Medzi chladiacim a zahrievacím cyklom nevidno výrazný rozdiel v magnetizácii vzorky. To môže byť spôsobené širokým rozsahom martenzitickej transformácie, kde celková zmena prebieha postupne v širokom rozhasu teplôt, čím je hysterézia potlačená. Curieho teplota okolo 400 K ukazuje možnosť využitia vzorky ako senzor. Vysokoteplotná fáza dosahuje nasýtenie magnetizácie pri poli 6 kOe a nízkoteplotná fáza pri 2,3 kOe. To naznačuje, že nízkoteplotná fáza má vyššiu magnetokryštalickú anizotropiu, opačne ako v prípade vzoriek $Co_{49}Ni_{21}Ga_{30}$. a $Co_{37}N_{34}iAl_{29}$.

Napäťovo deformačné krivky boli namerané pri rôznych teplotách za účelom potvrdenia superelasticity. Na vzorke bol zároveň pozorovaný vplyv tréningu, keď po niekoľkých cykloch bolo znížené nevratné predĺženie z 1% na 0,1%. Maximálne vratné predĺženie bolo 1,7%. Napäťovo deformačné krivky boli doplnené aj o merania zmeny permeability. Maximálne vratné predĺženie dosiahlo hodnotu 1%. Počas merania klesla permeabilita o 12%. Permeabilita vykazuje iba drobnú hysteréziu medzi zaťažením a odľahčením vzorky. Úzka hysterézia je totiž dôležitým faktorom pre výrobu presného senzoru predĺženia. Navyše, rozdiel v permeabilite pri nulovom pnutí pred a po meraní poukazuje na fakt, že zmena permeability je spôsobené fázovou premenou a rozdielom vo vlastnostiach fáz a nie kvôli závislosti permeability od pnutia.

Posledná superelastická vzorka má zloženie $Co_{51}Cr_{27}Ga_{11}Si_{11}$ a bola pripravená vo forme sklom potiahnutého mikrodrôtu. Pod elektronovým mikroskopom bolo možné odlíšiť kovové jadro od skleneného obalu a odmerať ich geometrické vlastnosti. Celkový priemer drôtu je 25 μm a priemer kovového jadra je 6,7 μm. Avšak, polykryštalický charakter vzorky nebol pozorovaný ako v prípade pások. EDX analýza bola vykonaná na 2 rôznych kúskoch mikrodrôtu s odhaleným kovovým jadrom. Výsledky EDX analýzy ukazujú že pripravené zloženie ($Co_{51.39}Cr_{25.99}Ga_{11.33}Si_{11.29}$) je v zhode so želaným zložením (± 1 at.%).

Prítomnosť jednej fázy bola potvrdená röntgenovou analýzou. Mikrodrôt kryštalizuje v B2 štruktúre s priestorovou symetriou $Pm\bar{3}m$ a s mriežkovým parametrom 2,8615 Å. Medzi najzaujímavejší objav na tomto mikrodrôte patrí detekcia spätne odrazených elektrónov. Tieto merania boli vykonané na viacerých kusoch mikrodrôtu a kryštalografický smer je <111> pre všetky zrná rovnobežne s osou mikrodrôtu. Žiadne hranice zŕn neboli pozorované.

Magnetické merania potvrdili prítomnosť martenzitickej transformácie v teplotnom rozsahu od 100 K do 300 K. Hysterézne slučky boli namerané pri teplotách 10 K a 300 K. Nízkoteplotná fáza má nižšiu anizotropiu v porovnaní s vysokoteplotnou fázou čo bolo určené z rozdielu nasýtenej magnetizácie medzi vysokoteplotnou (280 Oe) nízkoteplotnou (50 Oe) fázou.

Napäťovo deformačné krivky boli namerané na zväzku 19 mikrodrôtov. Maximálne dosiahnuté vratné predĺženie bolo 1,65% s veľmi malým nevratným predĺžením 0,13%. Treba podotknúť, že nízka hodnota nevratného predĺženia bola dosiahnutá bez trénovania, hneď počas prvého merania. To môže byť spôsobené vhodnou orientáciou kryštálov a neprítomnosťou hraníc kryštálov. Predĺženie bolo dosiahnuté aj bez nutnosti žíhania vzoriek.

Mikrodrôty so zložením $Cu_{80}Co_{20}$, $Cu_{90}Co_{10}$ a $Cu_{95}Co_5$ boli študované za účelom zistenia vplyvu žíhania na jav obrovskej magnetorezistencie. Vzorky boli žíhané pri teplote 673 K po dobu 10, 30, 60 minút a 2, 5, 10, 24 hodín. Takisto bolo prevedené nízkoteplotné žíhanie s rôznymi teplotami (423 K a 473 K) a čase žíhanie 2, 10, 24 hodín.

Pomocou röntgenovej analýzy boli identifikované 2 rôzne fázy vo všetkých Cu-Co vzorkách; *fcc* mriežka medi a *hcp* mriežka kobaltu. Jednotlivé intenzity reflexií naznačujú prítomnosť preferovanej orientácie kryštálov. Ústup preferovanej orientácii kryštálov možno pozorovať hlavne v prípade mikrodrôtu so zložením $Cu_{95}Co_5$. Po vyžíhaní vzorky so zložením $Cu_{90}Co_{10}$ a $Cu_{80}Co_{20}$ nevidno výrazné zmeny v intenzite reflexií.

Na štúdium mikroštruktúry vzoriek bola použitá transmisná skenovacia mikroskopia. Keďže rozpustnosť kobaltu v medi je okolo 6%, dá sa predpokladať, že vo vzorkách s vyšším obsahom kobaltu sa objavia granulárne štruktúry. Za účelom objavenia týchto granulárnych štruktúr bola vykonaná bodová EDX analýza v mikrodrôte na rôznych miestach. Avšak granulárna štruktúra bola objavená iba v prípade vzorky $Cu_{80}Co_{20}$. Bodová EDX analýza zbiera údaje zo 45 nm okolia. Pre účely lepšieho pokrytia plochy boli vytvorené TEM mapy chemického zloženie. Avšak podobne ako v predchádzajúcom prípade, objavené granulárne štruktúry boli len v prípade vzoriek $Cu_{80}Co_{20}$.

Magnetické merania poskytli lepší pohľad na distribúciu kobaltových atómov. Napríklad, hysterézne slučky pre $Cu_{90}Co_{10}$ pri rôznych teplotách sú lineárne pred žíhaním okrem krivky meranej pri 5 K. Avšak, po žíhaní prejavujú mikrodrôty feromagnetické správanie aj pri vyšších teplotách ako 5 K, čo naznačuje ich zvýšený výskyt.

Po žíhaní vzoriek pri teplote 673 K nastalo výrazné zlepšenie javu obrovskej magnetorezistencie. Napríklad, magnetorezistencia pre vzorku Co_5Cu_{95} dosiahla pred žíhaním 1% zmenu odporu a po desaťhodinovom žíhaní až 7,5% a pre vzorku $Cu_{80}Co_{20}$ jav obrovskej magnetorezistencie vzrástol z 8% na 19% pri rovnakých podmienkach žíhania.

Vnútorné pnutia vytvorené rôznym konštantami teplotnej rozťažnosti môžu byť jednou z príčin zvýšenia javu obrovskej magnetorezistencie. Táto možnosť však bola vylúčená meraniami zmeny odporu na vzorkách s nízkoteplotným žíhaním, pretože pnutia vytvorené rôznou teplotnou rozťažnosťou by sa uvoľnia už pri žíhaní nad teplotu 373 K. Avšak z röntgenovej difrakcie pre vzorky žíhané pri 373 K a 423 K nevidno výraznú zmenu v štruktúre. Nebol pozorovaný ani nárast magnetorezistencie na týchto vzorkách. Z toho vyplýva, že vnútorné pnutia v mikrodrôte kľúčovú rolu na nárast javu obrovskej magnetorezistencie.

Nárast magnetorezistencie môže byť vysvetlený spinodálnou dekompozíciou, ktorá predstavuje rýchlu segregáciu kobaltových iónov v mikrodrôte po žíhaní. Nárast veľkosti a množstva kobaltových častíc počas žíhanie tak vedie k nárastu magnetoresistencie. Z grafov s maximálnymi zmenami magnetorezistencie v magnetickom poli 5 T je možné porozovať odchýlky od očakávaného priebehu. To je však možné vysvetliť tým, že mikrodrôt nie je homogénny po celej dĺžke.

Na vzorkách bol takisto pozorovaný Kondov jav, ktorý predstavuje výskyt minima v teplotnej závislosti odporu pri poklese teploty pri nízkych teplotách. Kondov jav je spôsobený prítomnosťou magnetických nečistôt v kovovom materiáli, na ktorých dochádza k rozptylu vodivostných elektrónov. Avšak, zvyčajne sa Kondov jav objavuje ak je v materiáli malé množsto týchto nečistôt zvyčajne v rozmedzí 0,002-0,02%. Takto, ani vzorka s najmenším obsahom kobaltu nemôže byť považovaná za klasický materiál vykazujúci Kondov jav. V klasickom prípade Kondovho javu ho magnetické pole potláča. Merania vplyvu magnetického poľa na teplotnú závislosť odporu na nežíhaných vzorkách však ukazujú, že ani veľké magnetické pole (5 T) nedokáže úplne potlačiť Kondov jav. Naopak, v prípade žíhaných vzoriek je možné potlačiť Kondov jav už pri magnetickom poli 1 T.

Medzi najzaujímavejšie výsledky na superleastických vzorkách je považovaný výskum pásky so zložením $Fe_{43.5}Mn_{34}Al_{15}Ni_{7.5NiAl}$ a výskum na mikrodrôte so zložením

$Co_{51}Cr_{27}Ga_{11}Si_{11}$. Vzorka $Fe_{43.5}Mn_{34}Al_{15}Ni_{7.5}$ ukázala zaujímavé vlastnosti, ktoré možno využiť pri tvorbe senzoru. Zároveň má vhodné mechanické vlastnosti a je jednoduché ju pripraviť. Ďalší výskum je možné zamerať na vplyv žíhania na superelastické vlastnosti. Žíhaním sa však uvoľnia aj vnútorné pnutia, ktoré môžu mať vplyv na začiatok fázovej premeny.

V prípade vzorky $Co_{51}Cr_{27}Ga_{11}Si_{11}$ neboli pozorované žiadne hranice zŕn. Z toho vyplýva, že mikrodrôt by mohol byť monokryštalický po celej dĺžke mikrodrôtu. Avšak, merania boli uskutočnené len z povrchu mikrodrôtu. Merania z prierezu by ukázali štruktúru vo vnútri mikrodrôtu čím by potvrdili alebo vyvrátili túto hypotézu. Možnosť pripraviť mikrodrôt s vhodne orientovanými kryštálmi predstavuje výhodu v nižšej cene a v kratšom čase prípravy oproti materiálom pripravenom inými metódami.

Aj keď bolo doteraz vyvinutých veľa aplikácií, ešte stále je možné prísť s novými nápadmi a s potencionálnymi aplikáciami. Častice krehkých superelastických vzoriek môžu byť vložené do iných materiálov za účelom sledovania ich deformácie. Navyše, príprava týchto zložení vo forme sklom potiahnutých mikrodrôtov môže odstrániť problém s krehkosťou, ak sklo stabilizuje kovové jadro. Sklený obal môže poskytnúť biokompatibilitu a využitie týchto materiálov v medicíne.

Na vzorkách s obrovskou magnetorezistenciou by bolo zaujímavé vidieť, akým spôsobom spinodálna dekompozícia vo vzorke postupuje s časom žíhanie. S využitím transmisného elektrónového mikroskopu by bolo možné pripraviť mapy chemického zloženia na drôtoch s rôznymi podmienkami žíhania.

9 Resumé in Spanish

La presente tesis doctoral se fundamenta en la preparación de materiales magnéticos funcionales por el enfriamiento ultrarrápido y en la caracterización de sus propiedades. Los dos primeros capítulos son dedicados a la explicación teórica de la memoria de forma, la súper elasticidad, y la magnetorresistencia gigante. La memoria de forma es un proceso que permite al material deformado regresar a su forma original después del calentamiento térmico. La súper elasticidad es el comportamiento específico de los materiales en el cual el material recupera su forma original sin activación térmica, inmediatamente después de la liberación de las tensiones aplicadas. Los materiales policristalinos son capaces de lograr la extensión súper elástica de hasta 13%, en cuanto los mono-cristales hasta 20%. Estas aleaciones ya tienen uso comercial en la robótica, la biomedicina, la automoción y la aviación.

Existen tres tipos principales de efectos de memoria de forma:

- Memoria de forma unidireccional: la aleación recupera su forma original después de la activación térmica.
- Memoria de forma bi-direccional: la aleación recuerda su forma bajo las temperaturas baja y alta. La deformación mecánica no es indispensable.
- Súper elasticidad: la aleación retorna a la forma original inmediatamente después del descenso de tensión.

La transformación de fase es un proceso inevitable para las aleaciones con la memoria de forma. Este proceso se efectúa únicamente en estado sólido entre dos fases. Es generalmente conocido como la transformación martensítica. La fase de temperatura baja (estabilizada con tensión) se denomina la martensita y la fase de temperatura alta (estable sin tensión) se conoce como la austenita. El efecto de memoria se activa con el movimiento cooperativo de los átomos a las distancias más cortas que la distancia interatómica. La transformación martensítica transcurre en una forma organizada de tal modo que los átomos adyacentes siguen siendo los mismos, y así difiere de la deformación plástica. Para poder describir el fenómeno de memoria de forma, es necesario definir los siguientes términos:

- Las temperaturas de transformación: son temperaturas en las cuales comienza o termina la transición de una fase a otra, para la austenita y la martensita describimos la temperatura inicial y final. Por lo tanto, las temperaturas de transformación nos indican la amplitud de las operaciones donde se pueden aprovechar sus características.

- Extensión: para describir los componentes individuales de deformación (que transcurren simultáneamente) utilizamos siguientes términos: ε_{irr} es la deformación plástica irreversible. La deformación elástica reversible ε_{rec} es típica para todos los materiales y sigue el modelo de elasticidad de Young. La deformación reversible súper elástica se debe al fenómeno de memoria de forma y su tamaño es determinado por el cambio de la estructura cristalina y de su constante de red.

La aleación con el fenómeno de memoria de forma más utilizada y conocida es la del níquel y titanio, también conocida como Nitinol. Más de 90% de las aplicaciones se constituyen en la base de aleaciones de titanio y níquel. Sin embargo, la investigación no termina con el fin de descubrir una nueva aleación, pero se centraliza en las aleaciones con las temperaturas de funcionamiento adecuada con altos valores de extensión máxima. El descubrimiento de las aleaciones ferromagnéticas con fenómeno de memoria de forma abrió una nueva gama de aplicaciones en las cuales el actuador también puede actuar como un sensor.

Algunos modelos seleccionados de las aleaciones de Heusler son a la vez ferromagnéticos y exhiben la memoria de forma o la súper elasticidad. Las aleaciones de Heusler se dividen en dos categorías principales:

- Medias aleaciones de Heusler que tienen la estequiométrica y los componentes XYZ se cristalizan en general en una estructura cúbica con ninguna simetría central (grupo espacial no. 216, $F\bar{4}3m$, $C1_b$)
- Aleaciones de Heusler completos que tienen fórmula estructural X_2YZ y se cristalizan en una estructura cúbica (grupo espacial no. 225, $Fm\bar{3}m$, $L2_1$)

El átomo en la posición X se encuentra generalmente en la segunda mitad de los elementos d, el elemento Y es uno de los lantánidos y en la primera mitad de los d-elementos. Los elementos de Z son normalmente de metales s y semimetales. Su recíproca estructura atómica está fuertemente ligada a las propiedades de las aleaciones de Heusler. Incluso pequeñas impurezas pueden modificar la estructura atómica y así las propiedades de las aleaciones de Heusler. Por lo tanto, es muy importante conocer los criterios que denominan la estructura.

El segundo tipo de las muestras que describimos en esta tesis son materiales con la magnetorresistencia gigante. La magnetorresistencia es el cambio de la resistencia eléctrica por la causa del campo magnético externo. Se puede encontrar en todos los metales reales y su amplitud es ligeramente diferente para diferentes tipos de metales, pero generalmente se nota como un pequeño cambio en la resistencia hasta 0,1%. La magnetorresistencia gigante se manifiesta como un cambio notable en la resistencia del campo magnético (hasta 50%), causada por la orientación de la magnetización de las partículas magnéticas, rodeadas por un material conductor, pero no magnético. La reducción de la resistencia en el campo magnético se debe a la orientación de los momentos magnéticos en la capa magnética. Si el campo magnético externo es cero (o bastante pequeño) los momentos magnéticos se orientan al azar. Si los electrones de conducción tienen el espín opuesto a la capa magnética, se produce la dispersión de los electrones y alta resistencia. Sin embargo, cuando se enciende el campo magnético externo, los momentos magnéticos individuales se hacen girar en una sola dirección. Este procedimiento permite pasar a una parte de los electrones libres sin dispersión y esto provoca la reducción de la resistencia.

Este fenómeno fue observado por primera vez en 1988 por dos grupos de investigación independientes dirigidos por A. Fert y P. Grünberg. Por este descubrimiento obtuvieron el Premio Nobel en 1997. La magnetorresistencia gigante fue descubierta en un film fino compuesto de dos capas de hierro separadas por una capa de cromo no magnética. Estas capas finas se normalmente preparan por la pulverización catódica, o por la electrodeposición. Estos métodos son muy caros y exigen mucho tiempo. La magnetorresistencia gigante se descubrió más tarde en el material granular también, en el cual las partículas magnéticas se distribuyen aleatoriamente en un material conductor, pero no magnético. Un ejemplo de tal material se puede preparar usando el método de Taylor-Ulitovsky con enfriamiento rápido. Los métodos de enfriamiento rápido ofrecen una gama de ventajas en comparación con los métodos normales de la preparación de muestras:

- aumentan la solubilidad de las muestras, a menudo en orden,
- ofrecen la posibilidad de preparar las muestras con diferente composición,
- dan la oportunidad de preparar unas fases metaestables e inconstantes,
- reducen el número y el tamaño de las fases segregadas no solicitadas,

Para los fines de esta tesis se usaron dos métodos de enfriamiento rápido; El Melt spinning (torneado en estado de fusión) y el método de Taylor-Ulitovsky con la preparación de microhilos revestidos por vidrio. Las aleaciones madres se prepararon mediante fusión por arco eléctrico y luego se utilizaron para la preparación de los materiales de enfriamiento rápido.

Las cintas superelásticas con la composición $Co_{49}Ni_{21}Ga_{30}$., $Co_{37}N_{34}iAl_{29}$ y $Fe_{43.5}Mn_{34}Al_{15}Ni_{7.5}$ se prepararon utilizando el método de torneado en estado de fusión. Usando este método en nuestras condiciones es posible preparar las cintas policristalinas de hasta 3 mm de ancho y de 25-55 µm finas. En primer lugar la aleación madre se almacena en un tubo con agujero y se funde por calentamiento de inducción. Después de la adquirir la temperatura adecuada se dispara sobre el cilindro giratorio. Las cintas se disparan con la presencia de la atmósfera protectora de helio que impide a la oxidación del material al mismo tiempo permite el intercambio de calor. La velocidad de la rotación del cilindro para todas las muestras preparadas ha sido establecida a 20 ms^{-1}.

El método de Taylor-Ulitovsky se utilizó para preparar un microhilo superelástico con la composición $Co_{51}Cr_{27}Ga_{11}Si_{11}$ y para preparar los microhilos magnetorresistivos CuCo. La principal ventaja de este método es la posibilidad de:

- repetir y escalar la producción de masas,
- variar y controlar la geometría (el diámetro del núcleo metal y el espesor del vidrio) durante la preparación de los microhilos y así influir los resultados de las las propiedades físicas
- preparar los microhilos largos ininterrumpidos hasta de 10 km,

Durante la preparación de la aleación madre, ésta se coloca en un tubo de ensayo y se calienta por una fusión de inducción. Posteriormente, cuando la aleación se funde y la temperatura es bastante alta para poder ablandar el vidrio, se puede empezar a preparar el microhilo. Con el toque de la varilla de vidrio se recoge el vidrio ablandado y tirándolo hacia abajo, mediante el efecto capilar, se produce el microhilo revestido por vidrio. Las muestras han sido examinadas aplicando siguientes métodos:

- microscopía electrónica de barrido SEM (JEOL 6100),
- microscopía electrónica de transmisión TEM (Philips CM200 y SuperTwin Tecnai G2 20 TWIN),
- la detección de rayos X por energía dispersiva EDX,
- difracción de electrones por retrodispersión EBSD,
- difracción de rayos X XRD (Bruker D8 Advance),
- medición de la dependencia de la magnetización del campo magnético y la temperatura (Quantum Design MPMS),

- medición de la dependencia de la resistencia del campo magnético (Quantum Design PPMS),
- medición de las curvas de tensión-deformación (DMA Q800 TA),
- medición de las curvas de tensión-deformación en el aparato complementada con la medición del cambio de la permeabilidad

La primera muestra ha sido preparada en forma de cinta con la composición $Co_{49}Ni_{21}Ga_{30}$. Se prepararon sólo piezas cortas de cinta del tamaño hasta 1 cm. Con el microscopio electrónico de barrido revelamos el carácter policristalino de las muestras. También observamos el crecimiento de los cristales en la dirección perpendicular a la superficie de la cinta, que se probablemente debe a la gran diferencia de la temperatura creada por el enfriamiento rápido. El tamaño del cristal variaba de 10-30 µm. El análisis EDX ha sido realizado en cinco posiciones diferentes y en tres piezas diferentes de la cinta. La composición química media de la cinta era $Co_{49.4}Ni_{20.6}Ga_{30.0}$. La desviación de la composición deseada no sobrepasaba ±1,49%. Se obtuvo la homogeneidad suficiente de la muestra sin la necesidad del recocido de las aleaciones madre y las cintas preparadas.

El análisis de rayos *X* a temperatura ambiente ha revelado la presencia de una fase. Se trata de una estructura *B2* denominada, en la cual ocurre una ocupación aleatoria de las posiciones *Y* y *Z* de los átomos de Ni y Ga. El parámetro de red para esta fase es 2.857 Å.

De las medidas magnéticas podemos notar la presencia de una transformación de fase que transcurre a la temperatura ambiente. Se produce la histéresis de la cual se establecen las temperaturas de transformación. La temperatura austenítica de inicio fue 179 K y su temperatura final 252 K. La martensita empieza a formarse a la temperatura de 216 K y termina en 149 K. Los ciclos de histéresis se midieron a dos temperaturas diferentes, a 90 K cuando la aleación estaba en una etapa martensítica absoluta y a 265 K cuando la fase de la aleación estaba totalmente austenítica. Los ciclos muestran que la temperatura alta y la fase de temperatura baja tienen la anisotropía magnetocristalina diferente. El valor de la magnetización de saturación del campo, de hecho, demuestra la presencia de una anisotropía mayor en el caso de la fase de temperatura baja. Ésta tiene una magnetización saturada si el valor del campo magnético externo es de 1,25 kOe, mientras que la fase de temperatura baja se satura cuando el campo es de 7 kOe.

Teniendo en cuenta la dependencia de la temperatura de la resistencia eléctrica podemos observar un cambio de transformación martensítica a las temperaturas más altas. La temperatura inicial de martensita se ha desplazado de 216 K a 230 K.

La segunda muestra ha sido preparada con la composición de cinta $Co_{37}N_{34}iAl_{29}$. Después de preparar las cintas, se han formado piezas de unos pocos centímetros de largo. Bajo el microscopio electrónico de barrido observamos claramente la estructura policristalina y el tamaño de los granos individuales que era entre 1-2 µm. El espesor de la cinta se midió entre 25 y 40 µm. También observamos las áreas con el crecimiento de cristales vertical en la superficie a la cinta y una estructura granular orientada al azar. Los cristales pequeños tienen la ventaja porque sus límites actúan como centros de nucleación para cambio de fase, la cual de este modo se ejecuta más rápido. Esto reduce el tiempo de reacción de la transformación martensítica. El análisis químico se llevó a cabo en tres cintas de piezas diferentes y con la composición química media $Co_{38.3}Ni_{33.4}Al_{28.2}$ tomando en cuenta que las diferencias en la composición fueron ± 2,7.

La difracción de rayos X a temperatura ambiente confirmó la presencia de una fase, que se considera una variante (*B2)* de la fase de Heusler $L2_1$ similar a la aleación de la composición $Co_{49}Ni_{21}Ga_{30}$.. El parámetro de red para esta fase es 2,8499 Å.

La dependencia de la temperatura de la magnetización indica la presencia de la transformación martensítica en las condiciones de temperatura ambiente. Las temperaturas de transformación no quedan definidas claramente. El inicio de la transformación de fase a la martensita se determinó a partir de la dependencia de la temperatura de la magnetización a 150 K, y su final a 75 K. La austenita comienza a cristalizar a la temperatura de 80 K y termina a 170 K. Los ciclos de la histéresis se midieron a una temperatura de 10 K (la aleación está en la martensita) y a 190 K (la aleación está en la austenita). A partir de la forma de los ciclos de la histéresis podemos observar que la fase de alta temperatura tiene una mayor anisotropía magnetocristalina. Este efecto es aún más visible en las curvas de magnetización inicial. La magnetización saturada se debe a que la fase de temperatura alta ha alcanzado el campo magnético de 4 kOe, y la fase de baja temperatura en el campo de 9 kOe. Las mediciones de resistencia muestran la presencia de transformación de fase, mientras que empujan a la temperatura de inicio martensítica y austenítica a las temperaturas más altas. Las variaciones de las temperaturas de transformación de los distintos campos se pueden ver en la tabla 1.

El retorno máximo alcanzado por la extensión de la muestra $Co_{37}N_{34}iAl_{29}$ fue de 0,8% con la extensión irreversible de 0,3%. También se ha medido el alargamiento de 0,2% a la tensión de casi cero, que se consigue solamente por enderezar de la muestra y no es el resultado de la superelasticidad. La extensión crítica ha alcanzado el valor de 1,7%. Junto con una extensión de 0,8% causado por el enderezamiento de las muestras.

La tercera muestra súperelástica muestra una estructura $Fe_{43.5}Mn_{34}Al_{15}Ni_{7.5}$. El análisis por microscopía electrónica reveló una estructura policristalina con el crecimiento del cristal vertical similar a la de la muestra con la composición $Co_{49}Ni_{21}Ga_{30}$. Por otra parte, en el lado que estaba en contacto con el rodillo refrigerado se han observado los crecimientos de cristales granulares, que indican una alta tasa de enfriamiento. La cinta es de alrededor de 40-55 µm de espesor.

Tab. 1 las temperaturas de transformación martensítica

Medida	M_s	M_f	A_s	A_f
M(T)	150 K	75 K	80 K	170 K
R(T) 1T	175 K	95 K	65 K	175 K
R(T) 2T	160 K	100 K	105 K	165 K
R(T) 5T	165 K	105 K	110 K	170 K

M (T) es una medida de la dependencia de temperatura de la magnetización
R (T) es una medida de la dependencia de temperatura de la resistencia

La difracción de rayos X a temperatura ambiente ha mostrado la presencia de dos fases, designados como α y la γ'. La fase α se cristaliza en una red cúbica y la γ' cristaliza en la red cúbica espacialmente orientada. La fase martensítica se considera la red γ' con el parámetro de red a_{bcc} = 2,9086 Å. El parámetro de red de la fase α es a_{fcc} = 3,6604 Å. Mediante la comparación de las intensidades para determinar la proporción relativa del volumen de las dos fases encontramos que a temperatura ambiente, 88% de la aleación está en la fase austenítica y 12% en la fase martensítica.

A partir de la dependencia de la temperatura de la magnetización no fue posible detectar la presencia de la transformación martenzitická. Entre los ciclos de enfriamiento y calentamiento no se puede observar ninguna diferencia significativa en la magnetización de la muestra. Esto puede ser causado por una amplia gama de la transformación martenzitická, donde el cambio ocurre gradualmente en un amplio rango de temperaturas, con lo cual se suprime la histéresis. La temperatura de Curie, que es aproximadamente 400 K, muestra la posibilidad de utilizar las muestras como un sensor. La fase de temperatura alta alcanza la magnetización de saturación con el campo de 6 kOe y la fase de temperatura baja con el de 2,3 kOe. Esto sugiere que la fase de temperatura baja tiene mayor anisotropía magneto cristalina, al contrario que el caso de muestras $Co_{49}Ni_{21}Ga_{30}$ y $Co_{37}N_{34}iAl_{29}$.

Las curvas de tensión-deformación han sido medidas a diversas temperaturas con el fin de confirmar la superelasticidad. En la muestra también observamos el efecto de entrenamiento, cuando después de varios ciclos se redujo el alargamiento irreversible de 1% a 0,1%. La extensión máxima reversible fue 1,7%. Las curvas de tensión-deformación se complementaron con mediciones de cambios de la permeabilidad. La extensión máxima reversible alcanzó el valor de 1%. Durante la medición de la permeabilidad se redujo en 12%. La permeabilidad muestra solo una histéresis menor entre la carga y la descarga de las muestras. La histéresis estrecha es de hecho un factor importante para la fabricación de un sensor preciso de extensión. Además, la diferencia en la permeabilidad en la tensión cero antes y después de las mediciones significa que el cambio de la permeabilidad es debido al cambio de la fase y a las diferencias de las propiedades de las fases y no se debe a la dependencia de la permeabilidad de la tensión.

La última muestra superelástica con la composición $Co_{51}Cr_{27}Ga_{11}Si_{11}$ se preparó en forma de un microhilo revestido por vidrio. Bajo el microscopio de electrones fue posible distinguir el núcleo metálico del recipiente de vidrio y medir sus propiedades geométricas. El diámetro total del microhilo es de 25 μm y el diámetro del núcleo de metal es de 6,7 μm. Sin embargo, el caracter policristalino de las muestras ha sido observado como en el caso de las cintas. El análisis EDX se realizó en 2 diferentes piezas de microhilos con un núcleo de metal expuesto. Los resultados de los análisis EDX nos indican que la composición preparada ($Co_{51.39}Cr_{25.99}Ga_{11.33}Si_{11.29}$) coincide con la composición deseada (± 1% at.).

La difracción de rayos X confirmó la presencia de una sola fase. El microhilo cristaliza en la estructura *B2* con la simetría espacial y con un parámetro de red 2,8615 Å. Uno de los descubrimientos más interesantes es la detección de electrones retrodispersados en este microhilo. Estas mediciones se realizaron en varias piezas de microhilo con una dirección cristalográfica <111> para todos los granos, paralela al eje del microhilo. No se han observado ningunos límites de los granos.

Las mediciones magnéticas confirmaron la presencia de la transformación martensítica en el intervalo de temperatura de 100 K a 300 K. Los ciclos de histéresis se midieron a temperaturas 10 K y 300 K. La fase de temperatura baja tiene una anisotropía menor en comparación con la fase de temperatura alta que se determina a partir de la diferencia entre la magnetización saturada de la temperatura alta (280 Oe) y por la fase de temperatura baja (50 Oe).

Las curvas de tensión-deformación se midieron en el conjunto de 19 microhilos. La extensión máxima reversible fue 1,65% con la poca extensión irreversible 0,13%. Cabe señalar que el valor bajo de la extensión irreversible se logró sin entrenamiento, solo en la primera medición. Esto se puede deber a la orientación apropiada de los cristales y la ausencia de los límites de cristales. La extensión se logró sin la necesidad recocer las muestras.

Los microhilos con la composición $Cu_{80}Co_{20}$, $Cu_{90}Co_{10}$ y $Cu_{95}Co_{5}$ se estudiaron con el fin de determinar el efecto del recocido sobre el fenómeno de magnetorresistencia gigante. Las muestras se recocieron a 673 K durante 10, 30, 60 minutos y 2, 5, 10, 24 horas. También se hizo un recocido a temperatura baja a diferentes temperaturas (423 K y 473 K) y con tiempo de recocido de 2, 10, 24 horas.

Por medio de rayos X se identificaron dos fases diferentes en todas las muestras de CuCo. La estructura cristalina de Cu es *fcc* y la estructura cristalina de cobalto es *hcp*. Las intensidades de las reflexiones indican la presencia de una orientación preferida de los cristales. El eclipse de la orientación preferida de los cristales se puede observar especialmente en el caso del microhilo con la composición $Cu_{95}Co_{5}$. Después de recocer las muestras con la composición $Cu_{90}Co_{10}$ y $Cu_{80}Co_{20}$ no observamos cambios significativos en la intensidad de las reflexiones.

Para el estudio de la microestructura de las muestras se utilizó el análisis de la microscopía electrónica de transmisión. Puesto que la solubilidad del cobalto en el medio es de aproximadamente 6%, se cree que en las muestras con un mayor contenido de cobalto, aparece la estructura granular. Con el fin de descubrir estas estructuras granulares en diferentes ubicaciones en el microbio se hizo el análisis de punto EDX. Sin embargo, la estructura granular fue descubierta sólo en el caso de la muestra $Cu_{80}Co_{20}$. El análisis de punto EDX recoge los datos de contornos de 45 nm. Con el propósito de cubrir mejor el área, se crearon los mapas de TEM de la composición química. Sin embargo, como en el caso anterior, las estructuras granulares se descubrieron sólo en el caso de las muestras $Cu_{80}Co_{20}$.

Las mediciones magnéticas nos ofrecieron un mejor plano de la distribución de los átomos de cobalto. Por ejemplo, los ciclos de la histéresis para $Cu_{90}Co_{10}$ a diferentes temperaturas son lineares antes de recocer excepto de la curva medida a 5 K. Con todo, después de recocer, los microhilos presentan un comportamiento ferromagnético a temperaturas mayores de 5 K, lo que nos indica su presencia aumentada.

El fenómeno magnetorresistencia gigante mejora significativa ocurrió después de recocer las muestras a 673 K. Por ejemplo, la muestra Co_5Cu_{95} magnetorresistencia alcanzó antes del recocido un cambio de 1% en la resistencia y después de diez horas del recocido hasta 7,5% y el fenómeno de magnetorresistencia gigante para la muestra $Cu_{80}Co_{20}$ ha aumentado de 8% a 19% con las mismas condiciones al recocer.

Las tensiones internas creadas por diversas constantes de la expansión térmica pueden ser una de las razones detrás del creciente fenómeno de la magnetorresistencia gigante. Sin embargo, esta opción se descartó al medir el cambio de la resistencia en las muestras con el recocido a temperatura baja, porque las tensiones creadas bajo diferentes temperaturas se desalojan durante el recocido de más de 373 K. Sin embargo, de la difracción de los rayos X hecha en las muestras recocidas a 373 K y 423 K no aparece ningún cambio de la estructura. De esto resulta que las tensiones internas en el microhilo tienen una función clave en el aumento de la magnetorresistencia gigante.

El aumento de la magnetorresistencia se puede explicar por la descomposición espinodal, que representa una rápida segregación de los iones de cobalto en el microhilo después del recocido. El aumento del tamaño y de cantidad de las partículas de cobalto durante el recocido resulta en el aumento de la magnetorresistencia. De los grados de los cambios máximos de la magnetorresistencia en el campo magnético de 5 T podemos observar las desviaciones del curso esperado. Sin embargo, esto se puede explicar por el hecho de que el microhilo no es homogéneo en toda su longitud.

En las muestras también se observó efecto de Kondo que representa la presencia de un mínimo en la dependencia de la temperatura de la resistencia al bajar las temperaturas. El efecto de Kondo es causado por la presencia de las impurezas magnéticas en el material metálico en el que hay una conductividad de electrones de dispersión. Sin embargo, por lo general el fenómeno condón se produce cuando el material de un pequeño número de estas impurezas es de 0,002 a 0,02%. Por lo tanto, incluso la muestra que contiene un mínimo de cobalto no puede ser considerada un material clásico con el efecto de Kondo. En un caso clásico del efecto de Kondo suprime el campo magnético. Las mediciones del impacto del campo magnético a la dependencia de la temperatura de la resistencia en muestras no apareadas muestran que incluso el campo magnético grande (5 T) no puede completamente suprimir el efecto de Kondo. Al contrario, en las muestras recocidas es posible suprimir el efecto de Kondo ya en el campo magnético de 1 T.

Uno de los resultados más interesantes consideramos la investigación de las cintas superelásticas con la composición $Fe_{43.5}Mn_{34}Al_{15}Ni_{7.5}$ y las investigaciones sobre la composición de los microhilos $Co_{51}Cr_{27}Ga_{11}Si_{11}$. La $Fe_{43.5}Mn_{34}Al_{15}Ni_{7.5}$ reveló unas propiedades interesantes que se pueden utilizar en el desarrollo del sensor. Incluso tiene propiedades mecánicas útiles y es fácil de prepararla. Otra investigación se puede centrar en el impacto del recocido a las propiedades superelásticas. Con el recocido se liberan incluso las tensiones internas que puede influir al inicio de la fase de transformación.

En el caso de las muestras $Co_{51}Cr_{27}Ga_{11}Si_{11}$ no observamos los límites de granos. De esto deducimos el que microhilo podría ser monocristalino a lo largo de toda su longitud. Sin embargo, las mediciones se realizaron sólo en la superficie del microhilo. Las mediciones de la sección transversal de la estructura dentro del microhilo podrían confirmar o desmentir esta hipótesis. La oportunidad de preparar el microhilo con los cristales orientados correctamente tiene la ventaja del coste más económico y el ahorro del tiempo en comparación con la preparación del material producido por otros métodos.

A pesar de que hasta ahora se han desarrollado muchas aplicaciones, todavía es posible llegar con nuevas ideas y con aplicaciones potenciales. Las partículas de las muestras superelásticas frágiles se pueden incorporar a otros materiales con el fin de observar su deformación. Además, la preparación de estas composiciones en la forma de microhilos revestido por vidrio puede eliminar el problema con la fragilidad cuando el vidrio estabiliza el núcleo de metal. El envase de vidrio puede proporcionar la biocompatibilidad y el aprovecho de estos materiales en la medicina.

En las muestras con una magnetorresistencia gigante sería interesante ver de que manera la descomposición espinodal en la muestra avanza con el tiempo del recocido. El uso del microscopio electrónico de transmisión sería posible desarrollar los mapas de la composición química de los alambres con diferentes condiciones del recocido.

10 References

1 L. Lecce, A. Concilio, Shape memory alloy engineering (2015), 1st edition, Butterworth-Heinemann, Oxford

2 K. Yamauchi, I. Ohkata, K. Tsuchiya, S. Miyazaki, Shape memory and superelastic alloys, 1st edition, Woodhead Publishing Limited, Cambridge

3 Jani, J.M.; Leary, M.; Aleksandar, S.; Gibson M.A.; A review of shape memory alloy research, applications and opportunities; *Mater. Design* **56** (2014), 1078

4 Y. Tanaka, Y. Himuro, R. Kainuma, Y. Sutou, T. Omori, K. Ishida, Ferrous Polycrystalline Shape-Memory Alloy Showing Huge Superelasticity, *Science* **327** (2010), 1488

5 J.Ma, I.Karaman, R.D.Noebe, High temperature shape memory alloys *Int. Mater. Rev.* **55** (2010), 257

6 Arne Ölander, An Electrochemical Investigation of Solid Cadmium-Gold Alloys, *J. Am. Chem. Soc.* **54** (1932), 3819

7 L.B. Vernon, H.M. Vernon. Process of manufacturing articles of thermoplastic synthetic resins. In US Patent 1941, No. 2234993

8 A. Cladera, B. Weber, C. Leinenbach, C. Czaderski, M. Shahverdi, M. Motavalli, Iron-based shape memory alloys for civil engineering structures: An overview, *Constr. Build. Mater.* **63** (2015), 281

9 A.N. Vasil’ev, V.D. Buchel’nikov, T. Takagi, V.V. Khovaĭlo, É.I. Éstrin, Shape memory ferromagnets, *Phys-Usp+* **46** (2003), 559

10 L. Feng, E.K. Liu, W.X. Zhang, W.H. Wang, G.H. Wu, First-principle investigation of electronic structure, magnetism and phase stability of Heusler-type $Pt_{2-x}Mn_{1+x}Ga$ alloys, *J. Magn. Magn. Mater.* **377** (2015), 40

11 Duerig T.W., Pelton A.R., Ti–Ni shape memory alloys. Materials Properties Handbook, Titanium Alloys, Materials Park, OH: *American Society for Metals* (1994), 1035

12 T. Omori, K. Ando, M. Okao, X. Xu, Y. Tanaka, I. Ohnuma, R. Kainuma, K. Ishida, Superelastic Effect in Polycrystalline Ferrous Alloys, *Science* **333** (2011) 68

13 Y. C. Shu, K. Bhattacharya, The influence of texture on the shape-memory effect in polycrystals, *Acta Mater.* **46** (1998), 5457

14 K. Bhattacharya and R. V. Kohn, Symmetry, texture and the recoverable strain of shape-memory polycrystals, *Acta Mater.* **44** (1996)**,** 529

15 M. N. Baibich, J. M. Broto, A. Fert, F. Nguyen Van Dau, F. Petroff, P. Etienne, G. Creuzet, A. Friederich, J. Chazelas, Giant Magnetoresistance of (001)Fe/(001)Cr Magnetic Superlattices, *Phys. Rev. Lett.***61** (1988), 2472

16 G. Binasch, P. Grünberg, F. Saurenbach, W. Zinn, Enhanced magnetoresistance in layered magnetic structures with antiferromagnetic interlayer exchange, *Phys. Rev. B* **39** (1989), 4828

17 The Nobel Prize in Physics. Published online by The Nobel Foundation at <http://nobelprize.org/nobel_prizes/physics/laureates/2007/index.html>; 2007

18 Ch. Kittel, Introduction to Solid State Physics (2005), 8th edition, John Wiley & Sons ISBN 0-471-41526-X

19 A. Bid, A. Bora, A. K. Raychaudhuri, Temperature dependence of the resistance of metallic nanowires of diameter ⩾15nm: Applicability of Bloch-Grüneisen theorem, *Phys. Rev. B* **74** (2006), 035426

20 J. Kondo, Sticking to My Bush, *J. Phys. Soc. Jap.* **74** (2005), 1

21 B. D. Cullity C. D. Graham, Introduction to magnetic materials, Addison-Wesley Publishing Company 1972

22 L. Péter, I. Bakonyi, Electrodeposition and properties of nanoscale magnetic/non-magnetic metallic multilayer films. In: Staikov G, editor. Electrocrystallization in nanotechnology. Weinheim (Germany): Wiley-VCH; 2007. p. 242–60

23 J. Kondo, Resistance Minimum in Dilute Magnetic Alloys, *Prog. Theor. Phys.* **32** (1964), 37

24 W. J. de Haas, J. de Boer, G. J. van dën Berg, The electrical resistance of gold, copper and lead at low temperatures, *Physica* **1**, 1115

25 V.M. Fedosyuk, O.I. Kasyutich, D. Ravinder, H.J. Blythe, giant magnetoresistance in granular electrodeposited CuCo films, *J. Magn. Magn. Mater.* **165** (1996), 345

26 A. E. Berkowitz, J. R. Mitchell, M. J. Carey, A. P. Young, S. Zhang, F. E. Spada, F. T. Parker, A. Hutten, G. Thomas, Giant magnetoresistance in heterogeneous Cu-Co alloys, *Phys. Rev. Lett.* **68** (1992), 3745

27 C.L. Chien, J.Q. Xiao, J.S. Jiang, Giant negative magnetoresistance in granular ferromagnetic systems, *J. Appl. Phys.* **73** (1993), 5309

28 I. Bakonyi, L. Peter, Electrodeposited multilayer films with giant magnetoresistance (GMR): progress and problems. *Prog. Mater Sci*. **55**, (2010) 107

29 R.M. Bozorth, Magnetoresistance and domain theory of iron-nickel alloys. *Phys Rev* **70 (**1946) 923

30 R.M. Bozorth, Ferromagnetism, New York: Van Nostrand; 1951.

31 R.C. O'Handley. Modern magnetic materials – principles and applications, New York, Wiley, 2000

32 J.L. Gittleman, Y. Goldstein, S. Bozowski, Magnetic properties of granular nickel films, *Phys Rev B* **5** (1972) 3609

33 B.J. Hickey, M.A. Howson, S.O. Musa, N. Wiser. Giant magnetoresistance for superparamagnetic particles: melt-spun granular CuCo, *Phys. Rev. B* **51** (1995), 667

34 J. Kondo, Theory of dilute magnetic alloys (1969), *Solid State Phys.* **23**, 248

35 T. A. Costi, Kondo Effect in a Magnetic Field and the Magnetoresistivity of Kondo Alloys, *Phys. Rev. Lett.* **85** (2000), 1504

36 B. Knook: Ph. D. thesis, Leiden University, 1962

37 V. Zhukova, J. J. del Val, M. Ipatov. A. Granovsky, A. Zhukov, Magnetic and Transport properties of Co-Cu Mircrowires, *Proceedings of the 8th internation Conference on Sensing Technology*, (2014) Liverpool, UK

38 P. W. Anderson, Localized Magnetic States in Metals, *Phys. Rev.* **124** (1961), 41

39 T. Graf, C. Felser and S. S. P. Parkin, Simple rules for the understanding of Heusler compounds, *Prog. Solid State Ch.* **39** (2011), 1

40 T. Graf, J. Winterlik, L. Müchler, G.H. Fecher, C. Felser, S.S.P. Parkin, Magnetic Heusler Compounds (2013) *Handbook of Magnetic Materials* **21**, 75

41 F. Heusler, Über magnetische Manganlegierungen, *Ver. Deut. P.* **5** (1903), 219 *In German*

42 E. Şaşioğlu, First-principles study of the exchange interactions and Curie temperature in Heusler alloys, Faculty of Natural Sciences III, Martin Luther University Halle-Wittenberg, *Disseration thesis*, 2006

43 H. H. Potter, X-ray structure and magnetic properties of single crystals of Heusler alloy, *Proc. Phys. Soc.***41** (1929), 135

44 A. J. Bradley, J. W. Rodgers, The crystal structure of the Heusler alloys, *Proc. R. Soc. London Ser. A* **144** (1934), 340

45 D. P. Morris, R. R. Preston, I. Wialliams, Search for New Heusler Alloys, *Proc. Phys. Soc.* **73** (1959), 520

46 K. Takezawa, T. Shindo, S. Sato, Shape memory effect in β1-CuZnAl alloys, *Scripta Metall.* **10** (1976), 13

47 R.A. de Groot, F.M. Mueller, P.G. van Engen, K.H.J. Bushow, New Class of Materials: Half-Metallic Ferromagnets, *Phys. Rev. Lett.* **50** (1983) 2024

48 H.C. Kandpal, V. Ksenofontov, M. Wojcik, R. Seshadri, C. Felser, Electronic structure, magnetism and disorder in the Heusler compound Co_2TiSn, *Phys. D: Appl. Phys.* **40 (**2007), 1587

49 D.J. Hartl, D.C. Lagoudas, Aerospace applications of shape memory alloys, *Proc. Inst. Mech. Eng. Part. G: J. Aerospace End.* **221** (2007) 535

50 S. Spinner, A.G. Rozner, Elastic Properties of NiTi as a Function of Temperature, *Journal of the Acoustical Society of America*, **40** (1966), 1009

51 A. N. Vasilʹev. V. D. Buchelʹnikov, T. Takagi, V. V. Khovaĭlo, É. I. Éstrin, Shape memory ferromagnets, *Phys. – Uspekhi* **46** (2003), 559

52 C. W. Nan, L. Liu, N. Cai, J. Zhai, Y. Ya, Y.H. Lin, L.J. Dong, C.X. Xiong, A three-phase magnetoelectric composite of piezoelectric ceramics, rare-earth iron alloys, and polymer, *Appl. Phys. Lett.* **81** (2002), 3831

53 W. Mei, T. Okane, T. Umeda, Magnetostriction of Tb-Dy-Fe crystals, *J. Appl. Phys.* **84** (1998), 6208

54 K. Ullakko, J. K. Huang, C. Kantner, R. C. O’Handley, V. V. Kokorin, Large magnetic-field-induced strains in Ni2MnGa single crystals, *Appl. Phys. Lett.* **69** (1996), 1966

55 R. Tickle, R.D. James, T. Shield, M. Wuttig, V.V. Kokorin, Ferromagnetic shape memory in the NiMnGa system, *IEEE Trans. Magn.* **35** (1999), 4053

56 O. Heczko, A. Sozinov, K. Ullakko, Giant field-induced reversible strain in magnetic shape memory NiMnGa alloy, *IEEE Trans. Magn.* **36** (2000), 3266

57 S. J. Murray, M. Marioni, S. M. Allen, R. C. O’Handley, T. A. Lograsso, 6% magnetic-field-induced strain by twin-boundary motion in ferromagnetic Ni–Mn–Ga, *Appl. Phys. Lett.* **77** (2000), 886

58 G. H. Wu, C. H. Yu, L. Q. Meng, J. L. Chen, F. M. Yang, S. R. Qi, W. S. Zhan, Giant magnetic-field-induced strains in Heusler alloy NiMnGa with modified composition, *Appl. Phys. Lett.* **75** (1999) 2990

59 O. Söderberg, Y. Ge, N. Glavatska, O. Heczko, K. Ullakko, V.K. Lindroos, The behaviour of Ni-Mn-Ga martensitic alloys in magnetic field, J. Phys. IV France 11 (2001) Pr8-287

60 B.D. Shaninaa, A.A. Konchitsa, S.P. Kolesnika, V.G. Gavriljukb, I.N. Glavatskijb, N.I. Glavatskab, O. Soderberg, V.K. Lindroosc, J. Foct, Ferromagnetic resonance in non-stoichiometric $Ni_{1-x-y}Mn_xGa_y$, *J. Magn. Magn. Mater.* **237** (2001), 309

61 V.A. Chernenko, V.A. L'vov, M. Pasquale, S. Besseghini, C. Sasso, D.A. Polenur, Magnetoelastic behavior of Ni-Mn-Ga martensitic alloys, *Int. J. Appl. Electromag. Mech.* **12** (2000) 3

62 C. H. Yu, W. H. Wang, J. L. Chen, G. H. Wu, F. M. Yang, N. Tang, S. R. Qi, W. S. Zhan, Magnetic-field-induced strains and magnetic properties of Heusler alloy $Ni_{52}Mn_{23}Ga_{25}$, *J. Appl. Phys.* **87**, (2000) 6292

63 N. Lanska, O. Söderberg, A. Sozinov, Y. Ge, K. Ullakko, V.K. Lindroos, Composition and temperature dependence of the crystal structure of Ni-Mn-Ga alloys, J. Appl. Phys. **95** (2004) 8074

64 K. Rolfs, A. Mecklenburg, J.M. Guldbakke, Crystal Quality boosts responsiveness of magnetic shape memory single crystals, J. Magn. Magn. Mater. **321** (2009) 1063

65 L. Straka, H. Hänninen, A. Soroka, A. Sozinov, Ni-Mn-Ga Single crystals with very low twinning stress, J. Phys. Conf. Ser.**303** (2011) 012079

66 D. Kellis, A. Smith, K. Ullakko, P. Müllner, Oriented single crystals of Ni-Mn-Ga with very low switching field, *J. Cryst. Growth* **359** (2012) 64

67 I. Aaltio, X.W. Liu, M. Valden, et al., Nanoscale surface properties of Ni-Mn-Ga 10M magnetic shape memory alloy, *J. Alloy Compd.* **577** (2013) S367

68 K. Schlüter, B. Holz, A. Raatz, Principle design of actuators driven by magnetic shape memory alloys, *Adv. Eng. Mater.***14** (2012) 682

69 M. Kohl, D. Brugger, M. Ohtsuka, B Krevet, A ferromagnetic shape memory actuator designed for large 2D optical scanning, *Sensor Actuat. A-Phys.* **135** (2007) 92

70 Sohmura, Taiji, Oshima, Ryuichiro, Fujita, Francisco Eiichi Thermoelastic fcc-fct martensitic transformation in Fe-Pd alloy, *Scripta Metall.* **14** (1980) 855

71 M. Sugiyama, R. Oshima, F.E. Fujita, Martensitic Transformation in the Fe-Pd Alloy System, *Trans JIM* **25** (1984) 585

72 R.D. James, M. Wuttig, Magnetostriction in Martensite, *Philos. Mag. A* **77** (1998) 1273

73 J. Koeda, Y. Nakamura, T. Fukuda, T. Kakeshita, T. Takeuchi, K. Kishio, Giant magnetostriction of Fe-Pd single crystal exhibit martensitic transformation *Trans. Mater. Res. Soc. Jpn.* **26 (**2001), 215.

74 R.F.C. Farrow, The role of molecular beam epitaxy in research on giant magnetoresistance and interlayer exchange coupling, *IBM J Res Dev* **42** (1998), 43

75 D.H. Mosca, F. Petroff, A. Fert, P.A. Schroeder, W. P. Pratt Jr, R. Laloee, Oscillatory interlayer coupling and giant magnetoresistance in Co/Cu multilayers, *J. Magn. Magn. Mater.* **94** (1991), L1

76 S.S.P. Parkin, R. Bhadra, K.P. Roche, Oscillatory magnetic exchange coupling through thin copper layers, *Phys. Rev. Lett*. **66** (1991) 2152

77 H. Kubota, S. Ishio, T. Miyazaki, Z.M. Stadnik, Giant magnetoresistance and interlayer exchange coupling in Ni–Co/Cu multilayer films, *J. Magn. Magn. Mater.* **129** (1994), 383

78 S.S.P. Parkin, Giant Magnetoresistance in Magnetic Nanostructures. *Annu. Rev. Mater. Sci.* **25** (1995), 357

79 J.Q. Xiao, J.S. Jiang, C.L. Chien, Giant magnetoresistance in nonmultilayer magnetic system. *Phys. Rev. Lett.* **68** (1992), 3749

80 W. Rössler; J. Zimmer, T. Bever, K. Prügl, W. Granig, D. Hammerschmidt, E. Katzmaier, Integrated giant magneto resistors—A new sensor technology for automotive applications. In: *Advanced Microsystems for Automotive Applications*; Springer: Berlin, Germany; Heidelberg, Germany, 2006; pp. 323–342

81 C: Reig, S. Cardoso, S. Mukhopadhyay, Giant magneto resistance (GMR) Sensors: From Basis to State-of-the-Art applications. In *GMR Sensors in Automotive Applications*; Springer: Berlin, Germany; Heidelberg, Germany, 2013; pp. 133–156

82 C. Giebeler, T. Kuiper, J.B.A.D. van Zon, M. Doescher, G. Schulz, D. Oelgeschlaeger, Robust GMR Sensors for Automotive Applications. *Tech. Mess.* **68** (2001),

83 M. Hawraneck, J. Zimmer, K. Pruegl, W. Raberg, T. Bever, L. Alff, Stablity investigations of GMR sensors for automotive applications. In *Proceedings of*

the 9th Symposium Magnetoresistive Sensoren und Magnetische Systeme: Grundlagen-Herstellung-Anwendungen, Wetzlar, Germany, 13–14 March 2007; pp. 129–136.

84 R.D. Baselt, G.U. Lee, M. Natesan, S.W. Metzger, P.E. Sheehan, R.J. Colton, A biosensor based on magnetoresistance technology, *Biosensors and Bioelectronics*, **13** (1998), 731

85 I. Ennen, D. Kappe, T. Rempel, C. Glenske, A. Hütten, Giant Magnetoresistance: Basic Concepts, Microstructure, Magnetic Interactions and Applications, *Sensors* **16** (2016), 904

86 P. Allia, M. Knobel, P. Tiberto, and F. Vinai, Magnetic properties and giant magnetoresistance of melt spun granular Cu100-x Cox alloys, *Phys. Rev*. **52** (1995), 15 398,

87 A.R. Yavari, P. J. Desré, T. Benameur, Mechanically driven alloying of immiscible elements, *Phys. Rev. Lett.* **68** (1992), 2235

88 A. Zhukov, C. Garcia, M. Ilyn, R.Varga, J. J. del Val, A. Granovsky, V. Rodionova, M. Ipatov, V. Zhukova, Magnetic and transport properties of granular and Heusler-type glass-coated microwires, *J. Magn. Magn. Mater.* **324** (2012), 3558

89 I.S. Miroshnichenko and I.V. Salli, A device for the crystallization of alloys at a high cooling rate, *Zav. Lab.* **2**, p (1959) 1398

90 K. Klement K., R.H. Wilens and P. Duwez, Non-crystalline structure in solidified Gold-Silicon alloys, *Nature,* **187** (1970), 869

91 M. E. McHenry, M. A. Willard, D. E. Laughlin, Amorphous and nanocrystalline materials for applications as soft magnets, *Progress in Materials Science* **44** (1999) 291

92 G. Herzer, Anisotropies in soft magnetic nanocrystalline alloys, J. Magn. Magn. Mater. Vol. **294** (2005) 99

93 M.P.C. Vergara, J.C. Cezar, H.C.N. Tolentino, M. Knobel, Structural evolution of Co clusters on $Cu_{90}Co_{10}$ upon annealing, *Physica B,* **320** (2002) 143

94 M. G. M. Miranda, E. Estevez-Rams,G. Martinez, M. N. Baibich, Phase separation in $Cu_{90}Co_{10}$ high-magnetoresistance materials, *Phys. Rev. B,* **68** (2003), 014434

95 H. Chiriac, M. Lostun, G. Ababei, and T.A. Ovari, Comparative study of the magnetic properties of positive and nearly zero magnetostrictive submicron amorphous wires, J. Appl. Phys. **109** (2011), 07B501

96 Compact Arc Melter MAM-1 [online] [cit. 15.5.2015] Available at: http://www.edmund-buehler.de/index.php?lan=2&nav=9&sub=21&sel=100

97 Y. H. Qu, K. J. Yang, Y. T. Zhou, Y. Mao, W. Zhang, S. Y. Xu, "Phase Selection in Sub-Rapidly Solidified Au-20Sn Alloys", *Mater. Sci. Forum* **817** (2015), 325

98 J. L. Sánchez Llamazares, T. Sanchez, J.F. Santos, M.J. Pérez, M.L. Sanchez, B. Hernando, Ll. Escoda, J.J. Suñol, R. Varga, Martensitic phase transformation in rapidly solidified $Mn_{50}Ni_{40}In_{10}$ alloy ribbons, *Appl. Phys. Lett* **92** (2008), 012513

99 H. H. Liebermann and C. D. Graham, Jr. Production of Amorphous Alloy Ribbons and Effects of Apparatus Parameters on Ribbon Dimension, *IEEE T. Magn.* **12** (1976)

100L. Ptáček et al., Náuka o materiálu I, 2nd edition, Akademické Nakladatelství CERM, s.r.o., Brno, pp. 371-413

101 L. Reimer, Scanning Electron Microscopy (1998), 2nd edition, Springer-Verlag Berlin Heidelberg, ISBN: 978-3-540-38967-5

102 M. Birkholz, Thin Film Analysis by X-Ray Scattering, Edition October 2005, ISBN 978-3-527-31052-4

103 S. Foner, Versatile and Sensitive Vibrating-Sample Magnetometer, *Rev. Sci. Instrum* **30** (1959), 548

104 Q800 DMA [online] [cit. 20.5.2015] Available at: http://www.tainstruments.com/q800/

105 I. Bakonyi, J. Tóth, L. Goualou, T. Becsei, E. Tóth-Kádár, W. Schwarzacher, Giant magnetoresistance of electrodeposited $Ni_{81}Cu_{19}$/Cu multilayers, *J. Electrochem. Soc*. **149** (2002) C195

106 K. Oikawa, T. Ota, F. Gejima, T. Ohmori, R. Kainuma, K. Ishida, Phase Equilibria and Phase Transformations in New B2-type Ferromagnetic Shape Memory Alloys of Co-Ni-Ga and Co-Ni-Al Systems, *Mater. Trans.*, **42** (2001), 2472

107 Y. Kishi, C. Criaciunescu, M. Sato, T. Okazaki, Y. Fyruya, M. Wuttig, Microstructures and magnetic properties of rapidly solidified CoNiGa ferromagnetic shape memory alloys, *J. Magn. Magn. Mater.* **262** (2003), L186

108 J. Liu, H. Xie, Y. Huo, H. Zheng, Z. Li, Martensitic Transformation, Structure and Magnetic Properties of Co-Ni-Ga Ferromagnetic Shape Memory Alloys, *J. Alloy Compd.* **420**, (2006) 145

109 V. Yamakov, J.D. Hochhalter, W.P. Leser, J.E. Warner, J.A. Newman, G.P. Purja Pun, Y. Mishin, Multiscale modeling of sensory properties of Co–Ni–Al shape memory particles embedded in an Al metal matrix, *J. Mater. Sci.* **51** (2016), 1204

110 J. Ju, F. Xue, H. Li, Microstructure and Magnetic Property Variation with Addition of Rare Earth Element Dy in Co-Ni-Al Ferromagnetic Shape Memory Alloy, *J. Iron Steel Res. Int.* **22** (2015), 858

111 Y. Tanaka, K. Oikawa, Y. Sutou, T. Omori, R. Kainuma, K. Ishida, Martensitic transition and superelasticity of Co–Ni–Al ferromagnetic shape memory alloys with $\beta + \gamma$ two-phase structure, Mater. Sci. Eng. A-Struct. **438–440** (2006), 1054

112 D. Wang, S. Hou, Y. Wang, X. Ding, S. Ren, X. Ren, Y. Wang, Superelasticity of slim hysteresis over a wide temperature range by nanodomains of martensite, *Acta Mater.*, **66** (2014), 349

113 X. Xu, T. Omori, M. Nagasako, A. Okubo, R. Y. Umetsu, T. Kanomata, K. Ishida, R. Kainuma, Cooling-induced shape memory effect and inverse temperature dependence of superelastic stress in Co2Cr(Ga,Si) ferromagmetic Heusler alloys, *App. Phys. Lett.* **103** (2013), 164104

114 A.R. Yavari, P.J. Desré, T. Benameur, Mechanically Driven Alloying of Immiscible Elements, *Phys. Rev. Lett.* **68** (1992), 2235

115 M.N. Baibich, G. Martíznez, M.G.M. Miranda, A.T. da Rosa, J. González, A. Zhukov, Ribbons and micro-wires of CuCo segregated alloys, *J. Magn. Magn. Mater.* **320** (2008), e29

116 M. Ilyn, V. Zhukova, C. Garcia, J.J. del Val, M. Ipatov, A. Granovsky, A. Zhukov, Kondo Effect and Magnetotransport Properties in Co-Cu Microwires, *IEEE Trans. Magn.* **48** (2012) 3532

117 A. Zhukov, J. M. Blanco, J. González, M. J. Garcia Prieto, E. Pina, M. Vázquez, Induced magnetic anisotropy in Co–Mn–Si–B amorphous microwires, *J. App. Phys*. **87** (2000); 1402

118 M.G.M. Miranda, E. Estevez-Rams, G. Martinez, M.N.Baibich, Phase separation in $Cu_{90}Co_{10}$ high-magnetoresistance materials *Phys. Rev. B.* **68**, (2003) 014434

119 M.J. Garcia Prieto, E. Pina, A.P. Zhukov, V. Larin, P. Marin, M. Vázquez and A. Hernando, Glass coated Co-rich Amorphous Microwires with Improved Permeability, *Sensors & Actuators A* **81** (2000) 227

120 P. Allia, K. Knobel, P. Tiberto, F. Vinai, Magnetic properties and giant magnetoresistance of melt-spun granular Cu_{100-x}–Co_x alloys *Phys. Rev. B.* **52** (1995), 15398

121 A.Vedyaev , A.Granovsky**,** Electroresistivity of amorphous ferromagnetic alloys in the Ziman-Faber model, *Phys.Metal.Metalloved*. **63** (1987) 1076

122 V. Zhukova, C. Garcia, J.J. del Val, M. Ilyn, A. Granovsky, A. Zhukov, Magnetic and transport properties of Co–Cu microwires with granular structure, *Thin Solid Films* **543** (2013), 142

123 H. Sato, Y. Kobayashi, Y. Aoki and H. Yamamoto, Transport properties in granular Co-Ag alloys, *J. Phys.: Condens. Matter*. **7** (1995) 7053

124 C. Manohar, The Kondo effect and the spin-flip scattering, *Phys. Lett.* **31** (1970), 344

11 Attachments

IEEE TRANSACTIONS ON MAGNETICS, VOL. 51, NO. 1, JANUARY 2015 4000903

Structural and Magnetic Characterization of Fe–Mn–Al–Ni Pseudo-Heusler Alloy

Jakub Mino[1], Vladimir Komanicky[1], Martin Durisin[2], Karel Saksl[2], Jozef Kovac[2], and Rastislav Varga[1]

[1]Faculty of Sciences, Institute of Physics, Univerzita Pavla Jozefa Šafárika v Košiciach, Košice 041 80, Slovakia
[2]Institute of Experimental Physics, Slovak Academy of Sciences, Košice 04 001, Slovakia

In this paper, the production and structural, superelastic, thermoelastic, and magnetic properties of melt-spun $Fe_{43.5}Mn_{34}Al_{15}Ni_{7.5}$ alloy have been investigated with the aim to employ it for contactless strain measurements. Structural properties were observed by scanning electron microscope and X-ray diffraction, which shows the existence of two phases (fcc and bcc). Magnetic properties were studied by vibrating sample magnetometer and LCR-Bridge. Superelasticity was investigated by straining a ribbon. Measured superelastic strain at room temperature was ∼0.5%. Within that range we achieved 12% change of permeability that arises from the structural transition between two recognized phases. It proves that $Fe_{43.5}Mn_{34}Al_{15}Ni_{7.5}$ superelastic alloy is a promising potential contactless sensor of strain.

Index Terms—**Contactless sensor, Heusler alloy, magnetic material, superelasticity.**

I. INTRODUCTION

SUPERELASTIC (pseudoelastic) materials are able to recover high amount of strain [1]. Superelastic and shape memory behavior is granted by solid to solid phase transformation between two different phases, generally known as martensitic transformation, which is transformation between austenite (high-temperature phase, stable without stress) and martensite (low-temperature phase, stabilized by stress). The maximum strain is given by the difference between lattice parameter of two existing phases [2], [3]. Phase transformation can occur under the following conditions: 1) applied stress; 2) temperature; or 3) magnetic field change [4], which makes it a potential solid state sensor or actuator [1]. However, most used superelastic material based on Ni–Ti composition is not ferromagnetic [1], [5]. Superelastic material with appropriate magnetic properties could be a possible candidate for production of a contactless sensor of strain. Heusler alloys are possible choice for magnetic shape memory effect and for closely-related pseudoelastic effect.

Ferrous shape memory and superlelastic alloys have some advantages comparing with Ni–Ti-based alloys; they are cheaper and exhibit ferromagnetic behavior. Recently, the new ferrous superelastic $Fe_{43.5}Mn_{34}Al_{15}Ni_{7.5}$ alloy was discovered [3]. Two different phases with bcc and fcc structure are responsible for superelastic properties in this composition. The mentioned alloy was prepared by arc-melting method and aged at 200 °C for 6 h and subsequently cold-rolled at a reduction rate in thickness by 80%. Such a long production process has disadvantage for practical applications.

However, a few years ago, a melt-spinning method of preparing Heusler alloys was successfully employed. This method provides two advantages for the production of alloys: 1) the avoiding or reduction of annealing and 2) the synthesis of highly textured polycrystalline ribbons [6]. Ribbons prepared by melt spinning are more homogeneous than bulks prepared by arc melting [7].

In the given contribution, preparation of $Fe_{43.5}Mn_{34}Al_{15}Ni_{7.5}$ alloy is described and structural, magnetic, superelastic, and thermoelastic properties of melt-spun alloy are characterized.

II. EXPERIMENT

Master alloy with composition $Fe_{43.5}Mn_{34}Al_{15}Ni_{7.5}$ was prepared by arc melting in argon atmosphere, starting from highly pure elements (>99.9%). Ribbon was produced by melt spinning in an argon atmosphere at a wheel linear speed of 20 ms^{-1}. Ribbon's width ∼2.0–3.0 mm and uninterrupted length of one piece was ∼1.5 m. Bulks were prepared by suction casting method from master alloy. After production, no annealing was applied. Microstructure and element compositions were examined using a scanning electron microscope (SEM, JEOL 6100) equipped with an X-ray energy dispersive spectroscopy (EDS, Inca Energy 200) system. In addition, X-ray diffraction (XRD) patterns were obtained for phase identification. The XRD analysis were performed using Cu Kα (Kα_1 = 0.154089 nm) radiation at a room temperature. Magnetic properties were analyzed by vibrating sample magnetometer at the temperature of 20 °C and 300 °C. The stress–strain curves were obtained by force gauge FG20KG-RS23, superelastic, and thermoelastic strain were measured using DigimaticEA271122 Indicator ID-XC 543-390B. For sample straining Lustron Test Stand FS-1001 was used. The magnetic permeability was measured by Hameg HM8118 LCR-Bridge with test frequency of 100 kHz.

III. RESULTS AND DISCUSSION

The SEM micrographs of the fracture morphology are shown in Fig. 1, where an ordered columnar microstructure is observed. Individual columns grow perpendicularly to the ribbon plane following temperature gradient during quenching. There is also a thin layer of equiaxed crystallized grains

Manuscript received June 11, 2014; accepted August 2, 2014. Date of current version January 26, 2015. Corresponding author: J. Mino (e-mail: jakub.mino@student.upjs.sk).

Color versions of one or more of the figures in this paper are available online at http://ieeexplore.ieee.org.

Digital Object Identifier 10.1109/TMAG.2014.2348324

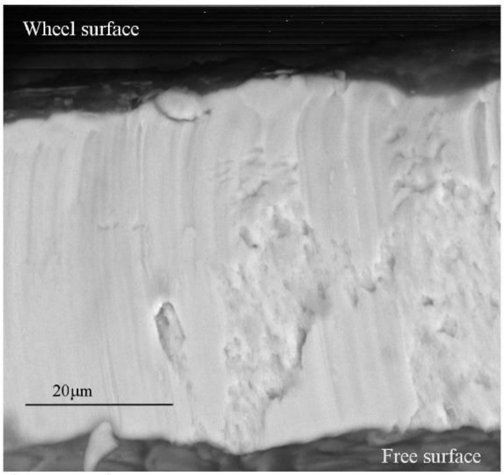

Fig. 1. SEM micrograph of the fracture $Fe_{43.5}Mn_{34}Al_{15}Ni_{7.5}$ ribbon with the marks of ribbon surfaces during the process of melt spinning.

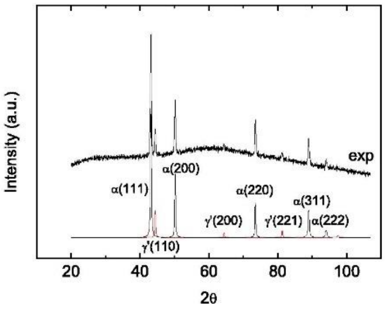

Fig. 2. XRD patterns with two different lattices of as-cast $Fe_{43.5}Mn_{34}Al_{15}Ni_{7.5}$ ribbon. Phases are identified as bcc (α) and fcc (γ') with comparison to experimental data (exp).

at the surface in contact with the wheel. The thickness of measured ribbon is ∼40–55 μm. The crystalline grain sizes are from 0.9 to 3.35 μm. During the examination, SEM ran in backscattering emission mode. The SEM/EDS microanalysis of selected area proved the homogeneous distribution of elements in the sample, which is typical for melt-spun ribbons [6]. In addition, a nominal composition is quite similar to average composition, which is $Fe_{42.49}Mn_{35.03}Al_{15.5}Ni_{6.94}$. Segregation of minor or major secondary phases was not observed.

Analysis of the XRD patterns reveals two different phases, as it is shown in the Fig. 2. The lattice parameter for an γ'-fcc lattice is $a_{\text{fcc}} = 0.36604$ nm and for α-bcc lattice it is $a_{\text{bcc}} = 0.29086$ nm. These parameters fit very well to the lattice constants acquired from [3] and [8]. The both phases coexist in the system and at the room temperature there was 87.7% of the alloy in the fcc phase and 12.3% of the bcc phase.

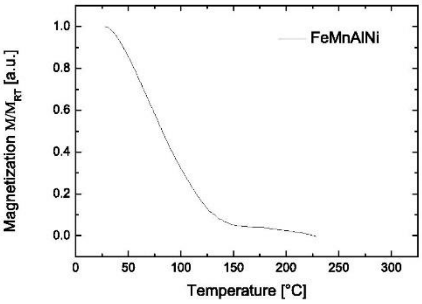

Fig. 3. M–T curve of $Fe_{43.5}Mn_{34}Al_{15}Ni_{7.5}$ taken in magnetic field of 200 kA/m with relative magnetization. M_{RT} represents magnetization at room temperature.

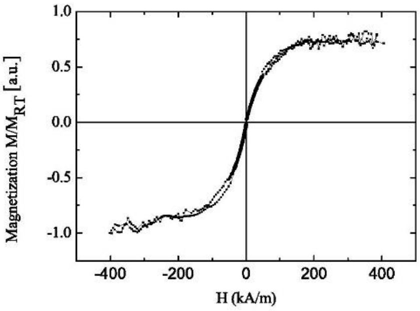

Fig. 4. Hysteresis loop of $Fe_{43.5}Mn_{34}Al_{15}Ni_{7.5}$ taken in room temperature with relative magnetization. M_{RT} represents magnetization at room temperature.

The magnetization versus temperature (M–T) curve of $Fe_{43.5}Mn_{34}Al_{15}Ni_{7.5}$ alloy was measured in magnetic field of 200 kA/m (shown in the Fig. 3). It shows typical ferromagnetic behavior with the magnetization decreasing with temperature. From the M–T curve, the Curie temperature was detected to be 125 °C similarly to [3]. Hysteresis loop (in Fig. 4) measured at room temperature confirms ferromagnetic nature of $Fe_{43.5}Mn_{34}Al_{15}Ni_{7.5}$ alloy.

To study superelastic properties, thermal dependence of strain was measured (Fig. 5). In the temperature range 25 °C–119 °C the maximum observed strain was 0.54%. In addition, thermal dependence of strain shows considerable hysteresis (14 °C), which is typical for superelastic materials [9]. The calculated linear coefficient of thermal expansion is $\alpha = 57.4\ \text{K}^{-1}10^{-6}$, which is significantly more than linear coefficient for others metals. According to high value of α, high strain cannot occur without phase transformation between two phases. The XRD proved the existence of two different lattices, so transformation runs between phases with bcc and fcc lattice.

Maximum theoretical strain $\varepsilon^{\max}$ can be calculated from lattice parameters [2]

$$\varepsilon_{100}^{\max} = \frac{\bar{2}a_{\text{bcc}} - a_{\text{fcc}}}{a_{\text{fcc}}}. \tag{1}$$

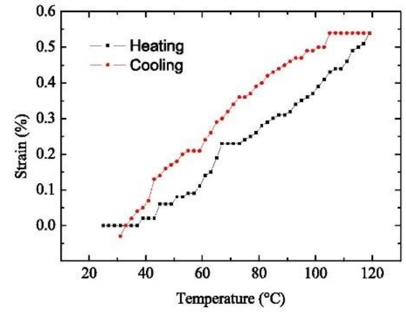

Fig. 5. Temperature dependence of strain of $Fe_{43.5}Mn_{34}Al_{15}Ni_{7.5}$ ribbon. No stress was applied.

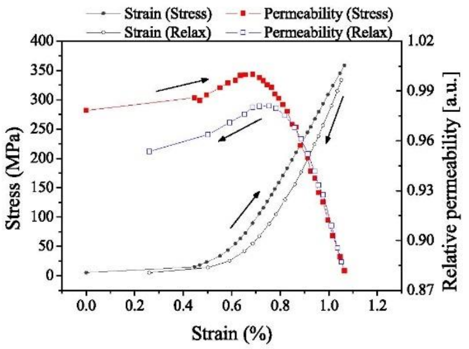

Fig. 6. Temperature dependence of permeability and stress on strain.

It works in whole range of superelastic behavior with total phase transformation between both lattice parameters, and suggested temperature range for $Fe_{43.5}Mn_{34}Al_{15}Ni_{7.5}$ is from 196 °C to 240 °C [3]. According to (1), the maximum strain is 12.3%, but it was not achieved in our case due to narrow experimental temperature range.

Stress–strain curves were taken up to 450 MPa of applied stress with simultaneous permeability measurement (Fig. 6).

Stress–strain measurement shows hysteresis typical for structural transition. The maximum induced strain was over 1%.

Phase transformation in $Fe_{43.5}Mn_{34}Al_{15}Ni_{7.5}$ triggers overall permeability of superelastic alloy due to the variation of magnetic properties of individual phases. This can be useful for contactless measuring of the strain through the change of permeability in material. Dependence of permeability on strain is linear until remarkable change of applied stress begins (Fig. 6). When applied strain grows up, $Fe_{43.5}Mn_{34}Al_{15}Ni_{7.5}$ alloy shows noticeable 12% change of permeability. There is only small hysteresis in permeability between positive straining and negative straining. In addition, the permeability at zero stress is different for two cases (relaxing and stressing), which points to the fact that permeability variations arises from structural transition between α and γ' phases rather than from stress dependence of permeability. Slim hysteresis is required for precise sensor or actuator [10].

IV. CONCLUSION

In this contribution, production of superelastic $Fe_{43.5}Mn_{34}Al_{15}Ni_{7.5}$ alloy by rapid quenching together with its structural and magnetic characterization is described. $Fe_{43.5}Mn_{34}Al_{15}Ni_{7.5}$ alloy prepared by melt-spinning method consists of α and γ' phase. Alloy shows ferromagnetic behavior with $T_C = 125$ °C. Permeability changes in characteristic range exhibit no hysteresis between stressing and relaxing in comparison with other properties, which confirms the fact that permeability variations are induced by the structural transition between α and γ' phases rather than from stress dependence of permeability. This attribute allows using $Fe_{43.5}Mn_{34}Al_{15}Ni_{7.5}$ as a potential sensor for measuring the strain.

ACKNOWLEDGMENT

This work was supported in part by the NanoCEXmat Project under Grant ITMS 26220120019 and in part by Slovak Grant Agency through the VEGA Project under Grant 1/0060/13 and Grant APVV-0027-11.

REFERENCES

[1] J. Ma, I. Karaman, and R. D. Noebe, "High temperature shape memory alloys," *Int. Mater. Rev.*, vol. 55, no. 5, pp. 257–315, Sep. 2010.
[2] Y. Tanaka, Y. Himuro, R. Kainuma, Y. Sutou, T. Omori, and K. Ishida, "Ferrous polycrystalline shape-memory alloy showing huge superelasticity," *Science*, vol. 327, no. 5972 pp. 1488–1490, Mar. 2010.
[3] T. Omori *et al.*, "Superelastic effect in polycrystalline ferrous alloys," *Science*, vol. 333, no. 6038, pp. 68–71, 2011.
[4] K. Ullakko, J. K. Huang, C. Kantner, R. C. O'Handley, and V. V. Kokorin, "Large magnetic-field-induced strains in Ni_2MnGa single crystals," *Appl. Phys. Lett.*, vol. 69, no. 13, pp. 1966–1968, Sep. 1996.
[5] C. D. J. Barras and K. A. Myers, "Nitinol—Its use in vascular surgery and other applications," *Eur. J. Vascular Endovascular Surgery*, vol. 19, no. 6, pp. 564–569 2000.
[6] J. L. S. Llamazares *et al.*, "Martensitic phase transformation in rapidly solidified $Mn_{50}Ni_{40}In_{10}$ alloy ribbons," *Appl. Phys. Lett.*, vol. 92, no. 1, p. 012513, 2008.
[7] B. Hernando *et al.*, "Thermal and magnetic field-induced martensite-austenite transition in $Ni_{50.3}Mn_{35.3}Sn_{14.4}$ ribbons," *Appl. Phys. Lett.*, vol. 92, no. 4, p. 042504, 2008.
[8] T. Omori, M. Nagasako, M. Okano, K. Endo, and R. Kainuma, "Microstructure and martensitic transformation in the Fe-Mn-Al-Ni shape memory alloy with B2-type coherent fine particles," *Appl. Phys. Lett.*, vol. 101, no. 23, p. 231907, 2012.
[9] J. M. Jani, M. Leary, A. Subic, and M. A. Gibson, "A review of shape memory alloy research, applications and opportunities," *Mater. Design*, vol. 56, pp. 1078–1113, Apr. 2014.
[10] D. Wang *et al.*, "Superelasticity of slim hysteresis over a wide temperature range by nanodomains of martensite," *Acta Mater.*, vol. 66, pp. 349–359, Mar. 2014.

Journal of ELECTRONIC MATERIALS, Vol. 45, No. 5, 2016
DOI: 10.1007/s11664-016-4351-6

Engineering of the GMR Effect in CuCo Microwires with Granular Structure

J. MINO,[1,2] V. ZHUKOVA,[2,5] J.J. DEL VAL,[2] M. IPATOV,[2,5] A. MARTINEZ-AMESTI,[4] R. VARGA,[1] and A. ZHUKOV[2,3,5,6]

1.—Institute of Physics, Faculty of Science, UPJS, Park Angelinum 9, 041 54 Kosice, Slovakia. 2.—Dpto. de Física de Materiales, Fac. Químicas, UPV/EHU, 20018 San Sebastián, Spain. 3.—Basque Foundation for Science, Ikerbasque, 48011 Bilbao, Spain. 4.—Fac. de Ciencia y Tecnología, UPV/EHU, 48940 Leioa, Spain. 5.—Dpto. de Física Aplicada, EUPDS, UPV/EHU, 200018 San Sebastián, Spain. 6.—e-mail: arkadi.joukov@ehu.es

We prepared $Cu_{100-x}Co_x$ (x = 5,10,20) glass-coated microwires by Taylor-Ulitovsky technique and studied the influence of annealing on structure and giant magnetoresistance (GMR) effect. We observed a significant improvement of the GMR effect in the samples annealed at high temperature (400°C) with longer annealing time. On the other hand low temperature annealing (150–200°C) only slightly affects the GMR effect. Considerable enhancement of the GMR effect related to structural changes of the studied samples after annealing is promising for technical applications.

Key words: Giant magnetoresistance, glass-coated microwires, Taylor-Ulitovsky, annealing

INTRODUCTION

Discovery of giant magnetoresistance (GMR) dates back to 1988 when change in the electrical resistance of the material was reported when an external magnetic field in magnetic multilayered films was applied.[1] The physical mechanism of the GMR effect is the spin-dependent scattering of electrons when travelling between two magnetic regions in a nanoscale non-magnetic metallic spacer.

From its discovery many new materials that exhibit the GMR effect have been developed. In particular, so-called granular materials consisting of small grains distributed inside a non-magnetic matrix can also exhibit the GMR effect.[2,3] Granular materials, usually formed by immiscible elements (Co, Fe, Ni)-(Cu, Pt, Au, Ag), have attracted considerable attention since the beginning of the 1990s.[2–5]

Similar to the case of multilayered thin films,[1,6,7] the GMR effect has been attributed to the spin-dependent scattering of conduction electrons within the magnetic granules as well as at the interfaces between magnetic and nonmagnetic regions.[2,3] Consequently, the size and spatial distribution of nano-sized ferromagnetic grains (usually of Co or Fe) inside the metallic matrix (typically Cu, Ag, Au or Pt) are crucial for obtaining high GMR effect.

These granular solids can be prepared by mechanical alloying[4] or different melt quenching techniques.[5,8,9]

One of the advantages of granular materials produced using the melt quenching method is that they can be easily obtained via the recrystallization of metastable alloys produced by various melt quenching techniques. This allows the preparation of large amounts of material and precise control of the structure of the material.

It is worth mentioning that during the last few years, studies of the composite microwires consisted of metallic nucleus surrounded by glass coating and prepared by the so-called Taylor-Ulitovsky technique involving melt quenching attracted considerable attention.[10–12] This method offers four main advantages: (i) with this method it is possible to prepare long and uniform glass-coated microwires (up to 10 km long) using rapid casting (about 100 m/min) with few grams of the master alloy. Consequently, this technique provides an opportunity for inexpensive mass production.[10–12] (ii) Moreover, the

---

(Received October 9, 2015; accepted January 12, 2016;

wide range of variation in geometrical and physical properties of microwires is adjustable.[11] (iii) Furthermore, glass-coating inflicts stress inside the metallic nucleus due to different thermal expansion coefficients of metallic nucleus and glass-coating. The strength of these stresses depends on the thickness of glass coating and metallic nucleus diameter, which provides another control mechanism of magnetoelastic anisotropy in the metallic nucleus.[11] (iv) Additionally, this type of material is quicker and much easier to prepare than multilayer films.

Glass-coated microwires from Fe-Ni-Co-based alloys containing metalloids (Si, B) can be prepared in an amorphous state and therefore usually present soft magnetic properties.[12]

A few years ago we employed this technique for preparation of Co-Cu and Fe-Cu microwires and reported on granular character of structure and GMR observation in as-prepared microwires.[9,12] However, reported GMR values were generally below 10%.

From previous knowledge on granular materials,[2–4] it is well-known that the GMR effect can be significantly improved by annealing allowing the recrystallization of metastable alloys.[2–4,13]

As was mentioned above, simultaneous rapid solidification of the composite wire consisting of metallic nucleus surrounded by the glass coating with rather different thermal expansion coefficients in the Taylor-Ulitovsky method induces strong internal stresses[14–18] (of the order of 100–1000 MPa) depending strongly on the ratio, ρ, between the metallic nucleus diameter, d, and total microwire diameter, D.[14,15] Existence of strong internal stresses reported in aforementioned publications[15–18] is essentially important for the formation of magnetic properties and the microstructure of glass-coated microwires. Thus, the magnetic properties of amorphous and crystalline glass-coated microwires are rather different from those of other amorphous materials.[19] Additionally, rather different structure and morphology of phases precipitating from amorphous precursor after the annealing of glass-coated microwires are reported elsewhere.[20,21] Aforementioned internal stresses can affect the recrystallization process of metastable microwires, the grain size of precipitating grains, the crystallization temperature, and even type of precipitating crystalline phases.[20–22]

Therefore, we can expect a different structure and consequently a different GMR effect in Co-Cu glass-coated microwires as compared to ribbons, thin films, and foils. Consequently in this work we studied the influence of annealing on GMR and the structure of glass-coated microwires with the compositions $Cu_{80}Co_{20}$, $Cu_{90}Co_{10}$, and $Cu_{95}Co_{5}$ prepared using the Taylor-Ulitovsky technique.

EXPERIMENTAL TECHNIQUE

We prepared Co_x-Cu_{100-x} ($5 \le x \le 20$ at.%) glass-coated microwires (typical total diameters, D, from 10 μm to 30 μm) consisting of a metallic nucleus (typical diameters, d, 5–20 μm) covered by an outer glass shell (typical thickness from 3 μm till 10 μm) using the Taylor-Ulitovsky technique described elsewhere.[11,12]

Samples have been annealed in a conventional furnace at fixed annealing temperatures, $T_{ann} = 400°C$ with varying annealing times, t_{ann} (10 min, 30 min, 60 min, 2 h, 5 h, 10 h, 24 h). Additional samples were annealed at an isothermal temperature ($T_{ann} = 150°C$ and 200°C) with varying annealing time, t_{ann}, up to 24 h.

Previously the x-ray diffraction (XRD) was successfully employed for studies of granular systems as well as prepared Co-Cu microwires.[23,24]

Therefore, in order to study the structure of the as-prepared and annealed samples we performed x-ray diffraction (XRD) studies using a BRUKER (D8 Advance) x-ray diffractometer with Cu K_α ($\lambda = 0.154$ nm) with a graphite monochromator located between the sample and the detector. XRD studies were made on the samples annealed at various temperatures and annealing times. As previously described,[22] cylindrical microwires are not the best samples for the XRD examination: they do not fit into the sample holder properly, so it is necessary to count with little shift in 2θ.

Transmission electron microscopy (TEM) work was done on a Philips SuperTwin CM200 and also on a TECNAI G2 20 TWIN, both operated at 200 kV and equipped with a LaB6 field emission gun and EDAX EDS microanalysis system. TECNAI G2 20 TWIN is also equipped with high angle annular dark-field scanning transmission electron microscopy (HAADF-STEM).

The samples for the TEM studies were prepared by ultramicrotomy. The Cu-Co microwires were embedded in an epoxy resin. Polymerization was performed at 70°C for 16 h followed by curing at room temperature for 1 week. Ultrathin sections, ~50 nm, were cut using an ultramicrotome (LKB-Ultratome III) equipped with a diamond-knife and the sections were supported on Mo-grids. To enable identification of wires in three sections, the resin blocks were trimmed to a trapezoidal shape. This shape is also essential in order to determine the cutting direction and to minimize sectioning artifacts such as compression and fractioning.

We used a quantum design physical property measurement system device for measurements of magnetic and magneto-transport properties in the 5–300 K temperature range under the external magnetic field up to 60 kOe.

The magnetoresistance (MR) has been defined as:

$$\Delta R/R(\%) = (R(H) - R(0)) \times 100/R(0). \qquad (1)$$

MR in all samples were tested under electric current $I = 10\ \mu$A.

EXPERIMENTAL RESULTS AND DISCUSSION

After annealing at 400°C, we generally observed considerable enhancement of the GMR effect in all studied samples. As an example, in the Co_5Cu_{95} microwire ($d = 13.3\ \mu$m, $\rho = 0.79$) we observed an increase of the GMI effect from 1% to 7.5% (see Fig. 1a) and an increase from 8% to 19% for the same annealing conditions in the $Cu_{80}Co_{20}$ microwire ($d = 13.3\ \mu$m; $\rho = 0.65$) (Fig. 1b). From XRD spectra we observed that the fabrication of microwires induces preferred grain orientation.

We identified two phases, fcc α-Co and fcc Cu. Most influenced by annealing is the sample with composition $Cu_{95}Co_5$ (Fig. 2a and c). After annealing of the sample $Cu_{95}Co_5$ we can observe a decrease of the preferred orientation. The first peak is appreciably increased and the relative intensities change with the annealing. In the very first peak we can observe merged peaks of both the Cu phase and the Co phase. For the sample $Cu_{80}Co_{20}$ (Fig. 2b and d), annealing does not significantly affect the XRD of Co-phase. The relative intensities of all the peaks are almost the same in the as-prepared and annealed $Cu_{80}Co_{20}$ samples. After annealing of the sample $Cu_{90}Co_{10}$ a remarkable preferred orientation persists. But more detailed analysis of the Cu and Co peaks allowed the observation that the peaks become more separated after annealing.

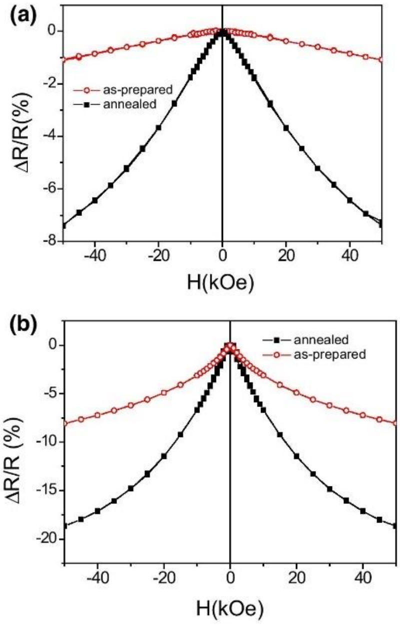

Fig. 1. $\Delta R/R(H)$ dependencies for Co_5Cu_{95} (a) and $Co_{20}Cu_{80}$ (b) microwires measured at 5 K in as-prepared and annealed at 400°C for 2 h.

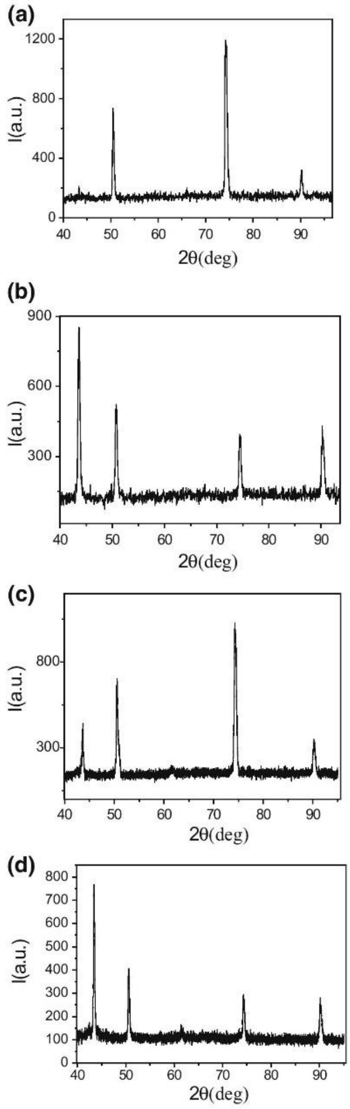

Fig. 2. XRD of as-prepared (a, b) and annealed at Tann = 400°C for 24 h (c, d) $Cu_{95}Co_5$ and $Cu_{80}Co_{20}$microwires, respectively.

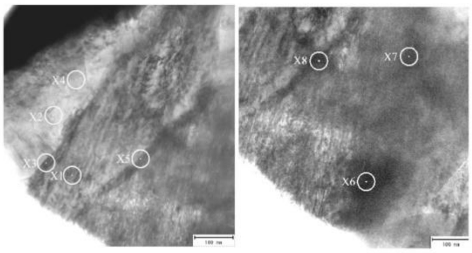

Fig. 3. TEM micrographs of $Cu_{80}Co_{20}$, where the circle marks the EDX beam. Chemical composition of analyses can be found in Table 1.

Table 1. Co and Cu content of EDX analyses in $Cu_{80}Co_{20}$ sample

$Cu_{80}Co_{20}$	Co (at.%)	Cu (at.%)
X1	4.5	95.5
X2	7.3	92.7
X3	4.9	95.1
X4	4.0	96.0
X5	2.2	97.8
X6	40.3	59.7
X7	15.3	84.6
X8	4.9	95.1

In order to prove the influence of the stress relaxation, isothermal annealing at lower temperatures was performed. Diffractograms of isothermally annealed samples were very similar to as-prepared samples.

TEM investigations show granular microstructure in the case of the $Cu_{80}Co_{20}$ sample. In the picture there are marked midpoints of energy-dispersive x-ray spectroscopy (EDX) analysis (the beam is 45 nm wide and illustrated by a circle) to show the chemical composition of grains (Fig. 3).

However, in the samples of $Cu_{90}Co_{10}$ and content $Cu_{95}Co_5$ granular microstructures were not observed. EDX analysis shows that all grains belong mostly to Cu-phase, but there are areas with increased Co. We observe low levels of Co content in the Cu matrix that can be related to the preparation process involving rapid quenching from the melt. Indeed, equilibrium of the Co-Cu phase diagram presents low Co solubility in Cu at room temperature (up to 8%). Areas with remarkably larger Co content (more than 10%) can be attributed to the relocated Co atoms in the Cu matrix after spinodal decomposition as previously observed.[9,25]

STEM mapping also suggests this hypothesis. In Fig. 4 maps are shown taken from grain-like areas in CuCo microwires. Grain structure was also only discovered in the $Cu_{80}Co_{20}$ sample. In the other two samples, the differences of Co or Cu content were negligible.

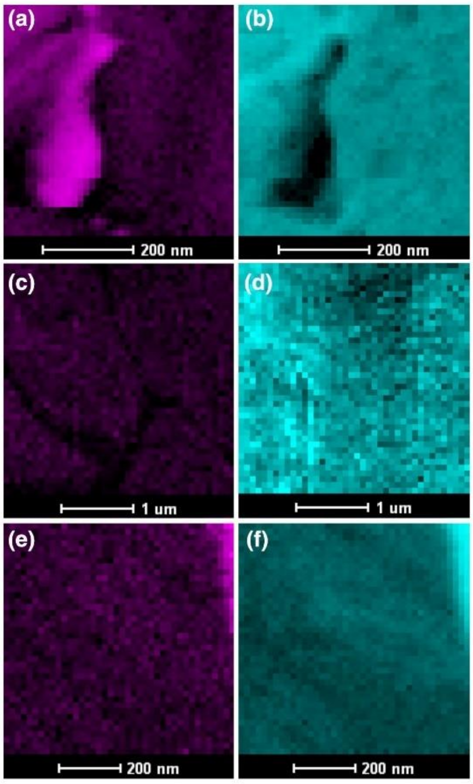

Fig. 4. STEM maps of Co and Cu content in all samples, Co map of samples (a) $Cu_{80}Co_{20}$ (c) $Cu_{90}Co_{10}$ (e) $Cu_{95}Co_5$ is indicated by purple colour. Cu map of samples (b) $Cu_{80}Co_{20}$ (d) $Cu_{90}Co_{10}$ (f) $Cu_{95}Co_5$ is indicated by teal colour.

As shown above, after annealing we observed remarkable improvement of GMR. Additionally after annealing of the $Cu_{80}Co_{20}$ sample, we can observe that there is a slight positive magnetoresistance that can be attributed to the anisotropic resistance related to ferromagnetic grain presence (Fig. 5).

Moreover we also measured GMR effect on samples annealed at 200°C with an annealing time of 24 h (sample was before annealed at 150°C for 10 h). The observed difference in $\Delta R/R(H)$ dependencies for Co_5Cu_{95} microwire is quite small (Fig. 6).

On the figures shown bellow (Fig. 7a–c), we summarize the results on studies of the effect of annealing at T_{ann} = 400° Con the GMR effect of all Co-Cu microwires.

In the graphs it is possible to see some irregularities from the expected state, which can be explained in three ways:

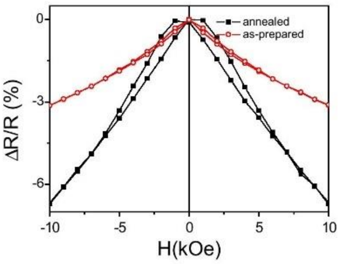

Fig. 5. $\Delta R/R(H)$ dependencies for $Co_{20}Cu_{80}$ (microwires measured at 5 K at low field region in as-prepared and annealed at 400 C for 2 h).

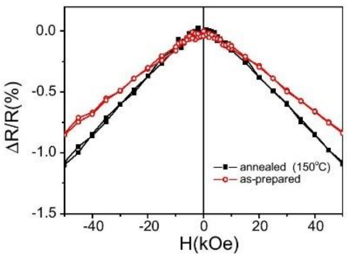

Fig. 6. $\Delta R/R(H)$ dependencies measured in as-prepared and annealed at 150°C for 10 h Co_5Cu_{95} microwires measured at 5 K.

(A) Annealing can release the stresses, which in principle influences the metallic core structure. However, this option is the least likely, because the stress relaxation occurs near 150–200°C[15] and measurements made on the samples annealed at low temperature do not show considerable change to the GMR effect (see Fig. 6).

(B) Another potential explanation was offered.[25] It can be described as a spinodal decomposition in CuCo samples. This means that the Co is distributed mainly in an oscillation of the concentration over most of the sample as shown for Co-Cu ribbons.

(C) Additionally it is possible that after production, microwires have inhomogeneous parts with higher or lower Co content.

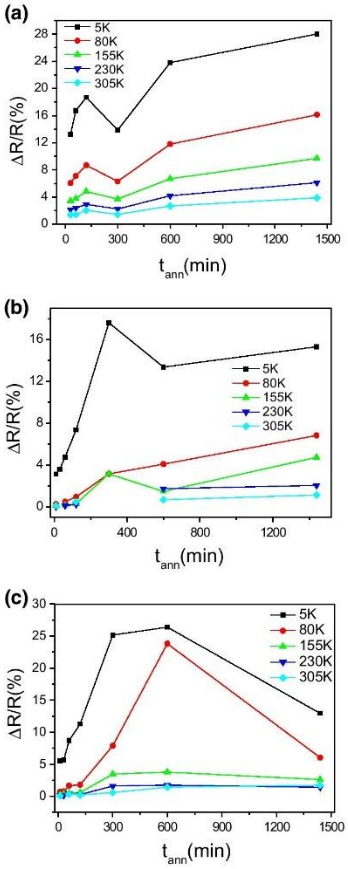

Fig. 7. Effect of annealing time on GMR effect measured in $Cu_{80}Co_{20}$ (a) $Cu_{90}Co_{10}$ (b) $Cu_{95}Co_5$ (c) microwires at different temperatures.

Internal stresses result in considerable texture among all the samples. We assume that after low-temperature annealing (T_{ann} = 150–200°C) stresses have been released, but XRD measurement shows that texture still persists after low temperature annealing. The GMR effect after low temperature annealing (i.e. after stress relaxation) was almost the same as in as-prepared microwires (see Fig. 6 for Co_5Cu_{95}). Comparison of Figs. 1a and 6 shows that maximum $\Delta R/R$ in the sample annealed at T_{ann} = 150°C for t_{ann} = 10 h at 5 K is just 1.2% (i.e. only slightly higher than for as-prepared sample), while for the same sample annealed at T_{ann} = 400°C for t_{ann} = 2 h $\Delta R/R \approx 7\%$ (see (Fig. 1b)). On the other hand after high-temperature annealing (T_{ann} = 400°C) we observed a considerable increase of the GMR effect in all the samples (Fig. 7).

It is worth mentioning that the maximum GMR ratio of about 28% obtained in annealed CoCu microwires in the magnetic field of about 10kOe is similar to the reported GMR values for other granular and multilayered materials.[2–8]

This GMR increase does not seem to be related with the stress relaxation and can be attributed to the short range ordering processes that cannot be distinguished by the XRD method.

Similar in all GMR systems is that high resistivity exists in the conducting medium, which is either magnetically inhomogeneous or disordered on the scale of the mean-free electron path.

On the other hand, the GMR appears only in samples with volume fraction Xv below the percolation volume fraction Xp. At Xv > Xp, all the particles form a connecting network with large ferromagnetic domains and low coercivity as in homogeneous ferromagnetic alloys and GMR decreases. Therefore, although we cannot detect any change of phase composition by XRD, observed dependence of the $\Delta R/R$ on T_{ann} must be attributed to the grain size and content change after annealing. The other possible reason for observed changes can be appearance of the nanostructures typical of spinodal decomposition after annealing.[8,25]

CONCLUSIONS

After annealing, a remarkable improvement of the GMR effect has been observed in all studied Co-Cu microwires. The largest GMR effect ($\Delta R/R \approx 28\%$) has been observed in $\mathrm{Cu_{80}Co_{20}}$. Similarly, for $\mathrm{Cu_{90}Co_{10}}$ and $\mathrm{Cu_{95}Co_{5}}$microwires we observed an increase of $\Delta R/R$ from 5.5% to 26% and from 3% to 17%, respectively. This GMR increase is not related to the stress relaxation and can be attributed to the short range ordering processes that cannot be distinguished by the XRD method.

ACKNOWLEDGEMENT

This work was supported by Spanish MINECO under MAT2013-47231-C2-1-P. The authors are thankful for technical and human support provided by SGIker of UPV/EHU and European funding (ERDF and ESF).

REFERENCES

1. M.N. Baibich, J.M. Broto, A. Fert, F. Nguyen van Dau, F. Petroff, P. Etienne, G. Creuzer, A. Friederich, and J. Chazeles, *Phys. Rev. Lett.* 61, 2472 (1988).
2. A.E. Berkowitz, J.R. Mitchell, M.J. Carey, A.P. Young, S. Zhang, F.E. Spada, F.T. Parker, A. Hutten, and G. Thomas, *Phys. Rev. Lett.* 68, 3745 (1992).
3. J.Q. Xiao, J.S. Jiang, and C.L. Chien, *Phys. Rev. Lett.* 68, 3749 (1992).
4. R. Yavari, P.J. Desré, and T. Benameur, *Phys. Rev. Lett.* 68, 2235 (1992).
5. P. Allia, K. Knobel, P. Tiberto, and F. Vinai, *Phys. Rev. B.* 52, 15398 (1995).
6. V.M. Fedosyuk, O.I. Kasyutich, D. Ravinder, and H.J. Blythe, *J. Magn. Magn. Mater.* 156, 345 (1996).
7. H.J. Blythe, V.M. Fedosyuk, and O.I. Kasyutich, *Mater. Lett.* 26, 69 (1996).
8. M.N. Baibich, G. Martínez, M.G.M. Miranda, A.T. da Rosa, J. González, and A. Zhukov, *J. Magn. Magn. Mater.* 320, 29 (2008).
9. M. Ilyn, V. Zhukova, C. Garcia, J.J. del Val, M. Ipatov, A. Granovsky, and A. Zhukov, *IEEE Trans. Magn.* 48, 11 (2012).
10. V.S. Larin, A.V. Torcunov, A. Zhukov, J. González, M. Vazquez, and L. Panina, *J. Magn. Magn. Mater.* 249, 39 (2002).
11. A. Zhukov, M. Ipatov, M. Churyukanova, S. Kaloshkin, and V. Zhukova, *J. Alloys Compd.* 586, S279 (2014).
12. A. Zhukov, J. Gonzalez, and V. Zhukova, *J. Magn. Magn. Mater.* 294, 165 (2005).
13. M.P.C. Vergara, J.C. Cezar, H.C.N. Tolentino, and M. Knobel, *Phys. B* 320, 143 (2002).
14. A. Zhukov, J.M. Blanco, M. Ipatov, A. Chizhik, and V. Zhukova, *Nanoscale Res. Lett.* 7, 223 (2013).
15. A. Zhukov, J. Gonzalez, J.M. Blanco, M.J. Prieto, E. Pina, and M. Vazquez, *J. Appl. Phys.* 87, 1402 (2000).
16. H. Chiriac and T.A. Ovari, *Prog. Mater Sci.* 40, 333 (1996).
17. S. Antonov, V.T. Borisov, O.V. Borisov, A.F. Prokoshin, and N.A. Usov, *J. Phys. D Appl. Phys.* 33, 1161 (2000).
18. J. Velázquez, M. Vazquez, and A. Zhukov, *J. Mater. Res.* 11, 2499 (1996).
19. A. Zhukov, M. Ipatov, and V. Zhukova, Advances in giant magnetoimpedance of materials, in *Handbook of Magnetic Materials*, ed. by K.H.J. Buschow, vol. 24 (2015), p. 98. doi: 10.1016/bs.hmm.2015.09.001.
20. J. Gonzalez, A. Zhukov, V. Zhukova, A.F. Cobeño, J.M. Blanco, A.R. de Arellano-Lopez, S. Lopez-Pombero, J. Martinez-Fernandez, V. Larin, and A. Torcunov, *IEEE Trans. Magn.* 36, 3015 (2000).
21. M. Zhukov, S. Churyukanova, V. Kaloshkin, S. Semenkova, M. Gudoshnikov, A. Ipatov, J.M. Talaat, V. Blanco, and J. Zhukova, *J. Alloys Compd.* 651, 718 (2015).
22. V. Zhukova, A.F. Cobeño, A. Zhukov, J.M. Blanco, V. Larin, and J. Gonzalez, *Nanostruct. Mater.* 11, 1319 (1999).
23. J.J. del Val, J. González, and A. Zhukov, *Phys. B* 299, 242 (2001).
24. L. Chien, J.Q. Xiao, and J.S. Jiang, *J. Appl. Phys.* 73, 5309 (1993).
25. M.G.M. Miranda, E. Estevez-Rams, G. Martinez, and M.N. Baibich, *Phys. Rev. B.* 68, 014434 (2003).

GMR and Kondo Effects in Cu-Co Microwires

V. Zhukova, J. Mino, J. J. Del Val, M. Ipatov, R. Varga, M. N. Baibich, G. Martinez, A. Granovsky & A. Zhukov

Journal of Superconductivity and Novel Magnetism
Incorporating Novel Magnetism

ISSN 1557-1939

J Supercond Nov Magn
DOI 10.1007/s10948-016-3767-9

Journal of
Superconductivity
and Novel
Magnetism

Volume 29 • Number 9
September 2016

10948 ISSN 1557-1939
29(9) 2221–2472 (2016)

Springer

Springer

J Supercond Nov Magn
DOI 10.1007/s10948-016-3767-9

ORIGINAL PAPER

GMR and Kondo Effects in Cu-Co Microwires

V. Zhukova[1,2] · **J. Mino**[1,3] · **J. J. Del Val**[1] · **M. Ipatov**[1,2] · **R. Varga**[3] · **M. N. Baibich**[4] · **G. Martinez**[4] · **A. Granovsky**[5] · **A. Zhukov**[1,2,6]

Received: 19 May 2016 / Accepted: 23 August 2016

Abstract We studied the effect of annealing on magneto-transport, magnetic, and structural properties of $Cu_{100-x}Co_x$ ($x = 5, 10, 20$) glass-coated microwires prepared using the Taylor-Ulitovsky technique. Both as-prepared and annealed samples exhibit magnetoresistance effect. We observed a Kondo-like effect in as-prepared and annealed $Cu_{95}Co_5$ microwire and a significant increase of the giant magnetoresistance (GMR) in all studied Co-Cu after annealing. The origin of GMR effect and Kondo-like behavior is discussed considering structural changes of the annealed samples.

Keywords Magnetic microwires · Giant magnetoresistance · Kondo effect · Granular alloy

✉ A. Zhukov
arkadi.joukov@ehu.es

[1] Dpto. de Física de Materiales, Fac. Químicas, UPV/EHU, 20018 San Sebastian, Spain

[2] Dpto. de Física Aplicada, EUPDS, UPV/EHU, 20018 San Sebastian, Spain

[3] Institute of Physics, Faculty of Science, UPJS, Park Angelinum 9, 041 54 Kosice, Slovakia

[4] Instituto de Física, UFRGS, C.P. 15051, 91501-970 Porto Alegre, RS, Brazil

[5] Moscow State "Lomonosov" University, Moscow, Russia

[6] IKERBASQUE, Basque Foundation for Science, 48011 Bilbao, Spain

1 Introduction

After discovery of giant magnetoresistance (GMR) in 1988 in magnetic multilayered films [1], many new materials with GMR have been developed. In particular, GMR was found in granular materials consisting of small grains distributed inside a non-magnetic matrix [2, 3]. A substantial advantage of granular materials is the preparation cost: multilayered materials must be fabricated using multisource MBE and sputtering with elevated fabrication. On the other hand, the granular materials can be fabricated with much simpler technologies, like mechanical alloying or rapid quenching [4–7].Consequently, granular materials formed by immiscible elements (Co, Fe, Ni)-(Cu, Pt, Au, Ag) attracted considerable attention since the beginning of the 1990s [2–5]. As in the case of multilayered thin films, the observed GMR has been attributed to spin-dependent scattering of conduction electrons within the magnetic granules as well as at the interfaces between magnetic and nonmagnetic regions [2, 3]. On the other hand, a novel rapid quenching method allowing the preparation of composite microwires consisting of a metallic nucleus surrounded by glass coating was developed during the last years [8]. The advantage of this method is that it is possible to prepare long uniform microwires (up to 10 km) with only a few grams of the master alloy [7–9]. Moreover, glass coating induces considerable stress inside the metallic nucleus (due to different thermal expansion coefficients) [9–11]. The strength of these stresses depends on the thickness of the glass coating and on the metallic nucleus diameter, which provides another control mechanism on its magnetoelastic anisotropy [10, 11]. Fe-Ni-Co-based compositions containing metalloids (Si, B) can be prepared in an amorphous state and is used to make soft magnetic microwires [9].

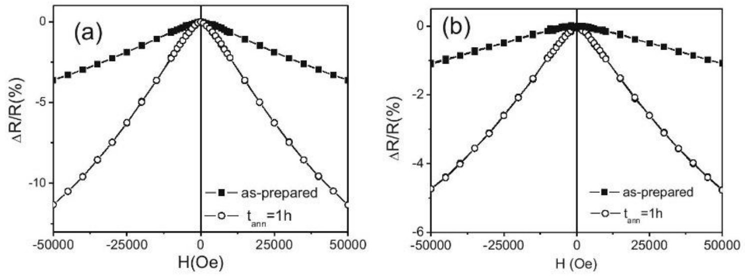

Fig. 1 $\Delta R/R(H)$ dependences for $Cu_{90}Co_{10}$ (**a**) and $Cu_{95}Co_5$ (**b**) microwires measured at 5 K in as-prepared and annealed at $T_{ann} = 673$ K for $t_{ann} = 1$ h

Few years ago, we employed this technique to prepare Cu-Co and Cu-Fe microwires and reported on granular character of its structure and GMR in as-prepared microwires [7, 12]. But reported GMR values were generally below 10 %.

From the previous knowledge on granular materials, it is well-known that GMR effect can be significantly improved by annealing of metastable alloys allowing precipitation of fine grains from the metastable alloys produced by rapid quenching from the melt [2–4, 13]. In the case of glass-coated microwire, annealing is also the way to release internal stresses [9, 14]. Such internal stresses can affect both the recrystallization process of the metastable microwires and the grain size of the precipitating grains [14, 15].

Additionally recently we reported that Co_5Cu_{95} microwires can present Kondo-like behavior exhibiting a minimum on temperature dependence of the resistance [16].

All these features can be affected by thermal treatment. Consequently, in this work, we study the influence of annealing on GMR and structure of glass-coated microwires with compositions $Cu_{80}Co_{20}$, $Cu_{90}Co_{10}$, and $Cu_{95}Co_5$ prepared using the Taylor-Ulitovsky technique.

2 Experimental Details

Studied $Cu_{100-x}Co_x$ ($5 \leq x \leq 20$ at %) glass-coated microwires (total diameters, D, from 10 to 30 μm) consisting of a metallic nucleus (diameters, d, 5–20 μm) have been prepared using the Taylor-Ulitovsky method [7, 8]. The samples have been annealed in conventional furnace at fixed annealing temperature, $T_{ann} = 673$ K varying the annealing time, t_{ann} (10, 30, and 60 min, and 2, 5, 10, and 24 h).

In order to study the structure of the samples, we performed X-ray diffraction (XRD) studies using a BRUKER (D8 Advance) X-ray diffractometer with Cu K_α ($\lambda = 0.154$ nm) with a graphite monochromator located between sample and detector.

A Quantum Design PPMS device was used to measure magnetic and magneto-transport properties at temperatures from 5 to 300 K with magnetic fields up to 60 kOe.

The magnetoresistance (MR) is defined as:

$$\Delta R/R(\%) = (R(H) - R(0)) \times 100/R(0) \qquad (1)$$

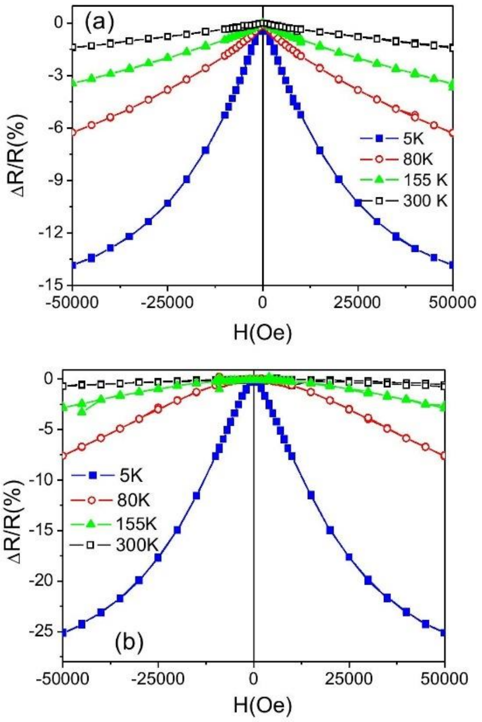

Fig. 2 $\Delta R/R(H)$ dependences for $Cu_{80}Co_{20}$ (**a**) and $Cu_{90}Co_{10}$ (**b**) microwires annealed at $T_{ann} = 673$ K for $t_{ann} = 5$ h measured at different temperatures

3 Experimental Results and Discussion

All studied samples exhibit GMR in the as-prepared state; but generally the maximum $\Delta R/R$ is below 5 % (see Fig. 1).

After annealing at $T_{\text{ann}} = 673$ K, we observed considerable enhancement of the GMR; for example, in $Cu_{90}Co_{10}$ microwire ($d \approx 14.7$ μm; $\rho = d/D = 0.73$), $\Delta R/R$ increases from 3 to 12 % after annealing for 1 h (Fig. 1a). For $Cu_{95}Co_5$ microwire, $\Delta R/R$ increases from 1 to 5 % after the annealing at the same conditions ($T_{\text{ann}} = 673$ K for $t_{\text{ann}} = 1$ h).

We observed considerable increasing of MR effect after annealing (Fig. 2). Moreover, increasing the annealing time generally further increasing of MR effect is observed (see Fig. 2): in the same sample and the same annealing temperature (with annealing for 5 h), $\Delta R/R$ reaches around 25 % (at $T = 5$ K) in studied $Cu_{90}Co_{10}$ microwire.

The behavior of $\Delta R/R(H)$ curves are typical for (standard, negative) GMR effect showing decreasing with magnetic field, H (Fig. 2). Moreover, $\Delta R/R(T)$ shows standard increase of the GMR ratio with decreasing the temperature for all samples (see Fig. 3).

The $Cu_{95}Co_5$ sample presents the lowest GMR measured (also showing considerable enhancement upon annealing) [16, 17], but the properties of this sample are probably the most unexpected: it presents a resistivity minimum on the temperature dependence (see Fig. 4). We observed this minimum in both as-prepared and annealed $Cu_{95}Co_5$ samples (Fig. 4a, b). The temperature of the minimum, T_{m}, of the as-prepared sample is considerably higher than that of the annealed sample (Fig. 4a).

The usual explanation for the resistivity minimum is the Kondo effect, related to magnetic impurities in non-magnetic metals. Usually, the Kondo effect is observed for very low contents of the impurities (0.002–0.02 %) [18], as the impurities cannot "see" each other in order to react independently to the conduction electron's spin. Thus, one of the features of the Kondo effect is that it can be suppressed by a magnetic field [19, 20].

As we can see from Fig. 4b, a magnetic field only slightly affects $R(T)$ of the as-prepared sample, but completely suppresses the minima of annealed ones.

In fact few different mechanisms might be considered to explain an increase of the resistivity of a metallic microwire at low temperatures: magnetic Kondo effect, weak localization, enhanced electron-electron interaction, scattering of conduction electrons by structural two-level system (TLS), and scattering of strongly spin-polarized charge carriers on diluted magnetic moments [16, 17].

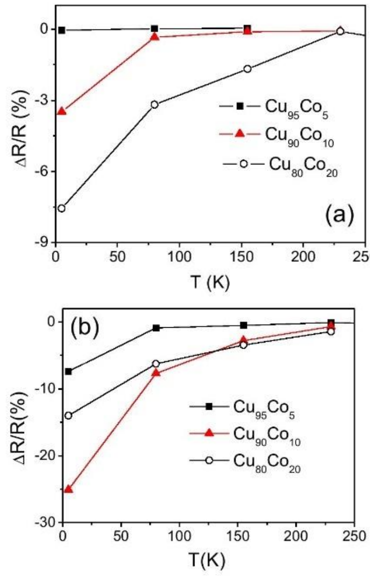

Fig. 3 Effect of temperature on GMR effect measured in as-prepared (**a**) and annealed at 673 K for 5 h (**b**) $Cu_{80}Co_{20}$, $Cu_{90}Co_{10}$, and $Cu_{95}Co_5$ microwires

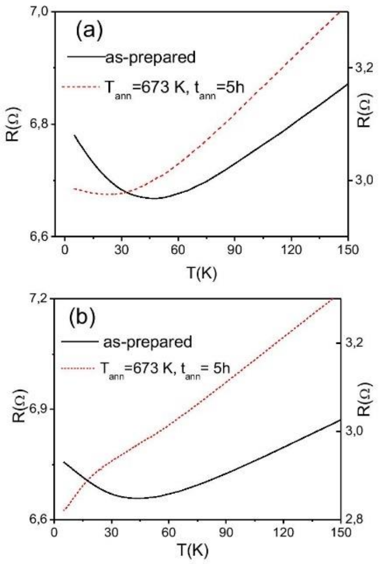

Fig. 4 $R(T)$ measured in as-prepared and annealed $Cu_{95}Co_5$ sample measured at $H = 0$T (**a**) and $H = 1$T (**b**)

The scattering processes on magnetic impurities could give rise to a resistivity contribution behaving as $\ln(T)$, and hence, provide a satisfactory explanation of the observed resistance minima. Figure 5 shows that the electrical resistivity exhibits roughly low-temperature $\ln(T)$ dependence for both as-prepared and annealed samples.

Magnetic measurements in principle can provide additional information on Co atoms distribution in the Cu matrix. Magnetization curves, $M(H)$, measured in as-prepared $Cu_{95}Co_5$ sample at 5 K exhibits saturation (see Fig. 6a). For higher temperatures (40, 50, 75, and 150 K), $M(H)$ dependences are virtually linear. Magnetization curves exhibiting saturation at 5 K might be associated with the presence of Co inhomogeneities or clusters.

After annealing ($T_{\mathrm{ann}} = 673$ K for $t_{\mathrm{ann}} = 5$ h) magnetic saturation can be observed up to much higher temperatures (see Fig. 6b). This can be explained considering the increasing of the Co inhomogeneities (or clusters) after annealing.

On the other hand, spinodal decomposition of the CoCu alloys characterized by long parallel Co-excess stripes [21], previously proposed by various authors, can be considered for the appearance of the Kondo effect in such high content alloys. For Kondo effect, one needs isolated magnetic entities inside the non-magnetic environment, which is only possible when one takes a non-uniform distribution of the impurity atoms, such as in spinodally decomposed materials.

X-ray diffraction (XRD) results can be interpreted as the existence of two phases: fcc Cu phase (Fig. 7) with main diffraction peaks at $2\Theta_1 \approx 43.23$ and $2\Theta_2 \approx 50.35°$ corresponding to atomic spacings of 2.09 and 1.81 Å and hcp α-Co with main diffraction peaks at $2\Theta_1 \approx 44.12°$ and $\Theta_2 \approx 51.57°$ corresponding to atomic spacings of 2.05 and 1.77 Å, respectively [22]. Those Cu and Co peaks are obviously quite close to each other. Owing to the low Co content in the sample the Co peaks are quite difficult to detect. Moreover the presence of an important texture further decreases the intensity of the main peak at $2\Theta_1 \approx 44.12°$.

Therefore these peaks are, in many cases overlapped (see Fig. 7a, b) and only a shoulder in the single peak corresponding to a small amount of the Co phase (presenting also small average grain size) can be observed in the main Cu peak. After annealing we observed broadening of the peaks (especially for $Cu_{95}Co_5$, see Fig. 7a) that can be attributed to the Co precipitation from the solid solution of Co in Cu. Recently we reported that we did not observe Co precipitations in as-prepared $Cu_{95}Co_5$ microwires [16]. These samples also present quite low MR effect in as-prepared state. In fact Co_5Cu_{95} alloy is not a classical diluted Kondo system not only because of large Co singleion concentration but also because a part of Co ions forms magnetic clusters and these clusters will create local magnetic fields and spin polarization of current carriers [23]. The presence of such clusters can be considered from the magnetization measurements at different temperatures, exhibiting saturation at low temperatures (Fig. 6). But even in the samples which do

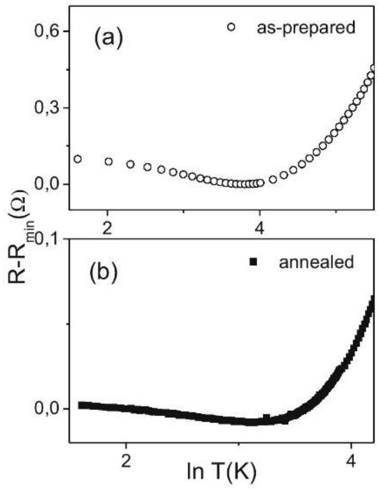

Fig. 5 R-$R_{\min}(\ln T)$ dependence for as-prepared (**a**) and annealed (**b**) $Cu_{95}Co_5$ samples

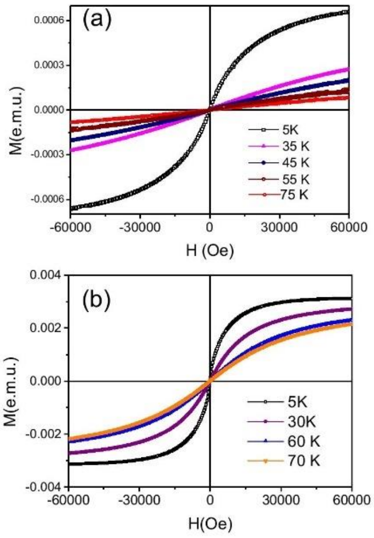

Fig. 6 Magnetization curves, $M(H)$, in as-prepared (**a**) and annealed at $T_{\mathrm{ann}} = 673$ K for $t_{\mathrm{ann}} = 5$ h (**b**) $Cu_{95}Co_5$ sample measured at different temperatures

Fig. 7 XRD of as-prepared $Cu_{95}Co_5$ (**a**) and $Cu_{80}Co_{20}$ (**b**) samples and annealed at $T_{\mathrm{ann}} = 673$ K for $t_{\mathrm{ann}} = 24$ h $Cu_{95}Co_5$ (**c**) and $Cu_{80}Co_{20}$ (**d**) microwires

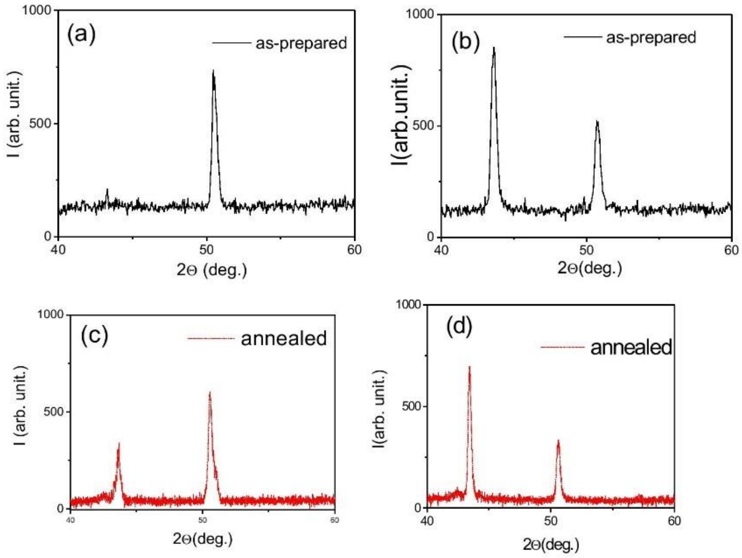

not present granular structure the other mechanisms like spindependent scattering in inter-granular spacers has been recently proposed [23].

As mentioned above the other peculiarity of the studied samples is the preferred grain orientation. After annealing we observed a decrease in preferred orientation. In the case of $Cu_{95}Co_5$ the first peak is appreciably increased and the relative intensities change with annealing. In the very first peak we can observe merged peaks of Cu and Co phases. For the sample $Cu_{80}Co_{20}$ (Fig. 6b) annealing does not affect the structure of the Co phase. The relative intensities of all the peaks of $Cu_{80}Co_{20}$ are less affected by annealing.

Although the peaks are merged (especially in the case of $Cu_{80}Co_{20}$ sample) we estimated the change of the relative intensities of the peaks at $2\Theta_1 \approx 44.12$ and $2\Theta_2 \approx 51.57°$, I_1/I_2: after annealing of $Cu_{95}Co_5$, I_1/I_2 increases from 0.27 to 0.57. For $Cu_{80}Co_{20}$ sample I_1/I_2 increases from 1.6 to 2.08. It is worth mentioning that usually the Co peaks at $2\Theta_1$ in Co-Cu granular alloys without texture present the highest intensity [22].

Consequently we cannot detect any change of phase composition by XRD and the observed dependence of the $\Delta R/R$ on T_{ann} must therefore be attributed to grain size and Co-content change after annealing. The other possible reason of the observed changes can be appearance of the nanostructures typical of the spinodal decomposition [21].

4 Conclusions

After annealing a remarkable improvement of the GMR effect has been observed in all studied CuCo microwires up to $\Delta R/R \approx 26$ %. In $Cu_{95}Co_5$, we observed a resistivity minimum typical of Kondo effect. The minimum temperature and magnetization curves of this sample as well as the magnetization curves are affected by the annealing. This GMR increasing could be attributed to the short-range-ordering processes that cannot be distinguished by the XRD method.

Acknowledgments This work was supported by Spanish MINECO under MAT2013-47231-C2-1-P and the Russian Science Foundation under the 16-19-10233 grants. Technical and human support provided by SGIker (UPV/EHU, MICINN, GV/EJ, ERDF, and ESF) is gratefully acknowledged. VZ and AZ wish to acknowledge the support of the Basque Government under Program of Mobility of the Researchers of the Basque Government (grants MV-2016-1-0025 and MV-2016-1-0018, respectively).

References

1. Baibich, M.N., Broto, J.M., Fert, A., Nguyen van Dau, F., Petroff, F., Etienne, P., Creuzer, G., Friederich, A., Chazeles, J.: Phys. Rev. Lett. **61**, 2472–2475 (1988)
2. Berkowitz, A.E., Mitchell, J.R., Carey, M.J., Young, A.P., Zhang, S., Spada, F.E., Parker, F.T., Hutten, A., Thomas, G.: Phys. Rev. Lett. **68**, 3745–3748 (1992)

3. Xiao, J.Q., Jiang, J.S., Chien, C.L.: Phys. Rev. Lett. **68**, 3749–3752 (1992)
4. Yavari, A.R., Desré, P.J., Benameur, T.: Phys. Rev. Lett. **68**, 2235–2238 (1992)
5. Allia, P., Knobel, K., Tiberto, P., Vinai, F.: Phys. Rev. B. **52**, 15 398–15 411 (1995)
6. Baibich, M.N., Martínez, G., Miranda, M.G.M., da Rosa, A.T., González, J., Zhukov, A.: J. Magn. Magn. Mater. **320**, e29–e31 (2008)
7. Ilyn, M., Zhukova, V., Garcia, C., del Val, J.J., Ipatov, M., Granovsky, A., Zhukov, A.: IEEE Trans. Magn. **48**(11), 3532–3535 (2012)
8. Larin, V.S., Torcunov, A.V., Zhukov, A., González, J., Vazquez, M., Panina, L.: J. Magn. Mater. **249**, 39–45 (2002)
9. Zhukov, A., Blanco, J.M., Ipatov, M., Chizhik, A., Zhukova, V.: Nanoscale Res. Lett. **7**, 223 (2012)
10. Chiriac, H., Ovari, T.A., Pop, G.: Phys. Rev. B **42**, 10105–10113 (1995)
11. Velázquez, J., Vazquez M, Zhukov, A.: J. Mater. Res. **11**(10), 2499–2505 (1996)
12. Zhukov, A., Gonzalez, J., Zhukova, V.: J. Magn. Magn. Mater. **294**, 165–173 (2005)
13. Vergara, M.P.C., Cezar, J.C., Tolentino, H.C.N., Knobel, M.: Physica B **320**, 143–145 (2002)
14. Zhukov, A., Ipatov, M., Garcia, C., Churyukanova, M., Kaloshkin, S., Zhukova, V.: J. Supercond. Nov. Magn. **26**, 1045–1054 (2013)
15. Aronin, A.S., Abrosimova, G.E., Kiselev, A.P., Zhukova, V., Varga, R., Zhukov, A.: Intermetallics **43**, 60–64 (2013)
16. Zhukova, V., Mino, J., Del Val, J.J., Ipatov, M., Martinez-Amesti, A., Varga, R., Churyukanova, M., Zhukov, A.: J. Alloys Compound. **266–271**, 674 (2016)
17. Mino, J., Zhukova, V., del Val, J.J., Ipatov, M., Martinez-Amesti, A., Varga, R., Zhukov, A.: J. Electron. Mater. **45**(5), 2401–2406 (2016)
18. Kondo, J.: Prog. Theor. Phys. **32**, 37–49 (1964)
19. Vedyaev, A., Granovsky, A.: Phys. Metal. Metalloved. **63**, 1076–1082 (1987)
20. Matho, K., Beal-Monod, M.: vol. 32 (1971)
21. Miranda, M.G.M., Estevez-Rams, E., Martinez, G., Baibich, M.N.: Phys. Rev. B. **68**, 014434 (2003)
22. del Val, J.J., González, J., Zhukov, A.: Physica B **299**, 242–250 (2001)
23. Granovsky, A., Ilyn, M., Zhukova, V., Zhukov, A., Gonzalez, J.: Phys. Solid State **53**, 320–322 (2011)

Journal of Alloys and Compounds 674 (2016) 266–271

Contents lists available at ScienceDirect

Journal of Alloys and Compounds

journal homepage: http://www.elsevier.com/locate/jalcom

Magnetoresistance and Kondo-like behaviour in Co_5Cu_{95} microwires

V. Zhukova [a, b], J. Mino [a, c], J.J. Del Val [a], M. Ipatov [a, b], A. Martinez-Amesti [d], R. Varga [c], M. Churyukanova [e], A. Zhukov [a, b, f, *]

[a] Dpto. de Física de Materiales, Fac. Químicas, UPV/EHU, 20018, San Sebastian, Spain
[b] Dpto. de Física Aplicada, EUPDS, UPV/EHU, 200018, San Sebastian, Spain
[c] Institute of Physics, Faculty of Science, UPJS, Park Angelinum 9, 04154, Kosice, Slovakia
[d] Fac. de Cienca y Tecnología, UPV/EHU, 48940, Leioa, Spain
[e] National University of Science and Technology «MISIS», Moscow, 119049, Russia
[f] IKERBASQUE, Basque Foundation for Science, 48011 Bilbao, Spain

ARTICLE INFO

Article history:
Received 12 January 2016
Received in revised form
4 March 2016
Accepted 7 March 2016
Available online 10 March 2016

Keywords:
Magnetic glass-coated microwires
Giant magnetoresistance effect
Taylor- Ulitvosky technique
Heat treatment
Magnetoresistance
Granular structure
Internal stresses
Taylor-Ulitovsky method
Glass-coated microwire
Annealing

ABSTRACT

We studied the effect of the annealing on the structure, transport properties and the magnetoresistance of $Cu_{95}Co_{95}$ glass-coated microwires prepared by Taylor-Ulitovsky technique. We observed a significant enhancement of the magnetoresistance, MR, effect in the samples annealed at 400 °C. On the other hand low temperature annealing (150–200 °C) allowed stress relaxation and elimination of the texture observed in as-prepared samples, although only slightly affects the MR effect. Annealing considerably affects the temperature dependence of resistivity. We observed resistivity minimum in both as-prepared and annealed samples associated with the Kondo effect. This minimum persists even under magnetic field in as-prepared samples. In annealed sample minimum disappears under applied magnetic field. Observed enhancement of the MR effect therefore must be attributed to the structural changes of the studied samples.

1. Introduction

Granular materials consisting of nano-sized ferromagnetic grains embedded into a nonmagnetic metallic matrix attracted continuous attention mostly owing to giant magnetoresistance (GMR) effect firstly reported in thin films [1] and slightly later reported for various granular materials [2–4]. Usually granular materials can be prepared from the immiscible elements, typically ferromagnetic elements such as Co or Fe, embedded into conductive metallic matrix (typically Cu, Ag, Au or Pt). The advantage of these granular materials is that they can be prepared using different rapid quenching [5–7] or mechanical alloying [8] techniques allowing fast and massive preparation of the samples.

The origin of the GMR effect in granular alloys has been explained considering the same nature as in the case of multilayered thin films, i.e. the spin-dependent scattering of conduction electrons within the magnetic entities as well as at the interfaces between the magnetic and nonmagnetic regions [1–8]. On the other hand there are still open questions as regarding the structure responsible for GMR effect in granular materials. Thus Co particles embedded in Cu matrix [5], small Co clusters within a Cu matrix [9], homogeneous spinodal decomposition characterized by long parallel Co-excess stripes [4] are proposed by various authors.

Rapid quenching techniques, allowing fabrication of metastable metallic alloys using the melt quenching, are quite common for preparation of the granular materials [4–6,9]. Usually, after appropriate recrystallization of the obtained alloys using annealing a more stable structures consisting of nano-sized inclusions into conductive metallic matrix can be obtained. Aforementioned precipitation of the small grains into conductive matrix is related to the phase diagram of the granular materials. Usually quite low solubility of the ferromagnetic metals in the metallic matrix metals at

---

[*] Corresponding author. Dpto. de Física de Materiales,Fac. Químicas,UPV/EHU, 20018, San Sebastian, Spain.
E-mail address: arkadi.joukov@ehu.es (A. Zhukov).

http://dx.doi.org/10.1016/j.jallcom.2016.03.039

room temperature takes place in phase diagrams of these metals. The source of the metastability is that in most of cases (i.e. Co–Cu) the solubility of ferromagnetic metal increases with temperature. Consequently, at room temperature a supersaturated solid solution can be obtained after the rapid quenching from high temperature. The appropriate annealing of such material may lead to the small particles precipitation form the matrix and formation of the materials consisting of fine grains of ferromagnetic elements embedded into the metallic non-magnetic matrix [5,7].

The most traditional well established rapid quenching technique allowing preparation of ribbons with either amorphous of metastable structure is planar melt spinning [4–6,10]. Quite different rapid quenching technique allowing fabrication of composite (glass-coated microwires) has been widely used for preparation of amorphous and nanocrystalline microwires [11,12]. This technique allows fabrication of long (up to few km) and continuous (up to 10 km continuous) microwires coated by glass and therefore recognized as quite promising from the view point of applications. The presence of the glass-coating with rather different thermal and mechanical properties can change considerable quenching conditions during the rapid quenching process. For instance, huge difference in thermal expansion coefficients of metallic nucleus and glass-coating induce strong internal stresses inside the metallic nucleus that can be tailored varying the glass-coating thickness and metallic nucleus diameter [11,13].

Consequently one can expect that the structure of the microwires with granular structure as well as GMR behaviour can be different and must be affected by the preparation parameters (quenching rate, internal stresses, annealing conditions …).

Recently we already reported on the influence of the internal stresses on crystalline structure, crystallization temperature and magnetic properties of microwires with nanocrystalline structure obtained after the recrystallization from the amorphous precursor [14–16]. Additionally we already reported on preparation of Co-Cu glass-coated microwires using Taylor-Ulitovsky exhibiting considerable GMR effect (below 10%) [17–19].

It is well-known that the structure of granular alloys can be considerably changed and the GMR effect can be significantly enhanced using adequate thermal treatment [2–6,19]. Moreover recently we observed electrical resistivity minimum in Co_5Cu_{95} glass-coated microwires [17].

Therefore in this paper we present our last experimental results on the influence of annealing on magnetic and transport properties of Co_5Cu_{95} glass-coated microwires.

2. Materials and methods

Co_5Cu_{95} glass-coated microwires (total diameters, $D \approx 16.9$ μm) consisted of metallic nucleus (with diameters, $d \approx 13.3$ μm) covered by outer glass shell (Durand glass) have been prepared by the Taylor-Ulitovsky technique [18].

X-ray diffraction (XRD) measurements were carried out by means of a D8-Advance (BRUKER) diffractometer provided with automatic divergence and receiving slits as well as graphite monochromator. CuKα (λ = 1.54 Å) radiation was used in all the patterns. Magnetic and magneto-transport properties have been measured at various temperatures within 5–300 K using suitable options of the Quantum Design magnetometer (PPMS). Magnetoresistance has been defined as:

$$\Delta R/R(\%) = (R(H) - R(0)) \times 100/R(0) \qquad (1)$$

Whenever the other was not stated the MR was measured for the field directed along the axis of the microwire, parallel to the current.

Samples have been annealed in conventional furnace at various annealing temperatures, T_{ann}, (150–400 °C) varying the annealing time, t_{ann}.

MR in all samples were tested under electric current I = 10 μA.

3. Experimental results and discussion

After annealing at 400 °C generally we observed considerable enhancement of the MR effect. For example we observed increasing of maximum $\Delta R/R$ from 1 to 13% after annealing at 400 °C for 10 h (Fig. 1). On the other hand annealing at lower temperature ($T_{ann} = 150°$ C) did not affect the MR effect: ΔR/R(H) curves of Co_5Cu_{95} sample after annealing at 150 °C: for 10 h is almost the same as in as-prepared samples (Fig. 1).

Consequently we systematically studied the influence of annealing time on magnetoresistance, MR, of Co_5Cu_{95} microwires annealed at 400 °C. The evolution of the maximum MR ratio on annealing time measured is shown in Fig. 2. Considerable enhancement of MR ratio after annealing at 400 °C (from 1% up to 17%) can be appreciated.

Low–temperature annealing has been performed in order to relax the internal stresses. From the previous knowledge on stress relaxation in glass-coated microwires we can assume that the relaxation processes run starting from 100 °C [20]. From Fig. 1 we can assume that the stress relaxation is not the key factor that affects the MR increasing (see Figs. 1 and 2) of studied samples.

Recently we reported that as-prepared Co_5Cu_{95} microwires exhibit a well pronounced minimum in temperature dependence of resistance at about 40 K, attributed by us to Kondo-like behaviour [17].

Consequently we measured temperature dependence of resistivity, R(T), in $Cu_{95}Co_5$ sample annealed at 400 °C. As can be seen from Fig. 3, the temperature of resistivity minimum, T_m, decreases after annealing (from 47 to 22 K). Additionally, the temperature coefficient of resistivity of annealed samples is much higher than of as-prepared $Cu_{95}Co_5$ sample.

These considerable differences must be associated with structural changes after annealing. Using XRD technique we observed the preferred grain orientation (texture) probably related to the fabrication method of microwires.

We observed presence of two phases, fcc α-Co and fcc Cu phase.

Annealing affects the XRD of $Cu_{95}Co_5$ sample (Fig. 4a and b). After annealing of the sample $Cu_{95}Co_5$ we observed decreasing of the preferred orientation. The first peak is appreciably increased

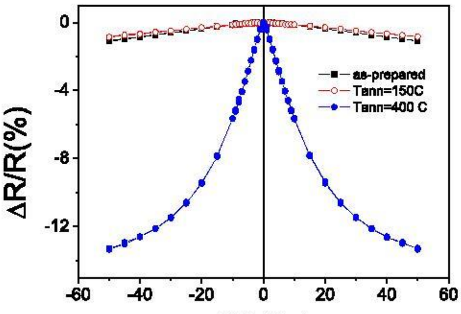

Fig. 1. ΔR/R(H) dependences measured in as-prepared, annealed at 150 °C for 10 h and at 400 C for 15 h Co_5Cu_{95} microwires measured at 5 K.

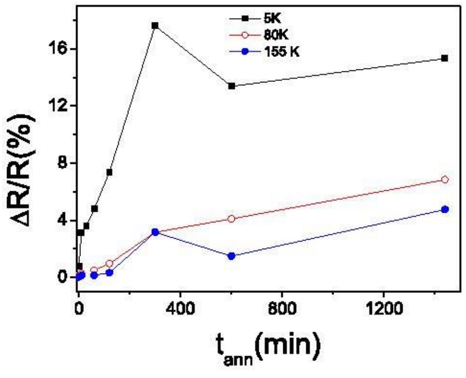

Fig. 2. Effect of annealing time on maximum MR ratio of the $Cu_{95}Co_5$ sample measured at different temperatures.

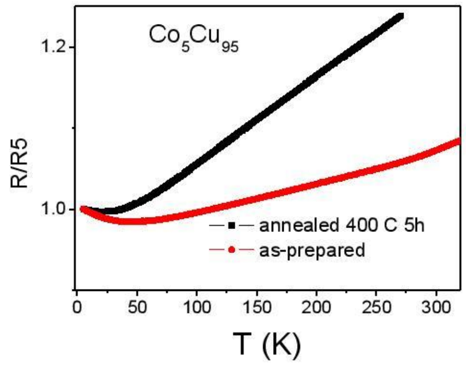

Fig. 3. R (T) measured in as-prepared and annealed $Cu_{95}Co_5$ sample.

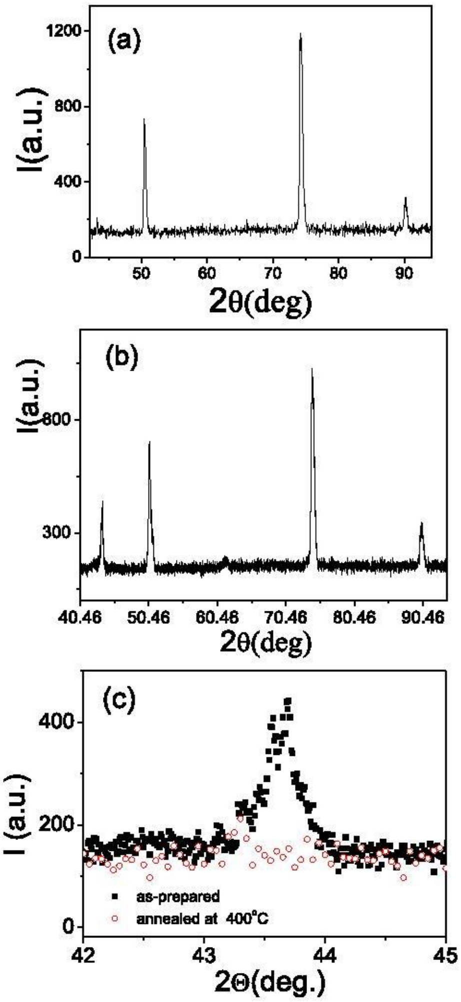

Fig. 4. XRD of as-prepared (a), annealed at T_{ann} = 400 °C for 24 h (b) $Cu_{95}Co_5$ microwires and comparison of first XRD peaks of as-prepared and annealed $Cu_{95}Co_5$ samples (c).

and the relative intensities change with the annealing. In the very first peak we can observe merged peaks of Cu and Co phases (see Fig. 4c).

On the other hand using STEM mapping we were not able to observed granular microstructures. EDX analysis shows that all grains belong mostly to Cu-phase, but there are areas with increased Co content. We observed small Co content in the Cu matrix that probably corresponds to solid solution of Co in Cu. In some areas the Co content was above 10% that can be attributed to the relocated spinodal decomposition of metastable CoCu alloys [4,13]. In the Fig. 5 are shown maps taken in grain-like areas in $Cu_{95}Co_5$ microwires. Grain structure was not observed in $Cu_{95}Co_5$.

Magnetic measurements can provide additional information on Co atoms distribution in Cu matrix. Magnetization curves, $M/M_{s5k}(H)$, measured at 5 K exhibits saturation (see Fig. 6). For higher temperature (40, 50, 75 and 150 K) $M/M_{s5k}(H)$ dependences are perfectly linear. Negative magnetization observed at 150 K must be attributed to diamagnetic contribution of glass. Magnetization curves exhibiting saturation at 5 K can be associated with the presence of Co inhomogeneities or clusters.

In crystalline materials few different mechanisms can be considered to explain an increase of the resistivity of a metallic alloys at low temperatures.

The common explanation of the resistivity minimum is the Kondo effect related to the magnetic impurities in metals. In classical Kondo-systems where the content of magnetic impurities in a metal is small (0.002–0.02%) it was recognized that the resistance minima is associated with magnetic impurities in the metallic host being one which has a local magnetic moment due to the spin of unpaired electrons in its atomic-like d or f shell [21]. The scattering processes from magnetic impurities (those in which the internal spin state of the impurity and scattered electron are exchanged) could give rise to a resistivity contribution behaving as ln(*T*), and hence provide a satisfactory explanation of the observed resistance

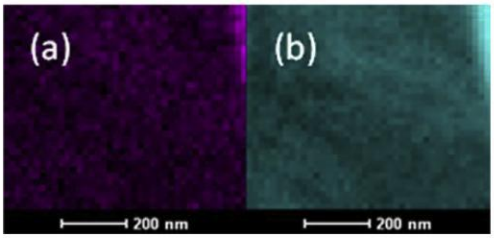

Fig. 5. STEM maps of Co and Cu content in $Cu_{95}Co_5$ where Cu indicated by purple colour map (a) and Co indicated by teal colour (b). (For interpretation of the references to colour in this figure legend, the reader is referred to the web version of this article.)

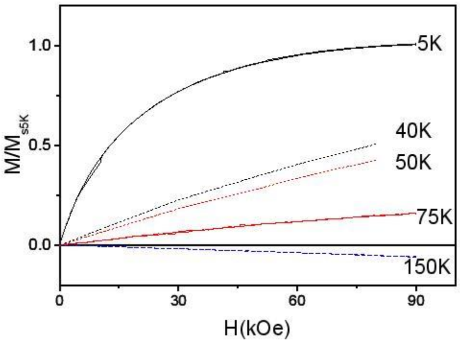

Fig. 6. Magnetization curves, $M/M_{s5k}(H)$, in as-prepared $Cu_{95}Co_5$ sample measured at different temperatures.

minima. Additionally, magnetic field usually suppresses the resistivity minimum [21,22]. But usually in classical Kondo-systems the minimum temperature is much lower. In our case the Co content is relatively high (5%) and consequently minimum temperature can be higher [23,24]. Indeed, strictly speaking the Kondo scattering mechanism only applies to metallic systems with very small amounts of magnetic impurities (dilute magnetic alloys). This is because the impurities can interact indirectly through the conduction electrons (RKKY interaction), and these interactions can clearly be expected to become important as the number of magnetic impurities is increased. But, certain non-dilute alloys with magnetic impurities can show a resistance minimum [25]. In many cases the Kondo mechanism provides quite satisfactory quantitative explanation of the R(T) dependences in these cases. In these systems the inter-impurity interactions are relatively small, and at intermediate and higher temperatures the magnetic ions act as independent scatterers. As a result, in this temperature regime, the Kondo mechanism is applicable.

To prove aforementioned mechanism we measured the effect of magnetic field on R(T) for both as-prepared and annealed $Cu_{95}Co_5$ samples (Fig. 7a and b) and plotted R-R_{min} versus ln T. As can be observed from Fig. 7 (a–c) in our case we do observe certain similarities with classical Kondo effect. Magnetic field considerably affects the resistivity minimum. It is worth mentioning that if the resistivity minimum of as-prepared samples Co_5Cu_{95} is not completely suppressed even by high magnetic field (H = 5T), resistivity minimum of annealed sample is completely suppressed by H = 1T. Surprisingly, in contrast to the other granular systems where R(T) minimum has been reported [24], we observed huge effect of annealing on minimum temperature, T_m: in our case T_m decreases after annealing from 47 to 22 K.

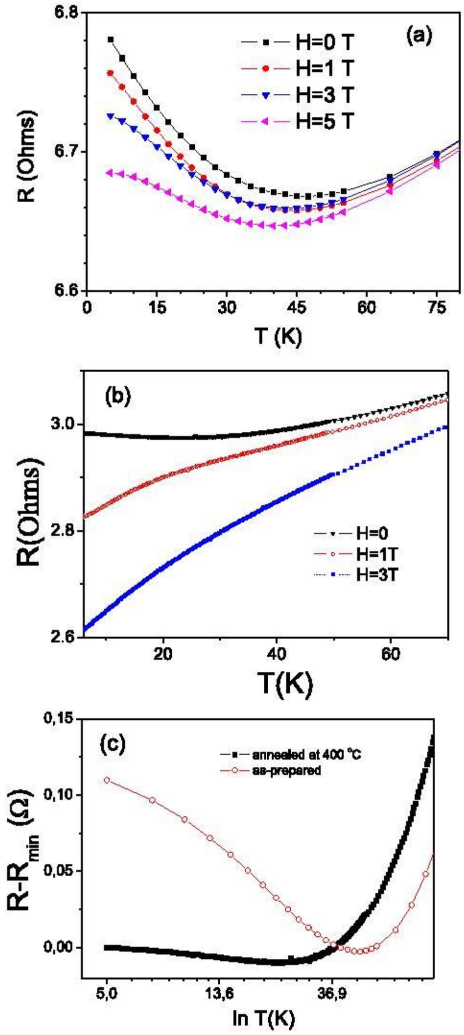

Fig. 7. Effect of magnetic field on temperature dependence of resistance, R, in as-prepared (a)and annealed at 400 °C (a) $Cu_{95}Co_5$ microwires and R-R_{min} (ln T) dependence for both samples (c).

Additionally Fig. 7c shows that the electrical resistivity exhibits an approximate low-temperature ln T dependence on T for both the as-prepared and annealed (T_{ann} = 400 °C) samples. From structural studies we did not observe Co-grains that means that Co is dissolved in Cu matrix.

Magnetization curves measured in Co-Cu microwires exhibit saturation at 5 K that can be associated with not uniform distribution of Co atoms in the Cu matrix, i.e. with the presence of Co inhomogeneities or clusters. Therefore studied Co_5Cu_{95} microwire is not a classical diluted Kondo system not only because of large Co single–ion concentration but also because a part of Co ions forms magnetic clusters and these clusters will create local magnetic fields and spin-polarization of current carriers [18].

Consequently both as-prepared and annealed Co_5Cu_{95} microwires present certain features typical for the classical Kondo effect related to the magnetic impurities in metals. But the resistivity minimum in as-prepared sample is not completely suppressed even at 7 T, the temperature of resistivity minimum is quite high for diluted Kondo alloys and the concentration of the Co ions distributed randomly in the Cu-matrix is not low. Therefore we cannot exclude interaction between magnetic Co-ions and, as a result, we can expect partial suppression of Kondo effect. Considering that studied samples present magnetic saturation at 5 K we must assume that the Co-ions are not uniformly distributed in the Cu-matrix: the regions with higher Co-ions content are responsible for the presence of Co inhomogeneities or clusters, while the regions with lower Co-ions content behave as the magnetic impurities in the metallic host.

We cannot exclude the role of other mechanisms, like TLS. TLS involves atomic motion. Although is known that atomic diffusion in disordered (amorphous) materials is higher than in crystalline materials [26], the TLS mechanism is less appropriate in the present case.

The other mechanisms, like weak localization, enhanced electron–electron interaction, scattering of conduction electrons by structural TLS and scattering of strongly spin-polarized charge carriers on diluted magnetic moments are also usually considered [22,27–29]. Above we reported that magnetic field considerably affects the resistivity minimum of as-prepared and annealed Co_5Cu_{95} microwire and therefore Kondo effect and TLS are more appropriated for the explanation of the observed Kondo-like anomaly.

Previously the temperature-dependent electrical resistivity with $T_m \approx 20$ K of granular Au/Fe superlattices was discussed in terms of a model related to the Kondo effect associated with loose spins proposed by Slonczewski [29,30]. Similarly to our case after annealing the resistivity minimum temperature decreased form 20 to 10 K was observed. However, a modelling considering small number of magnetic impurity forming a "quasi-bound state" between the magnetic moment of a localized impurity and the average moment of the itinerant electrons in its vicinity [31] gave an exaggerated Kondo temperature, $T_{K,}$ (about 100 K for Co-Ag). Additionally the T_m-values for as-prepared and annealed $Au_{1-x}Co_x$ ($x = 27,2$ and 42%) were lower in spite of higher Co content.

It is worth mentioning that unusual R(T) dependence has been reported for various amorphous materials [32–36]. From 1970-th it is known that many amorphous materials present a well-defined minimum in the resistivity–versus–temperature curve [31–36]. Moreover in many metallic glasses and disordered alloys the temperature dependence of the resistivity, R(T) is anomalous in that over a wide range of temperature the resistivity decreases with the temperature increasing. This is in contrast to the normal behaviour for ordered crystalline metals, where the temperature coefficient of resistivity, α, is large and positive.

There are few mechanisms explaining the origin of the resistivity minimum of amorphous materials. Some of them related to the role of metalloids that typically contain amorphous materials. In our case we must exclude the explanation related to the metalloids contribution.

But in our case the disordered structure arising from the rapid quenching from the melt can be the reason of the negative temperature coefficient of the resistivity, α [37,38]. Therefore, although they present crystalline structure (see Fig. 4) they can present high degree of disorder typical for amorphous alloys produced by the melt quenching.

Moreover after annealing releasing the internal stresses and the disorder we observed considerable growing of α.

Additionally after high-temperature annealing ($T_{ann} = 400$ °C) we observed considerable increasing of the MR effect in all the samples. Together with decreasing of T_m it can be interpreted as decreasing of the magnetic impurity content related to disorder degree decreasing, stress relaxation and segregation of the Co related to the spinodal decomposition.

This MR increasing is not seems to be related with the stress relaxation and must be attributed to the short range ordering processes that cannot be distinguished by the XRD method. The other possible explanation of observed experimental results can be related to the nanostructures typical of the spinodal decomposition reported after annealing of Co-Cu ribbons [4,13].

4. Conclusions

In summary, after annealing remarkable improvement of MR effect has been observed in Co_5Cu_{95} microwires (up to 17%). The increase in MR is not related with the stress relaxation and must be attributed to the short range ordering processes that cannot be distinguished by the XRD method. Additionally annealing considerably affects the temperature dependence of the resistivity. We observed resistivity minimum in both as-prepared and annealed samples associated with the Kondo-like behaviour. This minimum persists even under magnetic field in as-prepared samples. In annealed sample minimum disappears under applied magnetic field. We discussed observed results considering disorder, stress relaxation and spinodal decomposition of studied sample.

Acknowledgements

This work was supported by Spanish MINECO under MAT2013-47231-C2-1-P. AZ wishes to acknowledge the support of the Basque Government under Program of Mobility of the Investigating Personnel of the Department of Education, Universities and Investigation (grant MV-2016-1-0018). Technical and human support provided by SGIker (UPV/EHU, MICINN, GV/EJ, ERDF and ESF) is gratefully acknowledged. The authors acknowledge helpful discussions with Prof. A. Granovsky.

References

[1] M.N. Baibich, J.M. Broto, A. Fert, F.N. Vandau, F. Petroff, P. Etienne, G. Creuzet, A. Friederich, J. Chazelas, Giant magnetoresistance of (001)Fe/(001)Cr magnetic superlattices, Phys. Rev. Lett. 61 (1988) 2472.
[2] A.E. Berkowitz, J.R. Mitchell, M.J. Carey, A.P. Young, S. Zhang, F.E. Spada, F.T. Parker, A. Hutten, G. Thomas, Giant magnetoresistance in heterogeneous Cu-Co alloys, Phys. Rev. Lett. 68 (1992) 3745–3748.
[3] J.Q. Xiao, J.S. Jiang, C.L. Chien, Giant magnetoresistance in nonmultilayer magnetic systems, Phys. Rev. Lett. 68 (1992) 3749–3752.
[4] M.G.M. Miranda, E. Estevez-Rams, G. Martinez, M.N. Baibich, Phase separation in Cu90Co10 high-magnetoresistance materials, Phys. Rev. B 68 (2003) 014434.
[5] P. Allia, M. Knobel, P. Tiberto, F. Vinai, Magnetic properties and giant magnetoresistance of melt granular $Cu_{100-x}Co_x$ alloys, Phys. Rev. 52 (1995), 15 398.
[6] W.C. Nunes, W.S.D. Folly, J.P. Sinnecker, M.A. Novak, Temperature dependence of the coercive field in single-domain particle systems, Phys. Rev.B 70 (2004) 014419.
[7] A.R. Yavari, P.J. Desré, T. Benameur, Mechanically driven alloying of immiscible elements, Phys. Rev. Lett. 68 (1992) 2235–2238.
[8] J.A. De Toro, J.P. Andres, J.A. Gonzalez, J.P. Goff, A.J. Barbero, J.M. Riveiro, Improved giant magnetoresistance in nanogranular Co/Ag: the role of interparticle RKKY interactions, Phys. Rev. B 70 (2004) 224412.
[9] M.P.C. Vergara, J.C. Cezar, H.C.N. Tolentino, M. Knobel, Structural evolution of

Co clusters on Cu90Co10 upon annealing, Phys. B 320 (2002) 143–145.

[10] A. Zhukov, J. Gonzalez, V. Zhukova, Magnetoresistance in thin wires with granular structure, J. Magn. Magn. Mater. 294 (2005) 165–173.

[11] V. Zhukova, J.M. Blanco, M. Ipatov, A. Zhukov, Effect of transverse magnetic field on domain wall propagation inmagnetically bistable glass-coated amorphous microwires, J. Appl. Phys. 106 (2009) 113914.

[12] M. Vazquez, H. Chiriac, A. Zhukov, L. Panina, T. Uchiyama, On the state-of-the-art in magnetic microwires and expected trends for scientific and technological studies, Phys. Status Solidi A 208 (2011) 493–501.

[13] M.N. Baibich, G. Martí¬nez, M.G.M. Miranda, A.T. da Rosa, J. González, A. Zhukov, Ribbons and micro-wires of CuCo segregated alloys, J. Magn. Magn. Mater 320 (2008) e29–e31.

[14] A. Zhukov, M. Ipatov, M. Churyukanova, S. Kaloshkin, V. Zhukova, Giant magnetoimpedance in thin amorphous wires: from manipulation of magnetic field dependence to industrial applications, J. Alloys Comp. 586 (2014) S279–S286.

[15] J. Gonzalez, A. Zhukov, V. Zhukova, A.F. Cobeño, J.M. Blanco, A.R. de Arellano-Lopez, S. Lopez-Pombero, J. Martinez-Fernandez, V. Larin, A. Torcunov, High coercivity of partially devitrified glass-coated finemet microwires: effect of geometry and thermal treatment, IEEE Trans. Magn. 36 (No 5) (2000) 3015–3017.

[16] A. Zhukov, M. Churyukanova, S. Kaloshkin, V. Semenkova, S. Gudoshnikov, M. Ipatov, A. Talaat, J.M. Blanco, V. Zhukova, Effect of annealing on magnetic properties and magnetostriction coefficient of Fe Ni-based amorphous microwires, J. Alloys Comp. 651 (2015) 718–723.

[17] M. Ilyn, V. Zhukova, C. Garcia, J.J. del Val, M. Ipatov, A. Granovsky, A. Zhukov, Kondo effect and magnetotransport properties in Co-Cu microwires, IEEE Trans. Magn. 48 (11) (2012) 3532–3535.

[18] V. Zhukova, C. Garcia, J.J. del Val, M. Ilyn, A. Granovsky, A. Zhukov, Magnetic and transport properties of Co–Cu microwires with granular structure, Thin Solid Films 543 (2013) 142–147.

[19] A.E. Berkowitz, J.R. Mitchell, M.J. Carey, A.P. Young, D. Rao, A. Starr, S. Zhang, F.E. Spada, F.T. Parker, A. Hutten, G. Thomas, Giant magnetoresistance in heterogeneous Cu–Co and Ag–Co alloy films, J. Appl. Phys. 73 (1993) 5320–5325.

[20] M.J. Garcia Prieto, E. Pina, A.P. Zhukov, V. Larin, P. Marin, M. Vázquez, A. Hernando, Glass coated Co-rich amorphous microwires with improved permeability, Sensors Actuators A 81 (1–3) (2000) 227–231.

[21] J. Kondo, Resistance minimum in dilute magnetic alloys, Prog. Theor. Phys. 32 (1964) 37–49.

[22] A. Vedyaev, A. Granovsky, Electroresisrivity of amorphous ferromagnetic alloys in the Ziman-Faber model, Phys. Metal. Metalloved. 63 (1987) 1076–1082.

[23] K. Matho, M. Beal-Monod, Concentration effect in the Kondo resistivity, J. Phys. Colloq. Suppl. 32 (no 2–3) (1971). C1-213–C1-215.

[24] C. Manohar, The Kondo effect and the spin-flip scattering, Phys. Lett. 31 (6) (1970) 344–345.

[25] A. Sumiyama, Y. Oda, H. Nagano, Y. Onuki, K.i Shibutani, T. Komatsubara, Coherent Kondo state in a dense Kondo substance: CexLa1-xCu6, J. Phys. Soc. Jpn. 55 (1986) 1294–1304.

[26] R.W. Cahn, Atomic transport in amorphous materials: an introduction, J. Vac. Sci. Technol. A 4 (6) (1986) 3071–3077.

[27] M. Csontos, T. Wojtowicz, X. Liu, M. Dobrowolska, B. Janko, J.K. Furdyna, G. Mihaly, Magnetic scattering of spin polarized carriers in (In, Mn) Sb dilute magnetic semiconductor, Phys. Rev. Let. 95 (2005) 227203.

[28] A. Granovsky, M. Ilyn, V. Zhukova, A. Zhukov, J. Gonzalez, Giant magnetoresistance of granular microwires: spin dependent scattering in intergranular Spacers, Phys. Solid State 53 (No. 2) (2011) 320–322.

[29] H. Sato, Y. Kobayashi, Y. Aoki, H. Yamamoto, Transport properties in granular Co-Ag alloys, J. Phys. Condens. Matter 7 (1995) 7053–7062.

[30] J.C. Slonczewski, Origin of biquadratic exchange in magnetic multilayers, J.Appl. Phys. 73 (1993) 5957–5962.

[31] M.D. Daybell, W.A. Steyert, Loca1ized magnetic impurity states in metals: some experimental relationships, Rev. Mod. Phys. 40 (2) (1968) 380–389.

[32] R. Hasegawa, C.C. Tsuei, s-d Exchange interaction in amorphous Cr-Pd-Si and Mn-Pd-Si alloys, Phys. Rev.B 2 6 (1970) 1631–1643.

[33] R. Hasegawa, Electrical resistivity of amorphous metallic alloys, Phys. Lett. A 36 5 (1971) 425–426.

[34] R. Cochrane, Resistivity of amorphous metallic alloys, J. Phys. Colloq. 39 (C6) (1978). C6-1540–C6-1544.

[35] 0 Rapp, J. Jiicklet, K. Frobose, Relation between electron-phonon coupling constant and resistivity of amorphous transition metal alloys, J. Phys. F. Met. Phys. 11 (1981) 2359–2366.

[36] K. Shirakawa, K. Fukamichi, T. Kaneko, T. Masumoto, Electrical resistivity minima of Fe-(Ni, Co)-Zr amorphous alloys, J. Phys. F. Met. Phys. 14 (1984) 1491–1499.

[37] S.R. Nagel, Temperature dependence of the resistivity in metallic glasses, Phys. Rev.B 16 (4) (1977) 1694–1698.

[38] S.R. Nagel, J. Vassiliou, P.M. Homf, B.C. Giessen, Temperature dependence of the resistivity of Nb:Ni glasses, Phys. Rev.B 17 (2) (1978) 462–467.

Journal of Alloys and Compounds 695 (2017) 976–980

Contents lists available at ScienceDirect

Journal of Alloys and Compounds

journal homepage: http://www.elsevier.com/locate/jalcom

GMR effect and Kondo-like behaviour in Co-Cu microwires

A. Zhukov [a, b, c, *], J. Mino [d], J.J. del Val [a], R. Varga [d], G. Martinez [e], M.N. Baibich [e], M. Ipatov [a, b], M. Churyukanova [f], V. Zhukova [a, b]

[a] Dept. Phys. Mater., University of Basque Country UPV/EHU, 20018, San Sebastian, Spain
[b] Dept. Appl. Phys., EUPDS, University of Basque Country UPV/EHU, 20018, San Sebastian, Spain
[c] Ikerbasque, Basque Foundation for Science, 48011, Bilbao, Spain
[d] Institute of Physics, Faculty of Science, UPJS, Park Angelinum 9, 041 54, Kosice, Slovakia
[e] Instituto de Fisica, Universidade Federal do Rio Grande do Sul, 91501-970, Porto Alegre, RS, Brazil
[f] National University of Science and Technology «MISIS», Moscow, 119049, Russia

ARTICLE INFO

Article history:
Received 14 September 2016
Received in revised form
20 October 2016
Accepted 22 October 2016
Available online 24 October 2016

Keywords:
Glass-coated microwires
Annealing
Giant magnetoresistance effect
Kondo-effect

ABSTRACT

The influence of annealing on structure and temperature and magnetic field dependences of resistance of $Cu_{100-x}Co_x$ (x = 5, 10, 20) glass-coated microwires prepared using Taylor-Ulitovsky has been studied.

All $Cu_{100-x}Co_x$ microwires present resistivity minimum at certain temperature, T_m. This minimum is very well defined for as-cast samples. T_m-values decrease after annealing (from about 50 K to about 25 K). Observed *R(T)* dependences and the minimum are well affected by applied magnetic field.

Additionally we observed a significant increasing of the GMR effect in the annealed samples (at 400 °C) with long enough annealing time (up to 34% GMR effect).

Considerable enhancement of the GMR effect related with structural changes of the studied samples is promising for technical applications.

1. Introduction

Since the discovery of the giant magnetoresistance (GMRΠ effect in magnetic multilayered films [1] and later in granular materials [2,3] numerous studies on a variety of systems have been reported [1–6].

Granular or inhomogeneous materials typically formed by immiscible elements (Co, Fe, Ni)-(Cu, Pt, Au, Ag) attracted considerable attention since the beginning of 1990s [2,3,5,6]. The main interest in granular materials is related to a substantial economic difference between the preparation cost of a multilayered thin films and granular materials: multilayered materials must be fabricated with multisource MBE and sputtering. On the other hand granular materials can be fabricated with much simpler technology, like rapid quenching or ball milling [6,7].

Using rapid quenching from the melt it is possible to prepare a variety of materials with amorphous, nanocrystalline or granular structures [6,8–10]. Most interest in rapidly quenched materials is related to soft magnetic properties of amorphous and nanocrystalline ferromagnetic alloys [10,11]. But additionally rapidly quenching technique can be successfully employed for fast preparation of metastable and granular materials [6,12].

The main interest in granular materials is related to the GMR effect [7]. The origin of the GMR effect in granular materials has been attributed to spin-dependent scattering of the conduction electrons within the magnetic granules, as well as at the interfaces between magnetic granules and nonmagnetic matrix [2,3,5,6]. Granular structure can be usually obtained after the recrystallization of the metastable alloys prepared from immiscible elements (typically Co-Cu or Co-Ag) through the annealing. Formation of such structure is related to the phase diagram of the immiscible elements. Typically the phase diagram of immiscible alloys at room temperature presents quite low solubility of the ferromagnetic elements in the metallic matrix. Consequently, after rapid quenching from the melt the obtained alloys at room temperature usually form a supersaturated solid solution [2,3,6,12]. Annealing at adequate conditions allows formation of aforementioned granular structure consisting of fine magnetic precipitations within the nonmagnetic conductive metallic matrix [2,3,6].

It is worth mentioning that the granular structure is not the unique origin of the GMR effect in materials prepared from immiscible elements: the alternative interpretation of GMR effect

---

[*] Corresponding author. Dept. Phys. Mater., University of Basque Country UPV/EHU, 20018, San Sebastian, Spain.
E-mail address: arkadi.joukov@ehu.es (A. Zhukov).

http://dx.doi.org/10.1016/j.jallcom.2016.10.214
0925-8388/

involves Co particles embedded in Cu matrix [9], Co clusters within a Cu matrix [13] or homogeneous spinodal decomposition characterized by long parallel Co-excess stripes [14].

One of the routes allowing miniaturization of rapidly quenching materials is the utilization of novel techniques for preparation of composite materials. Thus, Taylor-Ulitovsky technique involving simultaneous rapid quenching from the melt of thin metallic microwire coated by glass gained considerable attention [12,15]. This inexpensive and fast preparation process allows preparation of long uniform glass-coated microwires (up to 10 km) with only a few grams of the master alloy with the diameter of metallic nucleus typically ranging from 0.1 up to 70 μm [12,15].

It is worth mentioning that simultaneous rapid quenching from the melt of the metallic alloy surrounded by the glass coating giving rise to the internal stresses related to difference in thermal expansion coefficients of metallic alloys and glass [16–18].

During last few years aforementioned Taylor-Ulitovsky method has been employed for preparation of Co-Cu and Fe-Cu microwires exhibiting granular structure and magnetoreistance, MR, effect [12,19,20]. But as-prepared Co-Cu and Fe-Cu microwires generally present relatively poor MR effect (below 10%). Recently we reported that MR effect can be considerable improved by annealing [20]. Additionally we reported on observation of resistivity minimum on temperature dependence of resistivity in $Cu_{95}Co_5$ microwires [21].

Consequently in this paper, we present our last experimental results on the influence of annealing conditions on magnetic, transport and structural properties of $Cu_{100\text{-}x}Co_x$ glass-coated microwires paying attention on temperature dependence of resistivity.

2. Experimental method

Taylor-Ulitovsky technique [12,15–21] has been employed for preparation of $Cu_{100\text{-}x}Co_x$ ($x = 5,10,20$) glass-coated microwires.

Studied $Co_{10}Cu_{90}$ glass-coated microwires (total diameters, $D \approx 20.2$ μm, metallic nucleus diameter $d \approx 14.7$ μm have been prepared using the Taylor-Ulitovsky technique.

Structure and phase composition have been studied using a BRUKER (D8 Advance) X-ray diffractometer with Cu K_α ($\lambda = 1.54$ Å) radiation.

Magnetic and transport properties have been measured using a Quantum Design PPMS device (with applied magnetic field up to 90 kOe) in the temperature range 5–300 K. For magnetic and transport measurements we used 4–5 mm long samples.

The magnetoresistance ratio (MR) is defined as:

$$\Delta R/R(\%) = (R(H) - R(0))x100/R(0) \tag{1}$$

Where R(H) is resistance at given magnetic field, H, R(0) is the resistance at $H = 0$. Because of thin diameters the sample resistance is not small (a few Ohms). Consequently observed resistivity changes we of the order from 0.2 to 1 Ohms.

Samples have been annealed in conventional furnace at annealing temperatures, $T_{ann} = 673$ K varying the annealing time, t_{ann}.

3. Experimental results and discussion

After annealing at 673 K even for short time ($t_{ann} = 60$ min) we observed considerable increasing of the MR effect. As an example $\Delta R/R(H)$ dependences measured in as-prepared and annealed ($t_{ann} = 60$ min) $Cu_{80}Co_{20}$ samples are shown in Fig. 1.

As-prepared $Cu_{80}Co_{20}$ samples at 5 K present $\Delta R/R \approx 7\%$ similarly to that reported previously [12] (see Fig. 1a). After annealing we observed considerable increasing of $\Delta R/R$ (see comparison of $\Delta R/R(H)$ for as-prepared and annealed at T_{ann}, = 673 f K or $t_{ann} = 60$ min in Fig. 1b). Observed $\Delta R/R(H)$ dependences are typical for GMR effect showing decreasing with magnetic field, H, increasing (Fig. 1). It is worth mentioning that recently we already reported on increasing of $\Delta R/R$ up to 25% for $Cu_{80}Co_{20}$ and $Cu_{90}Co_{10}$ microwires after annealing [21].

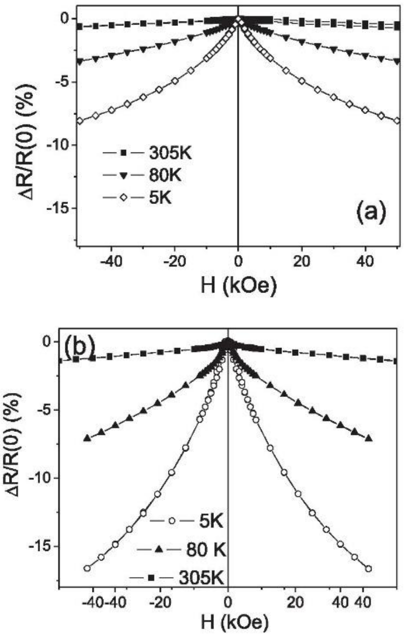

Fig. 1. ΔR/R(H) dependences for as-prepared (a) and annealed at 673 K for 60 min (b) $Cu_{80}Co_{20}$ microwires measured at different temperatures.

The other difference of as-prepared and annealed samples can be observed in magnetization curves: after annealing magnetic field dependence of magnetization (normalized to the value at maximum applied field), $M/M_{Hmax}(H)$ measured in $Cu_{90}Co_{10}$ and $Cu_{95}Co_5$ samples at 75 K presents saturation, while saturation is not observed in as-prepared samples measured at the same temperatures (see Fig. 2).

Recently we also reported on resistivity minimum versus temperature, $R(T)$, observed in as-prepared and annealed $Cu_{95}Co_5$ microwire [20].

We measured $R(T)$ dependences in $Cu_{90}Co_{10}$ and $Cu_{80}Co_{20}$ microwires (see Figs. 3 and 4).

As-prepared $Cu_{90}Co_{10}$ microwire presents well defined resistivity minimum on $R(T)$ dependence at about 50 K (Fig. 3a). After annealing the minimum on $R(T)$ dependence still takes place (Fig. 3b), but the minimum temperature decreases from 50 K to 27 K.

Similar $R(T)$ dependences are observed for $Cu_{80}Co_{20}$ microwire: well defined resistivity minimum on $R(T)$ dependence of as-prepared $Cu_{80}Co_{20}$ microwire is observed at about 50 K (Fig. 4). In annealed $Cu_{80}Co_{20}$ sample the minimum on $R(T)$ dependence is still appreciable, but similarly to $Cu_{90}Co_{10}$ sample the minimum temperature decreases from 50 K to 27 K (Fig. 4).

Usually the resistivity minimum on R(T) dependences is

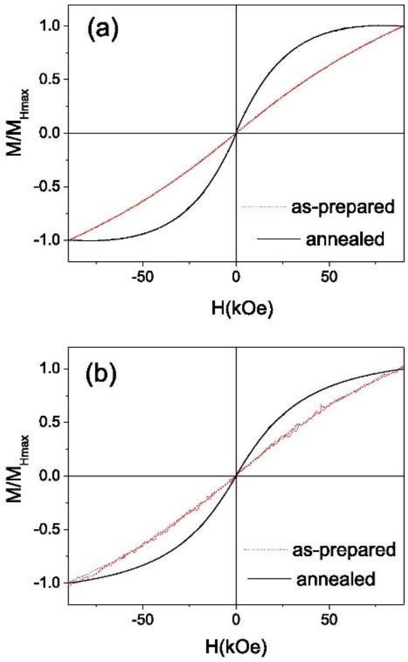

Fig. 2. Magnetization curves, M/M_{Hmax} (H), in as-prepared and annealed at 673 K for 10 h $Cu_{90}Co_{10}$ sample (a) and $Cu_{95}Co_{5}$ sample (b) measured at 75 K.

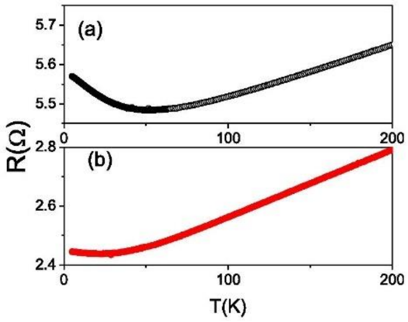

Fig. 3. Temperature dependence of resistance, R, measured in as-prepared (a) and annealed at 673 K (b) $Cu_{90}Co_{10}$ microwire.

attributed to the Kondo effect related to the effect of magnetic impurities on electron scattering in metals. But in classical Kondo-systems the content of magnetic impurities in a metal is rather small (0,002–0,02%) [22]. One of the features of the classical Kondo effect is the suppression of the *R(T)* minimum by external magnetic field. Consequently we studied the influence of magnetic field on *R(T)* dependences for both samples. In both as-prepared samples quite high magnetic field (of the order of 50 kOe for $Cu_{90}Co_{10}$ and 30 kOe for $Cu_{80}Co_{20}$) is needed to suppress the resistivity minimum (see Figs. 5a and 6a).

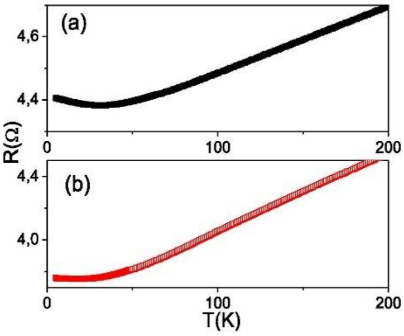

Fig. 4. Temperature dependences of resistance, R, measured in as-prepared (a) and annealed at 673 K (b) Cu_{80} Co_{20} microwire.

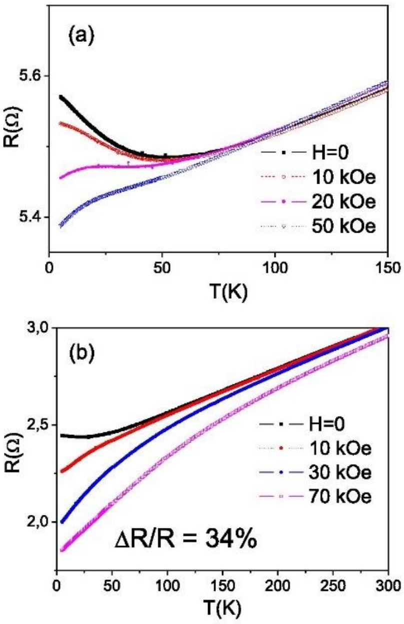

Fig. 5. Effect of magnetic field on temperature dependence of resistance, R, in as-prepared (a) and annealed at 673 K (b) $Cu_{90}Co_{10}$ microwires.

It is worth mentioning that from *R(T)* dependences measured under different external magnetic field the ΔR/R value can be estimated. For $Cu_{90}Co_{10}$ microwire after annealing at 673 K for 600 min the $\Delta R/R \approx 34\%$ at 5 K (for $Cu_{80}Co_{20}$ microwire $\Delta R/R \approx 32\%$). These quite singificant *ΔR/R* can be attractive for technical applications.

Similar tendencies have been recently observed by us in $Cu_{95}Co_{5}$ microwires [20].

The other feature of the classical Kondo effect is a resistivity contribution behaving as ln(*T*). In order to prove it we re-plotted *R(T)* dependences in a semi-logarithmic scale. As can be observed

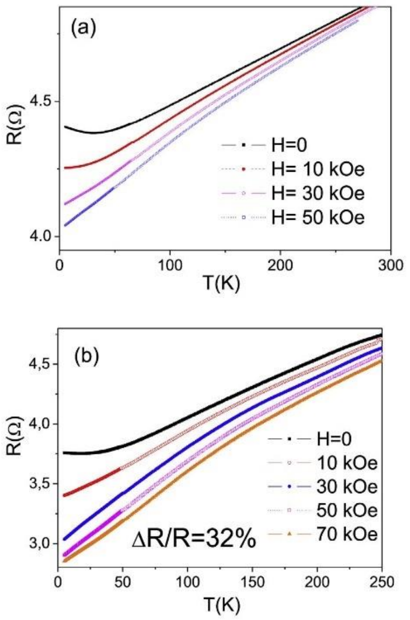

Fig. 6. Effect of magnetic field on temperature dependence of resistance, R, in as-prepared (a) and annealed at 673 K (b) $Cu_{80}Co_{20}$ microwires.

for as-prepared $Cu_{90}Co_{10}$ sample the $R\text{-}R_{min}(\ln T)$ dependence is not perfectly linear, although for annealed $Cu_{90}Co_{10}$ sample linear dependence fits better (Fig. 7).

Generally $R\text{-}R_{min}(\ln T)$ dependence for $Cu_{80}Co_{20}$ microwire can be described much better by the linear approximation (see Fig. 8).

As mentioned above in our case the Co content is relatively high (10–20%) and consequently minimum temperature can be higher than in classical Kondo-systems with low impurity content [23,24].

Indeed, certain non-dilute alloys with magnetic impurities can show a resistance minimum [25,26]. In some cases the Kondo mechanism provides quite satisfactory quantitative explanation of the $R(T)$ dependences in these cases. In these systems the interimpurity interactions are relatively small, and at intermediate and higher temperatures the magnetic ions act as independent scatterers. As a result, in this temperature regime, the Kondo mechanism is applicable.

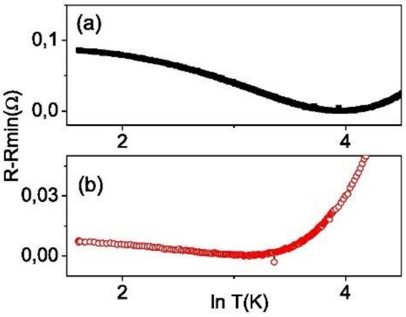

Fig. 7. R-R_{min}(ln T) dependence for as-prepared (a) and annealed at 673 K for 600 min (b) $Cu_{90}Co_{10}$ samples.

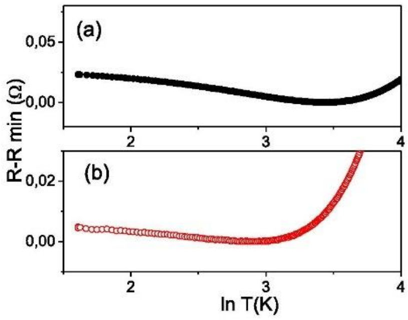

Fig. 8. R-R_{min}(ln T) dependence for as-prepared (a) and annealed at 673 K for 600 min (b) $Cu_{80}Co_{20}$ samples.

More detailed structural studies can provide the answer on origin of $R(T)$ minimum.

Consequently we employed the X-ray diffraction (XRD). The structure of the metallic core can be interpreted as granular with two phases: the main one, *fcc* Cu (lattice parameter 3.61 Å), found in all samples and small amount of *hcp* Co (lattice parameters 2.51 Å and 4.07 Å) with grain size between 20 and 40 nm (the estimation is provided using Debye–Scherrer correlation). The diffraction peaks of both phases in observed XRD spectra are quite close to each other and even overlapped (see Fig. 9) and only a shoulder in the single peak corresponding to a small amount of the Co phase (presenting also small average grain size) can be observed in the main Cu peak.

After annealing we observed also broadening of the peaks (as can be seen for $2\Theta \approx 50°$ see Fig. 9) that can be attributed to the Co precipitation from the solid solution of Co in Cu.

Consequently, we can assume that, after annealing the precipitation of fine Co grains from the metastable structure of $Co_{10}Cu_{90}$ microwire takes place. This assumption is confirmed by observation of magnetization saturation in annealed samples (see Fig. 2).

Considering described above $R(T)$ dependences we can assume that after annealing in solid solution of Co in Cu we'll have less Co content and this sample can be more similar to the classical Kondo-

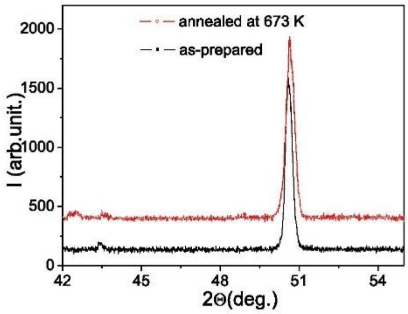

Fig. 9. XRD patterns of as-prepared and annealed at 673 K for $Co_{10}Cu_{90}$ microwires.

system (lower *R(T)* minimum temperature, stronger influence of magnetic field on *R(T)* dependence, better semi-logarithmic fitting). The redistribution of Co in the studied sample after annealing and formation of either Co grains or lamellar nanostructures can therefore explain observed dependences.

It is worth mentioning that the other possible reason of the observed changes can be related to appearance of the nanostructures typical for the spinodal decomposition [14].

On the other hand for similar Co content in Co-Ag system the nonmonotonic resistivity temperature dependence was explained using the two-current model without involving a Kondo mechanism [26].

Consequently, although in most cases our samples present features typical for the classical Kondo effect, we must consider also the other mechanisms responsible for the *R(T)* minimum, like weak localization, enhanced electron-electron interaction, scattering of conduction electrons by structural TLS and scattering of strongly spin-polarized charge carriers on diluted magnetic moments.

4. Conclusions

We prepared and studied the magnetic properties and magnetoresistance of $Cu_{100\text{-}x}Co_x$ (x = 5,10,20) glass-coated microwires. As-prepared microwires present MR generally below 7%. After annealing we observed considerable enhancement of the GMR effect up to 34% in $Cu_{90}Co_{10}$ microwire and up to 32% in $Cu_{80}Co_{20}$ microwire. We also observed the resistivity minimum on temperature dependence. The temperature of minimum is affected by the annealing. In both as-prepared and annealed samples *R(T)* dependence is affected by external magnetic field.

The obtained results can be interpreted considering the formation of the fine Co grains inside the Cu matrix as well as appearance of lamellar nanostructures allowing enhancement of the MR effect after annealing.

Considerable enhancement of the GMR effect of the studied samples after annealing can be useful for technical applications.

Acknowledgment

This work was supported by Spanish MINECO under MAT2013-47231-C2-1-P grant. VZ and AZ wish to acknowledge the support under Program of Mobility of the Researchers of the Basque Government (grants MV-2016-1-0025 and MV-2016-1-0018 respectively). Technical and human support provided by SGIker (UPV/EHU) is gratefully acknowledged.

References

[1] M.N. Baibich, J.M. Broto, A. Fert, F. Nguyen Van Dau, F. Petroff, P. Etienne, G. Creuzet, A. Friederich, J. Chazelas, Giant magnetoresistance of (001)Fe/(001) Cr magnetic superlattices, Phys.Rev.Lett. 61 (1988) 2472–2475.
[2] A.E. Berkowitz, J.R. Mitchell, M.J. Carey, A.P. Young, S. Zhang, P.E. Spada, F.T. Parker, A. Hutten, G. Thomas, Giant magnetoresistance in heterogeneous Cu-Co alloys, Phys. Rev. Lett. 68 (1992) 3745–3748.
[3] C.L. Chien, J.Q. Xiao, J.S. Jiang, Giant negative magnetoresistance in granular ferromagnetic systems, J. Appl. Phys. 73 (1993) 5309–5314.
[4] I. Bakonyi, L. Peter, Electrodeposited multilayer films with giant magnetoresistance (GMR): progress and problems, Prog. Mater Sci. 55 (2010) 107–245.
[5] J.Q. Xiao, J.S. Jiang, C.L. Chien, Giant magnetoresistance in nonmultilayer magnetic system, Phys. Rev. Lett. 68 (1992) 3749–3752.
[6] P. Allia, M. Knobel, P. Tiberto, F. Vinai, Magnetic properties and giant magnetoresistance of melt spun granular Cu100-x Cox alloys, Phys. Rev. 52 (1995) 15398–15411.
[7] A.R. Yavari, P.J. Desré, T. Benameur, Mechanically driven alloying of immiscible elements, Phys. Rev. Lett. 68 (1992) 2235–2238.
[8] I.S. Miroshnichenko, I.V. Salli, A device for the crystallization of alloys at a high cooling rate, Zav. Lab. 2 (1959) 1398.
[9] K. Klement, R.H. Wilens, P. Duwez, Non-crystalline structure in solidified Gold-Silicon alloys, Nature 187 (1970) 869–870.
[10] M.E. McHenry, M.A. Willard, D.E. Laughlin, Amorphous and nanocrystalline materials for applications as soft magnets, Prog. Mater. Sci. 44 (1999) 291–433.
[11] G. Herzer, Anisotropies in soft magnetic nanocrystalline alloys, J. Magn. Magn. Mater 294 (2005) 99–106.
[12] A. Zhukov, C. Garcia, M. Ilyn, R. Varga, J.J. del Val, A. Granovsky, V. Rodionova, M. Ipatov, V. Zhukova, Magnetic and transport properties of granular and Heusler-type glass-coated microwires, J. Magn. Magn. Mater. 324 (2012) 3558–3562.
[13] M.P.C. Vergara, J.C. Cezar, H.C.N. Tolentino, M. Knobel, Structural evolution of Co clusters on $Cu_{90}Co_{10}$ upon annealing, Phys. B, 320 (2002) 143–145.
[14] M.G.M. Miranda, E. Estevez-Rams, G. Martinez, M.N. Baibich, Phase separation in $Cu_{90}Co_{10}$ high-magnetoresistance materials, Phys. Rev. B, 68 (2003) 014434.
[15] H. Chiriac, M. Lostun, G. Ababei, T.-A. Ovari, Comparative study of the magnetic properties of positive and nearly zero magnetostrictive submicron amorphous wires, J. Appl. Phys. 109 (2011) 07B501.
[16] A. Zhukov, J. Gonzalez, A. Torcunov, E. Pina, M.J. Prieto, A.F. Cobeño, J.M. Blanco, V. Larin, S. Baranov, Ferromagnetic resonance and structure of Fe-based glass-coated microwires, J. Magn. Magn. Mat. 203 (1999) 238–240.
[17] H. Chiriac, T.A. Ovari, Gh Pop, Internal stress distribution in glass-covered amorphous magnetic wires, Phys. Rev. B 42 (1995) 10105–10113.
[18] P.A. Ekstrom, A. Zhukov, Spatial structure of the head-to-head propagating domain wall in glass-covered FeSiB microwire, J. Phys. D. Appl. Phys. 43 (2010) 205001.
[19] A. Zhukov, J. Gonzalez, V. Zhukova, Magnetoresistance in thin wires with granular structure, J. Magn. Magn. Mater. 294 (2005) 165–173.
[20] V. Zhukova, J. Mino, J.J. Del Val, M. Ipatov, A. Martinez-Amesti, R. Varga, M. Churyukanova, A. Zhukov, Magnetoresistance and Kondo-like behaviour in Co_5Cu_{95} microwires, J. Alloys Compd. 674 (2016) 266–271.
[21] J. Mino, V. Zhukova, J.J. del Val, M. Ipatov, A. Martinez-Amesti, R. Varga, A. Zhukov, Engineering of the GMR effect in CuCo microwire with granular structure, J. Electron. Mater. 45 (5) (2016) 2401–2406.
[22] J. Kondo, Resistance minimum in dilute magnetic alloys, Prog. Theor. Phys. 32 (1964) 37–49.
[23] K. Matho, M. Beal-Monod, Concentration effect in the Kondo resistivity, supplement, 32 no 2-3, J. de Physique Colloques (1971). C1-213-C1-215.
[24] C. Manohar, The Kondo effect and the spin-flip scattering, Phys. Lett 31 (6) (1970) 344–345.
[25] A. Sumiyama, Y. Oda, H. Nagano, Y. Onuki, K.I. Shibutani, T. Komatsubara, Coherent Kondo state in a dense Kondo substance: CexLa1-xCu6, J. Phys. Soc. Jpn. 55 (1986) 1294–1304.
[26] A. Gerber, A. Milner, I.Ya. Korenblit, M. Karpovsky, A. Gladkikh, A. Sulpice, Temperature dependence of resistance and magnetoresistance of nanogranular Co-Ag films, Phys. Rev. B 57 (21) (1998) 13667.

Kondo-like behavior and GMR effect in granular $Cu_{90}Co_{10}$ microwires

V. Zhukova, J. Mino, J. J. del Val, R. Varga, G. Martinez, M. Baibich, M. Ipatov, and A. Zhukov

Citation: AIP Advances **7**, 055906 (2017); doi: 10.1063/1.4973291
View online: http://dx.doi.org/10.1063/1.4973291
View Table of Contents: http://aip.scitation.org/toc/adv/7/5
Published by the American Institute of Physics

AIP ADVANCES **7**, 055906 (2017)

Kondo-like behavior and GMR effect in granular $Cu_{90}Co_{10}$ microwires

V. Zhukova,[1,2] J. Mino,[3] J. J. del Val,[1] R. Varga,[3] G. Martinez,[4] M. Baibich,[4]
M. Ipatov,[1,2] and A. Zhukov[1,2,5,a]
[1]*Dept. Phys. Mater., University of Basque Country UPV/EHU, 20018 San Sebastian, Spain*
[2]*Dept. Appl. Phys., EUPDS, University of Basque Country UPV/EHU,*
20018 San Sebastian, Spain
[3]*Institute of Physics, Faculty of Science, UPJS, Park Angelinum 9, 041 54 Kosice, Slovakia*
[4]*Instituto de Fisica, Universidade Federal do Rio Grande do Sul, 91501-970 Porto Alegre,*
RS, Brazil
[5]*IKERBASQUE, Basque Foundation for Science, 48011 Bilbao, Spain*

(Presented 3 November 2016; received 13 September 2016; accepted 12 October 2016;
published online 27 December 2016)

We observed a significant increase of the giant magnetoresistance (GMR) effect (up to 32% after the adequate annealing) and Kondo-like behavior in $Cu_{90}Co_{10}$ glass-coated microwires. Observed enhancement of the GMR effect can be interpreted considering the formation of the fine Co grains inside the Cu matrix as well as appearance of lamellar nanostructures allowing enhancement of the MR effect after annealing. Observed experimental data are discussed considering the regions with higher Co-ions content responsible for the presence of Co inhomogeneities or clusters and the regions with lower Co-ions content behaving as the magnetic impurities in the metallic host. Observed resistivity minimum on temperature dependence can be described considering Kondo effect mechanism involving magnetic impurities in metals. But the other mechanisms responsible for the resistivity minimum have been considered. [http://dx.doi.org/10.1063/1.4973291]

I. INTRODUCTION

Rapid quenching from the melt is quite fast and an effective method for preparation of novel metastable materials with crystalline, amorphous, nanocrystalline or granular structures with a new combination of physical properties (mechanical, magnetic, electrochemical…).[1–4] Most attention has been paid to studies of amorphous soft magnets presenting excellent magnetic softness.[3,4] This magnetic softness is originated from the absence of magnetocrystalline anisotropy in amorphous alloys.[3,4]

On the other hand, granular or inhomogeneous materials typically formed by immiscible elements (Co, Fe, Ni)-(Cu, Pt, Au, Ag) attracted considerable attention since the beginning of 1990s.[5,6] The main interest in granular materials is related to giant magnetoresistance (GMR), previously discovered in magnetic multilayered films.[7] A substantial economic difference between multilayered thin films and granular materials is the preparation cost: multilayered materials must be fabricated with multisource MBE and sputtering. The high fabrication cost is an obstacle. On the other hand, granular materials can be fabricated with much simpler technology.[3,4,8–11]

The origin of the GMR effect in granular materials has been attributed to spin-dependent scattering of conduction electrons within the magnetic granules, as well as at the interfaces between magnetic and nonmagnetic regions.[5,6] These granular inhomogeneous solids can be prepared by different techniques including mechanical alloying and rapid quenching techniques.[8–10]

---

[a] Corresponding author: A. Zhukov (e-mail: arkadi.joukov@ehu.es; phone: +34-943018611; fax:+34-943017130)

2158-3226/2017/7(5)/055906/8

Conventional route for optimization of the GMR effect in granular inhomogeneous materials involves appropriate recrystallization of the prepared metastable alloys through the annealing allowing formation of a structure consisting of magnetic nano-sized precipitations into conductive metallic matrix.[9,10] Formation of such structure is related to the phase diagram of the immiscible elements. Typically, at room temperature the ferromagnetic metals present quite low solubility in the metallic matrix. Consequently, rapidly quenched immiscible alloys at room temperature usually form a supersaturated solid solution.[9,10]

During last few years studies of glass-coated magnetic microwires prepared using Taylor-Ulitovsky technique involving rapid quenching from the melt gained considerable attention.[4,11] This inexpensive and fast preparation process method allows preparation of long uniform microwires (up to 10km) with few grams of the master alloy.[4] The diameter of metallic nucleus typically ranges from 1 up to 70 μm, although preparation of nanowires using almost the same technique is reported.[12]

Amorphous magnetic microwires can present excellent magnetic properties (giant magnetoimpedance effect and fast magnetization switching.[4,13] Moreover the developed technology is suitable for mass production.[4]

On the other hand, strong internal stresses may be induced during the simultaneous rapid solidification of the metallic wire surrounded by the glass coating. The origin of these stresses is related to different thermal expansion coefficients of metal and glass-coating. The strength of these stresses depends on thickness of the glass coating and metallic nucleus diameter, which provides another control mechanism of the magnetoelastic anisotropy in the metallic nucleus.[14–16]

Essentially the same fabrication method can be employed for preparation of Co-Cu and Fe-Cu microwires exhibiting granular structure and GMR effect.[11,17] But as-prepared microwires Co-Cu and Fe-Cu generally present GMR effect below 10%.

Quite recently we reported on considerable improvement of the GMR effect after annealing of Cu-Co microwires and on observation of Kondo-like behavior in $Cu_{95}Co_5$ microwires.[17,18]

On the other hand, there are still open questions as regarding the origin of the GMR effect in materials prepared from immiscible elements. Thus Co particles embedded in Cu matrix, small Co clusters within a Cu matrix, homogeneous spinodal decomposition characterized by long parallel Co-excess stripes are considered by various authors.[9,19,20] Moreover Kondo-like behavior reported for $Cu_{95}Co_5$ microwires is quite unusual even for alloys containing 5% Co. Indeed, classical Kondo-effect is usually observed in alloys with quite low content of magnetic impurities (0,002-0,02 %).[21]

Consequently, in this paper, we present our last experimental results on the influence of annealing conditions on magnetic, transport and structural properties of $Cu_{90}Co_{10}$ glass-coated microwires.

II. EXPERIMENTAL METHOD

Studied $Cu_{90}Co_{10}$ glass-coated microwires (total diameters, $D \approx 20.2$ μm, metallic nucleus diameter, $d \approx 14.7$ μm have been prepared using the Taylor-Ulitovsky technique.[4,12–16] A $Co_{10}Cu_{90}$ master alloy has been prepared by arc melting of the pure elements in Ar atmosphere. The master alloy ingot was first placed into a Pyrex tube inside an inductive coil. Once the composite material was melted (metallic alloy and Pyrex glass coating), it was drawn and wound onto a motorized cylinder shaped spool. A water jet has been applied to the moving wire for enhancing the quenching rate. Thin metallic wires ($D \approx 20.2$ μm, $d \approx 14.7$ μm) covered by a Pyrex glass have been obtained using aforementioned technique.

Structure and phase composition have been studied using a BRUKER (D8 Advance) X-ray diffractometer with Cu K_α (λ = 1.54 Å) radiation.

Magnetic and transport properties have been measured using a Quantum Design PPMS device (with applied magnetic field up to 90 kOe) in the temperature range 5 - 300 K. For magnetic and transport measurements we used 4-5 mm long samples. Electrical contacts were prepared by mechanically removing the insulating glass coating at the very end of microwires. The electrical resistance has been measured using four probe method.

The magnetoresistance ratio (MR) is defined as:

$$\Delta R/R\,(\%) = (R\,(H) - R\,(0))\,x100/R\,(0) \tag{1}$$

Where *R(H)* is resistance at given magnetic field, *H*, *R(0)* is the resistance at $H = 0$. Because of thin diameters the sample resistance is not small (a few Ohms). Consequently, observed resistivity changes we of the order from 0.2 to 1 Ohms.

Samples have been annealed in conventional furnace at annealing temperatures, $T_{ann} = 400°C$ varying the annealing time, t_{ann}. Since all the samples are coated by the insulating glass coating the annealing has been performed on air (without any inert gas or vacuum).

III. EXPERIMENTAL RESULTS AND DISCUSSION

The magnetization curves, *M(H)*, of studied $Cu_{90}Co_{10}$ microwires measured at temperatures 5 -150 K are shown in Fig. 1. *M(H)* of as-prepared sample measured at 5 K exhibits saturation (see Fig. 1). For higher temperature (above 75 K) *M(H)* dependences are almost linear. After annealing the saturation has been observed at least up to 80 K in the same sample (Fig. 1(b)).

As-prepared $Cu_{90}Co_{10}$ samples present magnetoresistance, $\Delta R/R$, of about 5% similarly to that reported previously[11] (see Fig. 2(a)). After annealing we observed gradual increasing of $\Delta R/R$ (see comparison of $\Delta R/R(H)$ for as-prepared and annealed at 400°C for t_{ann} = 1h and 5h). After long enough annealing we observed increasing of $\Delta R/R$ up to 32% (see Fig. 2(b)). This behavior is similar to that recently reported by us for $Cu_{95}Co_5$ and $Cu_{80}Co_{20}$ microwires.[17,18] But $\Delta R/R$ values observed in studied $Cu_{90}Co_{10}$ microwires ($\Delta R/R \approx 32\%$) are higher.

The behavior of $\Delta R/R(H)$ curves is typical for GMR effect showing decreasing with magnetic field, *H*, increasing (Fig. 2(a)).

In order to analyze the origin of the GMR effect we compared the temperature dependence of $\Delta R/R$ and M^2 for studied as-prepared and annealed $Cu_{90}Co_{10}$ microwire (see Fig. 3). We observed qualitative correlation for all temperature range.

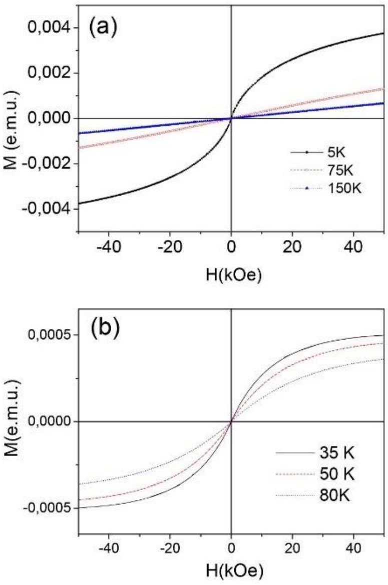

FIG. 1. Magnetization curves, M(H), in as-prepared (a) and annealed at 400°C for 10 h (b) $Cu_{90}Co_{10}$ sample measured at different temperatures.

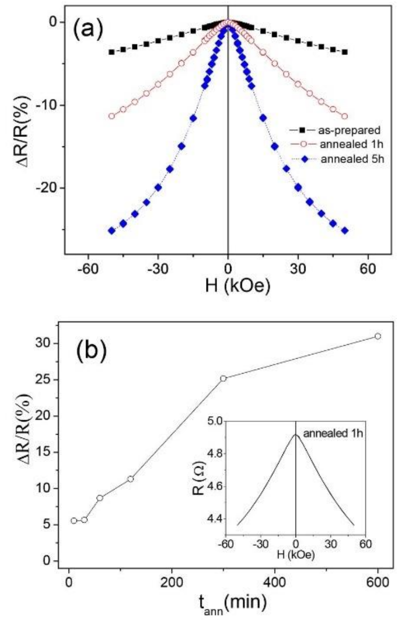

FIG. 2. Effect of annealing (T_{ann} =400°C) on GMR effect of $Cu_{90}Co_{10}$ microwires (a) and dependence of GMR effect on annealing time (b). Real resistance variation with magnetic field in the sample annealed at 400°C for 1 h measured at 5K is shown in the inset of Fig. 2(b).

As described elsewhere,[6] a number of magnetic systems exhibit large negative MR. In multilayers and granular systems, the MRs can be saturated under a sufficiently large magnetic field when ferromagnetic alignment is achieved. In our case we did not observe the saturation even at high magnetic field (see Figs. 2(a) and 2(b)). This behavior is typical for spin glasses and alloys containing small magnetic clusters, where the large negative MRs cannot be readily saturated by the field due to the inability to accomplish ferromagnetic alignment of all the moments. Consequently, we can only assume that studied samples are magnetically inhomogeneous or disordered on the scale of the mean-free path.

The other peculiarity of studied as-prepared $Cu_{90}Co_{10}$ samples is that surprisingly they present well-defined resistivity minimum at rather high temperature (about 50K, see Fig. 4). This minimum is affected by applied magnetic field, but in as-prepared sample can be totally suppressed by rather strong magnetic field (about 70 kOe). After annealing the resistivity minimum on *R(T)* dependence still persists, but this minimum can be suppressed by much lower magnetic field, i.e. by $H = 10$ kOe (Fig. 4(b)).

Usually the resistivity minimum is attributed to the Kondo effect related to the magnetic impurities in metals. But, as mentioned above, classical Kondo-effect is usually observed in alloys with quite low content of magnetic impurities (0,002-0,02 %) and the scattering processes on these magnetic impurities could give rise to a resistivity minimum on *R(T)* dependence.[21]

Typically in the case of classical Kondo effect the magnetic field suppresses the resistivity minimum. The temperature of *R(T)* minimum is usually much lower, but relatively high Co content can be the reason of the higher minimum temperature.[22] Considering high Co content we can expect the interaction between magnetic Co-ions and therefore suppression of the Kondo effect. The existence of Co inhomogeneities or clusters can be assumed from the magnetic saturation observed at low temperatures (see Fig. 1).

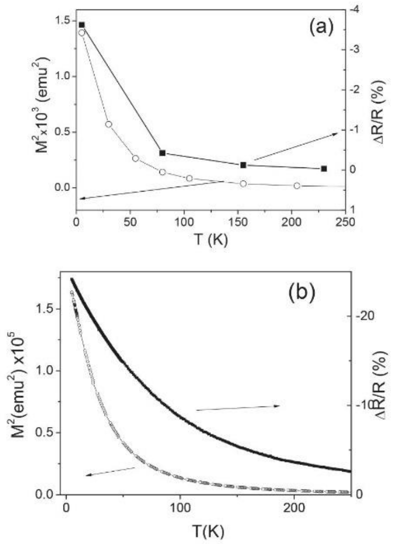

FIG. 3. Temperature dependences of Δ*R/R* and M^2 for as-prepared (a) and annealed at 400°C (b) $Cu_{90}Co_{10}$ microwires.

The other feature of the classical Kondo effect is a resistivity contribution behaving as $\ln(T)$. In order to prove it we re-plotted *R(T)* dependences in a semi-logarithmic scale (see Fig. 5). As can be observed, the R-$R_{min}(\ln T)$ dependence is not perfectly linear, although for annealed $Cu_{90}Co_{10}$ sample linear dependence fits better.

Consequently, after annealing magnetic and transport properties are rather different from as-prepared $Cu_{90}Co_{10}$ microwires.

More detailed structural studies can provide additional information on origin of R(T) minima.

Consequently, we employed the X-ray diffraction (XRD). The structure of the metallic core can be interpreted as granular with two phases: the main one, *fcc* Cu phase (lattice parameter 3.61 Å), found in all samples and small amount of *hcp* Co phase (lattice parameters 2.51 Å and 4.07 Å), obtaining an evaluation of the grain size between 20 and 40 nm. The grain size, *Dg*, of the crystals formed in each case can derived from Scherrer's equation:

$$D_g = \frac{K\lambda}{\varepsilon \cos 2\theta} \tag{2}$$

where, K is a dimensionless shape factor, with a value close to unity. The shape factor has a typical value of about 0.9, but varies with the actual shape of the crystallite. ε, is the half height width of the crystalline peak, and 2θ is the angular position of the maximum crystalline peak.

The Co phase shows a diffraction peak which is very close to the Cu one and, in fact, on those compositions with low Co concentrations, the Co peak is only seen as a shoulder in the high angle side of the Cu peak.[23] The diffraction peaks of both phases in observed XRD scans are quite close to each other and even overlapped (see Fig. 6(b)) and only a shoulder in the single peak corresponding to a small amount of the Co phase (presenting also small average grain size) can be observed in the main Cu peak. This fact is only observed when the peak in Fig. 6(b) is seen at very precise scale. The simple view of Fig. 6(b), where the annealed sample shows a wider peak than the as cast one in the high angle 2θ side, leads to deduce the existence of the peak corresponding to the Co phase.

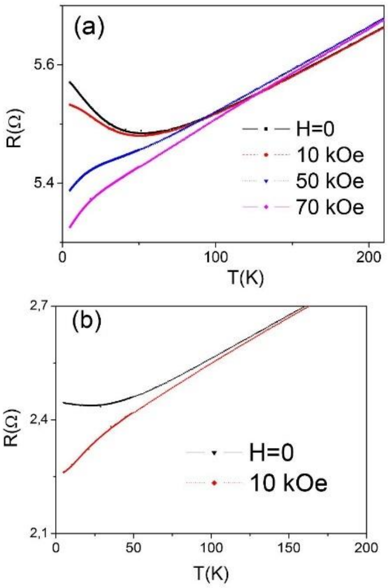

FIG. 4. Effect of magnetic field on temperature dependence of resistance, R, in as-prepared (a) and annealed (b) $Cu_{90}Co_{10}$ microwires.

Then, we deduced considerable preferred orientation of the grains visible from the peak intensities. Usually the peaks at 2 Θ≈43.95° in Co-Cu granular alloys without texture present the highest intensity.[23]

After annealing, it can still be found a marked preferred orientation in the sample, although intensities of each peak change with the treatment. When we look into the details, we clearly observed a broadening of the peaks (especially for ones at $2\Theta\approx50^0$, see Fig. 6(b)) that must be attributed to the Co precipitation from the solid solution of Co in Cu matrix. This broadening has been estimated as 0.3° to 0.5° (in the high angle side of the peak) and this means that the concentration of the Co phase is increased with the annealing.

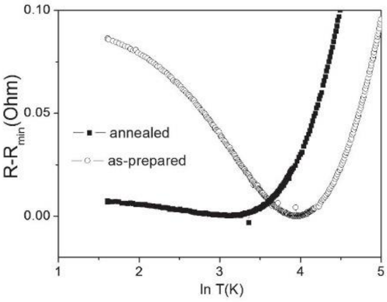

FIG. 5. $R\text{-}R_{min}(\ln T)$ dependence for as-prepared and annealed at 400°C $Cu_{90}Co_{10}$ microwires.

Consequently, we can assume that, after annealing the precipitation of fine Co grains from the metastable structure of $Co_{10}Cu_{90}$ microwire takes place.

It is worth mentioning that the other possible reason of the observed changes can be related to appearance of the nanostructures typical for the spinodal decomposition.[21]

On the other hand it is known that amorphous and disordered materials can exhibit a minimum on temperature dependence of resistivity or decreasing of the resistivity with temperature increasing.[24,25] Studied $Cu_{90}Co_{10}$ microwires present crystalline structure. But high degree of disorder related to the preparation method involving rapid quenching from the melt can be the origin of the unusual temperature dependence of resistivity.

Consequently, observed features of the resistivity minimum can be described considering Kondo effect mechanism involving magnetic impurities in metals. But, besides the classical Kondo effect, we must consider also the other mechanisms responsible for the *R(T)* minimum, like weak localization, enhanced electron-electron interaction, scattering of conduction electrons by structural TLS, scattering of strongly spin-polarized charge carriers on diluted magnetic moments and disordered structure. The fact that *R(T)* minimum is affected by the magnetic field supports the classical Kondo effect contribution. On the other hand, non-homogeneous and broad Co ions distribution and atomic disorder mentioned above can give rise to the other mechanisms.

It is worth mentioning that for similar Co content in Co-Ag system the nonmonotonic resistivity temperature dependence was explained using the two-current model without involving a Kondo mechanism.[26] Additionally recently we reported on similar behavior in Co_5Cu_{95} microwires with lower Co content.[17]

The fact that the minimum on *R(T)* dependence of annealed sample is suppressed by much lower magnetic field must be attributed to the redistribution of Co in the studied sample after annealing and formation of either Co grains or lamellar nanostructures.

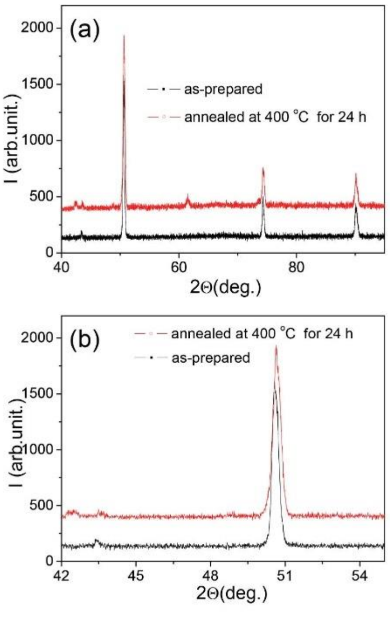

FIG. 6. XRD patterns of as-prepared (a) and annealed at 400°C for 24 h (b) $Cu_{90}Co_{10}$ microwires.

The fine granular structure obtained after annealing allows also the enhancement of the MR effect in the studied $Co_{10}Cu_{90}$ microwire up to 32%.

IV. CONCLUSIONS

We prepared and studied magnetic properties and magnetoresistance of $Cu_{90}Co_{10}$ microwires. As-prepared microwires present MR of about 5%. After annealing we observed considerable enhancement of the MR effect from 5 up to 32%. We also observed resistivity minimum on temperature dependence. The temperature of minimum is affected by annealing. In both as-prepared and annealed samples *R(T)* dependence is affected by external magnetic field.

The obtained results can be interpreted considering the formation of the fine Co grains inside the Cu matrix as well as appearance of lamellar nanostructures allowing enhancement of the MR effect after annealing. Observed resistivity minimum can be described considering Kondo effect mechanism involving magnetic impurities in metals. But, besides the classical Kondo effect, we must consider also the other mechanisms responsible for the *R(T)* minimum, like weak localization, enhanced electron-electron interaction, scattering of conduction electrons by structural TLS, scattering of strongly spin-polarized charge carriers on diluted magnetic moments and disordered structure.

ACKNOWLEDGMENTS

This work was supported by Spanish MINECO under MAT2013-47231-C2-1-P. VZ and AZ wish to acknowledge the support under Program of Mobility of the Researchers of the Basque Government (grants MV-2016-1-0025 and MV-2016-1-0018 respectively). Technical and human support provided by SGIker (UPV/EHU) is gratefully acknowledged.

[1] I. S. Miroshnichenko and I. V. Salli, Zav. Lab. **2**, 1398 (1959).
[2] K. Klement, R. H. Wilens, and P. Duwez, Nature **187**, 869 (1970).
[3] D. C. Jiles, Acta Mater. **51**, 5907 (2003).
[4] A. Zhukov, A. Talaat, M. Churyukanova, S. Kaloshkin, V. Semenkova, M. Ipatov, J. M. Blanco, and V. Zhukova, J. Alloys Compound. **664**(15), 235 (2016).
[5] A. E. Berkowitz, J. R. Mitchell, M. J. Carey, A. P. Young, S. Zhang, P. E. Spada, F. T. Parker, A. Hutten, and G. Thomas, Phys. Rev.Lett. **68**, 3745 (1992).
[6] C. L. Chien, J. Q. Xiao, and J. S. Jiang, J. Appl. Phys. **73**, 5309 (1993).
[7] M. N. Baibich, J. M. Broto, A. Fert, F. Nguyen Van Dau, F. Petron, P. Etienne, G. Creuzer, A. Friederich, and J. Chazelas, Phys.Rev.Lett. **61**, 2472 (1988).
[8] A. R. Yavari, P. J. Desré, and T. Benameur, Phys. Rev. Lett. **68**, 2235 (1992).
[9] P. Allia, M. Knobel, P. Tiberto, and F. Vinai, Phys. Rev. **52**, 15398 (1995).
[10] R. H. Yu, X. X. Zhang, J. Tejada, M. Knobel, P. Tiberto, and P. Allia, J. Appl. Phys. **78**, 392 (1995).
[11] A. Zhukov, C. Garcia, M. Ilyn, R. Varga, J. J. del Val, A. Granovsky, V. Rodionova, M. Ipatov, and V. Zhukova, J. Magn. Magn. Mater. **324**, 3558 (2012).
[12] H. Chiriac, M. Lostun, G. Ababei, and T.-A. Ovari, J. Appl. Phys. **109**, 07B501 (2011).
[13] P. A. Ekstrom and A. Zhukov, J. Phys. D: Appl. Phys. **43**, 205001 (2010).
[14] V. Zhukova, J. M. Blanco, V. Rodionova, M. Ipatov, and A. Zhukov, J. Appl. Phys. **111**, 07E311 (2012).
[15] H. Chiriac, T. A. Ovari, and Gh. Pop, Phys. Rev. B **42**, 10105 (1995).
[16] A. S. Antonov, V. T. Borisov, O. V. Borisov, A. F. Prokoshin, and N. A. Usov, J. Phys. D: Appl. Phys. **33**, 1161 (2000).
[17] V. Zhukova, J. Mino, J. J. Del Val, M. Ipatov, A. Martinez-Amesti, R. Varga, M. Churyukanova, and A. Zhukov, J. Alloys Compound. **674**, 266 (2016).
[18] J. Mino, V. Zhukova, J. J. del Val, M. Ipatov, A. Martinez-Amesti, R. Varga, and A. Zhukov, J. Electron. Mater. **45**(5), 2401 (2016).
[19] M. P. C. Vergara, J. C. Cezar, H. C. N. Tolentino, and M. Knobel, Physica B **320**, 143 (2002).
[20] M. G. M. Miranda, E. Estevez-Rams, G. Martinez, and M. N. Baibich, Phys. Rev. B **68**, 014434 (2003).
[21] J. Kondo, Progress of Theoretical Physics **32**, 37 (1964)
[22] K. Matho and M. Beal-Monod, Journal de Physique Colloques **32**, C1–213 (1971).
[23] J. J. del Val, J. González, and A. Zhukov, Physica B **299**, 242, (2001).
[24] R. Hasegawa, Physics Lett. A **36**(5), 425 (1971).
[25] K. Shirakawa, K. Fukamichi, T. Kaneko, and T. Masumoto, J. Phys. F: Met. Phys. **14**, 1491 (1984).
[26] A. Gerber, A. Milner, I. Ya. Korenblit, M. Karpovsky, A. Gladkikh, and A. Sulpice, Phys. Rev. B **57**(21), 13667 (1998).

Vol. **131** (2017) *ACTA PHYSICA POLONICA A* No. 4

Proceedings of the 16th Czech and Slovak Conference on Magnetism, Košice, Slovakia, June 13–17, 2016

Magnetic Characterization of Melt-Spun Co–Ni–Ga Ferromagnetic Superelastic Alloy

J. Mino[a,b,*], M. Ipatov[b], J. Gamcova[a], K. Saksl[a,c], M. Durisin[c], V. Zhukova[b],
Z. Vargova[a], A. Zhukov[b,d,e] and R. Varga[a]

[a]Institute of Physics, Faculty of Sciences, P.J. Safarik University, Park Angelinum 9, 041 54 Košice, Slovakia
[b]Material Physics Department, Faculty of Chemistry, University of the Basque Country, UPV/EHU,
Plaza Elhuyar, 2, 20018, San Sebastian, Spain
[c]Institute of Material Research, SAS, Watsonova 47, 040 01 Košice, Slovakia
[d]IKERBASQUE, Basque Foundation for Science, 48011 Bilbao, Spain
[e]Dpto. de Física Aplicada, EUPDS, UPV/EHU, 200018, San Sebastian, Spain

Ribbons of composition $Co_{49}Ni_{21}Ga_{30}$ have been prepared by melt-spinning method. X-ray diffraction investigation revealed single phase with $B2$ structure at room temperature. However, analysis of magnetization dependence of temperature suggests phase transition in the range 150–250 K. Resistivity measurements revealed similar transition with shift to higher temperatures in the presence of magnetic field.

DOI: 10.12693/APhysPolA.131.1075
PACS/topics: 62.20.fg

1. Introduction

Ferromagnetic superelastic alloys (FSA) have attracted scientific attention in recent years, since they are perspective materials that can be used as sensors and actuators [1]. Properties of superelastic change are mostly influenced by martensitic transformation (MT), which appears between two solid phases called martensite and austenite by coordinated shear relocation of atoms over very short distances (usually in order of Å). It can be triggered by a stress, by a temperature and, in the case of the ferromagnetic alloys [2], by a magnetic field change. Thus, ferromagnetic superelastic materials have advantage in having one more control parameter. Austenite is high temperature phase and it is stable without stress. Martensite is low temperature phase and it is stabilized by stress. Variations between crystal structures of both phases and their lattice parameters result in strain. It is known from studies on single crystals that we can achieve maximum strain in one direction that is strictly determined by shape of both changing crystal structures [3]. Some applications require preferred crystal orientation, which can be used to achieve maximum strain in defined direction.

So far, many alloys with aforementioned properties have been discovered, for example alloys NiMnGa [2–4], FePd [5], CoNi(Al or Ga) [6–9], FeMnAlNi [10, 11], Co2CrGaSi [12], or FSA are usually produced by arc-melting [6, 9, 11, 12], by rapid solidification method, or by growing of single crystals [4, 10] with additional annealing. However, melt spinning method can help to avoid long-term annealing (or at least significantly reduce it) keeping good quality of highly textured polycrystalline ribbons [13]. So far, there has been successful progress on rapidly quenched ribbons, where only short-term annealing is required to relax the induced internal stress [7].

In this work, we show that rapid quenching method is efficient method for producing a ferromagnetic superelastic alloy that is in a single phase at room temperature and shows phase transformation with different magnetic properties of both phases.

2. Experimental

Master alloy with off-stoichiometric composition of the Heusler alloys ($Co_{49}Ni_{21}Ga_{30}$) have been produced using arc melting method in an argon atmosphere from highly pure elements (Co — 99.9+%, Ni — 99.95+%, Ga — 99.99%). Ribbon have been produced from master alloy using melt spinning technique in a helium atmosphere. Tangential speed of surface of a copper wheel was set to 20 m s^{-1}. Scanning electron microscope (SEM) JEOL 6100 operated at 30 kV was used to examine the microstructure of the sample and it was equipped with X-ray energy dispersive spectroscopy system (EDX) Inca Energy 200. SEM ran in secondary electrons detection mode. X-ray diffractometer (XRD) RTG Philips Xpert Pro equipped with Cu anode ($K_{\alpha 1}$, $\lambda = 0.154089$ nm) was used to study structure of produced ribbons. Magnetic measurements were carried by Quantum Design physical property measurement system (PPMS) and by magnetic properties measurement system (MPMS) in the 5–400 K temperature range under the external magnetic field up to 50 kOe. Electric current used in resistivity measurements have been set to 1 mA. Sample was longitudinally oriented to the magnetic field in both measurement systems.

---

[*] corresponding author; e-mail: `jakub.mino@student.upjs.sk`

3. Result and discussion

Microstructure analysis provided by SEM revealed polycrystalline structure with a size of crystallites varying between 10 to 30 µm. Thickness of the ribbon is 30 µm (measured from the SEM picture of cross-section shown in Fig. 1). Directional growth of crystallites (perpendicular to ribbon plane) is most probably caused by strong thermal gradient created during rapid quenching. EDX analyses confirmed nominal composition $Co_{49.4}Ni_{20.6}Ga_{30.0}$, which corresponds well with desired one (Fig. 2). Analyses were taken from 5 sites on three different pieces of ribbon and deviation from nominal composition was ±0.8%. Sufficient homogeneity of sample was achieved without long-term annealing of master alloys comparing to [7].

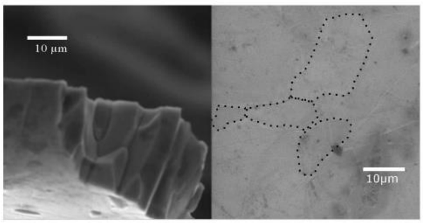

Fig. 1. SEM picture of ribbon cross-section and the surface of ribbon plane with marked grains.

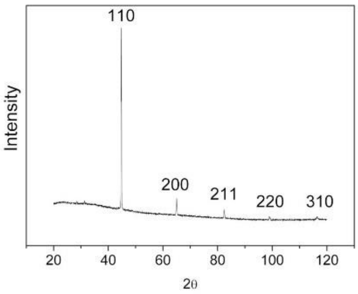

Fig. 2. X-ray diffraction pattern of $Co_{49}Ni_{21}Ga_{30}$ ribbon measured at room temperature.

X-ray diffractogram measured at room temperature shows single phase considered to be $B2$ crystal structure (Y–Z disorder of $L2_1$ Heusler alloy) [14]. Lattice parameter for the phase was determined to be 2.857 Å.

Magnetic characterization revealed a structural transition at the temperature below room temperature. Transformation occurs between high-temperature austenite and low-temperature martensite phase (Fig. 3). XRD of austenite phase corresponds to Ref. [6] and it crystallizes in body centered cubic (bcc) crystal structure, so according to [6] martensite phase should crystallize in face centered tetragonal (fct) structure at low temperature.

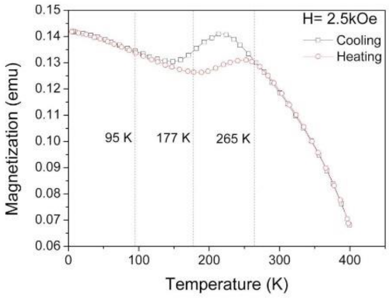

Fig. 3. Magnetization dependence on temperature of $Co_{49}Ni_{21}Ga_{30}$ ribbon determines phase transformation range. Dotted lines represent temperatures used for hysteresis loops measurement.

The phase transformation exhibits a hysteresis, from which MT temperatures were obtained. Austenite start temperature (A_s) was determined to be 179 K austenite finish temperature (A_f) to be 252 K. Martensite phase transformation starts (M_s) at 216 K and finish (M_f) at 149 K. The transition of polycrystalline sample is spread into the wilder temperature range contrary to single crystal [8].

Both phases have different saturated magnetization and magnetocrystalline anisotropy, that was confirmed by measurements of hysteresis loops.

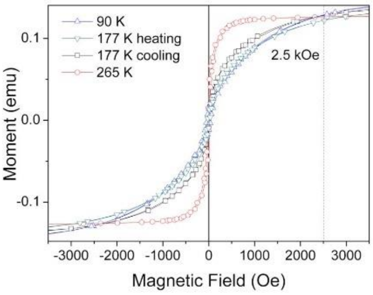

Fig. 4. Hysteresis loops of $Co_{49}Ni_{21}Ga_{30}$ ribbon in austenite, martensite, and in the middle of the MT. Dotted line represents magnetic field used for temperature dependence of magnetization.

Hysteresis loops (shown in Fig. 4) were taken at different temperatures: at full-martensite temperature (90 K), twice during the transition (177 K) on cooling and heating cycle, at full austenite temperature (265 K). Hysteresis loops indicate that low-temperature phase is more anisotropic.

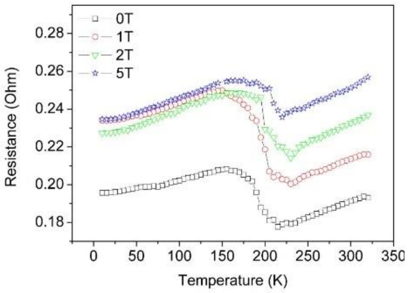

Fig. 5. Temperature dependence of resistance of $Co_{49}Ni_{21}Ga_{30}$ ribbon.

Resistivity dependence on temperature (Fig. 5) confirms MT with M_s = 215 K and for M_f = 155 K in accordance with magnetic measurements. M_s and M_f dependence on magnetic field does not reveal monotonic increase (Table I), since these temperatures are sensitive to local changes of structure in alloy. On the other side, inflex points of resistivity dependence on temperature (where major part of transition takes place) shows almost monotonic increase with applied magnetic field.

TABLE I

Martensitic transformation temperature taken from resistivity measurements.

	0 T	1 T	2 T	5 T
martensite start	215	230	230	220
inflex point	191	200	199	210
martensite finish	155	151	163	164

4. Conclusions

Ferromagnetic superelastic alloy $Co_{49}Ni_{21}Ga_{30}$ has been produced by melt spinning method. The alloy was characterized as single phase with $B2$ structure. Magnetic measurements revealed phase transformation in temperature range 149–252 K. From resistivity measurement, we can see that it is possible to shift MT temperatures to higher temperatures.

Acknowledgments

This work was supported by Spanish MINECO under MAT2013-47231-C2-1-P and Slovak project APVV-0027-011, VEGA grants No. 1/0164/16, VVGS-PF-2015-495 and VVGS-PF-2016-72614. Technical and human support provided by SGIker is gratefully acknowledged.

References

[1] J.M. Jani, M. Leary, A. Subic, M.A. Gibson, *Mater. Des.* , 56 1078 (2014).

[2] R. Kainuma, Y. Imano, W. Ito, Y. Sutou, H. Morito, S. Okamoto, O. Kitakami, K. Oikawa, A. Fujita, T. Kanomata, K. Ishida, *Nature* **439**, 957 (2006).

[3] V.A. Chernenko, J.M. Barandiarán, V.A. L'vov, J. Gutiérrez, P. Lázpita, I. Orue, *J. Alloys Comp.* **577**, S305 (2013).

[4] V.A. Chernenko, E. Villa, D. Salazar, J.M. Barandiaran, *Appl. Phys. Lett.* **108**, 071903 (2016).

[5] T. Okazaki, Y. Iwai, Y. Furuya, *Mater. Trans.* **49**, 360 (2008).

[6] J. Liu, H. Xie, Y. Huo, H. Zheng, Z. Li, *J. Alloys Comp.* **420**, 145 (2006).

[7] Y. Kishi, C. Criaciunescu, M. Sato, T. Okazaki, Y. Fyruya, M. Wuttig, *J. Magn. Magn. Mater.* **262**, L186 (2003).

[8] V.A. Chernenko, J. Pons, E. Cesari, A.E. Perekos, *Mater. Sci. Eng. A* **378**, 357 (2004).

[9] S. Dilibal, H. Sehitoglu, R.F. Hamilton, H.J. Maier, Y. Chumlyakov, *Mater. Sci. Eng. A* **528**, 2875 (2011).

[10] T. Omori, K. Ando, M. Okano, X. Xu, Y. Tanaka, I. Ohnuma, R. Kainuma, K. Ishida, *Science* **333**, 68 (2011).

[11] P. La Roca, J. Medina, C.E. Sobrero, M. Avalos, J.A. Malarria, A. Baruj, M. Sade, *MATEC Web of Conf.* **33**, 04005 (2015).

[12] X. Xu, T. Omori, M. Nagasako, A. Okubo, R.Y. Umetsu, T. Kanomata, K. Ishida, R. Kainuma, *Appl. Phys. Lett.* **103**, 164104 (2013).

[13] J.L. Sánchez Llamazares, T. Sanchez, J.D. Santos, M.J. Pérez, M.L. Sanchez, B. Hernando, Ll. Escoda, J.J. Suñol, R. Varga, *Appl. Phys. Lett.* **92**, 045002 (2008).

[14] T. Graf, C. Felser, S. Parkin, *Progr. Solid State Chem.* **39**, 1 (2011).